Assessment of Feasibility, Productivity and Product Quality during Laser Based Bending of Magnesium Alloy Sheets

A Thesis

Submitted in partial fulfillment of the requirements for the degree

of

DOCTOR OF PHILOSOPHY

by

Ravi Kant

(Roll No. 10610319)

Department of Mechanical Engineering

Indian Institute of Technology Guwahati, INDIA

2016

Dedication

This thesis is dedicated to my Late Grandparents, Family members, and Teachers, who taught me the purpose of life in countless ways

DECLARATION

I hereby declare that,

- I am the sole author of this thesis
- neither any part of this thesis nor the whole of the thesis has been submitted for a degree to any other University or Institution
- this thesis represents my ideas in my own words
- to the best of my knowledge, my thesis does not infringe upon anyone's copyright nor violate any proprietary rights; and that any ideas, techniques, quotations, or any other material from the other's work, are fully acknowledged in accordance with the standard referring practices
- I have adhered to all principles of academic honesty and integrity, and have not misrepresented or fabricated or falsified any idea/data/fact/source in my submission
- I understand that any violation of the above will cause for disciplinary action by the Institute and can also evoke penal action from the sources which have thus not been properly cited or from whom proper permission has not been taken when needed
- this is a true copy of my thesis, including any final revisions, as approved by my thesis review committee

Date: 09.05.2016

Ravi Kant
Roll No. 10610319

CERTIFICATE

This is to certify that the work contained in the Thesis entitled **"Assessment of Feasibility, Productivity and Product Quality during Laser Based Bending of Magnesium Alloy Sheets"** which is submitted by **Mr. Ravi Kant** in partial fulfillment of the requirement for the award of the degree of **Doctor of Philosophy** in Department of Mechanical Engineering, Indian Institute of Technology Guwahati, has been carried out under my supervision. The matter embodied in this thesis is original and has not been submitted elsewhere for the award of any other degree or diploma.

I wish him all the best for his bright future.

Dr. Shrikrishna N. Joshi
Assistant Professor,
Department of Mechanical Engineering,
Indian Institute of Technology Guwahati,
Guwahati, Assam, INDIA

Date: 09th May 2016

ABSTRACT

Magnesium alloys have low density, high specific strength and stiffness, superior damping capacity, high thermal conductivity and good electromagnetic shielding characteristics. They are the lightest metals among the available structural materials, and are widely used in the manufacture of components required for automobile, aviation, aerospace, and consumer electronics applications. Magnesium alloys have low ductility at room temperature due to the hexagonal crystal structure. This restricts precision bending of these alloys by using mechanical bending operations. In view of this, in present research work, systematic and extensive experimental as well as numerical studies have been carried out to assess the feasibility, productivity and product quality during the laser based bending of magnesium alloys.

Laser bending is a relatively new technique, which bends the workpiece by thermal stresses induced by the defocused laser beam irradiation instead of the mechanical force. Initially, experimental studies on laser bending of magnesium alloy M1A were carried out to assess the feasibility of the laser bending of magnesium alloy sheets. It was observed that the specimen did not catch the fire for any set of process conditions. Mechanical properties of the laser irradiated region were studied. The tensile properties of the magnesium alloy were found to be deteriorated due to the laser beam irradiation, however deterioration was very less and was limited to the irradiated region only. Experiments concluded that the magnesium alloys can easily be bent with the laser bending process without much deterioration in the mechanical properties of the heated region.

A three-dimensional non-linear coupled thermo-mechanical numerical model was developed for laser bending process using finite element method. The temperature and strain rate dependent material properties of magnesium alloy M1A were employed. The effect of melting was incorporated which made the developed model suitable for the wide range of process conditions. The mesh sensitivity analysis was carried out to obtain the optimum mesh parameters. Based on the stand-off distance between the laser head nozzle and worksheet surface, the beam diameter was computed. This formulation made the developed numerical process model more realistic.

The straight line laser bending of magnesium alloy M1A sheet was investigated by using the developed finite element based numerical model. The numerical model was first validated with experimental results, and found in good agreement. It was able to predict the bend angle

with an average absolute error of about 10.88%. The effects of process parameters, *viz*. laser power, scan speed and beam diameter on the performance parameters such as bend angle and edge effect were studied. The quality of laser bent worksheet was analyzed by studying the edge effect. It was observed that a combination of high laser power, slow scan speed and small beam diameter produced minimum edge effect.

In this work, a comprehensive numerical analysis of curvilinear laser bending process has been carried out. The laser beam was irradiated along a circular arc. The numerical model was validated with experimental results in terms of the bend angle, and found to be in good agreement with the experimental results. The numerical model predicted the bend angle with an absolute average error of about 4.71%. The validated numerical model was further used to study the effect of scanning path curvature on the edge effect, bend angle and deformation behavior.

In view of the lower productivity of single scan laser bending, experimental as well as numerical studies were carried out by employing multiple laser scans to obtain large bend angles (of the order of 10º) required for the industrial applications. The developed numerical model was validated with the experimental results. It was able to predict the bend angle after tenth laser scan with an average prediction error of about 12.41%. A series of numerical simulations were carried out to explore the change in bending mechanism, bend angle, edge effect, and temperature distribution during each scan of multi-scanning mode of laser irradiation.

In this work an integrated, simple and efficient technique – the laser assisted bending with moving pre-displacement has been developed. It combines together the advantages of thermal and mechanical bending operations. In this method, the mechanical load moves along the free edge of the worksheet simultaneously with the moving laser heat source. The moving mechanical load was applied in terms of the moving pre-displacement. An experimental setup was designed and developed to achieve the defined objectives. Initially, preliminary experiments were carried out to check the feasibility of the proposed technique. It was found that the proposed technique generates a large bend angle with a single laser scan. Three dimensional non-linear thermo-mechanical FEM based model was developed to carry out numerical simulations of the proposed methodology. The model was validated with the experimental results and was found to be in good agreement with the experimental results. The average prediction error of the numerical model was about 15.4%. The validated numerical model was further used to investigate the effects of laser power, scan speed, beam diameter

and pre-displacement on the bending mechanism, edge displacement, residual stresses, bend angle, edge effect and spring-back effect during the laser assisted bending with moving pre-displacement.

Overall the present research work has contributed systematic and extensive numerical as well as experimental studies on the laser bending of magnesium alloy M1A. This study covered important variants of the laser bending process, *viz*. straight line, curvilinear, multi-scan and laser assisted bending processes. Numerical simulations of all variants were validated with the experimental results. The efficiency of the process was improved by developing a simple laser based bending technique with an assistance of moving pre-displacement. The developed methodology of the moving pre-displacement can be employed in confidence to enhance the productivity and product quality of the laser bending process.

Chapter 1 presents introduction of the laser bending process and motivation of the present research work. Chapter 2 presents a critical review of literature and research gaps in the area of laser bending process. The objectives of the present work based on the research gaps identified in literature review are also presented. Chapter 3 presents assessment of the feasibility of laser bending of magnesium alloy M1A. Chapters 4 presents, in details, the development of FEM based thermo-mechanical numerical model for laser bending process. Chapter 5 presents numerical investigations on the single scan straight line laser bending process. Chapter 6 presents studies on the curvilinear laser bending process. Chapter 7 presents investigations on the multi-pass laser bending process to obtain large bend angles. Chapter 8 presents design and development of an integrated and simple laser assisted bending technique with moving pre-displacement. Chapter 9 presents important conclusions and specific contributions from the present research work with the scope for carrying out the future work in this area.

ACKNOWLEDGEMENTS

It has been a great experience for me to work on laser bending process. Many people have inspired, motivated and helped me during the entire course of this work and it is my heartfelt desire to acknowledge their immense goodwill and valuable support.

First, I thank Government of India and Indian Institute of Technology Guwahati for providing financial support and all sort of infrastructural facilities. I would like to acknowledge Advanced Manufacturing Laboratory, Material Science Laboratory, Central Workshop, and Central Instruments Facility of Indian Institute of Technology Guwahati for providing instruments to carry out the research work.

I shall forever remain obliged to my supervisor Dr. S. N. Joshi, Assistant Professor in the Department of Mechanical Engineering, for providing me a noble opportunity to work with him in the interesting field of laser bending process. His enthusiasm and zest to adopt and appreciate the latest trends in this research area and his eagerness to discuss and offer important suggestions have been a constant source of inspiration and encouragement. Each discussion carried out with him gave me confidence and clear direction of thought for my research work. I am especially thankful to him for critically reviewing the reports and research papers despite his busy schedule of academic and other administrative works. I owe him a lot for the valuable advice he has given whenever I needed.

I am sincerely thankful to Prof. U. S. Dixit, chairman of my Doctoral committee, who helped me a lot during this course of work. He gave many important suggestions and ideas to improve the quality of the work and the thesis report. I am also very thankful to other Doctoral Committee members, Prof. A. Khare, Dr. S. D. Kore, and the anonymous reviewers of my papers for their comments and suggestions which molded the course of this work.

I am thankful to Prof. Anoop K. Dass, Prof. Pinakeswar Mahanta and Prof. Debabrata Chakraborty, present and former Heads, Department of Mechanical Engineering, Indian Institute of Technology Guwahati, for providing various laboratory facilities and sanctioning funds without which completion of the work would not have been possible. Their co-operation had paved the way to my research work.

I am very much thankful to Dr. R. Ganesh Narayanan (M-Tech Project Supervisor), Shashikant (brother), Hema Gurung (wife), Mahesh Yadav (friend at IIT Kanpur) and Susanta Dey (friend in TATA Motors, Pune) for their technical support during this work. I am also

thankful to Mr. Lalit Saikia, Mr. Dhruba Saikia, Mr. Ranjan Patowary, Mr. Nandeswar Das, Mr. Nabajyoti Dutta, Mr. Raju Talukdar, Mr. Saimanta Das, Mr. Narayan Kalita, Ms. Trishna Choudhury, Mr. Labanu K. Konwar and Ms. Himadri Rajbongshi for their administrative.

I am grateful to Mr. Pranjol Paul, Technical officer and Mr. Jiten Basumatary, Mr. Saiffuddin Ahmed, Mr. Sanjib Sarma, Technical Superintendents in the Department of Mechanical Engineering for their valued support, time and patience to carry out my experimental studies without any hindrance. I extend my heartfelt thanks to Mr. Dilip Chetri, Mr. Minesh Medhi and Mr. Mrinal Sarma, Senior Technicians in Central Workshop, IIT Guwahati who helped me in the development and fabrication of experimental setups. Their valuable suggestions helped me to complete the experimental studies with better accuracy and repeatability.

I express my heartfelt gratitude to the present and past scholars who worked on laser bending process (Mr. Santosh Kumar**,** Mr. Hemanth, Mr. Parag Bhuyan, Mr. Kunwar Singh, Mr. Anil Mishra, Mr. Aghyad Eideh, Mr. Polash Dutta, Mr. Rosang, Mr. Biplab, Mr. Nagesh, Mr. Piyush, Mr. Himanshu, Mr. Pramod Sahu, Mr. Saurabh Garg). Their work was an important source of guidelines to me. I am thankful to my friends (Chandrahas, Vinod, Argha, Srikant, Satheesh, Saluja, Borad, Gururaj, Sunder, Devrani, Chandan, Akash, Arvind Shakya, Arvind Kumar, Mrityunjay, Debanjan, Praveen, Sathisha, Muthuraja, Prakash, Rasmi, Ojha, Rakesh, Jagannath, Simon, Mahto, Nilesh, Ajay, Nikhil) at IIT Guwahati for their timely help and moral support.

My sincere gratitude to my grand-father Late Sh. Mahadev Ram, grand-mother Late Smt. Mishri Devi, uncle Sh. Ramavtar, aunty Smt. Krishna Devi, father Sh. Ram Kishan, mother Smt. Kaushalya Devi, father-in-law Late Sh. Ashok Singh Gurung, Mother in Law Smt. Arati Gurung, brothers (Jitender, Laxmikant, Shashikant), sisters (Sumanlata, Saroj), and wife Hema Gurung, for their immense support during the course of my PhD work. Their patience, goodwill, caring nature and encouraging words kept me driving, and helped me to focus on my work. I dedicate this thesis to all of them.

Last, but not the least, I shall always be grateful to God for providing me such an awesome aura for research work.

Date: 09/05/2016 **Ravi Kant**

TABLE OF CONTENTS

NOMENCLATURE

H	Stand-off distance, distance between focal point and the worksheet surface
L	Worksheet length
P	Laser power
V	Scan speed
D	Beam diameter
t_s	Workpiece thickness
t_1	Thickness of the heated zone
A	Correction factor for the energy dissipation and counter-bending effect
k	Thermal conductivity
c	Specific heat of the material
F_0	Fourier number
S	Correlation coefficient
c_p	Heat capacity
R_t	Thermal effect index
E	Elastic modulus
M	Non-dimensional material parameter
k_s	Thermal conductivity of the shield gas
T_P	Laser pulse width
P_m	Maximum laser power of the machine
f	Frequency of the laser pulse
l	Half length of the plasticized zone
c_1, c_2	Constants dependent on materials properties
T_{max}	Maximum temperature
s	Reduction coefficient to account for the variation of yield strength and Young's modulus of elasticity with temperature
a_p	Characteristic length of the plastic zone
W	Worksheet width
L	Worksheet length
l_h	Width of the heated zone
T	Temperature
t	Time

K	Bulk modulus
q_c	Convective heat loss
q_r	Heat loss due to radiation heat flow
h	Convective heat transfer coefficient
T_s	Temperature at any point of the worksheet
T_0	Room temperature
T_s	Sheet temperature at a point
w_0	Laser beam waist
R	Laser beam radius
M^2	Beam quality factor
f	Focal length of the lens
R_L	Laser beam radius before lens (12 mm)
C	Strength coefficient
m	Strain rate sensitivity exponent
D_L	Beam diameter before focal lens
R_L	Beam radius before focal lens
I	Heat flux
r	Distance from center of the laser beam
u, v, w	Displacement in x, y, z direction, respectively
u_i, v_i, w_i	i^{th} node displacement in x, y, z direction, respectively
$[D^{eq}]$	Elasto-plastic stress-strain matrix
N_i	Individual shape function, related to i^{th} node
a_i	Generalized degrees of freedom
$[N]$	Interpolation or shape function matrix
$\{T_e\}$	Element nodal temperature matrix
$[B]$	General geometric matrix
$[C]$	Global heat capacity matrix
$[K_T]$	Global conductivity matrix
$\{Q\}$	Heat flux vector
$\{\delta u\}$	Virtual displacement vector
$\{F\}$	Body force in volume V
$\{F^a\}$	External applied force vector

$\{F^{nr}\}$	Internal force vector
$\{P\}$	Surface traction on surface S
$[K]$	Global tangential stiffness matrix
NT11	Temperature at node
PE	Plastic strain at node
S, Mises	Von-Mises stress at node
T_P	Laser pulse width
P_m	Maximum laser power

LIST OF GREEK SYMBOLS

η	Absorptivity
ρ	Material density
μ	Poisson's ratio
α_{th}	Coefficient of thermal expansion
α_d	Thermal diffusivity
α_b	Bend angle
λ_m	Latent heat
σ_y	Yield strength
λ	Wavelength of the laser beam
$\varepsilon_{\max}$	Maximum plastic strain at the heated surface
σ	Stress induced into the workpiece
λ and v	Lame's parameters
$\dot{\varepsilon}_{ii}$	Volumetric strain rate
$\{\delta\varepsilon\}$	Strain vector
$\dot{\varepsilon}_{total}$	Total strain rate
$\dot{\varepsilon}_{elastic}$	Elastic strain rate
$\dot{\varepsilon}_{plastic}$	Plastic strain rate
$\dot{\varepsilon}_{thermal}$	Thermal strain rate
$\theta_{\max}$	Maximum bend angle along the scanning line
$\theta_{\min}$	Minimum bend angle along the scanning line
$\theta_{average}$	Average bend angle along the scanning line
∇	Gradient operator
x, y, z	Three coordinate directions
ε_s	Surface emissivity of the workpiece
$\dot{\varepsilon}$	Strain rate
σ_s	Stefan-Boltzmann constant
θ	Half divergence angle

LIST OF ABBREVIATIONS

CNC	Computer numerical control
FEM	Finite element method
FDM	Finite difference method
TGM	Temperature gradient mechanism
BM	Buckling mechanism
UM	Upsetting mechanism
DOF	Degree of freedom
CW	Continuous wave
LVDT	Linear variable displacement transducer
RSM	Response surface methodology
CV	Coefficient of variation
ANN	Artificial neural network
GA	Genetic algorithm
SW	Scanning width
SS	Scanning step
STV	Scanning traverse speed
CPU	Central processing unit
ANFIS	Neuro-fuzzy interface system
HAZ	Heat affected zone
Nd:YAG	Neodymium-doped yttrium aluminum garnet
YLF	Yttrium lithium fluoride
CO_2	Carbon di-oxide

LIST OF FIGURES

LIST OF TABLES

CHAPTER 1: INTRODUCTION

Laser is a powerful, narrow, monochromatic, and directional beam of electromagnetic radiation. The radiation intensities of a high magnitude laser can be obtained with optical focusing that can melt, evaporate, bend, deposit or change the material characteristics of all metallic materials. Based on the lasing medium, the lasers can be classified as gas lasers, solid-state lasers, diode lasers, dye lasers, semiconductor lasers, excimer lasers and chemical lasers (Majumdar and Manna 2011). Nowadays, lasers are used in various manufacturing processes such as surface treatment (Palani et al. 2008, Subbu et al. 2009), cutting (Pallav et al. 2010, 2011), forming (Chakraborty et al. 2012), joining (Pandey et al. 2002), sintering, cladding (Santo and Davim 2011), engraving, marking, scribing, drilling (Singh and Melkote 2009, Singh et al. 2013), etc. These processes are widely used to produce the critical components of aerospace vehicles, bio-medical instruments, automobiles, and ships. Lasers can process a wide range of materials such as metals, non-metals, composites, ceramics (Santo et al. 2014, Ravindra and Patten 2014). Due to the capability of precise focusing and ease in controlling the heat energy, they can be used to process a variety of geometries such as sheets, plates, pipes, foils, complex curved surfaces.

Sheet bending, a material forming process, is widely used in the manufacturing industry. Tools and dies are generally employed in mechanical bending operations to manufacture the desired bend angle in the worksheet. The mechanical bending is cost effective and fast in view of the mass production of components. However, the cost associated with the equipment and alteration or adjustment of tools involved in the mechanical bending process is high, and therefore, it is not suitable for prototyping or low volume production. Spring-back effect, deformation of low ductility material and processing at the inaccessible region limit the applications of mechanical bending in precision manufacturing at micro as well as macro scale. Lasers helped to overcome some of these limitations. This motivates to pursue research work in the area of laser forming with an objective to assess the feasibility, productivity and product quality during laser based bending of difficult-to-form materials.

1.1 Laser Bending Process

The laser bending is similar to the flame bending that is used for the adjustment of welded construction in ship building industry. Forming of metal plates with the application of flame heating was initiated at the beginning of 19th century to shape the external metal plates of ship-

hull. However, the process is man-hour intensive and dependent on the skill of personnel. It is difficult to control and focus the flame on a small area (Ojeda and Grej 2009, Vollertsen and Sakkiettibutra 2010, Majumdar and Manna 2011). These problems were solved by applying a laser beam instead of a gas flame to deform the metal sheets. First application of the laser bending was patented by Martin in 1979 (Martin 1979). It was for automatic adjustment of leads of the relays using lasers. Then, in early 1980's, the application of laser for sheet bending was reported by Kitamura (Kitamura 1983).

Laser bending is a thermo-mechanical process that uses defocused laser beam to deform the workpiece. In the pure laser bending, the workpiece is deformed by means of thermal stresses without the use of any external mechanical force. Hard tooling such as tools, dies and presses are not required and the laser beam works as a non-contact virtual tool to deform the workpiece. This makes the process independent of tool inaccuracies those result in mechanical bending due to wear and deflection (Arnet and Vollertsen 1995, Dearden et al. 2003). The process can be used to bend sheets (Geiger 1994), plates (Lawrence et al. 2001), foils (Liu et al. 2009), tubes and pipes (Hao and Li 2003a,b) for a wide range of materials such as metals (Arnet and Vollertsen 1995), non-metals (Gärtner et al. 2001), composites (Chan and Liang 2000a, Edwardson et al. 2005a), plastics (Okamoto et al. 2004), and ceramics (Tam et al. 2001). Laser beam can be focused at a small spot (in the order of μm) that makes the process suitable for the processing of small meso/micro sized components.

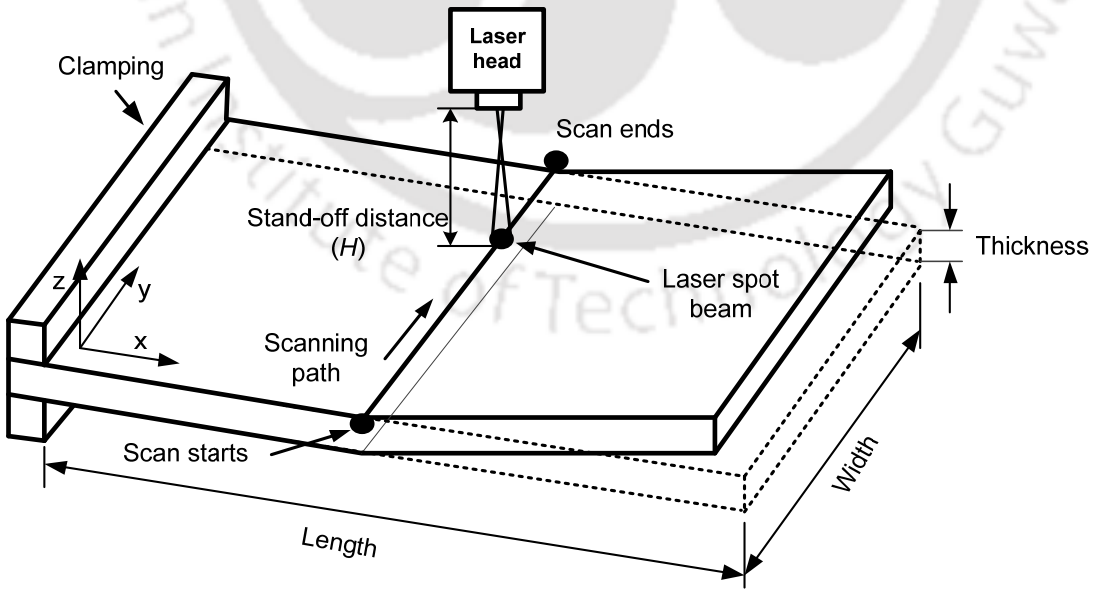

Figure 1.1. Schematic of laser beam irradiation.

Figure 1.1 shows schematic of the laser bending process for bending of a sheet metal workpiece (called as worksheet). The worksheet is clamped at one side on a computer numerical control (CNC) machine bed and the other side is free. The laser beam irradiates along a predefined scanning path. Either the CNC table or the laser head or both of them simultaneously move to generate a specified straight or curvilinear scanning path. The laser irradiation generates rapid localized heating which is followed by cooling as the laser beam moves to an adjacent area. Thermal expansion occurs in the heated region which is resisted by the surrounding cooler material. It induces compressive thermal stresses in the heated region and tensile stresses in the surrounding cooler material. During cooling, the irradiated material undergoes shrinkage, leading to the development of bend angle or change in shape of the worksheet (Geiger 1994, Shi et al. 2006).

1.2 Advantages and Limitations

Laser bending has many advantages in comparison with those of conventional bending operation. The important advantages are given as below (Vollertsen et al. 1995, Chen and Xu 2001, Magee and Vin 2002, Dearden and Edwardson 2003, Zhang and Xu 2005, Cheng et al. 2005a, Shen 2008, Casamichele et al. 2007, Shi et al. 2012a, Shidid et at. 2013):

1. The process is flexible and easy to control by using CNC controllers. It is easy to incorporate laser bending process into an automatic flexible manufacturing system due to the flexibility and easy control of laser beam.
2. The laser machine can be used for many applications such as cutting, forming, welding, marking, engraving, cladding, heat treatment, machining, etc., which makes the process suitable for small scale production and tool room applications.
3. External force setup, tools, dies and presses are not required. It reduces the cost of small batch production.
4. The process is fast due to the elimination of lead time associated with the design, manufacturing and placement of tools and dies as required in mechanical bending operation.
5. Precise, accurate and small bend angle can be obtained, which may not be possible with mechanical bending. The presence of inaccuracies due to spring-back, tool wear, and deformation limit the application of mechanical bending in precision operations.

6. Due to ease in transportation of the laser beam through flexible fiber optical cables, forming is possible in the areas where mechanical tools are not accessible.
7. The formability of material increases at an elevated temperature, therefore brittle and hard materials, such as magnesium alloys, titanium alloys, aluminum alloys, nickel alloys, ceramics can be processed easily.
8. Heat affected zone is small as the laser beam has narrow, concentrated and controlled area of irradiation.
9. Complex shapes can be generated with suitable irradiation strategies.
10. Laser bending uses localized heating to induce the controlled deformation instead of heating the entire workpiece. Therefore, it may have the advantage of energy efficiency as compared with other thermal bending operations.
11. Process can be used to bend materials with formability limitation (*e.g.*, aluminum oxide, glass, etc.) and size constraints (*e.g.*, very small parts required for miniaturization and large parts used in ship-building and aerospace industries).

In spite of various advantages, the laser bending has some limitations. These are as follows:

1. For mass production, the laser bending process is slow in comparison with traditional punch and die technique.
2. The process is not suitable for processing the workpiece with reflective surfaces. However, application of suitable coating can solve this problem.
3. The extensive heating due to the laser may melt the surface, which degrades the material properties of workpiece.
4. Mechanical and micro-structural properties of the irradiated region may deteriorate due to the presence of high temperature and thermal stresses.
5. High capital cost of the laser machine makes the process more expensive than the other variants of thermo-mechanical bending process, such as flame bending.

1.3 Applications of Laser Bending

Laser bending has many applications in automotive, aerospace, shipbuilding, medical, micro-electronics, and material processing industries (Li and Yao 2000a, Shen and Vollertsen 2009, Shi et al. 2012a). It finds a useful application to straighten the parts distorted at any stage of their production (Ueda 2009, Ueda 2011). Laser bending is used as an accurate and cost

effective process to adjust or align the mating parts in welded constructions, ship building industry and straightening of car body parts (Hennige 1997, Zhang and Xu 2005, Qi and Namba 2011). It is used to manufacture small parts used in micro-electromechanical systems (MEMS), chemical, and sensor industries (Vollertsen et al. 1995, Chen et al. 1998, Tam et al. 2001, Ocaña et al. 2007). The process is cost effective for low volume requirements such as forming of ship planks and production of aerospace fuselage (Zhou et al. 2013, Watkins et al. 2001). Due to high flexibility of the laser beam, it is well suited for the production of components in space. Laser bending is economical for maintenance work, when spare parts are not available (Dearden et al. 2006). It is suitable in processing of complex components in small-lot production and fabrication of individual parts for rapid prototyping (Laeng et al. 2000, Magee et al. 2000, Santos et al. 2006). It is also used to bend brittle materials that is not possible with conventional bending operations (Wu et al. 2010a,b, Bammer et al. 2011).

1.4 Motivation of the Work

Magnesium alloys have low density, high specific strength and stiffness, superior damping capacity, high thermal conductivity, and good electromagnetic shielding characteristics. They are the lightest metals among the available structural materials (Liu and Cui 2009). These are widely used to manufacture components required for automobile, aviation, aerospace, and consumer electronics applications (Mordike and Ebert 2001, Huo et al. 2009).

Magnesium alloys have low ductility at room temperature due to hexagonal crystal structure. This restricts precision bending of the magnesium alloys by using mechanical bending operations. Alexander (2007) and Bammer et al. (2011) reported that the mechanical bending generates cracks in the worksheet. To check this fact, the mechanical bending of magnesium alloy M1A worksheet was tried at the Central Workshop of IIT Guwahati. The worksheet was bent about an angle of 20°, and the bending edge was observed with an optical microscope. Figure 1.2 shows magnified view of the bent zone. It can be clearly seen that cracks are generated on the bottom surface of the sheet during mechanical bending operation. A bending radius of about 15.11 mm was obtained with the mechanical bending process. Therefore, generation of a large bend angle (of the order of 10°) with a small bending radius in magnesium alloy sheets was not thought to be feasible with the conventional mechanical bending operation.

Palaniswamy et al. (2004) reported that the formability of magnesium alloys increases at an elevated temperature due to the thermal activation of pyramid sliding planes in the

hexagonal closed pack structure. In view of this, laser bending can be an alternative for crack free precision bending of magnesium alloys. This motivated to carry out the assessment of feasibility of laser bending of magnesium alloy sheets. It was also thought to be interesting and important to study the behavior of magnesium alloy during laser bending operation.

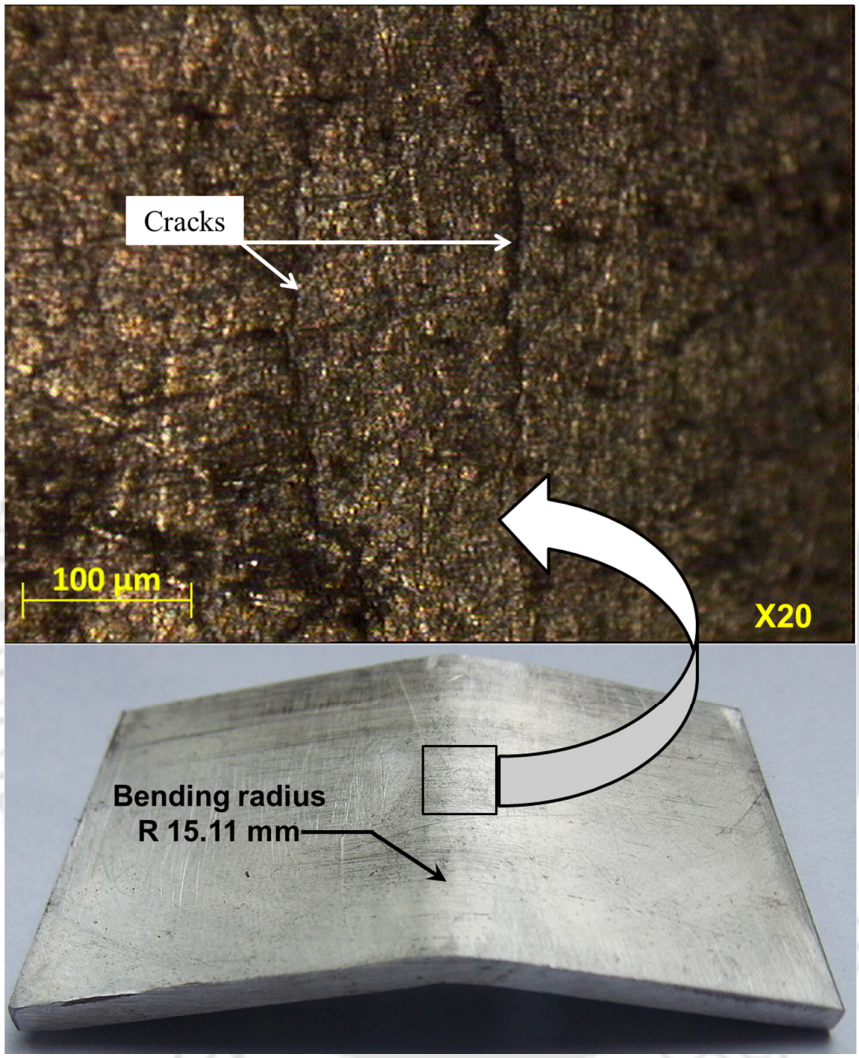

Figure 1.2. Optical microscope image showing cracks generated at the bottom surface during mechanical bending of magnesium alloy M1A sheet.

Literature reports numerical and experimental studies on various aspects of laser bending such as bending mechanisms, micro-structure studies and effects of process parameters, *viz*. power, scan speed, and beam diameter on the performance parameters *viz.* bend angle, edge effect, and surface quality. These studies are mainly focused upon straight line irradiation for 'single scan' only. The single laser scan produces a small bend angle (less than 2º). However, in real life applications, larger bend angles of the order of 10º are needed. It was

also reported that the bend angle is not uniform along the scanning path. This is not desirable in most of the practical applications. The non-uniform distribution of bend angle deteriorates the quality of the final product. Very scant research is reported on the studies to produce large and precise bend angles in difficult-to-form materials, such as magnesium alloys. This motivated to develop an efficient technique to manufacture large and precise bend angles using lasers. Also, a need was identified to carry out systematic numerical investigations to obtain the guidelines for an efficient and precise laser bending operation of difficult-to-form materials.

1.5 Organization of the Thesis

Chapter 1 presented an overview of the laser bending process in terms of its mechanism, advantages and limitations, and applications. The motivation for carrying out research in the area of laser bending of magnesium alloy has been brought out at the end of the chapter.

Chapter 2 presents an extensive literature review in the area of laser bending process. The current status of various aspects of laser bending, such as bending mechanisms, parametric analysis, laser bending with straight line, curvilinear, multiple scans is presented. The approaches towards the thermo-mechanical modeling of laser bending process as well as experimental studies are critically studied. The chapter concludes by summarizing important observations from the literature review, and stating the research objectives.

Chapter 3 presents, in detail, experimental studies carried out to check the feasibility of laser bending of magnesium alloys. Details regarding experimental set up and the associated procedures are presented. The mechanical properties of laser bent specimen were experimentally studied and presented in this chapter.

Chapter 4 describes, in detail, the development of three-dimensional non-linear coupled thermo–mechanical numerical model of laser bending process using finite element method (FEM). The governing equations, boundary conditions and solution methodology for the analysis are explained at length. The validation of predictions of numerical model for single-scan mode of laser bending is also presented.

Chapter 5 to Chapter 7 present numerical studies on laser bending of magnesium alloy M1A for three variants, *viz*. straight line, curvilinear and multi-scan laser beam irradiations. The validations of predictions of the simulations for the respective variant of laser bending operation are presented. For each variant of the process, the bending mechanisms and effect of various process parameters on the bend angle, edge effect and temperature distribution are discussed in detail.

Chapter 8 presents the design and development of an efficient laser based integrated technique for the improvement in productivity of the bending operation. Initially, details of the developed experimental setup are provided. Then, the validation of the predictions of numerical simulations of the proposed methodology is presented. At the end, parametric studies on the effect of various process parameters on the performance of laser bending with moving pre-displacement are presented in detail.

Chapter 9 presents the important observations and conclusions from the present research work. The scope for carrying out future work in this area is presented at the end of the chapter.

CHAPTER 2: LITERATURE REVIEW ON LASER BENDING PROCESS

2.0 Scope

This chapter presents a detailed literature review on research carried out in the area of laser bending process. It mainly covers a critical survey of research papers on experimental and numerical studies on bending mechanisms, process parameters, edge effects, and irradiation strategies of the laser bending process. Effects of the laser irradiation on mechanical and microstructural properties are also presented. The process planning and control of parameters to generate a desired shape is discussed. Various analytical, numerical, empirical, and soft-computing models are presented to predict the laser bending of a wide range of materials. The chapter concludes with a discussion on identification of gray areas of research in the laser bending process. In the end, objectives of the present research work are derived.

2.1 Laser Bending Mechanisms

In laser bending, a controlled laser beam scans over the workpiece surface. The outcome of laser scan involves complex interaction of laser process parameters, workpiece material properties, and the workpiece geometries (Geiger 1994, Vollertsen and Rödel 1994). Based on the temperature profile and stress-strain distribution, three mechanisms are operative, *viz.* temperature gradient mechanism (TGM), buckling mechanism (BM) and shortening or upsetting mechanism (UM). TGM and BM are responsible for the bending, and UM is responsible for the shortening and thickening of the workpiece (Geiger and Vollertsen 1993, Shi et al. 2006c). These mechanisms are discussed in details in the following sections.

2.1.1 Temperature gradient mechanism

Temperature gradient mechanism (TGM) is the most widely reported mechanism in the laser bending process. It can be used to bend the worksheet out of plane in the direction of laser source. The TGM occurs when energy parameters lead to a steep temperature gradient along the thickness direction (Arnet and Vollertsen 1995). The beam diameter is in the order of worksheet thickness (but can be larger), and the scan speed is fast enough to generate a steep temperature gradient along the worksheet thickness. The scan speed is faster for the materials with a higher thermal conductivity (Li and Yao 2001b).

Figure 2.1 illustrates various steps involved in the TGM. Initially, a steep temperature gradient generates along the thickness direction due to laser beam irradiation as shown in

Figure 2.1 (a). It results in the non-uniform thermal expansion in the heated region. The temperature of the top surface is higher, and therefore the thermal expansion is more at the top surface. It leads to the bending of worksheet away from the laser source as shown in Figure 2.1 (b). The thermal expansion of the heated region is restricted by the surrounding cooler material. It generates compressive thermal stresses in the heated region and tensile stresses in the surrounding cooler region. When these thermal stresses exceed temperature dependent flow stress, the plastic deformation occurs. The flow stress decreases with the increase in temperature, and hence the compressive plastic deformation occurs in the heated region. The cooler region does not undergo any deformation as the flow stress is high at a low temperature. The top irradiated surface has the highest temperature, and therefore the compressive deformation is more at the top surface. The plastic deformation is negligible at the bottom surface due to a lower temperature. The material contracts during cooling. The plastic compressive deformation causes a local shortening at the top surface. Thus, the worksheet finally bends towards the laser source as shown in Figure 2.1 (c). The bending occurs due to the difference between plastic deformation at the top and bottom surfaces (Lawrence 2002, Shi et al. 2006b, Shi et al. 2011). In general, a bend angle in the range of 0.1º to 3º can be achieved in a single laser scan (Lawrence et al. 2001).

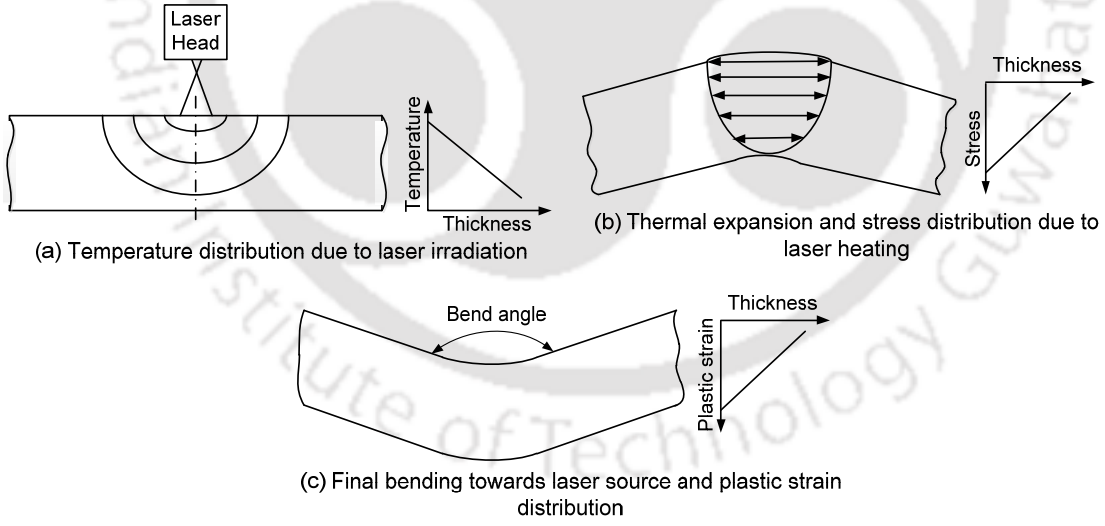

Figure 2.1. Process steps of the temperature gradient mechanism.

2.1.2 Buckling mechanism

Buckling mechanism (BM) occurs during laser bending of thin worksheets when the temperature gradient between top and bottom surfaces is negligible. It occurs when a thin worksheet of high thermal conductivity material is irradiated with a laser beam of large

diameter and slow scan speed. The beam diameter is about more than 10 times of the worksheet thickness (Hu et al. 2002).

Figure 2.2 illustrates various steps involved in the BM dominated laser bending process. The laser irradiation generates a high temperature isotherm along the thickness direction as shown in Figure 2.2 (a). It generates a large amount of lateral expansion in the heated region. The thermal expansion is uniform along the thickness direction, which is restricted by the surrounding cooler material. This induces compressive stresses in the heated region. The buckling stiffness of the worksheet is low due to a less thickness, and it reduces to a negligible value at a high temperature field caused by the laser beam irradiation. Due to the combined effect of large thermal expansion and negligible buckling stiffness, the buckle generates in the heated region as shown in Figure 2.2 (b). The buckling tendency is more when the worksheet is thin and the coefficient of thermal expansion and temperature dependent flow stress are high (Vollertsen et al. 1995). Once buckling is initiated, it extends along with the laser beam irradiation. When thermal stresses exceed the temperature dependent flow stress, the plastic deformation occurs in the buckle. Finally, based on the direction of the buckle, the worksheet bends towards or away from the laser source as shown in Figure 2.2 (c) (Lawrence 2002).

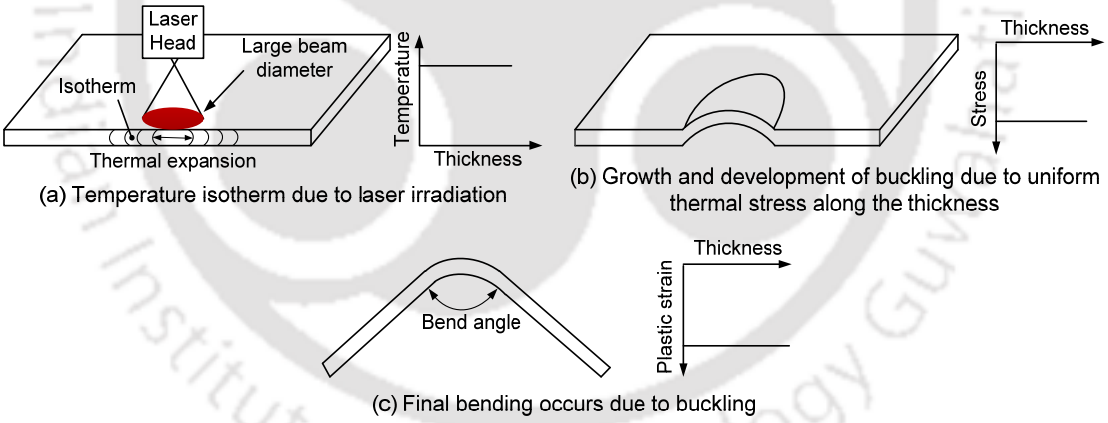

Figure 2.2. Process steps of the buckling mechanism.

In general, a bend angle between 1° to 15° can be achieved in a single laser scan using BM dominated process conditions, which is significantly higher than TGM. Unlike TGM, the counter bending does not occur in BM. The bending direction is not certain in BM, and determined by the pre-curvature of the sheet, internal stresses and external or gravitational forces acted on the worksheet (Shi et al. 2006c, Jamil et al. 2011a).

Li and Yao (2001b) postulated an irradiation scheme that starts from a location near the middle of the worksheet instead from an edge of the worksheet. The proposed irradiation

scheme is shown in Figure 2.3. First rightward and then leftward scanning was done from near the middle of the scanning path. The proposed scheme was able to provide a convex bending (away from laser source) in BM dominated process mechanism. It was due to the shift of starting point to the middle that added mechanical constraints to sustain the initial convex deformation. Jamil et al. (2011a) studied the effect of rectangular beam geometries with different transverse width to length aspect ratio on the buckling mechanism dominated laser bending of thin sheet. The beam geometry played an important role in the temperature distribution and deformation behavior. Vásquez-Ojeda and Ramos-Grez (2009) found that the directional certainty can be achieved with suitable modulation of the laser energy.

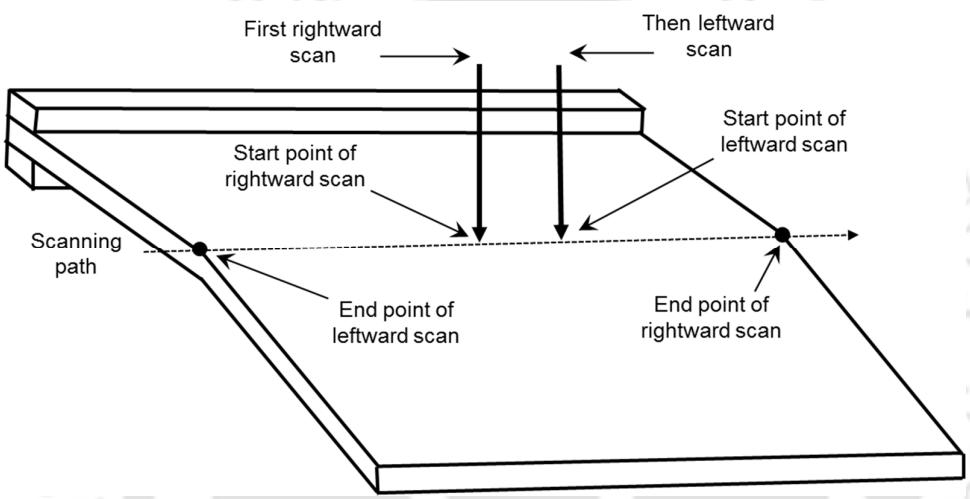

Figure 2.3. Irradiation scheme for the certain bending direction in buckling mechanism. Redrawn from Li and Yao (2001b), with permission (Appendix 2.1). Copyright © 2001, Elsevier.

Shi et al. (2006c) proposed a critical condition to know whether the process is dominated by the TGM or by the BM. The condition is given as

$$\frac{PD^{1/2}}{t_s^{2}V^{1/2}} > \frac{A\pi^{7/2}k^{1/2}\rho^{1/2}c^{1/2}}{41.52(1+\mu)\eta\alpha_{th}}, \tag{2.1}$$

where $P, D, t_s, V, A, k, \rho, c, \mu, \eta$ and α_{th} are laser power, beam diameter, sheet thickness, scan speed, correction factor, thermal conductivity, density, specific heat, Poisson's ratio, absorptivity and coefficient of thermal expansion, respectively. If a set of process parameters satisfies the inequality in Equation (2.1), it provides buckling mechanism dominated process conditions. The process condition for the dominating mechanism can also be assessed by the Fourier number which is given as (Shi et al. 2006c)

$$F_0 = \alpha_d D / t_s^{2} V, \tag{2.2}$$

where α_d, t_s, D and V are thermal diffusivity, sheet thickness, beam diameter and scan speed, respectively. Smaller value of the Fourier number corresponds to a TGM dominated laser bending, while BM plays a dominant role for a larger value of the Fourier number. Shi et al. (2008) derived a condition inequality to know the dominating mechanism and bending direction in the laser bending of sheets. The inequality is given as

$$\frac{P}{t_s^2}\left(\frac{D}{\rho c_p V h}-\frac{t_s}{3k}\right)\geq\frac{\pi^3}{20.76(1+\mu)\eta\alpha_{th}}. \tag{2.3}$$

For a workpiece, the BM plays a dominant role if inequality in Equation (2.3) is satisfied and the sheet produces a concave or convex forming. When the value of right hand side in Equation (2.3) is less than or equal to 2.8×10^5, the concave forming occurs in BM, and when this value is greater than or equal to 3.36×10^5, the convex forming can be achieved.

Chen et al. (2008) used 160 W diode laser for the laser bending of low carbon steel sheets of thicknesses 0.25 mm, 0.51 mm and 0.79 mm, respectively. It was observed that the BM dominated laser process parameters provided the largest bend angle, when the beam diameter to sheet thickness aspect ratio was close to four. For the aspect ratio less than 2, both TGM and BM contributed to the bend angle.

2.1.3 Upsetting mechanism

In the upsetting mechanism (UM), the workpiece shortens and thickens in the heated region, and therefore, it is also called shortening mechanism (Shen 2008). This mechanism is used for the shortening of small frames, pipe bending of various kinds of cross-sections, and aligning in micro-parts operations. The process conditions for the UM is similar to the BM, where the temperature gradient along the thickness is small. The only difference is that the workpiece is thick, and the beam diameter is less than the workpiece thickness. It makes the workpiece stiff enough to prevent the buckling. The UM occurs when thick workpiece is scanned with a slow scan speed and small beam diameter (Shi et al. 2012a). UM is illustrated in Figure 2.4.

In UM, a high temperature isotherm occurs along the workpiece thickness as shown in Figure 2.4 (a). It results in the uniform thermal expansion along the thickness. Due to uniform thermal expansion, the counter-bending does not occur. The thermal expansion is restricted by the surrounding cooler bulk material. It generates compressive thermal stresses in the heated region. The workpiece is thick and the beam diameter is small, therefore the buckling is prevented by the workpiece. When thermal stresses in the heated region exceed temperature dependent flow stress, the plastic deformation occurs. The plastic deformation is uniform and

compressive along the workpiece thickness. It results in a local shortening of the heated region, which is almost uniform along the workpiece thickness. During cooling, it results in local shortening and thickening of the workpiece in the heated region. As the workpiece is thick, a small temperature gradient is always present in the thickness direction, and therefore, the workpiece may bend a little as shown in Figure 2.4 (b) (Hu et al. 2002, Shi et al. 2006c).

Shi et al. (2012a) showed that a uniform plastic plane strain field can be obtained by simultaneously heating top and bottom surfaces with the same set of process condition. It helped to obtain a bend free deformation in the upsetting mechanism. When bending and shortening occurs simultaneously, it is called coupling mechanism (Shen 2008). In coupling mechanism, a steep temperature gradient occurs along the thickness, but the temperature at the bottom surface is high enough to generate the plastic deformation. Chakraborty et al. (2015) studied the effect of Fourier number and laser beam diameter on bend angle and increment in thickness during coupling mechanism dominated laser bending process. It was observed that the bend angle decreases and the increment in thickness increases with the increase in Fourier number, while both the bend angle and increment in thickness increases with the increase in beam diameter.

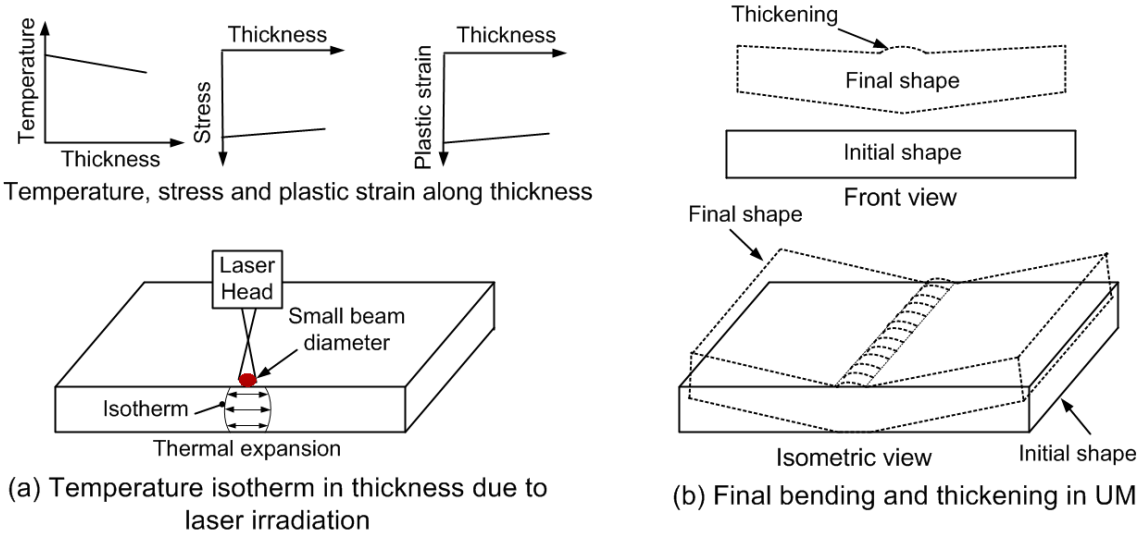

Figure 2.4. Process steps of the upsetting mechanism.

Observations

Laser bending mechanisms are the result of temperature and stress-strain distributions. In most of the research papers, the laser bending mechanisms are explained in view of deforming the metals. However, mechanisms of laser bending for plastic materials, composites, ceramics, and

laminated materials are still need to be explored. Further, the reported mechanisms explain the bending phenomenon for the single scan laser bending process. The bending mechanisms responsible for the production of large bend angles (of the order of 10º) during multi-scan laser bending and external mechanical load assisted laser bending processes are to be explored in detail.

2.2 Edge Effect in Laser Bending Process

The variation in thermal and mechanical constraints along the irradiation line results in the non-uniform bend angle from one end to another end of the irradiation line. This variation in bend angle along the irradiation line is called edge effect (Shen et al. 2010). The variation in bend angle along the scanning path as a result of edge effect is shown in Figure 2.5. The edge effect may result in different profiles along the scanning line. The edge effect occurs because the thermal and mechanical boundary constraints vary along the prescribed scanning path.

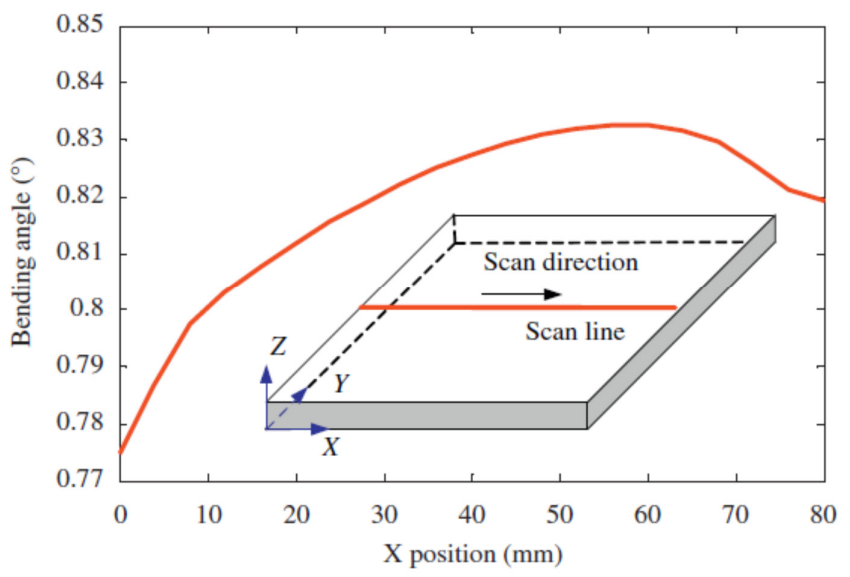

Figure 2.5. Variation in bend angle along the scanning line (edge effect). Shen et al. (2010), with permission (Appendix 2.1). Copyright © 2010, Elsevier.

Bao and Yao (2001) observed that the trends of bend angle distribution is concave (higher bend angle near the edges and lower at the middle of the scanning path) for TGM and convex for BM dominated process conditions. Jamil et al. (2011a) showed that the BM dominated process conditions produce a convex profile in the transverse direction and a concave along the scanning path. Jha et al. (2008) studied the edge effect in laser bending of AISI 304 stainless steel and found that the laser bending can render a multi-curvature along the scanning path. The multi-curvature phenomenon was found to be dependent on the scan speed.

It was reported that the extent of this effect was minimized with the use of multiple scans. Shi et al. (2013) investigated various scanning schemes to control the edge effect in multi-scan laser bending process. It was observed that the scanning schemes have a significant influence on the edge effect.

In general, the edge effect is not desirable, but in some cases it can be utilized to generate complex shapes and for alignments of sheets. A few attempts have been reported on the methods to control the edge effect. Shen et al. (2010) showed that a combination of acceleration and deceleration scanning scheme can minimize the edge effect. Hu et al. (2013) proposed two methodologies to reduce the edge effect. First method was to maintain a constant peak temperature along the scanning path, and the other method was to put an external mechanical constraint in the form of clamping at both ends of the scanning path. These methodologies significantly reduced the edge effect. Zahrani and Marasi (2013b) showed that the following parameters in order of significance directly influence the edge effect: (1) number of scans, (2) workpiece thickness, (3) scan speed, and (4) laser power. The edge effect decreases with increase in the number of scans, sheet thickness and scan speed, whilst it decreases with the decrease in the beam diameter. Safari and Farzin (2013) proposed an irradiation scheme to reduce the edge effect and multi-curvature bending phenomenon in laser bending of tailor machined blanks comprising of two different thicknesses. They investigated various scanning schemes, *viz.* equal speed method, half speed method, improved speed method and improved linear speed method to obtain uniform bend angle in laser bending of tailor machined blanks.

Review of literature also reveals the studies on the effect of material properties on the edge effect during laser bending process. Cheng and Yao (2005) found that the edge effect is influenced by the material anisotropy. The distribution of bend angle was different when laser was irradiated along the rolling direction and transverse direction of the worksheet. It was due to the variation in the strength of material along the two directions. Cheng and Yao (2001) performed numerical simulation with low carbon steel AISI 1010, and found that the bend angle slightly decreases, and then increases along the scanning path. Fan et al. (2005) found that in case of Ti–6Al–4V alloy, the bend angle first drops a little, and then increases in larger amount along the scanning path. Knupfer et al. (2012) studied the edge effect in aluminum–copper alloy (AA2024). It was reported that the bend angle first increases along the scanning line, remains constant around the middle of the scanning path, and then reduces. It was due to

increased temperature at the end of the scanning path, which reduced temperature gradient along the thickness direction.

Observations

It was noted that the edge effect affects the quality of the laser bent product. Some methodologies are proposed by the researchers to control the edge effect. These methodologies include the use of varying process conditions along the scanning line and the use of external mechanical constraints to prevent the edge effect. The use of varying scan speed along the scanning path is relatively easy to incorporate and does not need any special kind of experimental setup. However, the proposed techniques have limited scope of applications in the chosen range of process conditions, workpiece materials, and workpiece geometry. Thus, there is a need to explore the edge effect for various important materials, such as magnesium alloys, beryllium alloys and composites for a wide range of process conditions either by conducting systematic experiments or by carrying out numerical simulations using three-dimensional realistic numerical models.

2.3 Process Parameters

The laser bending process is controlled by various process parameters. These parameters can be categorized into four groups—laser parameters, workpiece material properties, workpiece geometry parameters and external constraints parameters. These are enlisted in Table 2.1. Effects of these parameters on laser bending process are discussed in the following sections.

Table 2.1. Parameters affecting the laser bending process.

S. No.	Laser Parameters	Material Properties	Geometry Parameters	External Constraint Parameters
1.	Laser power	Absorptivity	Length	Clamping
2.	Scan speed	Thermal properties	Width	Forced cooling
3.	Beam geometry	Mechanical Properties	Thickness	External mechanical load

2.3.1 Laser parameters

Important laser parameters which influence the laser bending process are laser power, scan speed and beam geometry. Generally, these parameters are used to control the process. Effects of these parameters on laser bending process are discussed below:

A. Laser power

Laser power directly controls the heat flux density of the laser beam, and the energy input into the worksheet surface. The heat flux density and energy input both increase with the increase in laser power. Shichun and Jinsong (2001), Lawrence et al. (2001) and Hsieh and Lin (2004b)

reported that in general, the bend angle increases linearly with the increase in laser power. However, further increase in laser power showed a marginal increase in the bend angle. Chen et al. (2004a) and Casamichele et al. (2007) observed that the bend angle decreases after attaining a peak value, when irradiated with slow scan speed. It may be due to melting occurred at higher laser power, and the energy is consumed into phase transformation instead of the worksheet bending. Paunoiu et al. (2008) noted that after melting, effectiveness of the process decreases with the increase in laser power. Lawrence (2002) observed that the laser bending is not possible below a certain laser power due to the reversible elastic effect or the threshold energy.

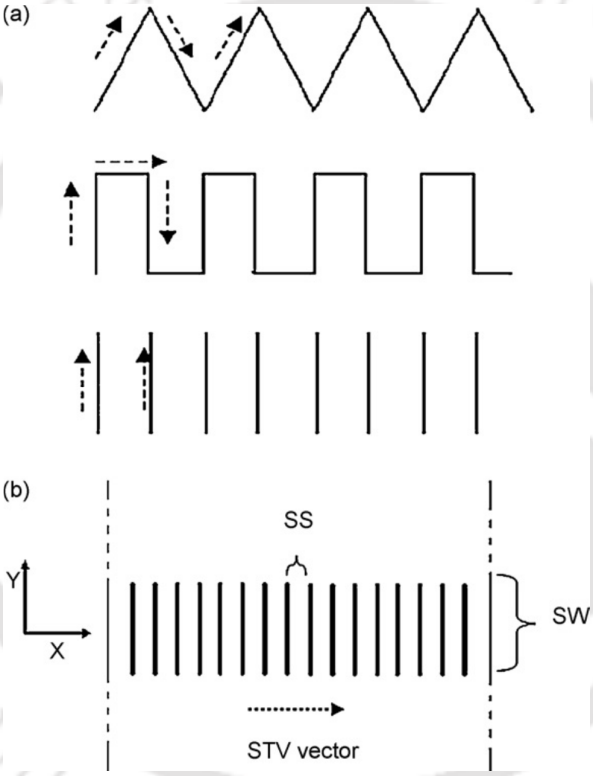

Figure 2.6. (a) Schematic of several scanning patterns: zig-zag pattern, squared pattern and stepped pattern. (b) Schematic of the step scanning patterns and its related parameters, scanning width (SW), scanning step (SS) and scanning traverse speed (STV). Vásquez-Ojeda and Ramos-Grez (2009), with permission (Appendix 2.1). Copyright © 2008, Elsevier.

Vásquez-Ojeda and Ramos-Grez (2009) worked on 60 W CO_2 laser machine with stepped scanning patterns. They used various scanning schemes using zig-zag pattern, squared pattern and stepped pattern at various scanning width (SW), scanning step (SS) and scanning traverse speed (STV). The scanning patterns are shown in Figure 2.6. The authors succeeded in obtaining large bend angle at low laser power with spatial modulation of energy and proper scanning pattern.

B. Scan speed or feed rate

The scan speed controls the heat input per unit length and the temperature gradient along the workpiece thickness (Vollertsen and Rödle 1994). The heat input per unit length decreases with the increase in scan speed as the contact time between laser beam and workpiece surface reduces. The decrease in heat input leads to the lower peak temperature and plastic deformation in the heated region, which reduces the bend angle with increase in the scan speed (Ji and Wu 1998, Kyrsanidi et al. 1999). Li and Yao (2000) investigated the effect of scan speed on bend angle by the concept of "constant peak temperature" at the upper surface of the plate. They determined various combinations of laser power and scan speed such that the peak temperature at the top surface remains constant. The bend angle decreased by 30% with 100% increase in the scan speed.

At slow scan speed, the temperature gradient increases with the increase in scan speed. When plastic deformation occurs on the bottom surface, the bend angle increases with temperature gradient (Li and Yao 2001a). Barletta et al. (2006) performed experiments on the laser bending of aluminum thin sheets, and found that the bend angle increases with the increase in scan speed at high laser power. Hu et al. (2001) found that the bend angle increases with the increase in scan speed even when the energy input is constant. It means that the bend angle is larger when workpiece is irradiated with higher laser power and faster scan speed. It is due to higher temperature gradient in the workpiece thickness. The scan speed also affects the edge effect. In general, the edge effect decreases with the increase in scan speed (Zahrani and Marasi 2013a).

Yau et al. (1998) studied the effect of line energy on bend angle. The line energy is defined as the ratio of the laser power to the scan speed. The authors observed that the bend angle varies with line energy into three ranges, *viz*. below threshold line energy where the bend angle is not produced, above threshold energy where bend angle increases linearly, and high line energy where bend angle increases marginally. It was concluded that the bend angle can be controlled by adjusting the laser power and the scan speed within the range where bend angle changes linearly with the line energy. Cheng and Lin (2000b) developed a model to obtain the bend angle as a function of line energy (P/V) using the least square estimation. The bend angle was given as

$$\alpha_b = -0.0047 + 3.7556\frac{P}{V} - 2.5968\left(\frac{P}{V}\right)^2 S^2, \tag{2.3}$$

where S is the correlation coefficient. Some other factors like beam diameter, thickness of the workpiece and length of the workpiece also affect the bend angle. Cheng and Lin (2000b) also proposed another model which computes bend angle as a function of volume energy instead of the line energy. The volume energy was defined as the ratio of the laser power and the product of scan speed, beam diameter (d) and workpiece thickness (t_s). The bend angle was given as

$$\alpha_b = 0.0121 + 2.9116\frac{P}{VDt_s} - 1.4255\left(\frac{P}{VDt_s}\right)^2 S^2 . \quad (2.4)$$

The results showed that the volume energy model was better than the line energy model for predicting the bend angle.

C. Beam geometry

Beam geometry includes total area and shape of the laser beam. In general, the laser beam has a circular shape. However, a variety of beam shapes such as line, rectangular, star, D-shape, annular, cross, etc. can be generated in a laser machine. The beam shaping can be carried out by using a mask, optical lens, beam scanners, field mappers, and beam integrators (Dickey and Holswade 2005, Shealy 2005).

The beam geometry controls the heat flux density (the ratio of laser power to the cross-sectional area of the beam). The heat flux density decreases with the increase in beam diameter. It results in the lower peak temperature, and hence less plastic deformation in the scanned region (Safdar et al. 2007). The beam diameter also controls the temperature gradient along the thickness direction. The temperature gradient decreases with the increase in beam diameter. In general, the bend angle decreases with the increase in beam diameter, but based on the dominating mechanism, it may also have the opposite effect (Chen and Xu 2001).

Safdar et al. (2006) and Sheikh and Li (2010) observed that the beam geometry provides a useful tool to control the temperature distribution, heating/cooling rates and thermal gradients. Therefore, it can be an important parameter to control and optimize the laser processing operation. Mazhukin et al. (2007) studied the effect of pulsed laser beam profiles (rectangular, triangular, Gaussian) on temperature distribution. It was observed that (1) the Gaussian and the right-angled triangular profile provides more depth of penetration, and (2) the choice of rectangular and rising triangular profile is more appropriate when the presence of the liquid phase is undesirable. Jamil et al. (2011b) studied the effect of triangular and rectangular beam geometries on TGM dominated process, and found that the beam geometry significantly controls the bend angle, edge effect, and bending edge radius.

Observations

Laser parameters are the main process controlling parameters, which have non-linear interaction among themselves and with other parameters, such as material properties and workpiece geometry. The effect of various combinations of process parameters on the performance parameters such as bend angle and edge effect was found to be difficult to generalize. Parametric studies (experimental and/or numerical) for various materials such as magnesium alloys, beryllium alloys and composites are still need to be explored. Very scant attempts have been reported on obtaining optimum laser parameters. This may be of interest to improve the productivity and product quality of the process.

2.3.2 Material properties

The laser bending is a thermo-mechanical process. The temperature distribution and stress-strain distribution are responsible for the desired process outcome. Thermal and mechanical properties of the workpiece affect the laser bending process (Shen and Vollertsen 2009). The important material properties which affect the laser bending process can be categorized in three groups: absorptivity, thermal properties and mechanical properties. These are discussed below.

A. Absorptivity

The laser energy is not completely absorbed by the workpiece surface. Some part of the energy is reflected to the surrounding. The part of laser energy absorbed by the workpiece is quantified as 'absorptivity'. Increase in absorptivity increases the energy input into the workpiece surface. Variation in absorptivity is affected by various parameters. It decreases with the increase in wavelength of the beam. Lawrence (2002) found that the diode laser is more efficient than CO_2 laser because the wavelength of diode laser is small, which enhances the absorptivity. The absorptivity also depends on the surface condition. Due to multiple reflections caused by peaks and valleys, absorptivity increases with the increase in surface roughness. In general, the metals have low absorptivity, however it increases due to the presence of rust, oxides, dust, contaminants, grease, oil or other foreign particles. The absorptivity can be increased by applying suitable coating of paint or graphite. The graphite coating is preferred due to its high absorptivity (60–80%), high melting point, low cost, and ease in application (Edwardson et al. 2006, Carey et al. 2007, Kannatey-Asibu 2009). The applied coating may react with the base material, which is not desirable in real practice (Chehrghani et al. 2012).

Dutta et al. (2013) observed that the bend angle is significantly high, when workpiece is coated with black enamel paint. They also found that the coating damages due to heat and

applying coating after each scan produces larger bend angle. Singh et al. (2013b) studied the effect of lime coating and graphite grease coating on the laser bending process. It was observed that the absorptivity can be enhanced by two and fifteen times of its value by using graphite grease and lime coating, respectively.

B. Thermal properties of material

Thermal properties control temperature distribution in the workpiece. The important thermal properties are thermal conductivity (k), heat capacity (c_p), density (ρ), and latent heat (λ). The thermal conductivity determines the heat flow into the surrounding material, and therefore, the temperature gradient and peak temperature are affected by the thermal conductivity (Bejan and Kraus 2003). The peak temperature and temperature gradient both decrease with the increase in thermal conductivity. It is due to quick heat dissipation in high conductivity material (Li and Yao 2001b, Hu et al. 2002). The increase in thermal conductivity, heat capacity, mass density, and latent heat decrease the peak temperature. This reduces the plastic deformation and bend angle (Guan et al. 2005). Shichun and Jinsong (2001) showed that the bend angle increases with a thermal effect index ($R= \alpha_{th} / \rho c_p$) in a piecewise linear fashion, where α_{th} is the coefficient of thermal expansion.

C. Mechanical properties of material

Mechanical properties of the material are responsible for the stress-strain distribution, elasto-plastic deformation and final distortion in the workpiece. The important mechanical properties which affect the laser bending process are coefficient of thermal expansion (α_{th}), yield strength (σ_y), elastic modulus (E), and Poisson's ratio (μ).

Guan et al. (2005) reported that the bend angle increases with the increase in coefficient of thermal expansion, which is due to more expansion of the heated region. It was observed that the bend angle decreases with the increase in temperature dependent yield strength and elastic modulus. Poisson's ratio determines thickening of the heated region because it is the negative ratio of transverse to axial strain (Dieter and Bacon 1988). However, there is no reported work on the study of the effect of Poisson's ratio on laser bending process.

Cheng and Yao (2005) found that the anisotropy in the mechanical properties of material decreases at higher laser power and slower scan speed. It is due to high temperature and large plastic strain, which result in the recrystallization of work surface. It was also noted that the anisotropy decreases with increase in the number of scans.

Gollo et al. (2011) defined a non-dimensional material parameter in order to quantify the mechanical and thermal characteristics of the materials. The non-dimensional material parameter (M) was given as

$$M = \frac{k\alpha_{th}\eta\sigma_y}{k_s\rho c_p}, \tag{2.5}$$

where k is the thermal conductivity of sheet, α_{th} is the coefficient of thermal expansion, η is the absorptivity, σ_y is the yield strength, k_s is the thermal conductivity of shield gas, ρ is the material density, and c_p is the specific heat. They found that the bend angle decreases with increase in the value of M.

Observations

Study on the effect of material properties is important to predict the process behavior of laser bending. Literature reports a need for the development of an efficient and cost effective surface coating technology for laser bending process to obtain precise and uniform bend angles.

2.3.3 Geometry parameters

During laser bending, the important geometry parameters to be considered are: length (perpendicular to scan direction), width (parallel to scan direction), and thickness of the worksheet. These parameters control the mechanical constraint provided by the bulk material and the heat flow into the surrounding material.

Workpiece thickness, an important geometry parameter, controls the temperature gradient along the thickness direction. Increase in the thickness leads to the change in the bending mechanism from BM to TGM. Geiger et al. (1993) reported that the bend angle is approximately inversely proportional to the square of the workpiece thickness. Lee and Lin (2002) numerically and experimentally studied the effect of worksheet thickness on bend angle, and observed that the bend angle decreases with the increase in thickness provided the peak temperature of the worksheet is below the melting point. Zahrani and Marasi (2013a) showed that the edge effect decreases with decrease in the workpiece thickness. Cheng et al. (2006a) studied the laser bending of varying thickness plate. The transition of bending mechanism was observed along the varying thickness. The bend angle was also affected by the transition of the laser bending mechanism.

The worksheet length does not have much influence on the bend angle (Chen et al. 2004a). Jha et al. (2008) reported that during the laser bending, stresses in the heated region decreases with the decrease in width of the workpiece. They stated that it could be due to more expansion along the irradiation line for lower width than that of the wider workpiece. Shichun and Jinsong (2001) conducted experimental studies on laser bending of AISI 1008 and observed that the bend angle increases with the increase in width of the worksheet. Shichun and Zhong (2002) observed from the simulation results that the counter-bending is less for wider worksheet because of the rigid-end effect. It leads to more compressive deformation in the heated region causing the increase in bend angle.

Cheng et al. (2005b) observed that the bend angle increases with the increase in width (along scanning path), provided the workpiece length is constant. This is due to the fact that the bend angle along the scanning path is non-uniform and influenced by the pre/post-bending effect. The bend angle decreases with the increase in worksheet length when worksheet width is constant. This is due to the increased heat sink effect with increasing sheet length. When both the workpiece length and width increase in the same proportion, the bend angle first increases and then decreases due to the competing effects. Shi et al. (2011) numerically and experimentally studied the effect of workpiece geometry on the bend angle along the scanning line to obtain precise bend angles. The precision in bending was found to be different for the various geometries, even when the laser parameters were kept constant. Shi et al. (2006a) studied laser bending of a plate under TGM and found that the length and width of plate have negligible effect on the bend angle, but they have significant effect on the bending radius.

Paramasivan et al. (2014) studied temperature distribution and bend angle for laser bending of an AISI 304 plate with a rectangular cut. They found that the bend angle decreases with the increase in width (along scanning line) of the cut. It is due to the reduced interaction time between the workpiece and the laser beam. However, the position and length of cut showed very less effect on the bend angle.

Observations

Geometry parameters: length, width and thickness of the worksheet affect the product quality during laser bending process. Workpiece thickness has a prominent effect in comparison with other parameters, *viz*. length and width. Literature mainly reports laser bending of the simple shapes, and scant literature is reported on the laser bending of workpiece with varying thickness and shape.

2.3.4 External constraint parameters

External constraints such as clamping, forced cooling and mechanical loading significantly affect the performance of the process. These are presented as below.

A. Clamping

Clamping is used to hold the workpiece, and it provides mechanical constraint to the workpiece bending along the scanning line. The choice of a clamping technique affects the stress distribution, bend angle and edge effect. Birnbaum et al. (2007) investigated the effect of clamping and observed that the effect of clamping depends on the distance between scanning line and the placement of the clamping. The effect of clamping on bend angle and edge effect was negligible, when it was placed at a far distance from the scanning line, while the significant effect was observed for a short distance. The bend angle and edge effect both decreased due to clamping. Hu et al. (2013) used clamping at both ends of the scanning line to control the edge effect. Shen et al. (2010) studied the effect of scan line position with respect to the edges of the workpiece. The bend angle was less when scan line was near to the edges due to lesser geometric constraint.

B. Forced cooling

Forced cooling of the workpiece affects the temperature profile which further alters the stress-strain distribution, and hence the deformation of the workpiece. Cheng and Yao (2001) found that the edge effect is reduced by the application of forced cooling. Shen et al. (2011) studied the effect of four different cooling conditions— (1) forced cooling at the top surface, (2) forced cooling at the bottom surface, (3) forced cooling at both top and bottom surfaces, and (4) no forced cooling. The forced cooling followed the laser beam by some delay of time. The use of forced cooling significantly reduced the peak temperature, but the temperature gradient did not increase along the workpiece thickness. The bend angle increased slightly when the cooling was applied either only on the top surface or on both top and bottom surfaces. The forced cooling did not increase the edge effect. Lambiase et al. (2013) studied the effect of passive water cooling to reduce the cooling time between consecutive scans. The passive water cooling was applied by partially immerging the workpiece into the stationary water. The employment of passive water cooling was found to be beneficial for the laser bending of thin sheets as significant reduction in cooling time, surface oxidation, and melting of the scanned surface was achieved. Shen et al. (2014) observed that a higher bend angle can be achieved when bottom surface of the sheet is immersed in the water during TGM laser bending of stainless steel sheets.

The water above the sheet decreased the bend angle due to decrease in the coupling energy. The water cooling also affects the heat affected zone (HAZ) significantly. Aghyad (2014) showed by FEM results that the application of forced cooling after laser scanning has insignificant effect on the final bend angle.

C. External mechanical load

The bend angle in a typical laser scan is small, and many a times, it is not sufficient for the practical applications. The use of external mechanical load with laser scanning can enhance the bend angle significantly (Dearden and Edwardson 2003). The mechanical load can be applied along with laser scan to combine the advantages of both laser bending and mechanical bending operations. It is called laser assisted bending (Alexander 2007). The presence of mechanical load in conjunction with laser scan affects the stress and plastic strain distribution in the workpiece (Schuöcker 2000).

Yanjin et al. (2003) carried out the numerical investigation on the laser bending of plates under pre-load at the free side. Results showed that the pre-load can increase the bend angle adequately, and a desired bending direction can be produced by controlling the direction and magnitude of the pre-load. Yao et al. (2007) carried out numerical investigations on the effects of various pre-load conditions on the bend angle. Four different pre-load conditions: pure compression, pure tension, pure bending towards the laser beam, and pure bending away from the laser beam were studied. The results showed that pure compression and pure bending toward the laser source increased the bend angle, whilst pure tension and pure bending away from laser source decreased the bend angle. Bammer et al. (2011) developed a laser-assisted bending system to generate a crack free large bend angle into the brittle material worksheet.

Gisario et al. (2011) studied the control of spring-back phenomenon in the bending process of aluminum sheets by hybrid bending process. The workpiece was constrained, and then pre-bent to the nominal shape and post-treated by laser to prevent the deformation of the pre-bent workpiece after release of the constraints. Shim and Kim (2011) proposed a practical method to control the effect of spring-back angle in stamped product. The appropriate laser scanning conditions were determined for the correction of spring-back angle.

Hsieh and Lin (2005) investigated the buckling mechanism dominated laser tube bending process with axial mechanical load, and found that the bend angle decreases with the increase in axial load. The bulging and the compressive stresses in the heated region were increased due to axial load. Liu et al. (2009) numerically studied the effect of pre-stresses on

the laser bending of AISI 304 stainless steel foils under buckling mechanism dominated process conditions. They reported that the bend angle and the bending direction can be controlled by changing the direction and value of the pre-stresses. Liu et al. (2010) observed the same behavior during experimental studies on AISI 304 stainless steel foils.

Observations

Literature reports a few attempts on the study of clamping and forced cooling methods on the performance of the laser bending process. However, further research can be carried out to choose suitable type of clamping and forced cooling condition for desired process performance. Some research work has also been reported on the use of concentrated and distributed stationary load along with laser beam irradiations. However, these load conditions may not be suitable for practical applications, especially for large sized sheets. Therefore, further research is envisaged to have a simple and efficient laser bending system with the assistance of mechanical load to manufacture large and precise bend angles.

2.4 Multi-Scan Laser Bending Process

In general, single laser scan produces a bend angle in the order of 0.1°–3°. Larger bend angles (of the order of 10º) can be obtained with the application of more than one laser scan. This is called multi-scan laser bending process. The bend angle increases with the number of laser scans. However, the effect of number of scans is not uniform. In general, the increment in bend angle after each laser scan decreases (Edwardson et al. 2006). The change in (1) workpiece thickness, (2) strain hardening, (3) absorptivity due to laser marking along with coating ablation, and (4) beam geometry due to workpiece bending are the important factors, which reduce the increment in bend angle after each laser scan (Edwardson et al. 2010a). The rise in temperature after each scan leads to the (1) melting of workpiece, (2) change in temperature dependent material properties, and (3) temperature gradient along thickness, which influences the effect of the subsequent laser scans (Edwardson et al. 2010b). Zahrani and Marasi (2013b) reported that in general, the edge effect decreases with the increase in the number of laser scans.

Cheng and Yao (2001) found that the cooling condition influences the laser bending process during multiple laser scans. They also observed that in multi-scan laser bending, a significant waiting time is necessary to cool down the workpiece so that a steep temperature gradient can be achieved in the next laser scan. The forced cooling after each scan can reduce the waiting time significantly. Carey et al. (2007) reported that the damage of surface coating increases with the number of scans.

Shen et al. (2007) studied the effect of overlapping of laser scans on the process performance. It was observed that the bend angle increases as the overlapping ratio decreases. Wu et al. (2010a) studied multi-scan laser bending of silicon sheets of 100 µm, 200 µm, and 300 µm thicknesses. The increment in bend angle was found to be decreased with increase in the number of scans. Griffiths et al. (2010) used FEM model to ascertain the contribution of various parameters towards the variation in bend angle per laser scan. Geometrical and absorptivity effects were found to be dominant during higher number of scans. Shi et al. (2013) numerically and experimentally studied various heating methods to reduce the edge effect in multi-scan laser bending process. Several heating methods used are shown in Figure 2.7. It was observed that the minimum edge effect can be obtained by adopting the heating method 4.

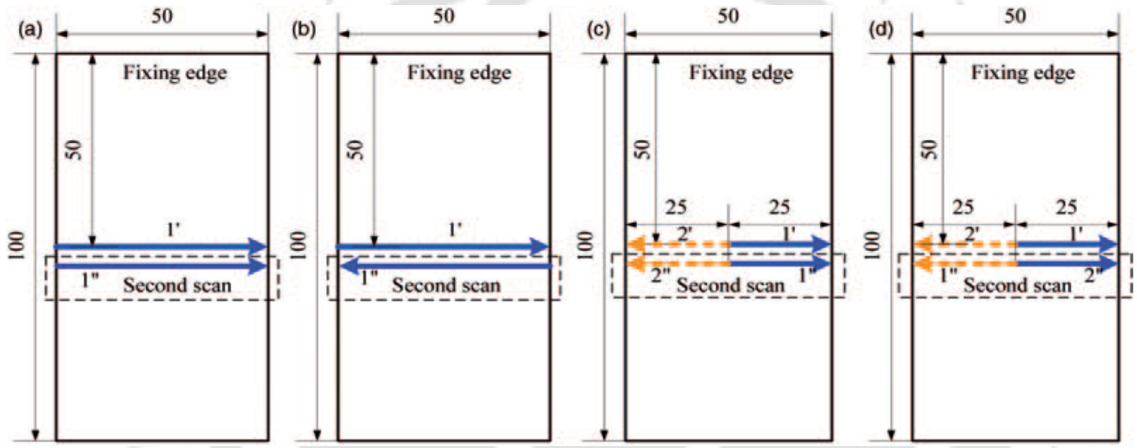

Figure 2.7. Heating methods used for multi-scan laser bending (a) scanning method 1, (b) scanning method 2, (c) scanning method 3, and (d) scanning method 4. Shi et al. (2013), with permission (Appendix 2.1). Copyright © 2013, SAGE Publications.

Observations

Multi-scan laser bending is an important method to obtain large bend angles in metal sheets. Proper selection of process parameters and cooling condition is essential for efficient and quality multi-scan laser bending process. Literature reports experimental work to study the effect of process parameters on bend angle and edge effect in multi-scan laser bending process. Numerical analysis is not yet explored systematically, which may provide better insight into the bending mechanism, bend angle and edge effect during successive laser scans. This can also help in the selection of proper process parameters for an efficient laser bending process.

2.5 Curvilinear Laser Bending Process

The straight line irradiation is generally used to produce simple parts, where bending is required about the scanning line axis. In many cases, parts have complex or spatially curved geometry

such as spherical dome or ship hull, which are difficult to manufacture with straight line irradiation. In those cases, the use of curved irradiations is more convenient and efficient as compared to the straight line irradiation. The laser bending with curved irradiation is called curvilinear laser bending process. Laser irradiation path significantly affects the temperature distribution and the deformation behavior. Chen et al. (2002) numerically and experimentally studied the curvilinear laser bending of titanium alloy sheets and found that the bend angle decreases with the increase in scanning path curvature. Chen et al. (2004a) experimentally studied the curvilinear laser bending of Ti–6Al–4V alloy. They reported that the curvilinear irradiation produces less bend angle and the bend angle decreases with the increase in scanning path curvature. It may be because the thermal stresses produce three-dimensional deformation instead of bend angle in the sheet and the proportion of stresses responsible for the sheet bending decreases with the increase in scanning path curvature.

Hennige (2000) investigated the differences in the forming behavior of sheet metal parts using straight and curved irradiations. Various irradiation strategies were studied to generate the spherical dome shapes. It was found that the bend angle significantly reduces in case of ring and circle irradiations as compared to linear irradiations. It was suggested that a combination of radial and concentric irradiation lines can be used for spherical structures. The concentric lines were used for stabilizing the initial flat plate against wrinkling. Chen et al. (2004b) studied the deformation behavior of laser curve bending of sheet and found that the deformation occurs only on one side of the scanning path along which the rigid constraint is relatively lower. The sheet was extended and slightly thinned on the relatively smaller side of irradiation paths. Zhang et al. (2007) showed that the peak temperature and warping increases with the increase in scanning path curvature. Zhang et al. (2009) investigated the deformation behavior of laser forming of ring shaped sheet metal. The results showed that the forming process fluctuates continuously, and the sheet edge is warped because of the rigid-ends effect. They also found that the warped curvature increased with the beam diameter. Venkadeshwaran et al. (2010) studied the deformation of a circular plate subjected to a circular scanning path. The discrete section heating in symmetry with shifting of the starting point in subsequent scans reduced the undesired waviness.

Observations

Curvilinear laser bending can be used to generate complex shapes. However, limited knowledge is available on the effect of scanning path curvature on temperature distribution,

stress-strain distribution, and distortions. It is important to investigate these aspects for practical applications of the curvilinear laser bending process.

2.6 Materials Processed by Laser Bending Process

The laser bending process can be applied to a wide range of materials including metals, non-metals, composites, plastics and ceramics. Researchers studied laser bending of various materials useful to the manufacturing industry, such as low or high carbon steel, high strength steel, stainless steel, aluminum alloys, titanium alloys nickel alloy, plastics. Table 2.2 summarizes the studies carried out in the laser bending.

With the recent developments in computer hardware and advanced simulation software, a number of researchers used numerical methods as a tool to simulate the laser bending of various materials such as metals, metal–matrix composite and non-metals (Cheng and Lin 2001, Chan and Liang 2001, Hu et al. 2001, Hu et al. 2002, Shichun and Zhong 2002, Zhang et al. 2002, Zhang et al. 2004, Zhang and Michaleris 2004, Hsieh and Lin 2004a, Liu et al. 2007). Chan and Liang (2000a) studied the deformation behavior of Al6013/SiC_p aluminium matrix composite sheets during the laser bending process. A smaller bend angle was obtained when the laser scanning direction was parallel to the rolling direction of the sheet in comparison with that obtained during transverse scanning to the rolling direction. Similar results were obtained by Chan and Liang (2000b) for two aluminium based metal matrix composites, *viz.* Al2009/20 vol% SiC_w and Al2009/20 vol% SiC_p. Chan and Liang (2001) studied the influence of reinforcement with 15% and 20% volume fraction of SiC particles on the coefficient of thermal expansion and bend angle on two metal-matrix composites (Al2024/15SiC_p and Al2024/20SiC_p).

Brittle materials such as ceramics and the materials with low formability, *viz*. aluminum oxide, glass, cast iron are difficult to form with conventional tools and dies since cracks may generate on the worksheet during the mechanical bending operation. The brittle materials like single crystal silicon, mono-crystalline silicon, borosilicate glass, aluminum oxide Al_2O_3, silicon, etc. have been deformed by researchers using laser bending process (Wu et al. 2010a,b). Okamoto et al. (2004) investigated the bending of plastic specimen with the Nd:YAG laser beam. Zhang et al. (2004) used low power lasers, including the continuous wave (CW) CO_2 laser, the Nd:YAG laser with a nanosecond pulse width and the fiber laser, to study the bending behaviors of ceramic, silicon and glass. They found that the bend angle over 1° can be obtained with higher laser power and multiple scans. Wang et al. (2011) studied laser bending of a single

Table 2.2. Summary of selected studies on the laser bending of various materials.

Reference	Material	Specimen size (mm)	Remarks
Akinlabi et al. 2014	Mild steel	200×50×3	It was observed that the number of scans, scan speed, laser power, beam diameter and cooling effect has a contribution of 32%, 27%, 21%, 18% and 2% respectively on the bend angle.
Kgomari and Mbaya 2010	High strength steel (A715)	3.5 mm thickness	A correlation was developed between microstructure and mechanical properties for both laser and mechanical forming.
Chen et al. 1999	Stainless steel AISI 301	10×0.8×0.1	Using a beam expander, a line shape laser beam was used to bend the worksheet.
Gisario et al. 2011	Aluminum alloy, AA 6082 T6	19×69×2	Spring-back control was investigated for the laser assisted bending process.
Chen et al. 2002	Titanium alloys, Ti – 6Al – 4V	50×40×1	Effect of scanning path curvature on the laser bending process was investigated.
Akinlabi 2013		90×30×1	Titanium alloy was successfully bent.
Okamoto et al. 2004	Plastics, high density polyethylene	20×5×1	Deformation mechanism of the plastic material was studied under the laser bending process.
Wu et al. 2010a	Silicon Sheet	20×5×0.1–0.3	A large bend up to 40° was produced.
Wu et al. 2010b	borosilicate glass and Al_2O_3	10–20×3–20×0.15	It was observed that an elevated substrate temperature needs to be applied to prevent the brittle fracture. The glass cannot be bent with Nd:YAG laser.
Chan and Liang 2000b	Al6013/SiC_p aluminium matrix	10 mm width, 0.32 mm thickness	Studied the effect of reinforcement on bend angle.
Shen et al. 2009	metal/ceramic bilayer	50×37.5×0.6	Numerically studied laser bending of the metal/ceramic bilayer material.
Carey et al. 2007	Fibre metal laminates	100×100×0.15	Studied the effect of various parameters on the laser bending of glass fibre based fibre metal laminates.

Size is given in the order as length×width×thickness (mm)

crystal silicon sheet of 0.2 mm thickness with the Nd:YAG laser. The mechanism of pulsed laser bending of thin silicon sheet was a hybrid mechanism of TGM and BM. A bend angle of up to 6.5º was achieved in silicon sheets with six laser scans. Xu et al. (2013) investigated the laser bending of the silicon sheet. They studied the bending mechanism of the brittle materials. It was observed that when the temperature is higher than the brittle–ductile transition threshold, the plastic deformation takes place and the sheet bends permanently.

Chen et al. (1998) produced deformation in the stainless steel and ceramic specimens with a precision of the order of tens of nanometers using a pulsed laser beam. The authors suggested that the process is suitable for removing distortions on magnetic head components to achieve a better contact between the magnetic disk head and the hard disk surface. Tam et al. (2001) used laser micro-bending process for fine adjustment of the bearing surface curvature of ceramic magnetic sliders. Zhang et al. (2001) studied the micro-scale bending of ceramic, silicon, and stainless steel samples using pulsed and continuous wave (CW) lasers. They observed that for similar stress affected zone, the CW laser produced more bending than the pulsed laser. However, the pulsed laser caused less surface composition change and thermo-mechanical damage to the specimens in comparison with that obtained for CW laser. In addition, the bend angle becomes larger with the increase in number of laser scans, once the temperature gradient in the scanning area is large enough. Matsushita (2003) used laser micro-bending technology for roll and pitch angle adjustment of the magnetic head suspension and air bearing surface adjustment of the magnetic head slider. Zhang and Xu (2005b) described a laser forming based technique to adjust curvatures of silicon micro-cantilevers used for chemical and biological detection. They were successful to adjust the curvatures by an amount of 3.5 μrad in cantilevers of dimension of length 110 μm, width 13 μm and thickness 0.6 μm. Ming et al. (2010) described the manufacturing of metallic micro-structures using lasers. Micro grid array structures were replicated on a metallic foil surface with high spatial resolution at micron levels.

Observations

A number of materials including metal, non-metals, ceramics and composites are successfully bent by laser irradiations. However, some important materials including magnesium alloys, beryllium alloys, composites, corrugated structures, functionally graded materials, smart materials and plastics are not investigated for the laser bending process. These are to be explored in detail by carrying out numerical as well as experimental investigations.

2.7 Lasers Used in Bending

As already discussed, the lasers are extensively used to deform a wide range of materials. A variety of lasers are employed by the researchers for the same. Table 2.3 summarizes types of lasers employed in bending of the various materials.

Table 2.3. Lasers used by researchers to bend the workpiece.

Reference	Laser used	Specifications	Workpiece	Remarks
Wu et al. 2010	Nd-YAG	millisecond pulse width Nd:YAG laser	Silicon sheet	Large bend angle up to 40° was produced in the brittle material.
Akinlabi 2013		Diode-Pumped 4.4 kW Nd: YAG laser	Ti6Al4V sheet	Titanium alloy was successfully bent with laser.
Dearden et al. 2003		Lamp-pumped Nd:YAG, Q-switched, maximum power of 47 W, *f*= 2kHz	Mild steel sheet	3-D complex shaped were generated.
Chen et al. 1999	Nd-YLF	10 ns, Pulsed, λ=1.047 μm,	Full-hard 301 stainless steels	Line shaped pulsed laser was used to bend the worksheet.
Naeini et al. 2007	CO_2	P_m=200 W, 3 DOF with CNC controller	ST37 steel sheet of 1–2 mm thickness	Studied the effect of sheet thickness, laser power, beam diameter, scan speed and sheet width on the bend angle.
Safari et al. 2013		CW, P_m=2 kW	Mild steel	Laser bending of tailor machined blanks was studied.
Lambiase et al. 2013	Diode laser	P_m=1.055 kW,	Stainless steel 304	Effect of the passive water cooling was studied.
Shen et al. 2014	Fiber laser	Pulsed laser, λ=1.07 μm	Stainless steel	Underwater pulsed laser bending of the stainless steel was studied.
Chen et al. 2008		CW, P_m=160 W, λ=0.94 μm,	cold-rolled grade 1008–1012 steel	TGM and BM laser bending was studied for the multi-path and multi-scan irradiations.
Maji et al. 2014		Yb fiber laser, CW, P_m=2 kW, λ=1.07 μm, 5-axes CNC	AISI 304 sheet	Dome shapes were generated.
Chen and Xu 2001	Argon ion laser	CW, P_m=4 W, λ=0.488 μm	full-hard 301 thin sheet	It was observed that the repeatability in the bend angle is good for the process conditions leading to the sheet bending without surface melting.

***T_P*=laser pulse width, λ=wavelength, CW=continuous wave, P_m=Maximum power, DOF=Degree of freedom, CNC=computer numerical control, *f*=frequency**

2.8 Effect on Mechanical and Micro-structural Properties

Laser scanning generates high temperature and localized deformation in the heated region due to which strain hardening, dynamic recrystallization, and phase transformation occur in the material. This changes mechanical and metallurgical properties of the heated region. Literature depicts studies on the effect of process parameters on micro-structural and mechanical properties of the laser deformed workpiece.

2.8.1 Studies on microstructural properties

Literature reveals a number of attempts on the microstructural studies during laser forming of the workpiece. Hu et al. (2001) analyzed the surface of the laser irradiated stainless steel plate and observed that the laser does not adversely affect the microstructure, and does not produce any cracks or porosity in the plate. The recrystallized grain size and the orientations of the grain were quite different from the base material. However, the authors expressed the possibility of a few scattered micro-cracks on the laser scanned surface, which may be associated with high cooling rate (Yilbas et al. 2012). Paunoiu et al. (2008) observed that the microstructure of stainless steel AISI 304 is affected by the laser beam. The annealing twins were appeared on the concave side of the laser scanned specimen. The annealing twins, density of the annealing twins, and the depth of their penetration increased with laser power. Yang et al. (2010) found that the overlapping of two laser pulses affect the interaction time between laser and material. It was noted that when the overlapping exist, the case-hardening of the heat affected zone occurs. Hardness and anti-corrosion properties were found to be increased in the irradiated zones.

Bartkowiak (2004) studied laser forming of Ti-6Al-4V sheets using continuous wave and pulsed Nd:YAG lasers, and found that the depth of the oxidation zone increases with the number of scans. They also found that the depth of heat affected zone after 15 and 30 scans was about double in the pulsed laser system as compared to that in continuous wave mode. Chen et al. (2004a) analyzed the microstructures of laser irradiated Ti–6Al–4V alloy and did not observe any obvious difference compared to the microstructure of the original material. The scanning at high laser energy density separated out the α-phase from β-grain boundaries, and therefore, β-grain size was increased. Fan et al. (2007) studied phase transformations in heat affected zone of AISI 1010 stainless steel. The grains were distinctly refined due to the phase transformation and recrystallization in the heat affected zone. After irradiation, a substantial amount of martensite was formed due to the high cooling rate.

Topić et al. (2007) observed that the residual strains vary in both the transverse (tensile in nature) and the longitudinal (compressive in nature) directions of the scanning path. Martensite phase transformation occurred due to rapid heating and cooling of the irradiated region. Grain refinement was observed at approximately 1.5 mm below the surface irradiated by the laser beam. Singh et al. (2013a) studied the microstructure of multi-scan laser bent mild steel. They observed that the average grain size in scanned region gradually decreased from the bottom to the top surface. The micro-structures at the top and the bottom surfaces are shown in Figure 2.8 (a) and Figure 2.8 (b). The reformation from coarse grain to fine grain was more at the top surface in comparison to that at the bottom surface. It was due to higher temperature and higher strain hardening at the top surface.

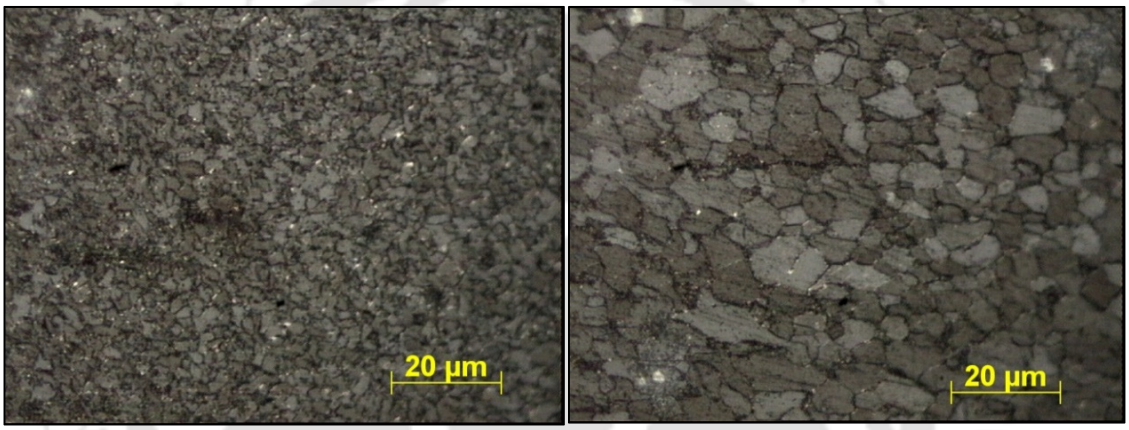

(a) (b)

Figure 2.8. Micro-structure after 20 laser scans (Laser power 400 W, Scan speed 300 mm/min) (a) at top surface, (b) at bottom surface (with e-mail consent of the author, Copyright © Singh et al. 2013a).

2.8.2 Studies on mechanical properties

Laser bending process involves strain hardening, compressive and tensile deformations, and generation of residual stresses in the heated region. These factors affect the mechanical properties like tensile strength, fatigue strength, hardness and ductility of the material (Merklein et al. 2001).

McGrath and Hughes (2007) reported that the fatigue life of workpiece materials enhanced after laser scanning. The endurance limit of the laser bent specimen was also increased. It was due to laser-hardening mechanism and compressive residual stresses induced due to laser beam irradiations. Thomson and Pridham (2001) studied the effects of laser scanning on the material properties of the mild steel. They found that the performance of laser formed parts was good. Due to laser scanning, the strength of the scanned region increased, the

ductility decreased and strain ageing apparently increased in laser forming of mild steel. Shen and Yao (2009) studied tensile behavior of laser bent low carbon steel workpiece, and observed improvements in the yield strength and tensile strength but reduction in the total elongation. Walczyk and Vittal (2000) studied material properties of laser bent titanium sheets and observed that the fracture toughness and fatigue strength of titanium deteriorates due to laser forming.

Singh et al. (2013a) carried out a 3-point flexure test on laser bent specimen. The flexural stiffness of laser bent specimen was more as compared to mechanically bent workpiece. It was found that the Young's modulus of elasticity was same for both the laser bent and mechanically bent workpiece, but the elasto-plastic stiffness of laser bent workpiece was more than that of the mechanically bent workpiece. Cheng and Yao (2001) observed that the intermediate cooling between laser scans moderately decreased the ductility of stainless steel. It was due to application of repeated work hardening cycles after respective softening of the work material. The hardening occurred due to plastic deformation and softening occurred because of recovery and recrystallization accompanied by each laser scan.

Majumdar et al. (2004) studied laser bending of AISI 304 stainless steel sheets and observed that the micro-hardness of the irradiated zone is increased by 1.5 to 2 times as a result of grain refinement. Fan et al. (2007) bent AISI 1010 stainless steel and noted that the micro-hardness decreases along the thickness of laser bent specimen. The hardness was influenced by both phase constitution and work hardening. Due to high cooling rate, a substantial amount of martensite formed at the top surface leading to high hardness. Kgomari and Mbaya (2010) compared the laser treated and mechanically formed high strength low alloy steels. It was observed that the phase changes from a fine-grain ferrite to predominantly coarse-grain ferrite at the laser scanned surface, and therefore, the hardness decreases significantly. Singh et al. (2013a) studied laser bending of mild steel sheet and found that the hardness increased with laser power due to higher peak temperature.

Carey et al. (2010) investigated the use of laser forming to shape thermosetting glass fibre based fibre metal laminates. It was found that TGM is the only mechanism which gives an out-of-plane bend without considerable damage to the laminate. BM dominated process parameters caused the delamination of the structure and the heat damage to the composite layer. UM could not be produced in fibre metal laminates.

Observations

The laser bending process involves localized high temperature and plastic deformation which significantly affect the mechanical and microstructural properties. Variation in these properties depends on process conditions and the type of workpiece material. Investigation on these properties is important to assess the feasibility of application of laser bending for various materials.

2.9 Process Modeling of Laser Bending Process

Experimental studies on the laser bending process are costly, time consuming, and limited to the available facilities. Physics based numerical and analytical studies can help to study the laser bending process at faster rate, and can predict the deformation for a wide range of process conditions. Literature reports a significant work on the numerical as well as analytical modeling the laser bending process. A review of various models reported in the literature is presented in the following sections.

2.9.1 Analytical models

Researchers developed various analytical models to predict the bend angle, temperature distribution and stress distribution in the workpiece. The analytical modeling of the laser forming process involves transient non-linear governing differential equations and boundary conditions. The non-linearity arises due to the factors, such as temperature dependent material properties, kinematic non-linearity, and the non-linearity of thermal boundary conditions. A brief review of analytical modeling of the laser bending process is presented in this section.

Vollertsen and Rödel (1994) developed a residual stress based model to calculate the bend angle. In the case, when plasticized zone is smaller than the sheet thickness (*i.e.* fast scan speed, thick worksheet and low thermal conductivity), the bend angle was given as

$$\alpha_b = \frac{\varepsilon_{\max} l t_1}{t_s^3}\left(3\pi t_s - 8t_1\right), \tag{2.6}$$

and for the other case, when plasticized zone is larger than the sheet thickness, which occurs when scan speed is slow and thermal conductivity is high, the bend angle was given as

$$\alpha_b = \frac{\varepsilon_{\max} l}{t_1 t_s^3}\left(6V^2\sqrt{t_1^2 - t_s^2} + 6t_s t_1^2 \arcsin\frac{t_s}{t_1} + 4\left(t_1^2 - t_s^2\right)^{3/2} - 4t_1^3\right), \tag{2.7}$$

where α_b is the bend angle, ε_{max} is the maximum plastic strain at the heated surface, l is the half length of the plasticized zone, t_s is the sheet thickness and t_1 is the depth of plastic zone.

Vollertsen (1994) derived an expression for the bend angle in TGM. The analytical expression is given by,

$$\alpha_b = \frac{3\alpha_{th} P\eta}{\rho c_p V t_s^2}, \tag{2.8}$$

where α_{th} is the coefficient of thermal expansion of the work piece, P is the laser power, η is the absorptivity, ρ is the density, c_p is the specific heat capacity, V is the scan speed and t_s is the sheet thickness. Magee et al. (1997) modified the Equation (2.8) for metal matrix composites by multiplying with a constant on the right hand side. The value of constant was 0.5 at slow scan speed and it was decreased linearly with the increase in scan speed.

Vollertsen's models did not include the effect of yield stress and Young's modulus of elasticity of worksheet material. Yau et al. (1998) included this effect in their model. The bend angle is given by,

$$\alpha_b = \frac{21\alpha_{th} P\eta}{2\rho c_p V t_s^2} - \frac{36 l\sigma_y}{hE}, \tag{2.9}$$

where E is the Young's modulus and σ_y is the yield stress.

Kyrsanidi et al. (2000) considered non-uniform temperature distribution throughout the thickness of the plate and applied the concept of basic mechanics of materials. Their model, although computationally efficient, requires programming and includes iterative steps. Cheng et al. (2006a) proposed analytical model for plate with varying thickness. The bend angle of the plate at the location with thickness, $t_s(x)$, is,

$$\alpha_b = b(1-\mu^2)\varepsilon_{\max}\left(\frac{3f(x)\pi}{2t_s^2(x)} - \frac{4f^2(x)}{t_s^3(x)}\right), \tag{2.10}$$

where

$$b = c_1\sqrt{P/V}, \tag{2.11}$$

and

$$f = c_2 P/(Vt_s), \tag{2.12}$$

where c_1 and c_2 are constants dependent on materials properties, $t_s(x)$ is the thickness of the sheet and μ is the Poisson's ratio. In Equation (2.10), $\varepsilon_{\max}$ is the maximum plastic strain at the heated surface. It is given by,

$$\varepsilon_{\max} = \alpha_{th} T_{\max} - \sigma_y / E \ , \tag{2.13}$$

where $T_{\max}$ is the maximum temperature attained.

The model of Shen et al. (2006c) is based on the assumption that the plastic deformation is generated only during heating, while during cooling the plate undergoes only elastic deformation. According to this model, the bend angle is given by,

$$\alpha_b = \left[4\beta_v + \frac{12 s \sigma_y}{E} \frac{2 a_p R}{t_s (t_s - a_p)} \right] \frac{t_s a_p}{(t_s - a_p)^2} , \tag{2.14}$$

where β_v is the bend angle provided by Equation (2.8), R is the laser beam radius, s is the reduction coefficient to account for the variation of yield strength and Young's modulus of elasticity with temperature and a_p is the characteristic length of the plastic zone. The constants s and a_p need to be evaluated empirically, which is a limitation of this model. The model is valid for TGM as well as BM.

Lambiase (2012) proposed an expression for the bend angle based on assumption of elastic-bending theory without considering the plastic deformation during heating and cooling phases. The bend angle is given by,

$$\alpha_b = \frac{3\eta P (t_s - t_1) \alpha_{th}}{\rho v c_p t_s (t_s^2 - 3 t_s t_1 + 3 t_1)} , \tag{2.15}$$

where t_s is the sheet thickness and t_1 is the thickness of heated volume, which is invariably estimated empirically. Lambias and Ilio (2013) developed a more rigorous analytical model to predict the deformation of thin sheets.

Kraus (1997) provided a closed–form expression for estimating the bend angle during upsetting mechanism. The bend angle is expressed as

$$\alpha_b = \frac{4\eta l P \alpha_{th}}{\rho c_p V (2 D t_s - t_s^{\,2})} - \frac{\sigma D}{E} , \tag{2.16}$$

where D is the beam diameter.

Shi et al. (2007a) provided a model for estimating the bend angle in an in-plane axis perpendicular to the scan direction. The bend angle is given by,

$$\alpha_e = \frac{6.92 \eta P \alpha_{th} W R^{1/2}}{\pi^{3/2} L^2 t_s \left(\rho c k V \right)^{1/2}} , \tag{2.17}$$

where W and L are the width and length of worksheet respectively, k is the thermal conductivity. Hu et al. (2013) expressed a model as a function of laser parameters, worksheet material parameters and worksheet geometry parameters to calculate the bend angle between various points on the scan line (edge effect).

Vollertsen et al. (1995) derived an expression for estimating the bend angle in buckling mechanism dominated process conditions, *i.e.* for bending of thin worksheets with high ratio of thermal conductivity to worksheet thickness. The proposed analytical model was dependent on important influencing parameters such as worksheet thickness (t_s), absorptivity (η), laser power (P), scan speed (V), coefficient of thermal expansion (α_{th}), specific heat (c), density (ρ), elastic modulus (E) and temperature dependent flow stress (σ_y). The expression is given as

$$\alpha_b = \left[36 \frac{\alpha_{th}\sigma_y}{c\rho E} \frac{\eta P}{V} \frac{1}{t_s^2} \right]^{1/3}. \tag{2.18}$$

Cheng et al. (2005b) introduced an another analytic model to capture the effects of change in width and length dimensions of the sheet,

$$\alpha_b = \frac{3 l_h \alpha_{th} \Delta T}{2 t_s}, \tag{2.19}$$

where l_h is the width of heated zone, ΔT is the temperature rise in the heated region.

Liu et al. (2005) introduced analytical model for laser bending of metal matrix composites. The model is given as

$$\alpha_b = \frac{9(1-2\mu_m)\eta A P \alpha_{th}}{\rho_m c_m V t_s^2} \frac{b + (c-b)V_p}{[b + (e-b)V_p][1 + (d-1)V_p]}, \tag{2.20}$$

where $b = \frac{1-2\nu_p}{1-2\nu_m}$, $c = \frac{\alpha_{thp} K_p}{\alpha_{thm} K_m}$, $d = \frac{\rho_p c_p}{\rho_m c_m}$, $d = \frac{E_p}{E_m}$ are the dimensionless quantities, A is a correction factor for energy dissipation and counter-bending effect, K is the bulk modulus. The indices m and p mean the corresponding quantity belongs to the matrix and particle, respectively.

Several other analytical models have also been proposed. Cheng and Lin (2001) considered that the final bend angle is a sum of angle induced during heating and cooling

cycles. The bend angle during heating process was assumed to be a function of the temperature distribution at the moment when the highest temperature was achieved, while the bend angle during cooling process was assumed to be a function of the surrounding temperature. McBride et al. (2004, 2005) presented an analytical model to describe the local curvature in terms of the interaction time and area energy induced. This model was used for the iterative laser forming of non-developable surfaces. Ueda et al. (2005) measured temperatures at both top and bottom surfaces using two color pyrometers with an optical fiber to determine the relationships between bend angle and beam diameter, surface temperature and sheet thickness. Shen et al. (2008) developed an analytical model based on force and moment balancing to predict the bend angle in metal/ceramic bi-layer material system of laser forming. Gollo et al. (2008) derived formulae based on laser process parameters using regression analysis to predict the bend angle. Gollo et al. (2011) developed a relationship based on the sheet thickness, material properties and laser parameters including the number of scans to predict the bend angle. Recently, Eideh et al. (2015) developed an analytical model based on the elastic-plastic bending of sheet to evaluate the bend angle in laser bending of metal sheets.

Several models are developed to find out the temperature distribution during laser bending process. Cheng and Lin (2000a) proposed a model to calculate the temperature field induced by laser scanning. Shi et al. (2007b) derived a simple analytical model to calculate the temperature distribution in the workpiece. They explored similarity of temperature distributions about the scan line axis during laser forming of sheets. Chen et al. (2010) proposed an analytical model to calculate the temperature distribution based on the similarity of temperatures at different thicknesses. Based upon the proposed temperature model, they developed an analytical model for the estimation of bend angle as a function of laser process parameters and dimensions of the plate.

The accuracy of the closed form expressions to predict the laser bending is not high. It typically ranges from 10 to 50%. Moreover, the closed form expressions provide limited information. Several FEM methods have been proposed to get better accuracy and deeper insight into the process. The important studies on numerical modeling of the laser bending process are presented in the following subsection.

2.9.2 Numerical models

As the development of high speed processing computers and user friendly solvers has increased the computational efficiency, the numerical simulations have been performed in order to

improve the fundamental knowledge of the process. Vollertsen et al. (1993) obtained the temperature distribution and bend angle using finite difference method (FDM) and finite element method (FEM). However, the models have limited applicability due to non-availability of the temperature dependent material properties. Holzer et al. (1994) conducted the FEM simulation of buckling mechanism using ABAQUS. Ji and Wu (1998) carried out FEM analysis of transient temperature field produced in the laser bending process. Kyrsanidi et al. (1999) numerically simulated the laser bending process to generate a sine shape from a flat workpiece. Hu et al. (2001, 2002) carried out computer simulation and on-line experimental investigation for laser bending of the workpiece. Hsieh (2004a) investigated the vibration phenomenon during pulsed laser bending of thin metal plates. Shen et al. (2006a, b) developed an FEM model for two parallel laser beams scanning over the workpiece. Shi et al. (2007a) predicted the temperature field by using a three-dimensional FEM model. They considered temperature dependent thermal properties of the workpiece. Liu et al. (2007) developed a numerical model for laser forming of aluminum matrix composites with different volume fractions of reinforcement. Shen et al. (2009) used FEM to investigate the laser bending for metal/ceramic bi-layer materials.

Many researchers worked on the improvement of the numerical models. Shichun and Jinsong (2001) introduced weight coefficients to handle the transition from elastic zone to plastic zone in an element of FEM. Zhang and Michaleris (2004) compared 3-D Eulerian and Lagrangian approaches of FEM formulation. It was found that the Eulerian approach takes lesser time than the Lagrangian approach in the prediction of bend angle. However, the results of Lagrangian approach were in better agreement with the experimental results. Cheng and Yao (2005) incorporated the material anisotropy in the FEM model. Fan et al. (2005) developed thermal–microstructural–mechanical numerical model for the laser bending of Ti–6Al–4V alloy. They incorporated the effect of phase transformations by considering phase transformation kinetics. The flow stress was predicted by the rule of mixtures. Liu et al. (2008) developed an FEM model integrated with a multi-particle cell model to examine the effect of particle spatial distributions on deformation behavior of a composite in laser bending. Sowdari and Majumdar (2010) developed an enthalpy based computational model to analyze the temperature distribution, solid-liquid interface location, and shape and size of the molten pool. Numerical models considering the strain rate and temperature effects usually give unsatisfactory results, when applied to the multi-scan laser bending operations. This is mainly due to the inadequate constitutive models employed to describe the hot deformation behavior.

Cheng and Yao (2002) developed a numerical model by considering the effects of microstructural change on the flow stress in multi-scan laser forming of low carbon steel. Incorporation of the effect of microstructural change on the flow stress increased the accuracy of the developed numerical model.

Various efforts have been put to reduce the computational time for simulations of the large workpiece. Yu et al. (2001) adopted a rezoning technique to reduce the simulation time. They studied the effects of mesh refinement on the temperature distribution and final distortion. Zhang et al. (2004) studied the effects of temporal and spatial discretization and mesh density on angular distortion to reduce the computational time. It was concluded that to obtain an accurate solution, the temporal discretization requires at least four time increments to pass through the beam radius and the spatial discretization requires at least two elements per beam radius and three elements along the workpiece thickness. Reutzel et al. (2006) developed a computationally efficient method based on the concept of differential geometry to analyze the thermal forming process. The developed numerical model was reasonably accurate and provided the errors less than 12%. The computational efficiency was found to be improved and the computational time was reduced by about 99.9%. Shi et al. (2006b) derived similarity theory to predict the temperature field and deformation behavior of much larger plates through the analysis of much smaller ones. Pitz et al. (2010) introduced the moving mesh approach to save the computational time. Hu et al. (2012) developed a simple, robust and accurate FEM model using multi-layered shell elements. This intelligent mesh reduced the number of elements which increased the simulation efficiency significantly. The model could predict the laser bending process with good accuracy and was suitable for the simulation of the large workpiece. Eideh (2014) showed by FEM results that the cooling rate after completion of the laser scan has insignificant effect on the final bend angle. Therefore, it is a good idea to apply forced cooling on the workpiece after laser beam irradiation for the numerical analysis of the process. It reduces the simulation time.

The numerical simulations offered satisfactory results in terms of temperature, stress, strain and displacement distributions. However, advanced analysis is required for laser bending to be a viable process for rapid prototyping, shape correction and micro-adjustment as FEM simulation takes several hours. The numerical simulations are not suitable for the online optimization and control (Kyrsanidi et al. 2000). Researchers developed some soft-computing models to overcome long simulation time of numerical models and poor predictability of the mathematical models.

2.9.3 Soft-computing models

Numerical models proved to be time and CPU memory consuming. Thus, they pose the disadvantage of high computational cost. On the other hand, the analytical models have been difficult and unsatisfactory. They require tedious and complex calculations. In this scenario, the soft computing can play an important role to predict the bend angle with certain parameters.

Cheng and Lin (2000b) used three supervised artificial neural networks (ANN), *viz.* two back propagation neural network with hyperbolic tangent function and logistic function respectively, and one radial basis function neural network to estimate the bend angles. Inputs to these neural networks were beam diameter, scan speed, laser power and workpiece geometries (thickness and length). Verification results showed that the radial basis function neural network model was superior in predicting the bend angle. Dragos et al. (2000) showed that the neural network is an excellent tool to improve automated manufacturing control and it can be used for on-line simulations in order to support an automatically controlled laser bending process. Casalino and Ludovico (2002) developed an ANN model to predict the bend angle and process conditions for TGM and BM dominated laser bending of sheets.

Barletta et al. (2009) developed an artificial neural network model to control the spring-back effect in laser assisted bending process. Gisario et al. (2011) used neural network solutions to predict, control and manage the spring-back in V-shaping of thin aluminum sheets. Maji et al. (2014a) developed neural networks and neuro-fuzzy system for pulsed laser bending of workpiece to establish the relationships between bend angle and process parameter. They adopted an inverse approach to determine the process parameters in order to achieve desired outputs. The bend angle and pulse duration were taken as inputs and laser power, scan speed and beam diameter were the outputs. The model was able to predict the process parameters for the desired bend angle. Maji et al. (2014b) developed neural network models to predict the dome height and the process parameters for obtaining a particular dome height for laser forming process.

Cheng and Yao (2004a) developed a genetic algorithm (GA) based methodology to determine the optimal process conditions during laser bending process to generate a desired shape. It was shown that the control parameters (laser power, scan speed and scanning path length) and type of fitness function have significant effects on GA synthesis results. The selection of proper fitness function is important to establish a balance among competing

objectives, such as geometric accuracy, forming time and energy consumption. Du et al. (2010) presented an improved back-propagation neural network model based on the double chain quantum genetic algorithm to predict the bend angle more accurately. Maji et al. (2013a) presented a GA-tuned neural network (GA-NN) and neuro-fuzzy inference system (GA-ANFIS) to predict the bend angle and to carry out the inverse analysis of the laser forming process. The prediction of bend angle was better in GA-NN approach, whilst the predictions of inverse analysis were comparable in both the approaches.

Observations

Significant research has been reported on the development of analytical, numerical and soft-computing based models for the prediction of bend angle, temperature distribution, stress-strain distribution, and edge effect. Many of these models are able to predict the process within acceptable error band. However, it was observed that the numerical modeling and simulation of multi-scan laser bending is not yet explored. Most of the presented models do not include the effect of melting, change in mechanical and microstructural properties, strain hardening and change in absorptivity occurring as a result of laser beam irradiation, and thus have limited applicability for a wide range of process conditions and materials.

2.10 Inverse Modeling and Optimization

As discussed in the previous section, various numerical and analytical models are developed to predict the process responses and to understand the physics of the process. One major difficulty in using these models is that many a times some of the properties of workpiece materials, laser beam and laser-workpiece interaction are not known. The inverse modeling is useful for finding out these unknown parameters. In inverse modeling, a suitable optimization technique is used to estimate the unknown parameters. The results obtained through analytical or numerical model are compared with experimental or known data. Based on the difference, values of the unknown parameters are adjusted. The values of the unknown parameters are optimized by minimizing the suitable error function. Some attempts have been reported on these aspects.

Mishra and Dixit (2013) determined absorptivity, thermal diffusivity and laser beam diameter by inverse heat conduction method. They measured temperature on centroid of the bottom surface at different time intervals and thermal properties were estimated using this measured temperature. The minimization of objective function was based on absorptivity, thermal diffusivity and beam diameter. The methodology was found to be efficient, however,

more than one combination of parameters can provide same temperature variation with time at a particular location. Further, Aghyad and Dixit (2013) improved their model and they carried out inverse determination by measuring temperature at two locations. The objective was to minimize combined errors between predicted and measured temperature at two locations. The proposed methodology was found to be efficient and robust. Xu et al. (2013) determined absorptivity based on the coupling of the experimental and simulation results.

The optimization of laser forming process is one of the promising area. There is hardly any comprehensive paper on the optimization of laser bending process. Kumar and Dixit (2008) combined a finite element module with the artificial intelligence (AI) module containing a neural network that learns with experience. In their work, inverse problem of determining the scan speed for the desired bend angle is solved using an optimization module. Maji et al. (2013b) used the response surface methodology for the modeling and optimization of the pulsed laser bending process.

Observations

Very few attempts have been made for the estimation of unknown parameters using inverse analysis and optimization. However, it is an effective methodology for the prediction of the unknown parameters like absorptivity, cooling coefficients, beam diameter, etc. Absorptivity significantly affects the laser bending process, however its behavior is difficult to predict under laser beam irradiations. Optimization of the laser bending process is another important area which is not yet explored by the research community. A need thus exists to carry out research work in the field of inverse modeling and optimization of the laser bending process.

2.11 Process Design of Laser Bending

Laser bending process parameters have non-linear effect on the bend angle and edge effect. Therefore, planning and control of irradiations are important for an efficient application of laser forming process in the industry. The laser forming can be used to generate various complex shapes using different irradiation strategies. The laser parameters such as laser power, scan speed, beam diameter and scanning path should be optimized to get the desired shape. Several methodologies are proposed by researchers for using the feedback of the bent specimen geometry to alter the irradiation strategies. Yu et al. (2000) presented an algorithm based on the non-linear optimization theory and the differential geometry to determine the minimal strain energy required to convert a 3-D bent geometry into a flat shape. The algorithm explained the heating path planning, but it did not provide an explicit method to determine the heating

conditions. Kim and Na (2009) proposed a method where the free surface was decomposed into a combination of plane patches. The forming data such as laser irradiation lines, bend angles, and shrinkage data along the forming lines were calculated and process parameters were matched to the forming data by using FEM data maps.

Liu et al. (2004) proposed an optimization approach for the determination of optimal laser scanning paths and heating conditions to produce doubly curved shapes. The approach includes strain field calculation based on the principal curvature formulation and minimal strain optimization. The heating directions were defined normal to the direction of the maximum principal curvature. Scanning paths and heating condition (laser power and scan speed) were determined by combining analytical and practical constraints. Edwardson et al. (2005b) developed a predictive model for the scanning strategies. An iterative process design was proposed which determined scanning paths either perpendicular to the contour lines of the resultant gradient vector or along the contour lines based on the differential geometry. The error between current and desired geometry was used to get a new scanning strategy. Edwardson et al. (2001) used various scanning strategies to produce a saddle shape in large sized mild steel sheets.

Cheng and Yao (2004b) developed a process design methodology for the laser forming of doubly curved thin plates. Initially, they calculated the strain field required to generate the desired shape. The scanning paths were decided based on the concept of in-plane strain, bending strain, principal minimal strain, and temperature gradient mechanism of laser forming. The database of minimal principal in-plane strain magnitudes as a function of laser power and scan speed was used to determine the heating condition. Liu and Yao (2005) developed FEM based design methodology to determine laser scanning paths and heating conditions. Strain fields were calculated by FEM and then decomposed into the in-plane and bending strains. Scanning paths were chosen perpendicular to minimum principal strain direction and heating conditions were decided based on the ratios of in-plane to the bending strain. Cheng et al. (2005a) proposed a strategy based on the temperature field and bending deformation for tapered thickness plate and compressor airfoils. The strategy utilized FEM to generate a deformation map from the initial to final configurations, and heating paths were determined by weighted-averages of the minimum principal in-plane and bending strains. A thickness dependent database was established by experiments and FEM simulations to determine the heating conditions. Cheng et al. (2006b) presented a similar approach for thin plates of the varying thickness.

Abed et al. (2007) used a predictive and adaptive approach to control the laser forming of mild steel and aluminum sheets into a desired surface. An incremental adaptive approach was used that utilized the error between the current and desired geometry to define a new scanning strategy. Carlone et al. (2008) developed a computational procedure based on the minimization of a vectorial fitness function for three-dimensional laser forming of sheets. The error minimization was carried out by comparing the target surface with reference deformed surfaces described by sixteen point bi-cubic patches. The reference deformed surfaces were described by the nodal displacements obtained from FEM based numerical simulations. Magee and Vin (2002) combined two forming techniques to improve the flexibility and accuracy of the bending process. They proposed that the collision problem can be largely circumvented by under-bending of components and then final finishing can be done by using the laser bending operation.

Observations

Laser bending is an effective tool to manufacture 3-D complex shapes. Proper selection of the irradiation strategies and the optimal selection of process parameters are the key factors to produce an accurate 3-D complex shape. Literature reports a few attempts on the generation of desired surfaces using computational geometry based irradiation strategies. Simple geometries like saddle and pillow shapes are generated using these irradiation strategies. There is a need to carry out further systematic studies to evolve efficient strategies to manufacture 3-D complex shapes of macro as well as meso sized components.

2.12 Feedback Based Control in Laser Forming

Laser forming process can be controlled by using the feedback obtained from the process performance. The feedback approach relies on sensors those are used to monitor the degree of deformation. The deformation achieved after laser scanning is compared with a target value, and based on the difference, the process parameters are adjusted. Hennige et al. (1997) used a feedback system for accurate laser bending of the sheets. The laser triangulation sensors and a noise filter was used to find the displacement due to laser scanning. The maximum sampling rate for the on-line measurement system was more than 50 Hz which is sufficiently good for the scan speed up to 200 mm/sec. The deviation of bend angle for the online system was less than 0.01°. The laser parameters for each successive scan were calculated based on the bending results of the previous scan. The developed system achieved an accuracy of at least 0.2° for a 10° of total bend angle (which means the error was less than 2%). Thomson and Pridham (1997)

developed a feedback control systems using linear variable displacement transducer (LVDT) sensor. The displacement error was used as feedback to control the laser scanning. The developed system improved the accuracy of final product and results showed a good achievement in single line laser forming. Later, Thomson and Pridham (1998) improved the control system by using increased feedback data sampling, time delays and a modified control algorithm. The forming rate in addition to the displacement error was used as feedback to control the process. These modifications improved the process tolerance significantly. The authors claimed that the feedback system can be used to produce simple parts such as door panel of a car.

Liu and Yao (2002) proposed a response surface methodology (RSM) based optimization method where propagation of error was used as an additional response for optimization, which made the process design more robust. Kim and Na (2003) proposed distance based and angle based criteria algorithms to generate laser scanning paths. The distance based method used the maximum distance between given sheet and the target shape as a criterion for a new irradiation point. When the maximum distance was larger than the offset distance, the point at the maximum distance was adopted as a new irradiation point. The second method used angles between tangent lines as a criterion for making an irradiation point. The angle gradually increases as the radius of curvature decreases, so that more forming points can be generated in a highly curved surface. Further, Kim and Na (2005) employed a feedback control scheme for 2-D laser curve bending. The feedback was obtained by means of laser displacement sensors. This scheme improved the accuracy of the final product.

Observations

Literature reveals that a few attempts have been made to generate desired shapes within acceptable accuracy by using feedback based control systems. These systems produce desired products with reasonable accuracy. However, development of the control systems which can determine irradiation strategies and process conditions to produce desired shape by considering the initial and final details of the workpiece is still a challenging task. Development of these kind of control systems will be very effective in the employment of laser bending process in the manufacturing industry.

2.13 Observations and Conclusions

Literature reports research on various aspects of the laser bending process such as bending mechanisms, effect of process parameters and material properties on the process responses,

irradiation strategies, edge effect, pre-load, etc. Significant research has also been reported on the empirical, analytical, numerical and soft-computing modeling of the process. The empirical works are concentrated on the study of effects of process parameters on the bend angle, edge effect and metallurgical variations. Analytical models are contributed to characterize the laser bending mechanisms. Finite element simulations are carried out to improve the fundamental knowledge of the process. The soft-computing models are used to predict the bend angle. This chapter has provided an overview of the established research work on the laser bending process. The key observations of the literature review are as follows:

- Various experimental and numerical studies on the laser bending of a wide range of materials are carried out by researchers worldwide. A number of materials useful to the manufacturing industry have been processed by the laser bending that includes steels, titanium alloys, aluminum alloys, nickel alloys, plastics and brittle materials like mono-crystalline silicon, borosilicate glass, and Al_2O_3 ceramics. Some work has also been reported on metal matrix composite and sandwiched material. However, there is hardly any published work available on the laser bending of ultra-high strength steels, magnesium alloys, and beryllium alloys. These materials are among some of the most important materials used in automobile, ship-building, aerospace, aviation, medical, instrumentation and electronics industries. There is a need for comprehensive study on the laser bending of these materials.
- In general, there are three mechanisms involved in laser bending process: temperature gradient mechanism (TGM), buckling mechanism (BM), and upsetting mechanism (UM). The bending mechanism is mainly determined by the temperature distributions produced inside the material. However, for some process conditions, there may be a transition zone exists between two mechanisms. Very scant systematic study has been reported on the transitions of mechanisms and deformation behavior for various important materials such as magnesium alloy, aluminum alloy and beryllium alloy.
- The laser bending process is quite complex to understand through experimental studies and analytical modeling. The numerical approaches are employed to enhance the insight into the process. The numerical simulations provided significantly accurate results for temperature distribution, stress-strain distributions, and distortions. However, presented models have limited applicability and they are not suitable for a wide range of process conditions. More accurate models are required by considering

the effect of microstructural changes, phase transformation, and molten metal flow in the laser bending process.

- In laser bending, the bend angle is not uniform along the scan line, which is called edge effect. The control of edge effect is a challenging task, however a suitable irradiation strategy, *e.g*. curvilinear irradiation can be used to control the edge effect. The curvilinear laser bending is also important to generate the complex shapes using lasers. The effect of curvilinear irradiation parameters, particularly, the effect of scanning path curvature on the deformation behavior, temperature distribution and warping of the worksheet is still need to be explored for the application of curvilinear laser bending process in real practice.
- Multi-scan laser bending obtains large bend angles (of the order of 10º) in metal sheets. Literature reports significant experimental studies on the effect of process parameters on bend angle and edge effect in multi-scan laser bending process. However, there is hardly any comprehensive work available on the numerical simulations of the multi-scan laser bending process, which may provide better insight into the bending mechanism, bend angle, and edge effect during each successive laser scans. This may also help in the selection of proper process conditions for an efficient laser bending process.
- In spite of several advantages of the laser bending process, on many occasions it is not able to compete with the conventional mechanical bending in terms of energy efficiency and production time. Due to this several researchers have augmented the laser heating with mechanical load, which is called laser assisted bending. Laser assisted bending can provide advantages of both laser bending and mechanical bending operations. The laser assisted bending, although beneficial, sacrifices flexibility of the process. Most of the presented work on laser assisted bending considered the distributed or concentrated mechanical load, which may not be suitable for many of the practical applications. Especially, in case of laser assisted bending of medium to large sized sheets, the use of concentrated or distributed load is not suitable due to the requirement of a large size force application system and the complexities involved in the space availabilities. Therefore, there is a need to design and develop a suitable technique for laser assisted bending to produce a large bend angle (of the order of 10º) in medium to large sized sheets.

2.14 Research Objectives

In the present work, an extensive review of the reported research work on the laser bending process has been carried out. Many research gaps have been identified which have provided the guidelines to define objectives of the proposed research work. Overall objective of the proposed work is to carry out numerical as well as experimental investigations to assess the feasibility, productivity and product quality during the manufacture of large (of the order of 10º) and precise bend angles in difficult-to-form material such as magnesium alloy using lasers. The specific objectives of the proposed work are as follows.

- To assess the feasibility of laser bending of magnesium alloys by conducting systematic experiments and to study the mechanical properties of the laser-bent magnesium alloy.
- To carry out comprehensive parametric studies on the important variants of laser based bending process, *viz*. single scan laser bending, curvilinear laser bending, multi-scan laser bending, and laser assisted bending with moving pre-displacement by using numerical simulations and experiments. The main objective of these studies is to assess the productivity and product quality of the laser bending process variants.
- To design and develop an efficient and simple technique – laser assisted bending with moving pre-displacement and further to develop an experimental setup for the same.
- To study the bending mechanism, edge effect and efficiency of the proposed technique, and to compare its performance with that of the laser bending process.

Chapter 3 presents the systematic experimental studies carried out to check the feasibility of bending of magnesium alloy using lasers.

CHAPTER 3: EXPERIMENTAL STUDIES ON LASER BENDING OF MAGNESIUM ALLOY M1A

3.0 Scope

This chapter primarily focuses upon the feasibility study of laser bending of magnesium alloy sheets. Initially, an overview of the work carried out during this research is presented. The need to carry out the feasibility study of laser bending of magnesium alloys is defined. Details of the experimental setup, worksheet geometry, coating, and heating conditions are presented. Experiments are conducted on magnesium alloy M1A worksheets, and the results are discussed. At last, the mechanical properties of the irradiated worksheet material are presented. The chapter is summarized with conclusions.

3.1 Overview of the Present Work

Figure 3.1 shows an overview of the present work. It primarily comprises a feasibility study on the laser bending of magnesium alloys by conducting experimental studies on magnesium alloy M1A, development of the numerical model for laser bending process, and then, the use of developed numerical model to improve process efficiency and product quality of the laser bending of the difficult-to-form material magnesium alloy M1A.

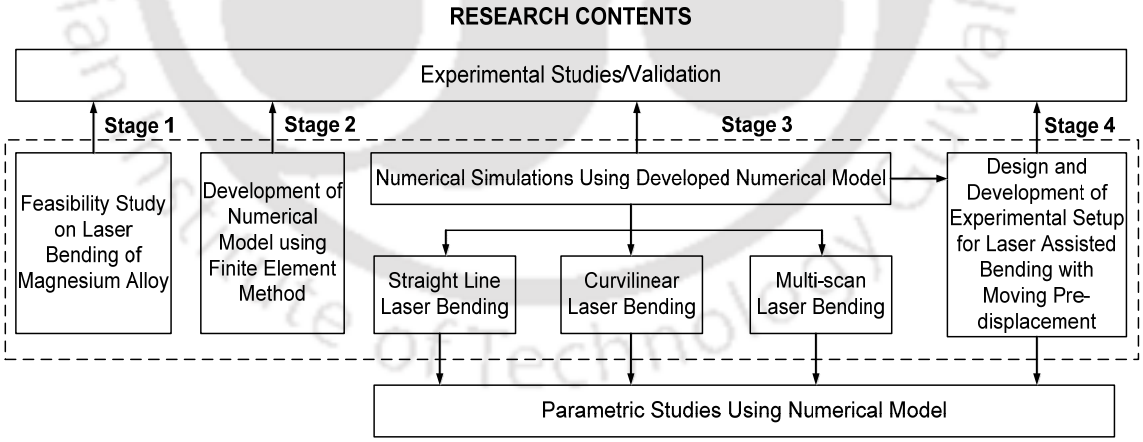

Figure 3.1. Overview of the present work.

The present work is carried out in the following sequence,

- First, experimental studies on laser bending of the magnesium alloy M1A sheet are carried out. Feasibility of the sheet bending using lasers and the effect of laser

irradiation on mechanical properties of the worksheet are studied. The details are presented in this chapter.

- Second, a three-dimensional non-linear thermo-mechanical finite element method (FEM) based numerical model is developed by considering the thermo-physical characteristics of the process. The results predicted by the developed numerical model are validated with those obtained in the experiments. Various details are presented in Chapter 4.
- Third, analysis of the important variants of laser bending process, *viz*. single scan laser bending, curvilinear laser bending, multi-scan laser bending is carried out by using the developed numerical model. Details of the single scan laser bending are presented in Chapter 5.
- The edge effect is observed in the straight line laser bending process and to control the edge effect, an analysis on the curvilinear laser bending process is carried out using developed FEM model. Details are presented in Chapter 6.
- Single laser scan produced quite low bend angle (of the order of 1º). To obtain larger bend angle, multiple scans have been employed. The detailed numerical as well as experimental analysis of multi-scan laser bending is reported in Chapter 7.
- The process efficiency of multi-scan laser bending is found to be less as compared with that of conventional bending operation. To overcome this limitation, a novel, simple, low cost and efficient technique is proposed. In this technique, the laser bending has been carried out in conjunction with an external mechanical load. This facilitated the utilization of advantages of both laser and mechanical bending of worksheet. An experimental setup for the implementation of the moving mechanical load strategy in terms of moving pre-displacement is designed and developed. At last, performance analysis of proposed technique has been carried out by using numerical simulations as well as experimental studies. Details are presented in Chapter 8.

This chapter presents details of experimental studies on laser bending of the magnesium alloy M1A. Experimental studies are carried out to check feasibility of the laser bending of magnesium alloys.

3.2 The Need

Literature reports very scant research work on laser bending of magnesium alloys. Magnesium alloys have high strength to weight ratio, and are widely used in the manufacture of low weight

components of automobile, aerospace, medical, sensor, instrumentation, electronics and household applications. Due to the low formability, it is quite difficult to obtain precise bend angle in magnesium alloys by using mechanical bending operations. In this scenario, the laser bending was thought to be an alternative to deform the magnesium alloys. However, these alloys may catch the fire when heated at high temperature in the presence of air. A need was thus identified to carry out the feasibility study of laser bending of magnesium alloys. Also, in a perspective of real life applications of laser bent magnesium alloy sheets, it was also thought to be worth to study the mechanical properties of the laser bent specimen.

The following sections present details of the experimental setup, specimen preparation and observations of the experimental results. The change in mechanical properties of the worksheet material due to the laser beam irradiation is also presented.

3.3 Experiments on Laser Bending of Magnesium Alloy M1A

Experimental studies on the laser bending of magnesium alloy M1A have been carried out to check the feasibility of the process for magnesium alloys. Various details of the experimental studies on laser bending of magnesium alloy M1A are presented in the following sections.

3.3.1 Specimen preparation

The experimental study was carried out on commercially available magnesium alloy M1A sheets. It was an Mg–Mn alloy, and approximate composition of the material was magnesium 98.07% and manganese 1.93%. The composition of the material was tested in Omkar Analab located in Mumbai (INDIA). A copy of the test report is given in Appendix 3.1.

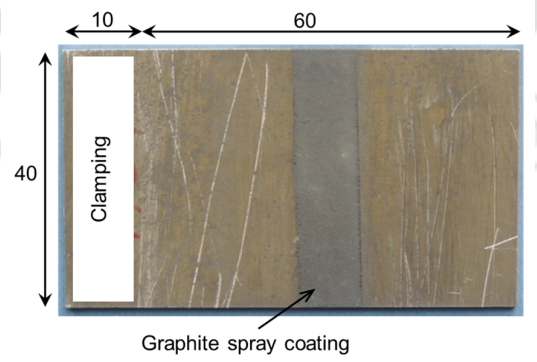

Figure 3.2. The graphite spray coated specimen for laser bending process (dimensions in mm).

Thickness of the sheet was about 1.9 mm. Specimens of size 70 mm length and 40 mm width were cut by using CO_2 laser cutting machine (LVD ORION 3015). The laser cutting was preferred over shear cutting as the lasers cut the specimen accurately with minimum distortion.

The length 70 mm was taken along the rolling direction of the worksheet. Along length, 10 mm was used for clamping and remaining 60 mm was freely hanging. The cut specimens were cleaned with a cloth to remove dust and fumes. Metals have high reflectivity, and therefore, the specimens were coated with graphite spray to increase the absorptivity. The coating also ensured the uniform absorption of the laser beam along the scanning path. The coated specimens were allowed to dry for about an hour under normal room conditions. Figure 3.2 shows a graphite spray coated worksheet specimen with dimensional details.

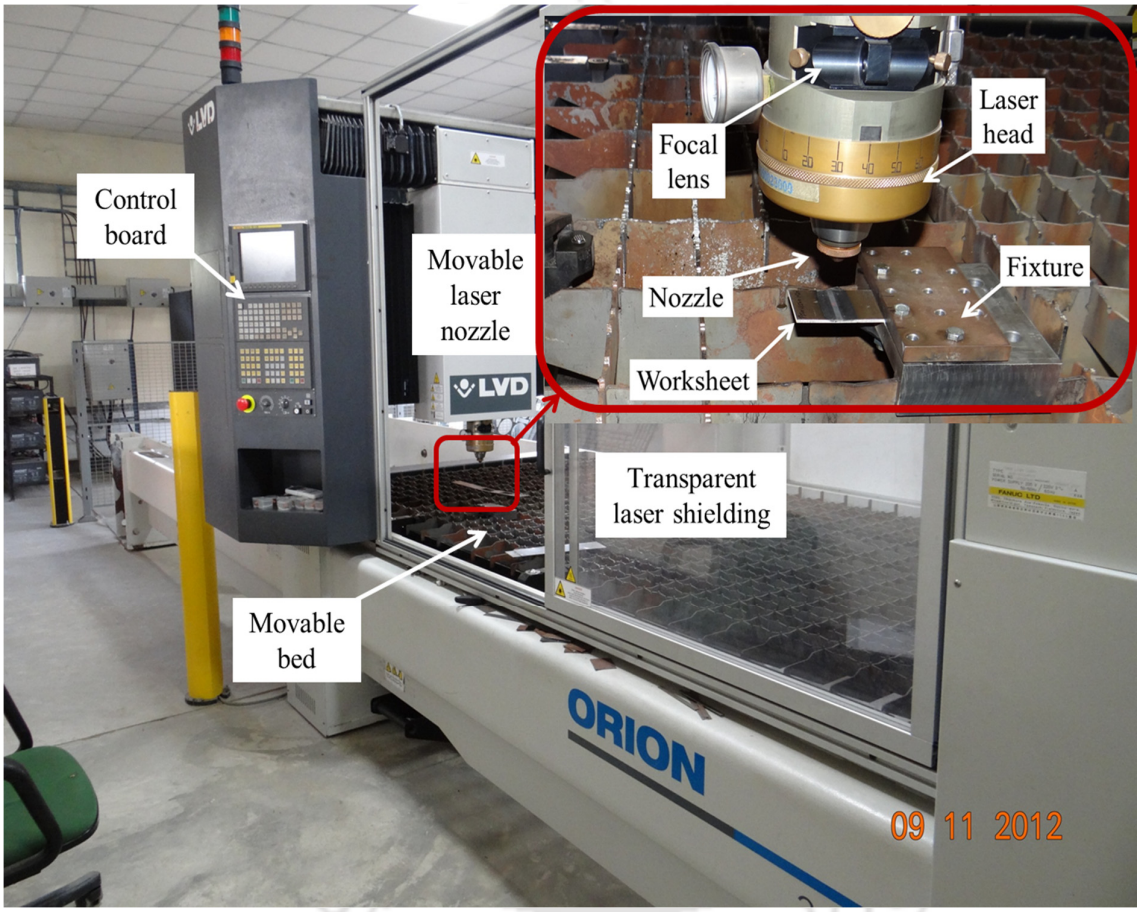

Figure 3.3. Details of laser machine setup.

3.3.2 Laser irradiation

The laser heating was performed by using LVD Orion 3015 2.5 kW continuous wave CO_2 laser machine shown in Figure 3.3. The duty cycle was set at 100%, so that the laser power is continuous during entire irradiation along the scanning length of the worksheet. Specifications of the machine are given in Appendix 3.2. The specimen was fixed over the laser machine bed by using a fixture as shown in Figure 3.3. The continuous wave CO_2 laser beam was irradiated

over the worksheet surface along a predefined scanning path. The coating was damaged due to the laser irradiation as shown in Figure 3.4. At high laser power, slow scan speed and small beam diameter, some melting was occurred over the specimen surface as shown in Figure 3.4. The specimens were allowed to cool naturally after the laser irradiation. Due to laser irradiation, the specimens were successfully bent as shown in Figure 3.5.

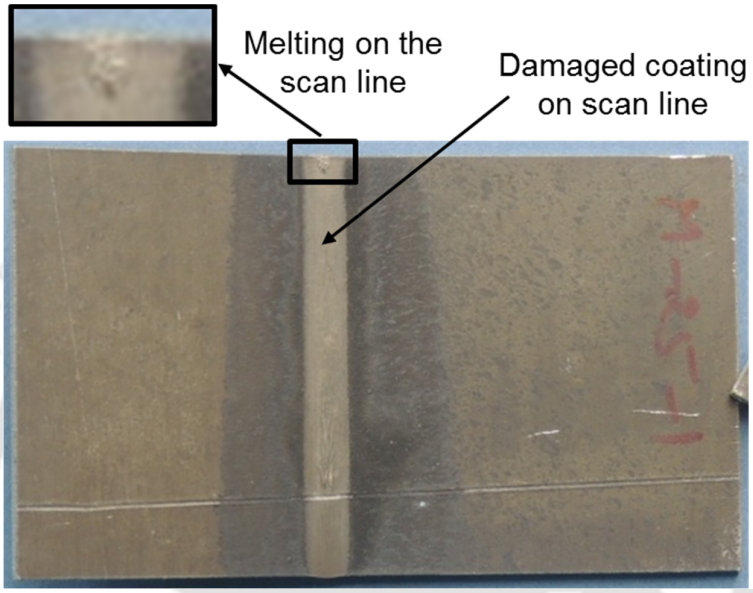

Figure 3.4. Laser irradiated specimen.

Figure 3.5. Laser bent specimen.

3.3.3 Bend angle measurement

The bend angle generated due to laser irradiation was measured at middle of the scanning path using Zeiss^{TM} make coordinate measuring machine (VISTA; 1620-14, DCC, BND, K) (Figure 3.6). The specifications of the machine are given in Appendix 3.3. The touch probe was moved along x, y and z axis to collect the data points on either side of the scan line. Two points were collected on each side of the laser scan line, which formed two lines on both sides of the scanning line. The bend angle was computed between these two lines. Figure 3.7 shows a schematic of data points located on the worksheet to obtain the bend angle as

$$\theta = \tan^{-1}\left(\frac{u_d - u_c}{L_{cd}}\right) + \tan^{-1}\left(\frac{u_a - u_b}{L_{ab}}\right), \tag{3.1}$$

where, notations used in Equation 3.1 are shown in Figure 3.7.

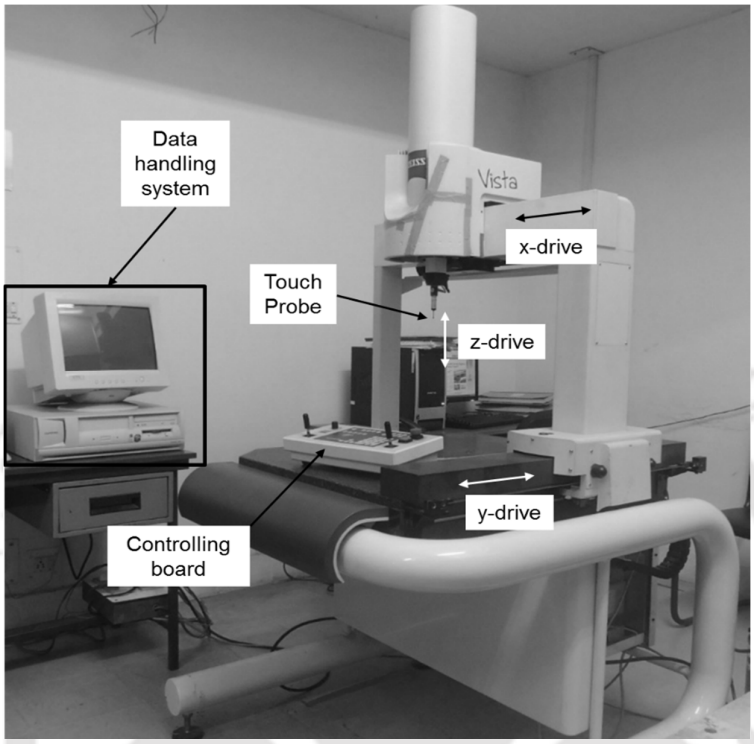

Figure 3.6. Coordinate measuring machine used to measure the bend angle.

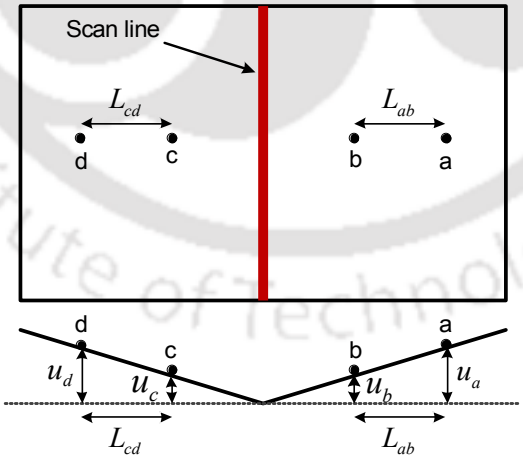

Figure 3.7. Schematic of bend angle measurement.

The process (laser) parameters, *viz.* laser power (P), scan speed (V) and beam diameter (D) were varied to control the laser bending operation. Levels of various laser process parameters are shown in Table 3.1. Full factorial experiments were carried out for the laser

bending process. Each experiment was performed thrice to record the repeatability of the response, *i.e*. bend angle. The bend angles obtained for all sets of process conditions are reported in Appendix 3.4. The average of three trials was considered as the experimental value. The coefficient of variation (*CV*) was calculated as the ratio of standard deviation to the mean of three trials. From the feasibility experiments, it was observed that a bend angle of about 1.4° can be achieved by using single laser scan. The process condition with low heat flux density, for example *P*=300 W, *V*=3000 mm/min and *D*=7.74 mm, did not bend the worksheet. During the course of experiments, it was also observed that a combination of high laser power, fast scan speed and small beam diameter produced larger bend angle. The effects of various process parameters on the bend angle and edge effect are discussed in details in Chapter 5.

Table 3.1. The range of laser process parameters used in the experiments.

S. No.	Laser Power (W)	Scan Speed (mm/min)	Stand-off Distance (mm)	Beam Diameter (mm)
1.	300	1000	20	3.87
2.	400	2000	30	5.81
3.	500	3000	40	7.74

Experimental studies on the laser bending of magnesium alloy M1A showed that the bend angle of about 1.4° can be achieved in single laser scan, which makes the process suitable for the micro-bending applications. However, many a times, a larger bend angle (of the order of 10º) needs to be generated in real practice. Larger bend angle can be generated by applying multiple scans instead of single laser scan. In the present work, the laser bending of magnesium alloy with multiple scans is also carried out to check feasibility of obtaining large bend angle using lasers in magnesium alloy sheets. Total ten number of scans were applied for the same set of process conditions used in the single scan laser bending process. All the ten scans were carried out in natural cooling conditions. Each laser scan was followed by a natural cooling of about 5 seconds. In this duration, the laser source was moved from the scan 'end' position to its 'start' position and prepared itself to start the next irradiation. The worksheet was cooled naturally during the complete scanning cycle of the process. The forced cooling was not applied at any stage of the experiments. Coating was applied only once before the first irradiation. The coating was ablated due to laser irradiation (see Figure 3.4), but it was not applied again before the start of next irradiation. After ten irradiations, the specimen was removed from the laser machine, and the bend angle was measured over the coordinate measuring machine (CMM).

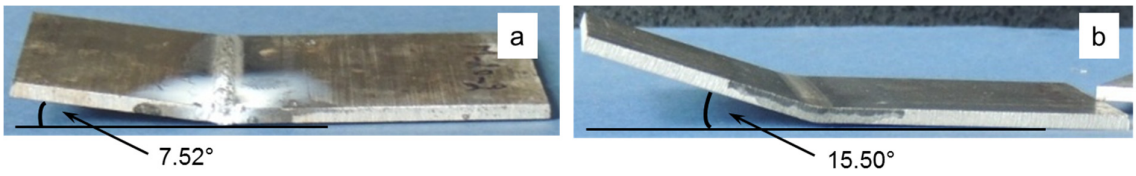

Figure 3.8. Laser bent specimens with multi-scan laser bending process.

Figure 3.8 shows the magnesium alloy M1A worksheet specimens undergone multi-scan laser bending process. It is observed that a significantly large bend angle can successfully be produced with multiple irradiations. For various set of process conditions as mentioned in the Table 3.1, the bend angles obtained after the completion of ten laser scans for all sets of process condition are presented in Appendix 3.5. It can be seen that a significantly large bend angle of about 15° was achieved with ten laser scans. The smallest bend angle produced is about 0.89°. Thus, it can be concluded that the laser bending process is suitable for both micro as well as macro bending of magnesium alloys. During the course of experiments, it was also observed that a combination of high laser power, slow scan speed and large beam diameter produces small bend angle. It may be due to high temperature at the bottom surface and low temperature gradient along the thickness direction. The detailed analysis on bend angle in multi-scan laser bending process is presented in Chapter 7.

Laser bent specimens after ten laser scans are shown in Figure 3.8. During experimental study, it was observed that the melting occurs when laser power is high, scan speed is slow and beam diameter is small as shown in Figure 3.8 (a). In some cases, the melting zone was very small (Figure 3.8 (b)), while in some cases, a significant melting was occurred in the irradiated region (Figure 3.8 (a)). However, the melting was noted to be localized, and occurred in the irradiated region only. It can clearly be seen that the bend angle is less when melting occurs in the heated region.

Figure 3.9 (a) shows the bottom surface of the laser bent specimen. It can be observed that the bending radius is about 4.6 mm which is very small as compared with that obtained in the mechanically bent specimen shown in Figure 1.2 (Chapter 1). The laser bent specimen has a sharp edge on the bending line. The laser bent specimen was seen under the optical magnification using ZEISS made optical microscope. The magnified image of the bottom surface (away from laser irradiation) of the laser bent specimen is shown in Figure 3.9 (b). It can be observed that the cracks are not generated during multi-scan laser bending of the

magnesium alloy M1A worksheet. For the similar bend angle of about 17.52°, many cracks were observed in the mechanical bending of worksheet as shown in Figure 1.2. Thus, the experimental study revealed that the multi-scan laser bending is suitable for producing crack-free large bend angle in magnesium alloy worksheets.

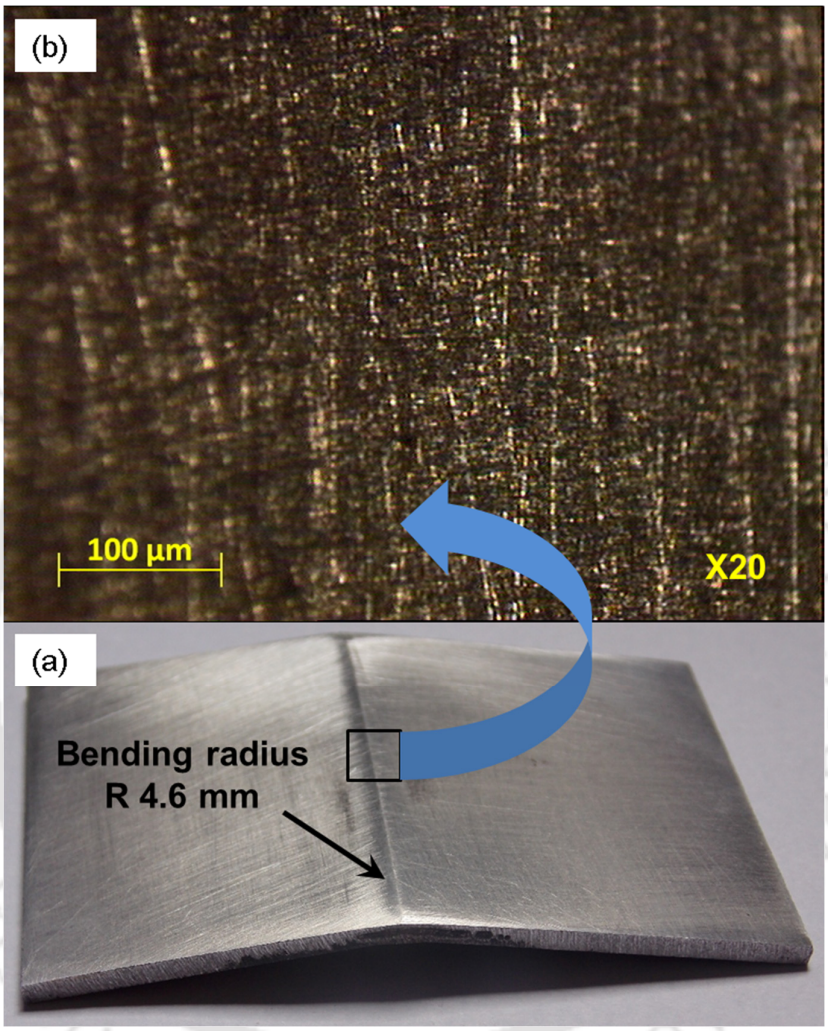

Figure 3.9. Laser bending of magnesium alloys (a) bent specimen and (b) magnified image.

3.4 Study on Mechanical Properties of Laser Bent Magnesium Alloy M1A

The laser bending process involves high temperature and localized distortions near the irradiated region. It may affect the mechanical properties of the worksheet. Therefore, the effect of laser irradiation on the tensile behavior of the magnesium alloy M1A is studied and compared with the base material. The process parameters for laser irradiation were taken as laser power=500 W, scan speed=3000 mm/min and beam diameter=3.87 mm. Details of the tensile experiments are shown in Figure 3.10. The laser was scanned perpendicular to the

rolling direction of the sheet and tensile specimens were cut along and perpendicular to the scanning direction by using CO_2 laser cutting machine. Dimensions and cutting details of the tensile specimen are shown in Figure 3.10. Tensile tests were carried out on Micro-Tensile machine by Deben (Deben Microtest MT10081). The machine was suitable up to 5 kN tensile load. The cross-head speed was maintained at 0.2 mm/min. The tensile tests were carried out at room temperature and under normal environmental conditions. The load-stroke data were monitored and converted into stress-strain values. The stress-strain behavior were studied along and perpendicular to the laser scanning direction.

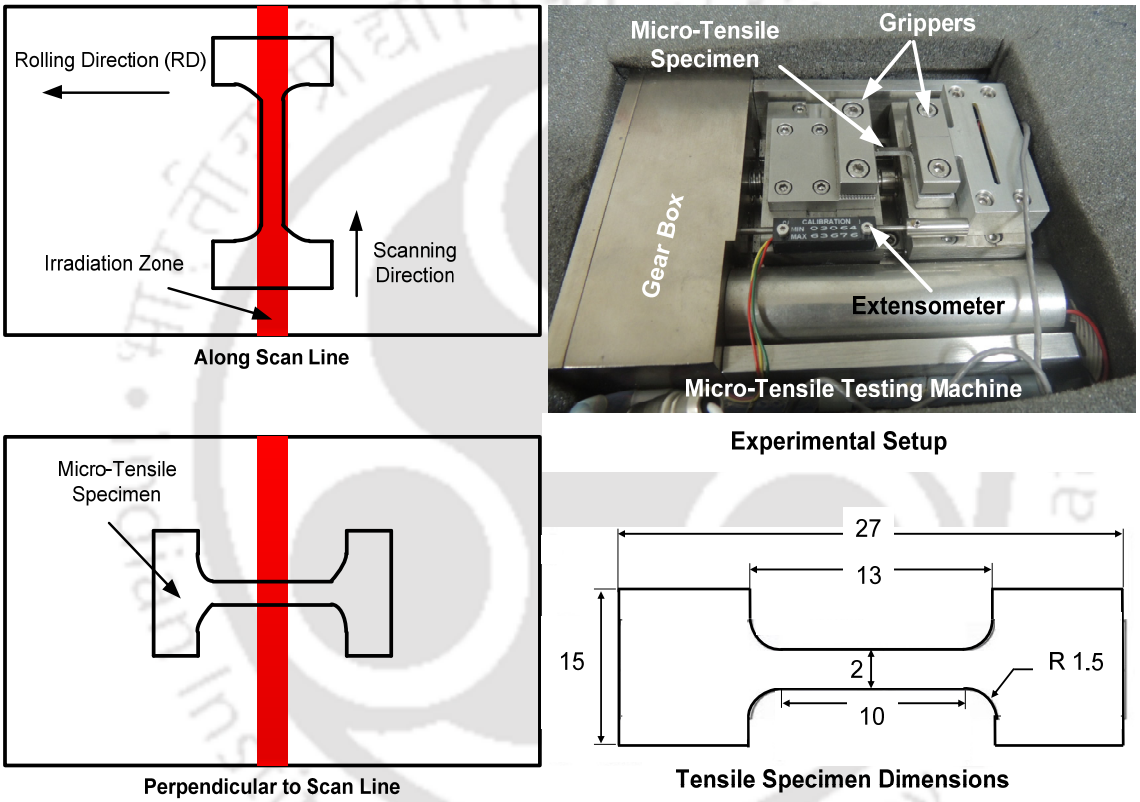

Figure 3.10. Details of tensile test.

Figure 3.11 shows tensile behavior along the laser scanning direction. The stress-strain behavior of the laser scanned specimen was compared with that of the base material. The mechanical properties were deteriorated due to laser irradiation. The tensile stress of base material and irradiated material were found to be about 250.9 MPa and 239.7 MPa, respectively, and the elongation at break was noted as 22.6% and 19.1%, respectively. It can be seen that the yield strength, tensile strength and ductility decrease due to laser irradiation. However, the decay in mechanical properties was not much significant.

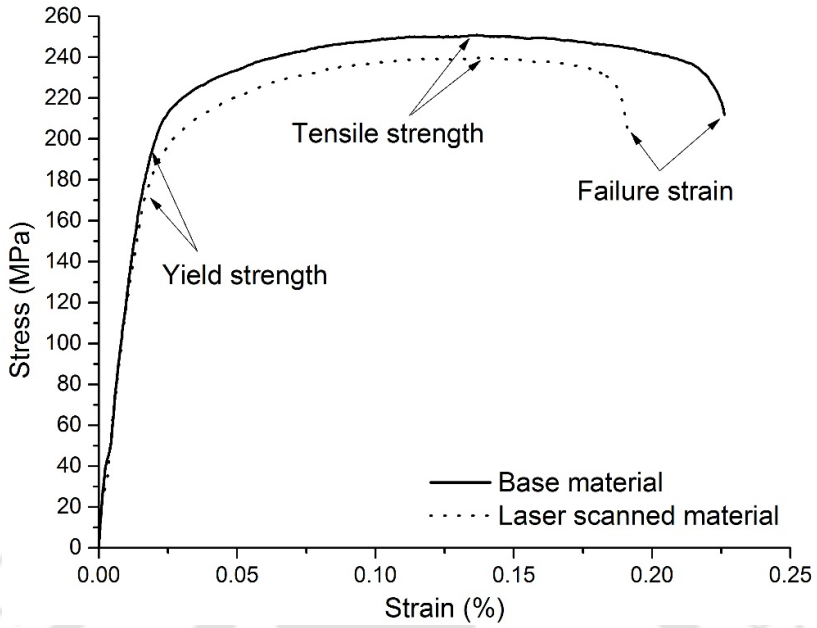

Figure 3.11. Tensile properties along the laser scan direction.

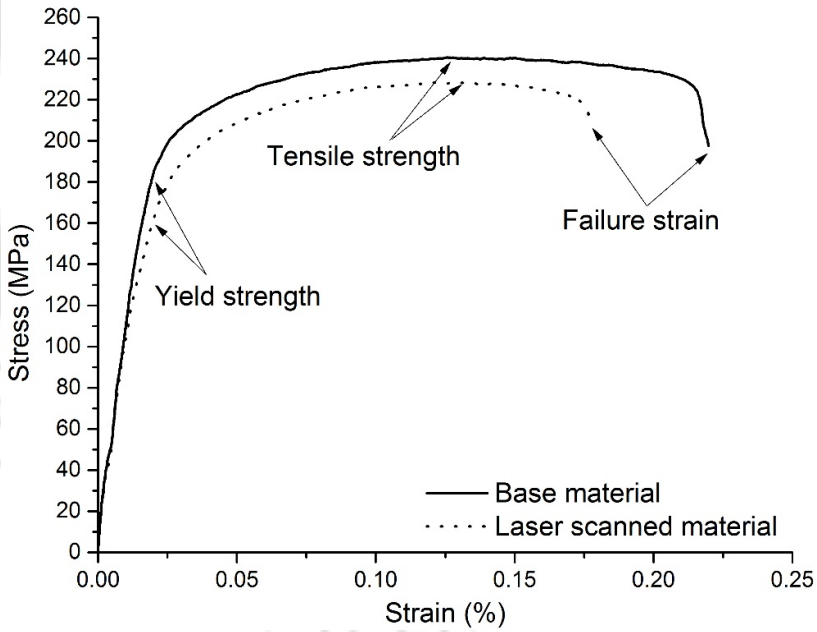

Figure 3.12. Tensile properties of specimen along a direction perpendicular to the laser scan.

Figure 3.12 shows tensile behavior of the base and laser irradiated specimen in the direction perpendicular to the scanning line. The tensile strength, elongation at break and yield strength was decreased due to laser irradiations. It is similar to the tensile behavior along the laser scanning line axis. The tensile strength of the base and laser irradiated specimens was about 240 MPa and 228 MPa, respectively, and the elongation at break was about 22% and

17.7%, respectively. The specimens were failed in the heated region. The results showed that the material properties of the base material deteriorate due to laser irradiations. However, degradation in the mechanical properties is marginal, but this factor should be considered while using laser bending process for the bending of magnesium alloys.

The Vickers micro-hardness test was also performed to measure hardness of the laser bent specimen. Hardness of the laser irradiated specimens was measured and compared with that of the base material specimens. The micro-hardness was measured in the irradiated zone shown in Figure 3.4. The test was performed on micro-hardness tester by BUEHLER™ shown in Figure 3.13. The hardness was measured at three positions in the irradiated region by using force of 500 g for both base material and laser irradiated specimens. The average of three was considered as the experimental value. The average hardness of the base material and laser irradiated specimens were found to be about 48.2 HV and 50.05 HV, respectively. Hardness of the laser irradiated specimen is slightly more which may be due to compressive deformation in the irradiated region.

Figure 3.13. Micro-hardness tester by BUEHLER.

Based on the encouraging results obtained during the experimental studies, it was thought appropriate to explore, in detail, the bending mechanism, bend angle and edge effect during laser bending of the magnesium alloy. The details of numerical modeling and the parametric studies based on the predicted results are presented in the next chapters.

3.5 Summary

In this part of research work, preliminary experimental studies on the laser bending of magnesium alloy M1A worksheets were carried out. These studies revealed that the magnesium alloys can successfully be bent with laser bending process. It was observed that the specimen did not catch the fire during the application of all sets of process parameters (Table 3.1). It was also observed that the laser bending process is not only suitable for the micro-bending applications, but also can easily be employed for the macro-bending of magnesium alloy sheets. In the scope of these experiments, a maximum bend angle of about 16° was produced with ten number of laser scans. Mechanical properties of the laser irradiated region have also been studied. Along the scanning direction, tensile strengths of the base material and laser scanned material were about 250.9 MPa and 239.7 MPa, respectively, and the respective elongations at break were about 22.6% and 19.1%. Perpendicular to the laser irradiation, tensile strength of the base material and laser scanned specimens were about 240 MPa and 228 MPa, respectively, and the respective elongation at break were about 22% and 17.7%. It was observed that the specimens were failed in the laser heated region. Overall, the yield strength and tensile strength of the laser irradiated specimens was decreased by about 4–5%. The hardness of the heated region increased marginally as compared with the base material. The mechanical properties were found to be deteriorated due to the laser irradiation, however, deterioration was marginal and was limited in the heat affected zone only. Thus, it can be concluded that the magnesium alloys can easily be bent with laser without much deterioration in the mechanical properties of the heated region. Based on this encouraging fact, it was thought appropriate to develop a numerical model using finite element method for the parametric study of the laser bending operation. The experimental results will also be used to validate the numerical model.

CHAPTER 4: 3-D THERMO-MECHANICAL NUMERICAL SIMULATION OF LASER BENDING PROCESS USING FINITE ELEMENT METHOD

4.0 Scope

This chapter presents details regarding finite element method based numerical simulation of the laser bending process. The need to carry out thermo-mechanical analysis of laser bending process is defined. Details of numerical simulations in terms of assumptions, governing equations, boundary conditions, and solution methodologies are presented. The mesh sensitivity analysis is carried out and the optimum mesh parameters are decided. In the end, a case study on the numerical simulation of laser bending using a commercial FEM solver ABAQUS^{TM} is presented.

4.1 The Need

Based on the encouraging results obtained in the feasibility studies, it was thought appropriate to study the effect of process parameters, *viz*. laser power, scan speed, beam diameter, number of scans and mechanical load on the performance parameters, *viz*. bending mechanism, bend angle, temperature distribution, stress-strain distribution, and edge effect during the laser bending operation of magnesium alloys. However, conducting exhaustive experiments is often costly, time consuming, and error prone. Also, it is very difficult to obtain the in-situ information about the bending mechanism, bend angle increment, temperature profile, and stress-strain histories during physical experiments. As the development of high speed processing computers and user friendly solvers has increased the computational efficiency, the numerical simulations have been performed in order to improve the fundamental knowledge of the process. These days, thermo-mechanical numerical studies are more viable and the use of numerical models as a research tool in both academic and industrial sectors are becoming more prevalent. Numerical simulations are used in order to improve fundamental knowledge of the process by predicting the process behavior in less time and low cost.

Thus, a need was identified to develop a numerical model for three-dimensional non-linear thermo-mechanical analysis of the laser bending of magnesium alloys for various sets of process condition. Details of the development of numerical model are given in the following sections.

4.2 Thermo-Mechanical Modeling of Laser Bending Process

To understand and improve the laser bending process, it is important to develop a mathematical model to establish a realistic relationship between input and output process parameters. This mathematical formulation is useful in describing the static and dynamic performance of the laser bending process.

The aim of this work is to analyze the deformation behavior in the laser bending of magnesium alloy under temperature gradient mechanism (TGM) by proposing thermal and mechanical analysis. Due to the ease in control and deterministic prediction of bending, it was decided to employ the process conditions prevalent to the TGM for laser bending of magnesium alloys. Details of the TGM are already discussed in Section 2.1.1.

The work mainly includes the following steps.

- Define governing equations and boundary conditions.
- Modeling of laser heat flux which includes continuous wave heat flux density, Gaussian heat flux distribution, beam shape, beam size, scan speed, and scanning path.
- Application of the material properties – mechanical and thermal.
- Solution of the problem using finite element method based tool ABAQUS^{TM} in transient mode.
- Determination of temperature distribution, stress-strain distribution, and distortions at various process conditions for the straight line laser bending, curvilinear laser bending, multi-scans laser bending, and laser bending with moving pre-displacement.
- Study on the effect of various process parameters on bend angle and edge effect using developed numerical model.

These steps are discussed at length one by one in the following sections.

4.2.1 Assumptions

In real practice, the laser bending process involves complex non-linear interaction between various laser, worksheet material, and worksheet geometry parameters. Incorporation of all the interactions is difficult which include material in-homogeneity and random variation in the worksheet geometries. Therefore, following assumptions were considered in the numerical modeling of laser bending process,

- Worksheet material is homogeneous and isotropic in nature.

- The worksheet material is considered as elastic–perfectly plastic. Strain hardening and Bauschinger's effects are neglected as the process involves high temperature in the deforming region. The yield stress reduces to a lower value at elevated temperatures.
- Von-Mises criterion is used for the plastic yielding which is suitable for the ductile materials.
- The worksheet is considered flat, weightless, and free of residual stresses.
- Energy dissipation due to plastic deformation is negligible as compared to the laser heat absorbed into the worksheet, and hence it is neglected.
- The material loses its mechanical properties (stiffness) beyond the melting temperature.
- Laser has Gaussian distribution of heat flux inside the beam diameter. For CO_2 lasers, it is quite close to the real condition and widely reported in the literature (Bao and Yao 2001, Cheng and Yao 2005, Li and Yao 2000).

4.2.2 Governing equations and boundary conditions

Primary mechanism of laser bending is the deformation occurred due to the stresses induced into the worksheet by the laser heating. Therefore, both thermal and mechanical analyses are need to be carried out. The governing equations and boundary conditions for laser bending process are presented in details as follows,

A. Thermal analysis: governing equations and boundary conditions

Governing equations

Laser bending is a result of non-uniform temperature distribution into the worksheet material. The laser heat transfers into the worksheet material as a result of thermal conduction and the heat flows into the surrounding by convection and radiation heat flow. This heat transfer problem is solved by the law of conservation of thermal energy. The transient temperature field generated in isotropic material due to the laser beam irradiation is determined by using,

$$\rho c \frac{\partial T}{\partial t} = \nabla.\left(k \nabla T\right) + \left(3\lambda + 2\nu\right)\alpha_{th} T \dot{\varepsilon}_{ii}, \tag{4.1}$$

where T is the temperature (°C), which is a function x, y, z and time t(s), ρ is the density of material (kg/m^3), c is the specific heat (J/kg-°C), k is the thermal conductivity vector of the material (W/m-°C), α_{th} is the coefficient of thermal expansion, $\dot{\varepsilon}_{ii}$ is the volumetric strain rate and λ and ν are the Lame's parameters. The last term of Equation (4.1) is the heat generated due to volumetric change of the worksheet and it is neglected due to its very less value in

comparison with the laser heat input into the worksheet surface. ∇ is the gradient operator which is given as

$$\nabla = \frac{\partial}{\partial x}\hat{i} + \frac{\partial}{\partial y}\hat{j} + \frac{\partial}{\partial z}\hat{k} \quad . \tag{4.2}$$

Boundary conditions

The initial thermal condition of the worksheet was set to room temperature,

$$T\big|_{t=0} = T_0 . \tag{4.3}$$

The thermal boundary conditions are modeled by using natural convection and radiation heat losses. The convection heat loss (q_c) is given as

$$q_c = h(T_s - T_0), \tag{4.4}$$

where $h(=25\ \mathrm{W/m^2\text{-}^\circ C})$ is the convective heat transfer coefficient, T_s is the worksheet temperature and $T_0(=20\ ^\circ\mathrm{C})$ is the environmental temperature. The heat loss due to radiation (q_r) is calculated as

$$q_r = \varepsilon_s \sigma_s (T_s^4 - T_0^4), \tag{4.5}$$

where $\sigma_s(=5.67\times10-8\ \mathrm{W/m^2\text{-}^\circ C^4})$ is Stefan-Boltzmann Constant, and $\varepsilon_s(=0.2)$ is the surface emissivity of the worksheet.

The effect of melting was incorporated by considering the latent heat near to the melting temperature. The solidus and liquidus temperature of the material is 648 °C and 649 °C, respectively (Avedesian and Baker 1999). Incorporation of the latent heat in such a small range of melting temperature destabilizes the process of solving the numerical problem. Therefore, the latent heat was considered to be distributed over the temperature range of 645 °C to 655 °C. The latent heat of the magnesium alloy M1A is 370 kJ/kg-°C, and the distributed latent heat for the range 645 °C to 655 °C was taken as 37 kJ/kg-°C.

Heat flux model

The laser beam was assumed to be circular with Gaussian distribution of heat flux. The beam diameter is controlled by changing stand-off distance (*H*) between laser head and worksheet

surface. A mathematical model based on standard beam propagation equations was used to calculate the beam diameter.

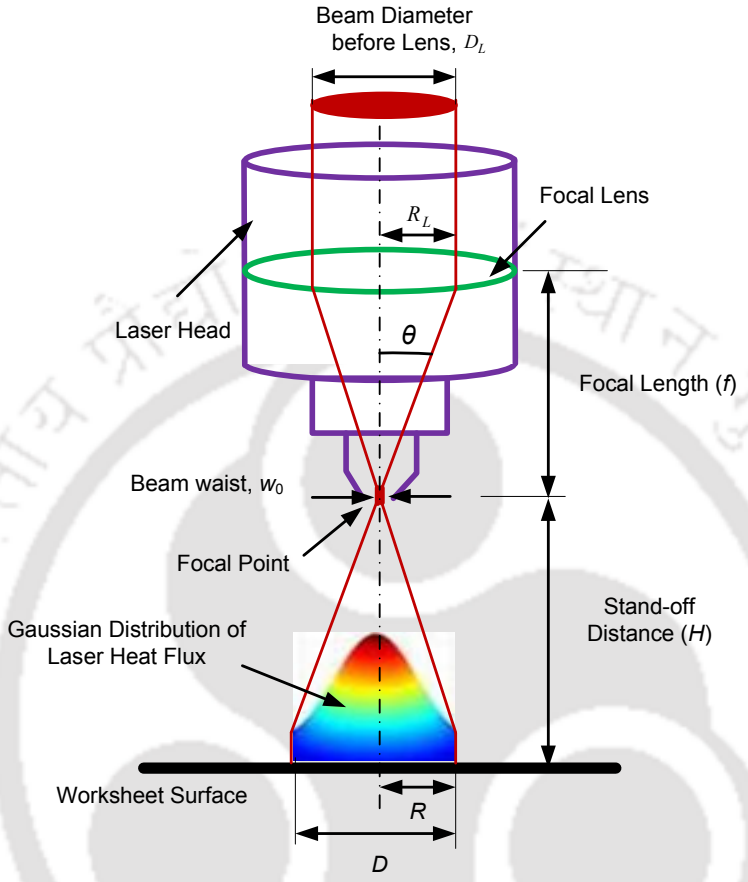

Figure 4.1. Schematic of laser beam profile.

Figure 4.1 shows schematic of the laser beam passing through the focal lens. The beam radius (R) is calculated from the stand-off distance (H) as (Sun 1998)

$$R = w_0\left[1+\left(\frac{M^2\lambda H}{\pi w_0^2}\right)^2\right]^{1/2}, \tag{4.6}$$

where w_0(=0.05 mm) is the laser beam waist which is the minimum beam radius at focal point, λ(=10.6 μm) is the wavelength of CO_2 laser beam, H is the distance between focal point to the worksheet surface and adjusted as equal to the stand-off distance, M^2 is the beam quality factor. It is equal to one for a perfect Gaussian beam but in actual it always has a greater value. The half divergence angle (θ) of the laser beam is given as (Sun 1998)

$$\theta = \frac{M^2 \lambda}{\pi w_0}. \tag{4.7}$$

Multiplying both sides by focal length (*f*), Equation (4.7) becomes,

$$f\theta = \frac{M^2 f \lambda}{\pi w_0} \tag{4.8}$$

where *f*(=127 mm) is the focal length of the lens used in this work. Now $f\theta = R_L$, therefore, Equation (4.8) can be written as

$$w_0 = \frac{M^2 \lambda f}{\pi R_L}, \tag{4.9}$$

where R_L is the laser beam radius before lens. The Equation (4.9) was used to calculate the M^2 and it was found to be 1.4.

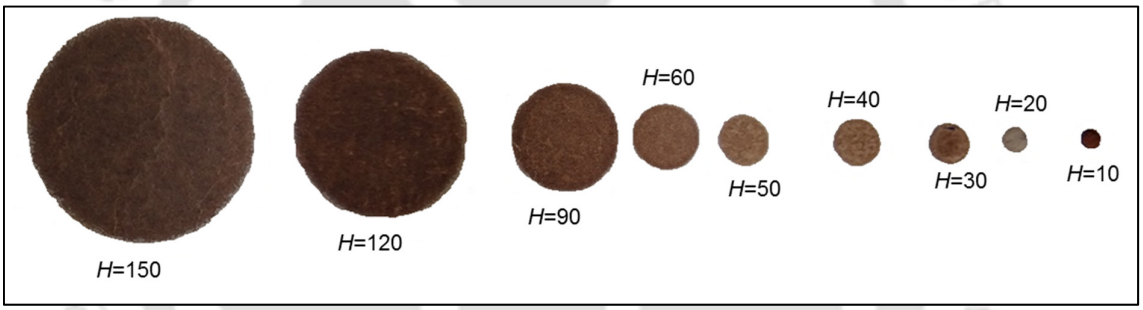

Figure 4.2. Burn prints at various stand-off distances (in mm) on photographic paper.

Table 4.1. Comparison between experimental and numerical laser beam diameter.

S. No.	*H* (mm)	Experimental Beam Diameter, *D* (mm)			Mathematical Value (mm)	Error (%)
		Major Axis	Minor Axis	Average		
1	10	1.989	1.916	1.953	1.938	0.74
2	20	3.898	3.873	3.886	3.872	0.35
3	30	5.852	5.830	5.841	5.807	0.58
4	40	7.5	7.280	7.39	7.743	4.78
5	50	9.903	9.617	9.76	9.678	0.84
6	60	11.691	11.253	11.472	11.337	1.18
7	90	17.546	16.557	17.052	17.006	0.27
8	120	23.528	22.173	22.851	22.674	0.77
9	150	29.355	27.931	28.643	28.342	1.05
***H* = Stand-off Distance**					**Average error = 1.17%**	

Beam diameter obtained from mathematical model was validated by taking burn prints on the photographic paper at various stand-off distances. During this process, the laser power was selected in such a way that a clear circular impression of the laser beam generates on the photographic paper, but the paper does not burn out completely. Images of burn prints on the

photographic paper are shown in Figure 4.2. It can be observed that the burn prints are slightly elliptical in shape. However, the difference between major and minor axes is small, and therefore, the beam can be considered as of circular shape. The measurement of major and minor axes of the laser beam was carried out on an optical surface profile projector. The comparison between experimental and calculated values of the beam diameter is shown in Table 4.1. The average error between experimental and calculated values of beam diameter is about 1.17%. Therefore, it can be concluded that the mathematical results are in good agreement with the experimental results, and Equation (4.6) can be used to compute the beam diameter at various stand-off distances.

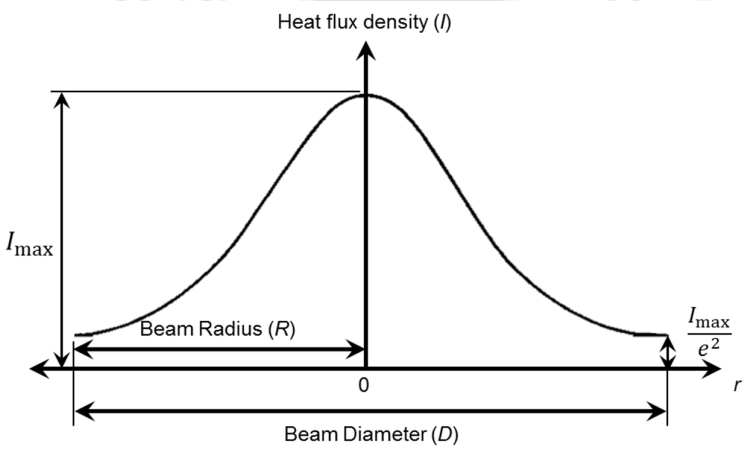

Figure 4.3. Heat flux distribution and beam diameter terminologies.

The heat flux into the laser beam obeys a normal distribution as shown in Figure 4.3. It has peak value (I_{max}) at the center of the beam. The heat flux distribution in Gaussian distributed circular shaped laser beam as a function of beam radius is defined as (Holzer et al. 1994)

$$I(r) = \frac{2\eta P}{\pi R^2} \exp\left(\frac{-2r^2}{R^2}\right), \tag{4.10}$$

where η is the absorptivity, P is the laser power, r is the distance from center of laser beam and R is the effective beam radius which is defined as the radius in which power density is reduced from the peak value (I_{max}) by a factor of the square of natural exponent $(1/e^2)$. The mean heat flux density within the area of laser beam can be calculated as (Hu *et al.* 2001)

$$I_m = \frac{1}{\pi R^2}\int_0^R I(2\pi r)\mathrm{d}r = \frac{2\pi}{\pi R^2}\int_0^R \frac{2\eta P}{\pi R^2}\exp\left(\frac{-2r^2}{R^2}\right) r\mathrm{d}r = \frac{0.865\eta P}{\pi R^2}. \tag{4.11}$$

B. Mechanical analysis: governing equations and boundary conditions

Governing equations

Thermal expansion caused by the laser heating induces thermal stresses in the heated region. These stresses lead to the plastic strains, and further, distortions in the worksheet. Total strain and strain rate can be decomposed into elastic, plastic, creep and thermal components of strain and strain rate. However, deformation occurs at relatively short time scale, and hence, the contribution of creep can be neglected. Total strain rate as a sum of elastic, plastic and thermal strain rate is given as

$$\dot{\varepsilon}_{total} = \dot{\varepsilon}_{elastic} + \dot{\varepsilon}_{plastic} + \dot{\varepsilon}_{thermal} . \tag{4.12}$$

Elastic strains are calculated through isotropic Hook's, law and yielding is determined by using von-Mises criterion as

$$\frac{1}{2}\left[(\sigma_1-\sigma_2)^2+(\sigma_2-\sigma_3)^2+(\sigma_1-\sigma_3)^2\right]=\sigma_y^2, \tag{4.13}$$

where σ_y is the temperature and strain rate dependent flow stress and σ_1, σ_2 and σ_3 are x, y and z components of the stresses, respectively. The material properties are significantly affected by temperature, strain and strain rate. Therefore, temperature, strain and strain rate dependent yielding should be considered in the numerical modeling of laser bending process. The strain rate dependent flow stress is given as

$$\sigma_y = C\dot{\varepsilon}^m \tag{4.14}$$

where C is the strength coefficient and m is the strain rate sensitivity exponent. The C and m are the temperature dependent parameters.

Boundary conditions

To avoid the rigid body movement, one side (clamped side) of the worksheet was fully constrained in mechanical analysis. The boundary conditions of zero displacement and zero rotation were applied on the clamped side of the worksheet. All other sides were free of mechanical boundary conditions.

4.2.3 Solution methodology

After formulating the problem in terms of governing equations and boundary conditions, finite element method (FEM) was used to solve the problem. FEM is a numerical technique to solve

the engineering problems in which the unknown function is approximated by piecewise defined functions. In this technique, the worksheet is discretized into elements. The collection of elements is called finite element mesh. Each element has nodes which are used to represent values of the field variables (for example, temperature, stress, strain, displacement, etc.) over the element by an interpolation function (sometimes called approximating function). FEM is preferred in structural analyses as it has good flexibility to model complex geometries, capability to handle general boundary conditions and variable material properties, availability of user friendly solvers, solid theoretical foundation which adds reliability and makes it possible to mathematically analyze and estimate the error in the approximate solutions.

Finite element formulation of the laser bending process is associated with heat transfer analysis and mechanical analysis. These analyses can be carried out in two ways: (1) sequential analysis, and (2) coupled thermo-mechanical analysis. In sequential thermo-mechanical analysis the temperature distribution does not depend on stress-strain solutions. The temperature distribution is calculated from the heat transfer analysis and the solution (*i.e.* temperature distribution) is applied as thermal loads for the mechanical analysis. In coupled analysis, it is assumed that the temperature distribution depends on stresses and deformation obtained in the mechanical analysis. Deformation and stresses also depend on the temperature distribution generated during each step of the solution. The coupled analysis is more realistic and represents the actual behavior.

4.3 Finite Element Formulation

In finite element method, the geometry considered for analysis is first discretized into finite number of small elements. The governing equation and boundary conditions are expressed in the form of a set of algebraic equations. Details of FEM formulation is given as below:

4.3.1 Continuum discretization

Laser bending process includes large strains in the heated region. Therefore, to account for large deformation 3-D eight-node or twenty-node brick elements should be used. The eight–node solid element consumes less computational time and provides significantly accurate results, and hence, mostly preferred in numerical modeling of the laser bending process (Chen et al. 1999, Li and Yao 2001, Jamil et al. 2011a,b, Stevens et al. 2012). The shape function of 3-D eight-node brick element is given as

$$u=\frac{1}{8}[u_1(1-\xi_1)(1-\xi_2)(1-\xi_3)+u_2(1+\xi_1)(1-\xi_2)(1-\xi_3)+u_3(1+\xi_1)(1+\xi_2)(1-\xi_3)+u_4(1-\xi_1)(1+\xi_2)(1-\xi_3)+$$
$$u_5(1-\xi_1)(1-\xi_2)(1+\xi_3)+u_6(1+\xi_1)(1-\xi_2)(1+\xi_3)+u_7(1+\xi_1)(1+\xi_2)(1+\xi_3)+u_8(1-\xi_1)(1+\xi_2)(1+\xi_3)+$$
$$a_1(1-\xi_1^2)+a_2(1-\xi_2^2)+a_3(1-\xi_3^2)]$$

$$v=\frac{1}{8}\left[v_1(1-\xi_1)(1-\xi_2)(1-\xi_3)+.....(\text{Analogous to } u)\right]$$

$$w=\frac{1}{8}\left[w_1(1-\xi_1)(1-\xi_2)(1-\xi_3)+.....(\text{Analogous to } u)\right] \quad (4.15)$$

Using summation operator, the above equations can be written as

$$u=\sum_{i=1}^{8}N_iu_i+a_1(1-\xi_1^2)+a_2(1-\xi_2^2)+a_3(1-\xi_3^2)$$

$$v=\sum_{i=1}^{8}N_iv_i+a_4(1-\xi_1^2)+a_5(1-\xi_2^2)+a_6(1-\xi_3^2)$$

$$w=\sum_{i=1}^{8}N_iw_i+a_7(1-\xi_1^2)+a_8(1-\xi_2^2)+a_9(1-\xi_3^2) \quad (4.16)$$

In the above equations u_i, v_i and w_i are the nodal degrees of freedom, *i.e.* nodal displacements and a_i are the generalized degrees of freedom. They may also be called "node less" degree of freedom. Displacement nodes associated with a_i are called "incompatible" or "non-conforming" because at locations other than nodes, they allow overlaps or gaps between adjacent elements.

4.3.2 Thermal analysis

The temperature field variable with the element is interpolated by,

$$T=[N]\{T_e\}, \quad (4.17)$$

and

$$T_{,x}=[B]\{T_e\}=\left[\frac{\partial}{\partial x}N\right]\{T_e\}, \quad (4.18)$$

where [N] is the interpolation or shape function matrix, $\{T_e\}$ is the element nodal temperature matrix and [B] is the general geometric matrix. Galerkin method is used to solve the above equations, and the resulting equations are expressed in the matrix form as

$$[C]\{T\}+[K_T]\{T\}=\{Q\}, \tag{4.19}$$

where $[C]$ and $[K_T]$ are the global heat capacity matrix and global conductivity matrix respectively, and are given as

$$[C]=\int_V \rho c[N][N]^T \mathrm{d}V, \tag{4.20}$$

$$[K_T]=\int_V k[B][B]^T \mathrm{d}V, \tag{4.21}$$

and $\{Q\}$ is the heat flux vector. Equation (4.19) are solved by Newton-Raphson method.

4.3.3 Mechanical analysis

In order to analyze the movement and the deformation of worksheet, the incremental form of virtual work is applied. According to the virtual work principle;

$$\int_V \sigma_{ij}\delta\varepsilon \mathrm{d}V=\int_V F_i\delta u_i \mathrm{d}V+\int_S P_i\delta u_i \mathrm{d}S \tag{4.22}$$

The above equation can be written as

$$\int_V \{\delta\varepsilon\}^T\{\sigma\}\mathrm{d}V=\int_V \{\delta u\}^T\{F\}\mathrm{d}V+\int_S \{\delta u\}^T\{P\}\mathrm{d}S \tag{4.23}$$

where $\{\delta\varepsilon\}$ is the strain vector, $\{\delta u\}=\lfloor \delta u\ \delta v\ \delta w \rfloor^T$ is the virtual displacement. The symbol δ has the same meaning as d for differential, but the convention δ is used when displacement is virtual. $\{F\}$ is the body force in volume V and $\{P\}$ is the surface tractions on surface S. The displacements $\{u\}$ are interpolated over an element as

$$\{u\}=[N]\{d\} \tag{4.24}$$

where $\{u\}=\lfloor u\ v\ w \rfloor^T$ and $\{d\}$ is the nodal displacement degree of freedom of an element. Strains are determined from displacement as

$$\{\varepsilon\}=[B]\{d\}, \tag{4.25}$$

where $[B]=[\partial][N]$. A discretization of this problem using standard finite element procedure and assembling we obtain a group of non-linear equations which are written in matrix form as

$$[K]\{\Delta u\}=\{F\}, \tag{4.26}$$

where $[K] = \int_V [B]^T [D^{eq}][B] \mathrm{d}V$ is the global tangential stiffness matrix, $[D^{eq}]$ is the elasto-plastic stress-strain matrix, and also called constitutive matrix, $\{\Delta u\}$ is the displacement incremental vector at the element nodes, and $\{F\}$ is the global force vector, including nodal force and force caused by the thermal strain.

$$\{F\} = \{F^a\}\{F^{nr}\}, \tag{4.27}$$

where $\{F^a\}$ is the external applied force vector and $\{F^{nr}\}$ is the internal force vector (sum of element stresses).

In coupled thermo-mechanical analysis both temperature and strain are calculated simultaneously. For coupled analysis, the basic equations of temperature (Equation 4.19) and displacement (Equation 4.26) used in sequentially coupled thermo-mechanical analysis are combined as

$$\begin{bmatrix} [0] & [0] \\ [0] & [C] \end{bmatrix} \begin{Bmatrix} u \\ T \end{Bmatrix} + \begin{bmatrix} [K] & [0] \\ [0] & [K_T] \end{bmatrix} \begin{Bmatrix} u \\ T \end{Bmatrix} = \begin{Bmatrix} \{F\} \\ \{Q\} \end{Bmatrix}. \tag{4.28}$$

This is the main governing equation for coupled thermo-mechanical analysis, and can be solved either by writing a computer code or by using commercially available software. In view of the time requirement in development of the computer code, it was thought appropriate to employ a commercial code with basic understanding of the finite element method. Therefore, a numerical model for the laser bending of magnesium alloy M1A was developed in commercially available finite element solver ABAQUS™. Details regarding development of numerical model are presented in the next section. Before carrying out the comprehensive analysis of the laser bending process, the numerical results were validated with those obtained in experiments. The validated numerical model was further used to study the laser bending process.

4.4 Development of Numerical Model for Laser Bending of Magnesium Alloy M1A Using FEM

A coupled thermo-mechanical numerical model is developed in ABAQUS™ where temperature and distortions were computed simultaneously. The distortions were used to analyze the bend angle and the edge effect. Inputs, outputs and various modules of numerical simulations are shown in Figure 4.4.

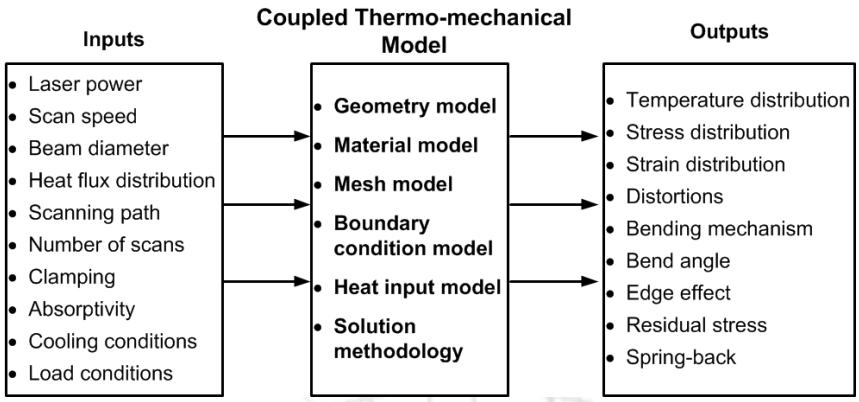

Figure 4.4. Schematic of coupled thermo-mechanical numerical model.

The development of general continuum problem using FEM follows an orderly step–by–step procedure, which is outlined below.

1. Worksheet geometry was modeled. Temperature dependent and strain rate dependent material properties were assigned to the worksheet. Details are given in Section 4.4.1.
2. Initial conditions, thermal boundary conditions such as convection heat flow, radiation heat flow and laser heat input were applied. Mechanical constraints for the clamping were also applied. Details are given in Section 4.2.2.
3. The energy parameters: laser power, scan speed, beam shape, beam size, heat flux distribution, and scanning path were employed by using a user subroutine DFLUX. The FORTRAN code was written to define these inputs. It is given in Appendix 4.1. Relevant information is presented in Section 4.2.2.
4. Worksheet domain is discretized with eight node hexahedral elements C3D8T. The irradiated and nearby regions were discretized with fine mesh so that accurate results can be obtained. Remaining region was discretized with coarse biased mesh to reduce the simulation time. The mesh sensitivity analysis was carried out to optimize the discretization. Various details of the discretization and mesh sensitivity analysis are given in Section 4.4.2.
5. Transient coupled temperature-displacement solution was carried out by adopting an automatic time step increments. The solution scheme is presented in Section 4.4.3 in details.
6. Solver computed the temperature, stress, strain and distortion at each node of domain at the end of the analysis. The node outputs were used to analyze the process. A case study to demonstrate the simulation by using the developed model is presented in Section 4.5.

4.4.1 Worksheet material and geometry

To carry out numerical simulations, a flat worksheet of dimensions 60 mm length, 40 mm width and 1.9 mm thickness was used. The temperature and strain rate dependent mechanical and thermal properties of magnesium alloy M1A sheets were employed. The temperature dependent material properties of the material are shown in Table 4.2 and Table 4.3. The melting temperature of magnesium alloy M1A is about 650 ºC. The stiffness of material decreases with the increase in temperature, and it reduces to a negligible at the melting point. Therefore, localized stiffness in the heated material is considered as negligible, once the temperature exceeds the melting point. This condition is implemented by employing a negligible yield strength and elastic modulus after exceeding the melting temperature of 650 ºC. The yield strength (MPa) and elastic modulus (GPa) both were considered as 10^{-6} after exceeding melting temperature as shown in Table 4.2.

Table 4.2. Temperature and strain rate dependent mechanical properties of magnesium alloy M1A (Data source: Avedesian and Baker 1999).

S. No.	Temperature (ºC)	Tensile Yield Strength (MPa) at Strain Rate per Minute				Elastic Modulus (GPa)	Poisson's Ratio
		0.005	0.05	0.5	5		
1	24	171	181	191	201	44	0.35
2	93	137	150	163	177		
3	149	82	107	133	163		
4	204	52	69	86	119		
5	260	33	46	58	83		
6	316	26	32	40	55		
7	371	18	23	29	34		
8	427	15	18	21	23		
9	482	10	12	14	21		
10*	650	10^{-6}	10^{-6}	10^{-6}	10^{-6}	10^{-6}	

*Assumed values after melting temperature

Table 4.3. Thermal and physical properties of magnesium alloy M1A (Data source: Avedesian and Baker 1999).

S. No.	Temperature (ºC)	Specific Heat (kJ/kg-ºC)	Coefficient of Thermal Expansion (µm/m-ºC)	Density (kg/m³)	Thermal Conductivity (W/m-ºC)
1	20	1.04	0.000025376	1730	138
2	100	1.042	0.00002688		
3	300	1.148	0.00003064		
4	550	1.338	0.00003534		
5	650	1.414	0.00003534		

4.4.2 Mesh model

The worksheet continuum was discretized with three-dimensional linear hexahedron eight node elements. The elements 'C3D8T' which are specially meant for the coupled thermo-mechanical analysis were used for the discretization. Mesh sensitivity analysis was carried out to mesh the worksheet for accurate prediction of the laser bending process in an optimum time frame. The heated and nearby region was discretized with uniform fine mesh. To reduce the computational time, outer region was discretized with coarse biased mesh. The worksheet geometry was fine meshed around the beam for more than 2 mm. In thickness direction, the uniform mesh was used. The meshing scheme is shown in Figure 4.5.

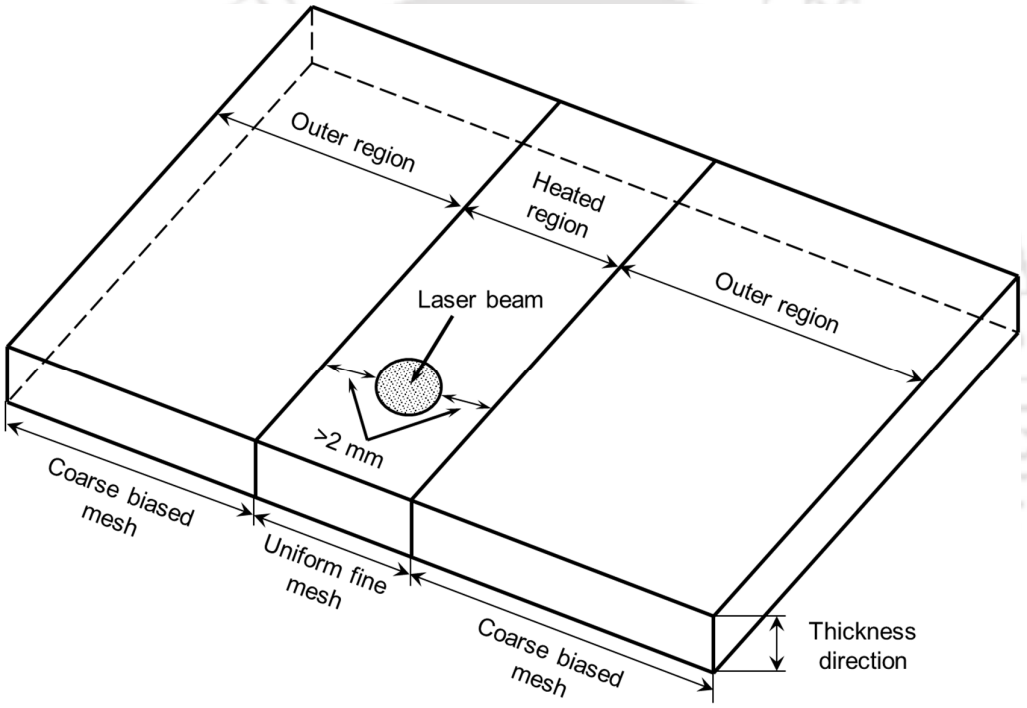

Figure 4.5. Schematic of the worksheet meshing.

Table 4.4. Results of the mesh sensitivity analysis for the fine mesh in the heated region.

S. No.	Length × Width	Bend angle	Change in bend angle %	CPU time (hrs)
1	2 X 2 mm	0.987	-	1.473
2	1.5 X 1.5 mm	1.098	-11.171	1.599
3	1 X 1 mm	1.079	1.656	4.146
4	0.75 X 0.75 mm	1.106	-2.441	6.315
5	**0.5 X 0.5 mm**	**1.092**	**1.284**	**11.361**

The mesh sensitivity analysis was carried out for a typical process condition: laser power=300 W, scan speed=1000 mm/min and beam diameter=3.87 mm. Table 4.4 shows the

various sizes of the element used to discretize the heated domain. It was found that the change in bend angle is the lowest, when the element size reduces from 0.75 mm × 0.75 mm to 0.5 mm × 0.5 mm in comparison with those obtained in other cases. Therefore, the element size of 0.5 mm × 0.5 mm was chosen for the discretization of heated region.

Table 4.5. Results of the mesh sensitivity analysis for coarse biased mesh in the outer region.

S. No.	No. of elements	Bend angle	Change in bend angle %	CPU time (hrs)
1	1	1.005	-	4.078
2	2	1.100	-9.376	4.576
3	3	1.098	0.160	5.292
4	5	1.094	0.370	6.588
5	7	1.093	0.109	8.258
6	9	1.092	0.038	10.401

Table 4.5 shows the results of mesh sensitivity analysis for the outer region where coarse biased mesh was used. It can be seen that the bend angle is significantly affected when the number of elements increases from one to two. However, further increment in the number of elements does not affect the bend angle significantly. During preliminary simulations, it was also observed that for some sets of process condition, the simulations were aborted for less number (2–4) of elements, therefore, in the present work, the number of elements in the outer region were taken from five to nine.

Table 4.6. Mesh sensitivity study for number of elements in thickness direction.

S. No.	No. of elements	Bend angle	Change in bend angle %	CPU time (hrs)
1	1	0.002	-	0.679
2	2	1.109	-68466.645	2.261
3	3	1.093	1.392	4.874
4	**4**	**1.092**	**0.134**	**9.011**
5	5	1.091	0.032	16.412

Table 4.6 shows the mesh sensitivity analysis for the number of elements in the thickness direction. It can be seen that the numerical model predicted a negligible bend angle when there was only one element in the thickness direction. However, further increase in the number of elements, a significant bend angle was observed. When the number of elements in thickness direction increases from 4 to 5, a marginal variation in bend angle takes place while the simulation time is increased from 9 to 16.4 hours.

Thus, based on the mesh sensitivity analysis, the heated and nearby region was discretized with uniform fine mesh of element size 0.5 mm. The outer region was discretized with coarse biased mesh, and equidistant four elements were taken in the thickness direction. A typical mesh model of the worksheet is shown in Figure 4.6.

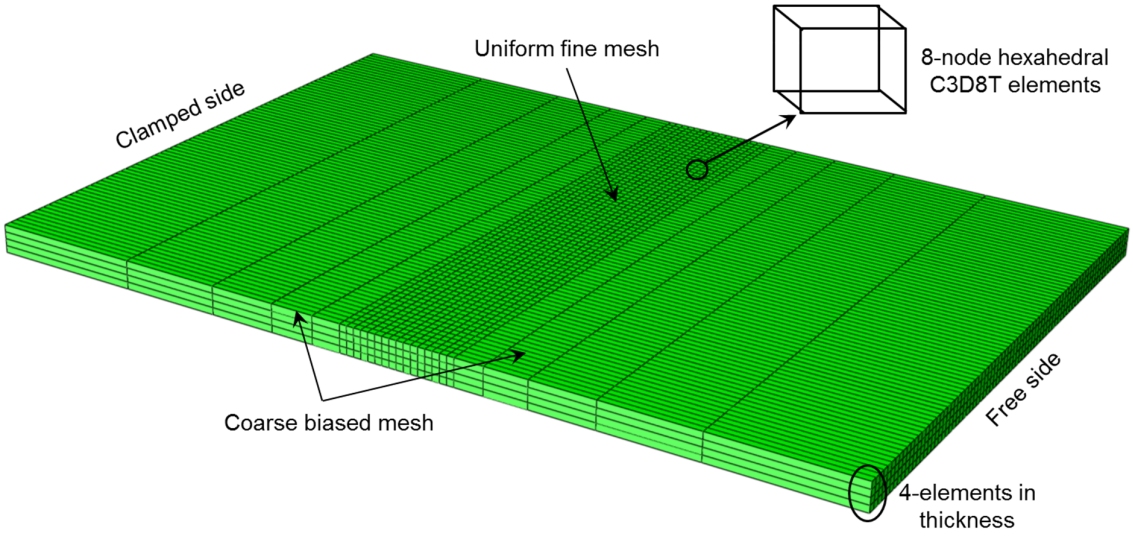

Figure 4.6. The worksheet mesh model.

4.4.3 Solution parameters

In the present work, for solving the thermo-mechanical laser bending problem, the automatic (self-adaptive) time step algorithm was used to select the time increment in a step. This is based on the tolerance in the maximum temperature change allowed in a time increment. In automatic time step algorithm, the increment is adjusted based on the maximum temperature change in a time step and the corresponding convergence rate.

Table 4.7. Sensitivity analysis for optimal time step increment.

S. No.	Maximum change in temperature in a step	Bend angle	Change in bend angle %	CPU time (hrs.)
1	5	1.091540862	-	14.72
2	10	1.09166224	0.01	7.13
3	20	1.091665752	0.00	2.61
4	30	1.091255551	-0.04	1.81
5	50	1.089384586	-0.17	1.27
6	70	1.087188941	-0.20	1.02
7	100	1.08720017	0.00	1.01

The effect of maximum permissible temperature change in a step was studied by carrying out the sensitivity analysis for a typical process condition: laser power=300 W, scan

speed=1000 mm/min and beam diameter 3.87 mm. The maximum temperature change in a step was varied from 5 to 100 °C and its effect on the bend angle was analyzed. This is shown in Table 4.7. It can be observed that the maximum temperature change in a step marginally affects the bend angle, however it significantly affects the simulation time. The maximum temperature change in a step was chosen from 10–50 °C. The maximum and minimum time steps size were taken as 0.02 and 0.0005 second, respectively. The equations solved in coupled thermo-mechanical analysis are equations of motion and heat conduction equation. These equations were solved by Full Newton technique. In this technique, the target stiffness matrix is evaluated at each iteration. This helps in getting proper convergence even when the guess value is far away from the solution. Also, the stiffness matrix is more accurate in each iteration which provides a better prediction accuracy. However, computationally, it is not as efficient as Modified Newton method, in which sometimes, convergence is not achieved (Bathe 1996).

4.5. A Case Study on Numerical Simulation of Laser Bending Process Using FEM

After the development of numerical model, it was tested for the predictions/results. The worksheet geometry, material properties, meshing and solution scheme were implemented as discussed in Section 4.4. In the heated region, elements of size 0.5 mm × 0.5 mm were taken, and in the outer region a coarse biased mesh with total five number of elements was modeled. The bias ratio of the biased mesh was five. Total four equidistance elements were taken in the thickness direction. As per this meshing scheme, the geometry was discretized into 8320 number of elements and 10935 number of nodes. The solution was carried out with automatic time step with maximum 10 °C increment in temperature in a step. The maximum time step was taken as 0.2 second, and the minimum time step was taken as 0.005 second.

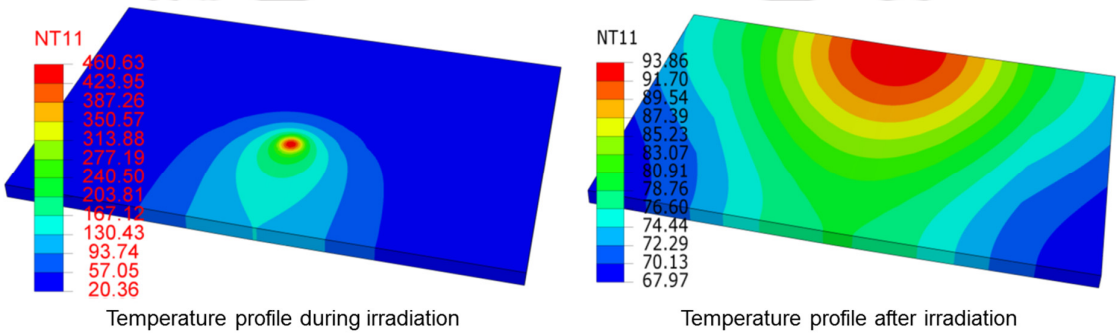

Figure 4.7. Temperature contour induced by the laser scan.

This case study was carried out for a typical process condition: laser power=300 W, scan speed=1000 mm/min and laser beam diameter=3.87 mm. The thermo-mechanical

numerical model was able to predict temperature distribution, stress-strain distributions and distortions. Figure 4.7 shows the temperature contours obtained during laser scan. It can be seen that the highest temperature occurs in the beam diameter region. The temperature distribution is symmetric about the irradiation line.

The increase in temperature generates thermal stresses in the heated region. Figure 4.8 shows contours of the various components of thermal stresses induced due to the laser scan. It can be seen that thermal stresses are not symmetric about the irradiation line. It is due to clamping on one side the worksheet. The clamping provides external mechanical constraint which results in the generation of thermal stresses.

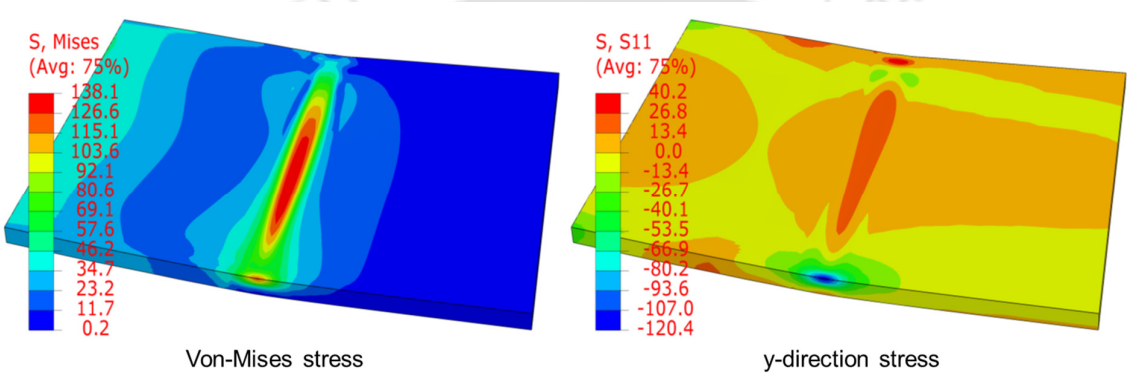

Figure 4.8. Thermal stresses contour induced by laser scan.

When induced thermal stresses exceed temperature dependent flow stress, the plastic deformation occurs. The contours for various components of plastic strains induced due to laser scan are shown in Figure 4.9. It can be seen that the plastic deformation is concentrated in the irradiated region. It justifies the use of fine mesh in the heated region and coarse biased mesh in the outer region.

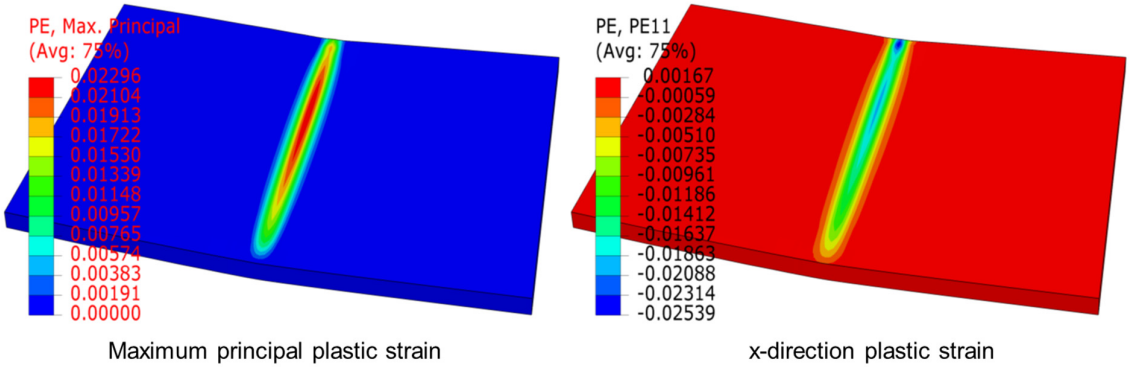

Figure 4.9. Plastic strains contour induced by laser scan.

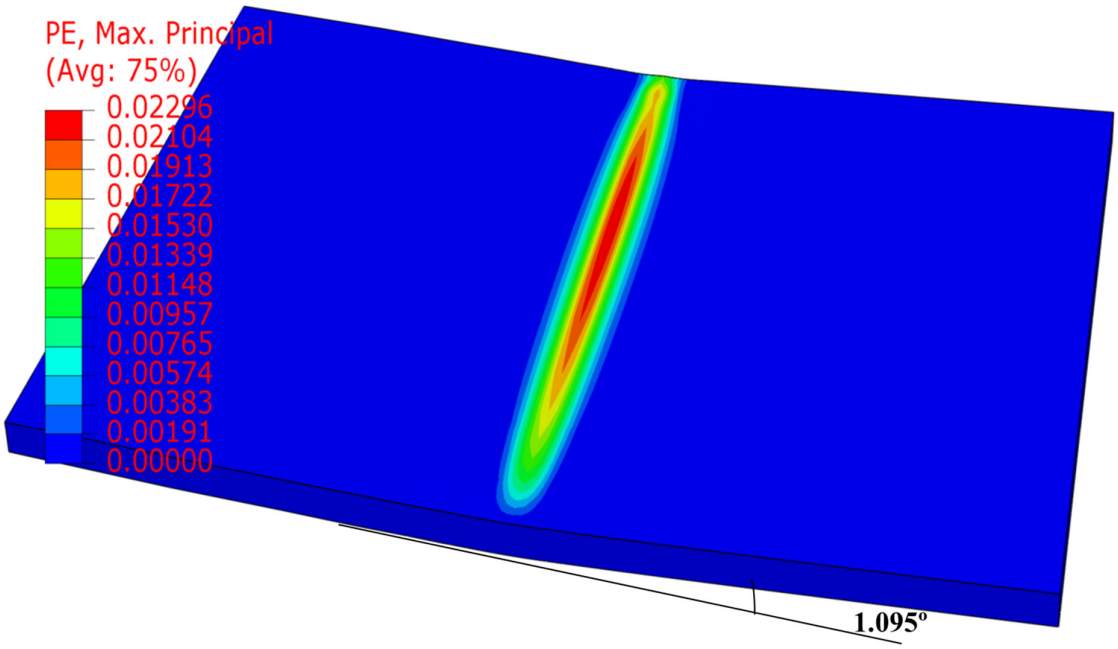

Figure 4.10. Laser bent worksheet.

The plastic strain generated due to laser scan produces distortions in the heated region. These distortions result in the worksheet bending. The bending profile generated by laser scan is shown in Figure 4.10.

The bend angle generated by laser scanning was measured by taking two points on each side of the scan line. These points formed two lines on both sides of the laser scanning line and the bend angle was measured between these two lines. Details of the bend angle measurement scheme is given in Section 3.3.3. The bend angle was not uniform along the laser scan line, and it varied from one end to another end as shown in Figure 2.5. This is called edge effect. Details of the edge effect are discussed in Section 2.2. The edge effect can be quantified by measuring the bend angle at five equidistance positions along the scanning line as shown in Figure 4.11. In the present work, the edge effect was quantified by calculating the relative variation in bend angle (*RVBA*) per unit length measured at five equidistant positions along the scan line as

$$RVBA\ (\mathrm{mm}^{-1}) = \frac{1}{L}\left(\frac{\theta_{\max} - \theta_{\min}}{\theta_{average}}\right), \tag{4.29}$$

where $\theta_{\max}$, $\theta_{\min}$ and $\theta_{average}$ are the maximum, minimum and average bend angle along the scanning line respectively, and L is the length of worksheet. The edge effect is more when the value of *RVBA* is higher, and vice-versa.

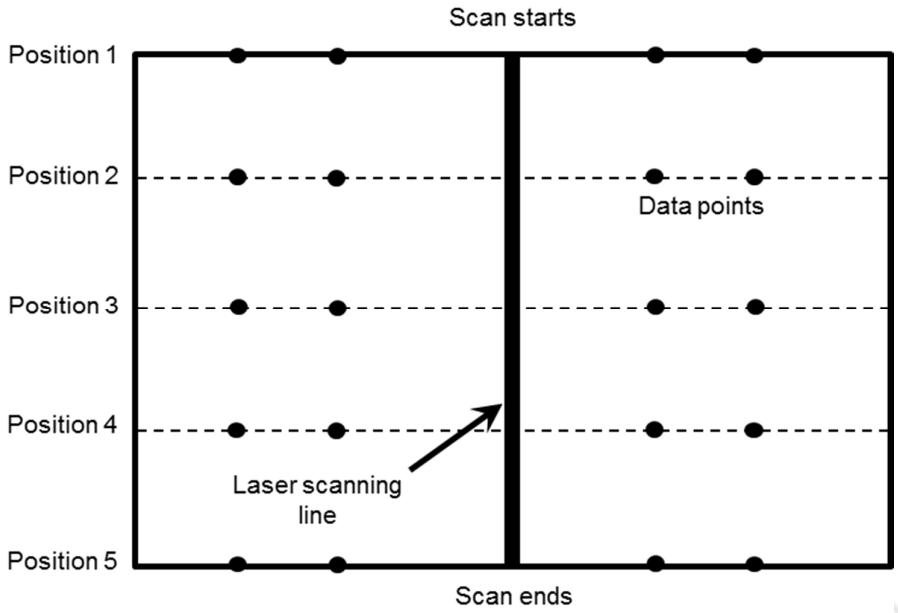

Figure 4.11. Bend angle positions to calculate the edge effect.

The bend angle predicted by using the numerical simulation was compared with that obtained in experiment. Details of the experimental procedure are reported in Chapter 3. In experiments three trials were carried out for the process condition: P=300 W, V=1000 mm/min and D=3.87 mm. Bend angles of about 1.007º, 1.106º and 1.094º was obtained in the three trials respectively, and the average of these three values (1.069º) was considered as the experimental result. It was observed that the numerical bend angle has an error of about 2.4% in comparison with that of the experimental bend angle. Therefore, it can be concluded that the numerical model predicts the bend angle quite accurately for the chosen process condition.

The case study shows that numerical model can simulate the laser bending process well. It is capable to predict the bend angle and edge effect based on the temperature distribution, stress-strain distributions, and distortions obtained during numerical computations. Predictions of the developed numerical model are validated with those obtained in the experimental studies for various cases of laser bending such as single scan, curvilinear, multi-scan, and with moving pre-displacement. Parametric studies have also been carried out using the developed numerical model. These are presented at length in the next chapters.

4.6. Summary

This chapter presented, in details, the development of a numerical (FEM) model for laser bending process. The three-dimensional non-linear coupled thermo-mechanical numerical

model for the laser bending of magnesium alloy M1A sheet is developed by using finite element method. Gaussian distributed continuous wave moving heat source is modeled and applied over the worksheet surface. Laser beam diameter is a critical parameter which affects the process significantly. A methodology to calculate the beam diameter using stand-off distance was presented. The presented methodology was experimentally validated by taking burn prints on the photographic papers and was found to be in good agreement. The convection and radiation heat loss were considered. The temperature and strain rate dependent material properties of magnesium alloy M1A were employed. The effect of melting was incorporated which made the developed model more realistic and suitable for a wide range of process conditions. Mesh sensitivity analysis was carried out for precise prediction accuracy over a range of process conditions. The governing equations and solution methodology was presented in details. A case study was carried out to see capabilities of the numerical model. The developed model was able to simulate the laser bending process. It was capable to predict the temperature distribution, stress-strain distributions, and distortions. Distortions can be used to calculate the bend angle and edge effect. The methodology to calculate the bend angle and edge effect were also discussed in details. The developed numerical model was validated with the experimental results and found to be in good agreement.

The next chapter presents experimental validation of the developed numerical model for straight line single scan laser bending of the magnesium alloys. The bending mechanism and the effect of process parameters on bend angle and edge effect are presented in details for laser bending of magnesium alloy.

CHAPTER 5: SINGLE SCAN STRAIGHT LINE LASER BENDING OF MAGNESIUM M1A ALLOY SHEETS

5.0 Scope

This chapter presents numerical studies on the single scan straight line laser bending of magnesium alloy sheets. The need to carry out investigations on the single scan laser bending is defined. Predictions of the developed numerical model have been validated with those obtained in experimental studies. Parametric studies based on the validated numerical model are presented. Effects of laser power, scan speed and beam diameter on the bend angle and edge effect are discussed at length. At last the conclusions are summarized.

5.1 The Need

Based on the feasibility experimental study carried out in this work, it was observed that the laser bending can be used for the micro as well as macro bending of the magnesium alloy sheets. The single scan laser bending produces bend angle of the order of 1°. This is called laser micro-bending. Laser bending is controlled by a number of interacting process parameters related to the laser irradiation, worksheet material, and worksheet geometry. These parameters have complex non-linear interactive effect on the performance of the laser bending process. Thus, a need was identified to carry out the parametric study of the laser bending process to produce precise micro-bend angles.

Literature reports that there may be the existence of the combination of two bending mechanisms during laser bending operation. However, very scant research is reported on the deformation behavior during transition between two mechanisms. It is thus important to explore the transition between two bending mechanisms. This information can be utilized to select the proper process conditions to obtain the desired stress-strain distribution, which will help in the enhancement of the process efficiency.

5.2 Experimental Validation of Numerical Simulations for Single Scan Laser Bending

In the present work, a three-dimensional non-linear thermo-mechanical numerical model is developed by using finite element method. Details regarding the governing equations, boundary conditions and solution methodology are presented in Chapter 4. In this chapter a parametric study on the effects of process parameters, such as laser power, scan speed, beam diameter on the bending mechanism, bend angle and edge effect is presented. Before carrying

out the simulations, the numerical model is validated by comparing the prediction results of the developed model with those obtained in experimental studies for similar process conditions.

Details of the experiments, such as experimental equipment, procedure, specimen preparation, bend angle, edge effect measurement methodology are presented in Chapter 3. Experiments were carried out with full factorial design of experiments. Figure 5.1 shows single scan straight line laser bent specimens for some typical sets of process conditions. It can be observed that a micro-bend angle is produced about the scanning line axis due to the laser beam irradiation. Also, the coating is damaged due to laser heating.

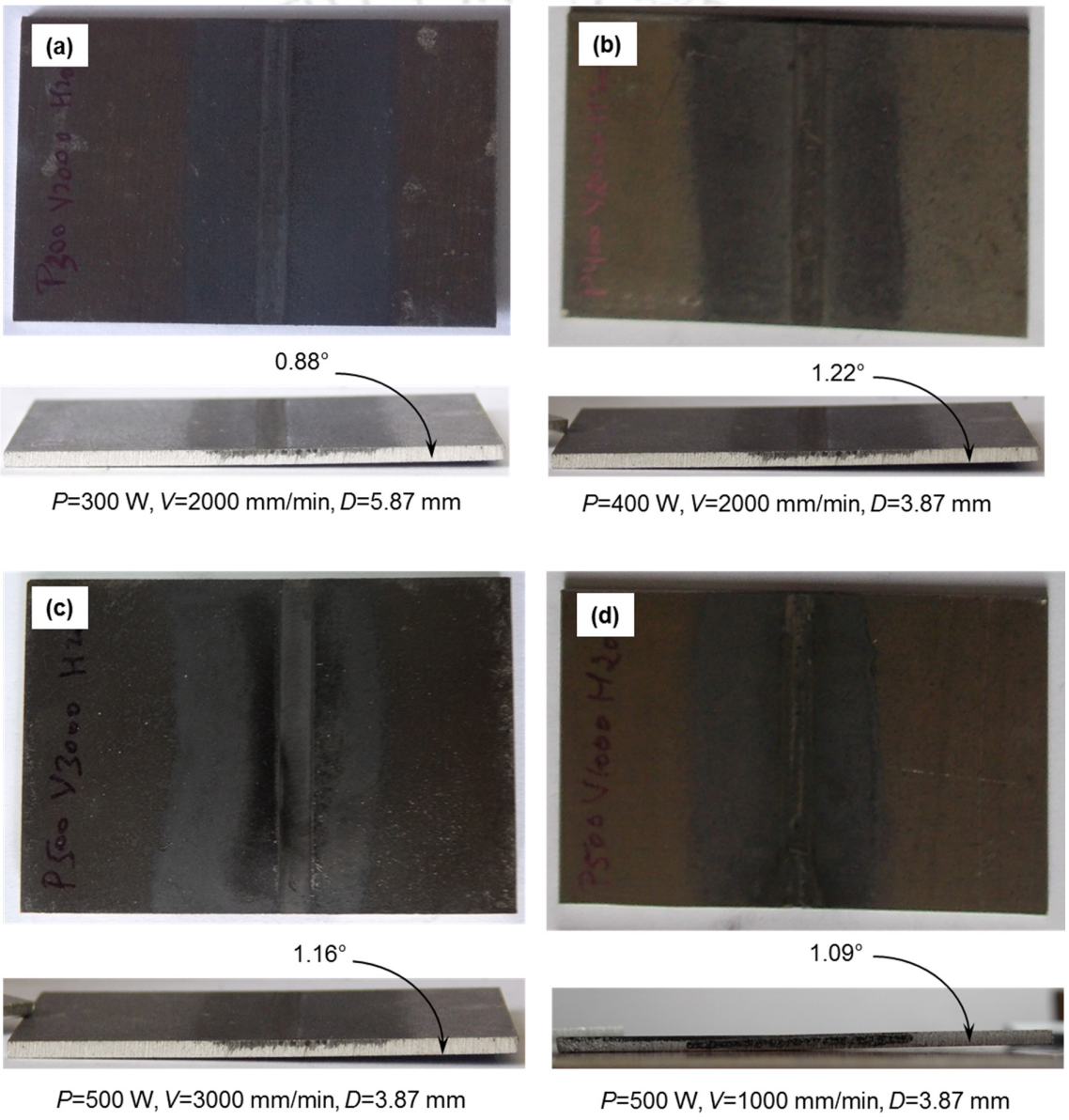

Figure 5.1. Laser bent specimens with straight line single scan laser bending process.

The process conditions and respective numerical and experimental results are presented in Table 5.1. Based on the comparison of results, it can be concluded that the numerical results are in good agreement with the experimental results. A bar chart of the dataset number and absolute error between numerical and experimental results is shown in Figure 5.2. The process conditions for the dataset number are given in Table 5.1. It can be seen that the numerical model is able to predict the bend angle within the error band of 1.76–24.47%. The average absolute error is about 10.88%, which can be considered as reasonably good for carrying out the numerical simulations for further study. The detailed analysis on the effect of process parameters on the bend angle is presented in Section 5.4.

Table 5.1. Comparison between numerical and experimental results.

Dataset No.	*P* (W)	*V* (mm/min)	*D* (mm)	Average Experimental Bend Angle (º)	*CV* (%)	Numerical Bend Angle (º)	Absolute Error (%)
1	300	1000	3.87	1.069	4.113	1.095	2.389
2	300	1000	5.81	0.731	3.137	0.718	1.769
3	300	1000	7.74	0.490	4.602	0.396	19.172
4	300	2000	3.87	0.836	3.961	0.932	11.511
5	300	2000	5.81	0.312	3.772	0.334	7.065
6	300	2000	7.74	*	*	0.083	*
7	300	3000	3.87	0.604	19.306	0.550	8.984
8	300	3000	5.81	0.139	18.621	0.105	24.472
9	300	3000	7.74	*	*	0.011	*
10	400	1000	3.87	1.281	6.365	1.250	2.461
11	400	1000	5.81	0.836	13.404	0.974	16.527
12	400	1000	7.74	0.771	7.096	0.739	4.228
13	400	2000	3.87	1.305	9.693	1.465	12.257
14	400	2000	5.81	0.766	3.911	0.860	12.286
15	400	2000	7.74	0.437	22.171	0.404	7.462
16	400	3000	3.87	1.113	10.989	1.158	3.994
17	400	3000	5.81	0.418	11.782	0.399	4.348
18	400	3000	7.74	*	*	0.098	*
19	500	1000	3.87	0.993	7.311	1.113	12.017
20	500	1000	5.81	0.940	1.441	1.053	12.054
21	500	1000	7.74	0.753	18.690	0.872	15.836
22	500	2000	3.87	1.425	15.450	1.591	11.674
23	500	2000	5.81	1.003	7.579	1.161	15.776
24	500	2000	7.74	0.721	13.982	0.709	1.760
25	500	3000	3.87	1.268	6.633	1.571	23.930
26	500	3000	5.81	0.838	15.930	0.771	8.018
27	500	3000	7.74	0.345	12.288	0.272	21.137
***=insignificant bend angle (<0.1°)**					**Average absolute error =**		**10.880**

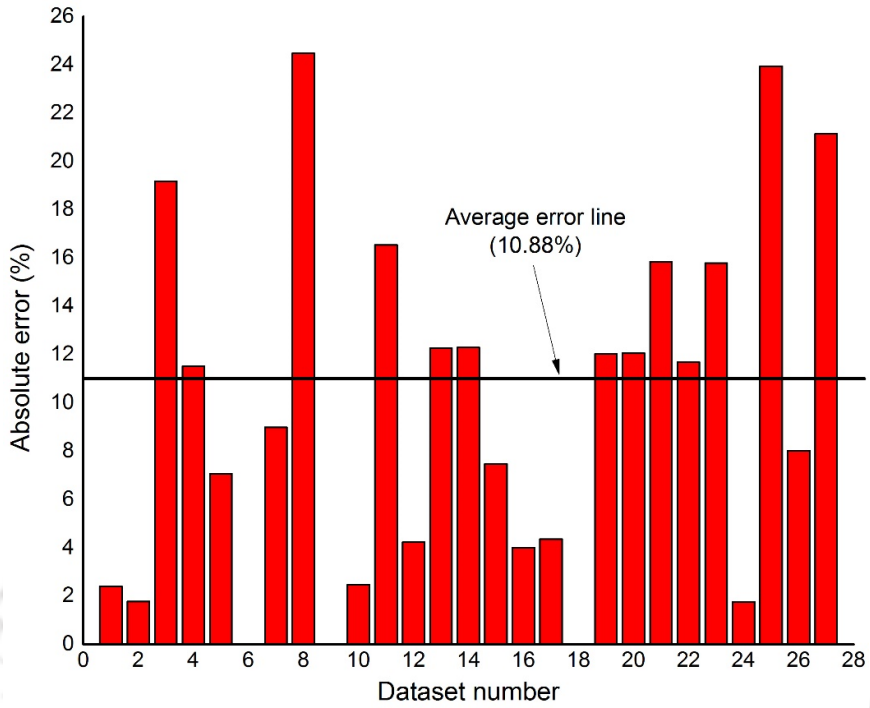

Figure 5.2. Absolute error for various dataset number.

Based on the confidence gained in the validation studies, the developed model was further used to investigate the straight line laser bending process. A study on the bending mechanism and the effect of various process parameters on deformation behavior is important for an efficient and quality laser bending process. This is presented in the following sections.

5.3 Bending Mechanism

Laser bending mechanism is important to understand in view of the non-linear and complex interaction of its process parameters, material parameters with temperature distribution, stress-strain distribution, and distortions. In this section an effort has been made to explain the dominating mechanism during laser bending of magnesium alloy M1A sheets. Using developed numerical model, the effects of process parameters, *viz*. laser power, scan speed and beam diameter on temperature distribution and stress-strain distribution are discussed.

5.3.1 Temperature distribution

Laser beam is irradiated, and the incident energy gets absorbed by the worksheet surface. It generates non-uniform temperature distribution, and stress-strain distribution into the worksheet. Figure 5.3 to Figure 5.5 show the temperature history at middle of the scanning surface (Point A) and at middle of the opposite surface (Point B) for various sets of process conditions. It can be seen that a steep temperature gradient occurs between top and bottom

surfaces. The temperature is higher at the top surface compared to the bottom surface which confirms the temperature gradient mechanism (Shi et al. 2006 a, b). The temperature gradient will be more at a faster scan speed. Therefore, the process is TGM dominating for the chosen process conditions. It can be observed that the peak temperature at the bottom surface has a marginal delay as compared with the top surface. It is because the laser is irradiated over the top surface and the heat energy takes some time to reach to the bottom surface through thermal conduction.

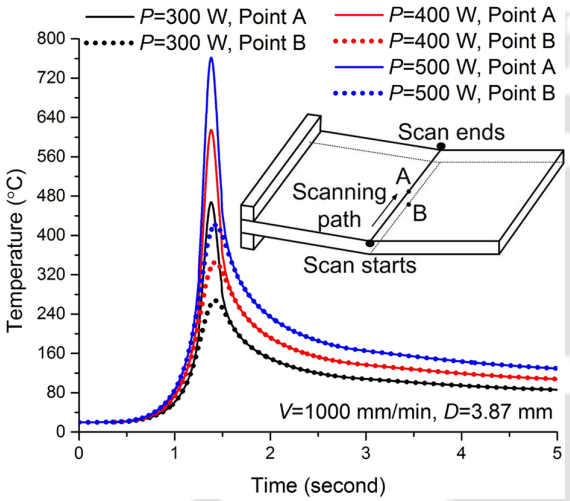

Figure 5.3. Effect of laser power on temperature distribution

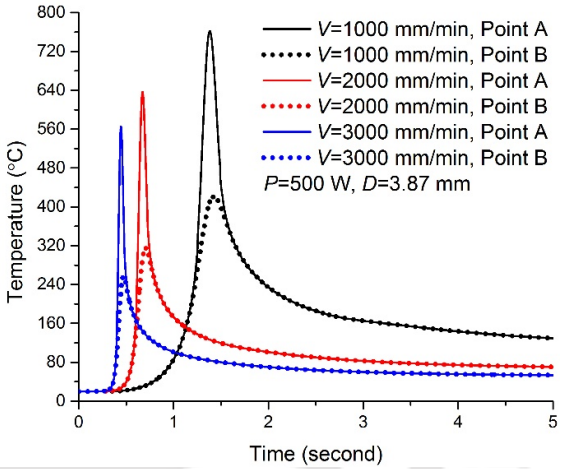

Figure 5.4. Effect of scan speed on temperature distribution

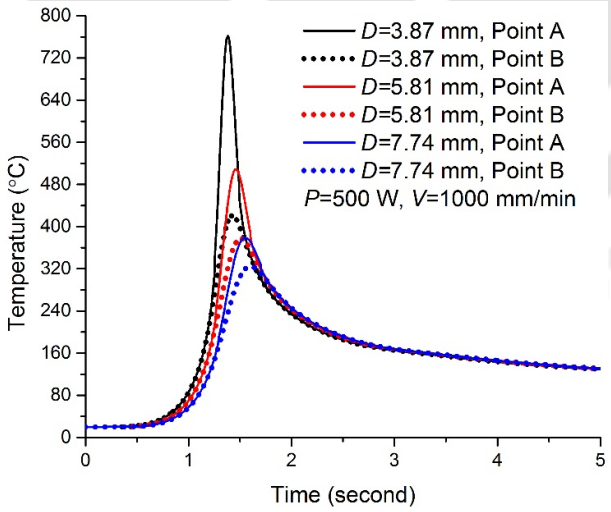

Figure 5.5. Effect of beam diameter on temperature distribution.

Figure 5.3 shows the effect of laser power on temperature history during laser bending process. It can be observed that the shape of the temperature profile is same for all sets of

process conditions. The peak temperature increases with the increase in laser power at both top and bottom surfaces. It is also observed that the temperature gradient is influenced by the laser power. The temperature gradient is calculated as the ratio of the difference between peak temperatures at the top and bottom surfaces to the thickness of the worksheet. The temperature gradient for the laser power 300 W, 400 W and 500 W is found to be 105.3, 141.7 and 179.2 K/mm, respectively. Therefore, it can be concluded that the temperature gradient increases with the increase in laser power at a constant scan speed.

Figure 5.4 shows the effect of scan speed on temperature history at the top and bottom surfaces. It can be seen that the scan speed significantly influence the temperature history during laser bending process. The peak temperature decreases with the increase in scan speed. It is because the contact time between laser beam and worksheet surface decreases with the increase in scan speed. Thus, the energy absorption per unit length decreases at faster scan speed. The temperature profile has a slow increase in the peak temperature at slower scan speed, and the sharpness of temperature curve near to peak temperature hike increases with the increase in scan speed. It is because at a slower scan speed the succeeding material gets preheated due to the thermal conduction, while at faster scan speed the laser beam quickly reaches to the Point A, and succeeding material gets less time to preheat. It also results in the earlier occurrence of the peak temperature at faster scan speed as shown in Figure 5.4. The temperature gradient at a scan speed of 1000 mm/min, 2000 mm/min and 3000 mm/min were found to be 179.2, 169.3, and 162.2 K/mm, respectively. It can be concluded that, the temperature gradient decreases with the increase in scan speed for a constant laser power.

Figure 5.5 shows the effect of laser beam diameter on temperature history at top and bottom surfaces. The peak temperature significantly reduces with the increase in beam diameter. A marginal delay in the peak temperature can also be observed at larger beam diameter. It is because of larger scanning path equal to the difference in beam diameter. As the laser beam starts from outside of the worksheet, and it irradiates until the laser beam completely comes out of the worksheet. The total scanning length is equal to the sum of width of the worksheet and beam diameter. Therefore, the scanning length increases with the increase in beam diameter, which leads to the delay in peak temperature at a larger beam diameter. The temperature gradient at a beam diameter of 3.87 mm, 5.81 mm, and 7.74 mm were found to be 169.3, 69.3, and 28.5 K/mm, respectively. Thus, it can be said that, the temperature gradient decreases with the increase in beam diameter for the constant levels of laser power and scan speed.

5.3.2 Stress distribution

During laser irradiation, the increase in temperature leads to the thermal expansion of the heated region. The thermal expansion is more at the top surface (Point A) as the temperature of the top surface is higher. Therefore, the worksheet bends away from the laser source, which is called counter-bending.

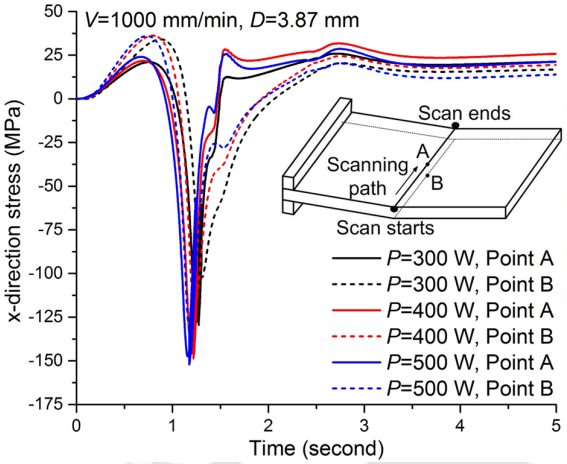

Figure 5.6. Effect of laser power on stress history at Point A and Point B.

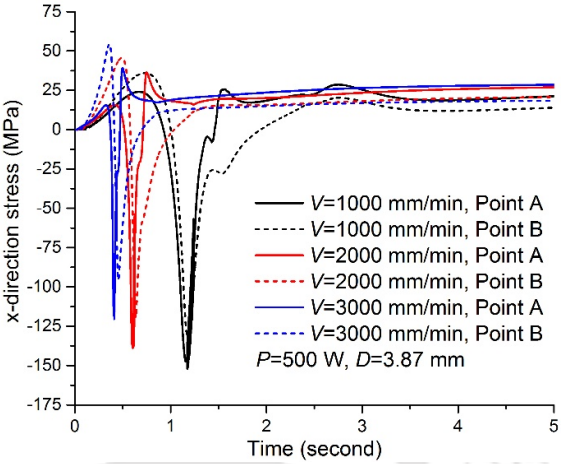

Figure 5.7. Effect of scan speed on stress history at Point A and Point B.

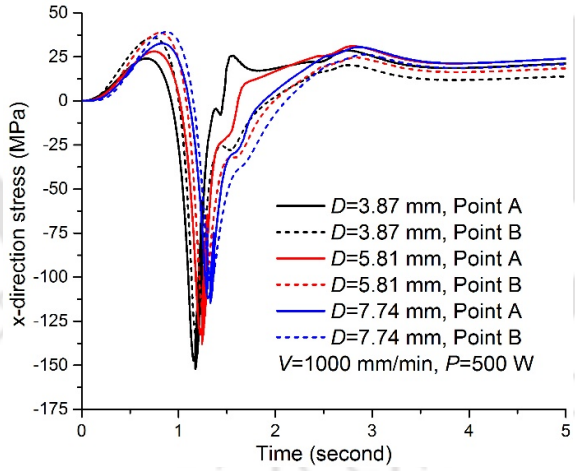

Figure 5.8. Effect of beam diameter on stress history at Point A and Point B.

The expansion of the heated region is resisted by the surrounding cooler material. It generates compressive thermal stresses in the heated region, and tensile thermal stresses in the cooler region as shown in Figure 5.6 to Figure 5.8. Comparing the temperature histories (Figure 5.3 to Figure 5.5) and the stress histories (Figure 5.6 to Figure 5.8), it can be observed that as the laser beam reaches near to the Point A, the compressive stresses are generated in the heated

region and tensile stresses in the cooler region. It can be seen that the magnitude of compressive stresses are more at the top surface as compared with the bottom surface. It is because the peak temperature is more at the top surface. From Figure 5.6 to Figure 5.8, it can be observed that the compressive stresses at both top and bottom surfaces increase with the increase in laser power, and decrease with the increase in scan speed and beam diameter. It is because the peak temperature increases with the increase in laser power and decreases with the increase in scan speed and beam diameter.

5.3.3 Strain distribution

During the laser based heating, when induced thermal stresses exceed temperature dependent flow stress, the plastic deformation occurs. Figure 5.9 to Figure 5.11 shows the x-direction plastic strain history at Point A and Point B. It can be observed that the plastic deformation is compressive at both top and bottom surfaces, but the plastic compressive deformation is more at the top surface. The bending occurs due to the difference between plastic deformation at the top and bottom surfaces. The plastic deformation is compressive and quantitatively more at the top surface as compared with the bottom surface, and therefore the bending occurs in the direction of the heating source (laser head). Figure 5.9 shows that the plastic strains at both top and bottom surfaces increase with the increase in laser power. It is due to more energy input at higher laser power. The difference between plastic deformations at the top and bottom surfaces also increases with the increase in laser power. It is because of the increase in temperature gradient along the worksheet thickness direction with increase in the laser power as discussed in Section 5.3.1.

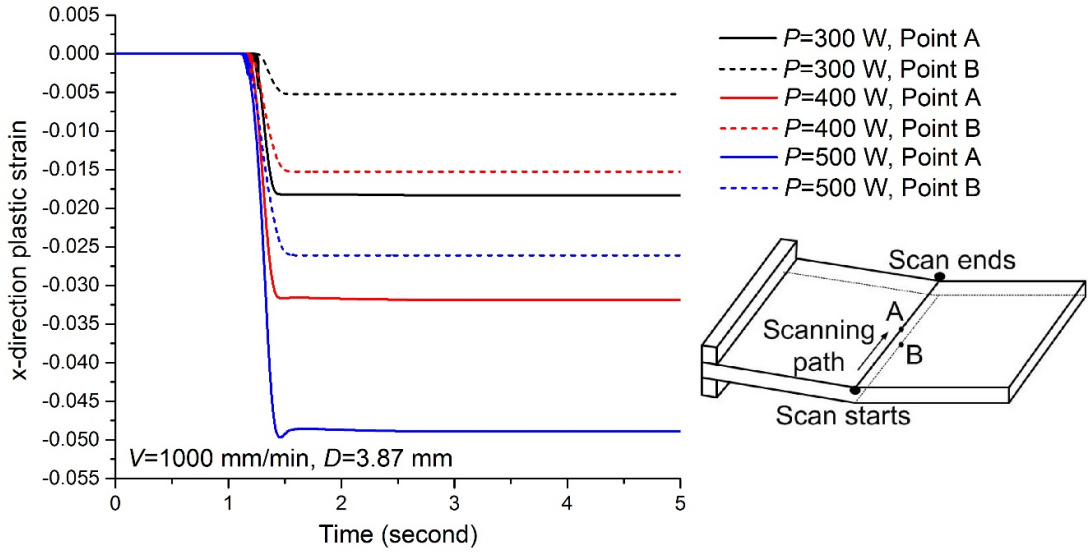

Figure 5.9. Effect of laser power on plastic strain history at Point A and Point B.

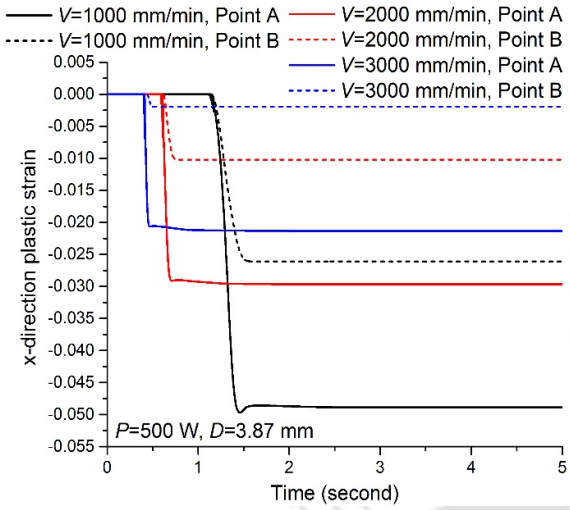

Figure 5.10. Effect of scan speed on plastic stain history at Point A and Point B.

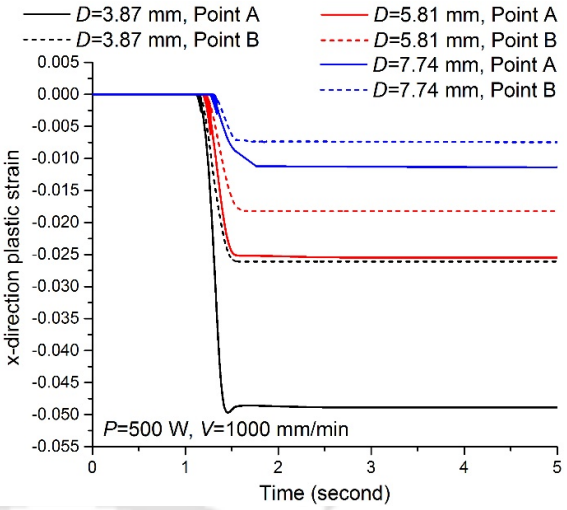

Figure 5.11. Effect of beam diameter on plastic stain history at Point A and Point B.

Figure 5.10 and Figure 5.11 show the effect of scan speed and beam diameter on plastic strain histories at Point A and Point B. It can be observed that the plastic strain decreases at both top and bottom surfaces with the increase in scan speed and beam diameter. It can also be observed that the difference between plastic deformation at the top and bottom surfaces decreases with the increase in scan speed and beam diameter. It is because of the decrease in temperature gradient along the worksheet thickness with increase in the scan speed and beam diameter as discussed in Section 5.3.1.

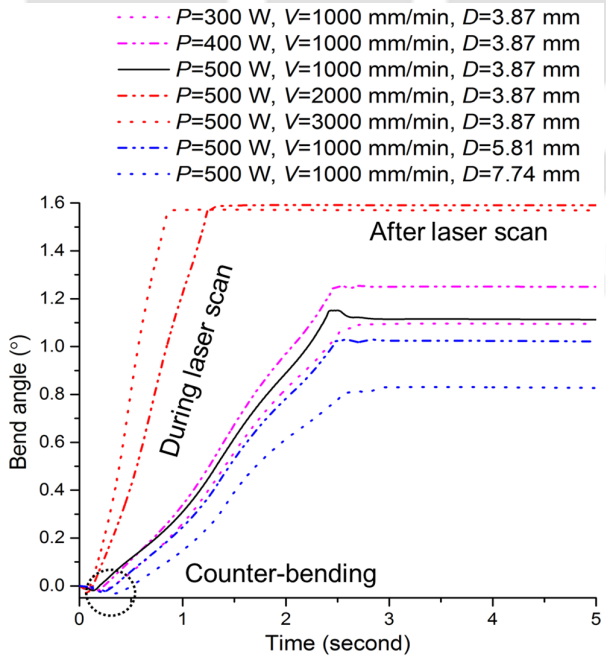

Figure 5.12. Bending history at middle of the scanning path (along Point A).

The worksheet bends due to the difference between the plastic deformations at top and bottom surfaces. Figure 5.12 shows the bending histories at middle of the scanning path for various process conditions. It can be seen that initially an elastic counter bending occurs away from the heating source. It is due to the thermal expansion of the material during heating phase. After heating, the irradiated region deforms plastically, and the compressive deformation is more at the top surface. Therefore, finally, the bending occurs towards the laser source. It can also be observed that after heating, there is no elastic recovery of the bend angle, and the bend angle remains constant after completion of the laser scan.

5.3.4 Residual stresses

Figure 5.13 shows the distribution of von-Mises and axial residual stresses along the scanning line. These residual stresses are obtained from the numerical simulation results. The x-directional residual stress is more at the start of the scanning line, and almost negligible along the rest of the scanning path. The x-directional stresses are compressive near the edges. The y-direction residual stresses are negligible near the edges and higher away from the edges. It is due to less mechanical constraint provided by the surrounding material near the edges.

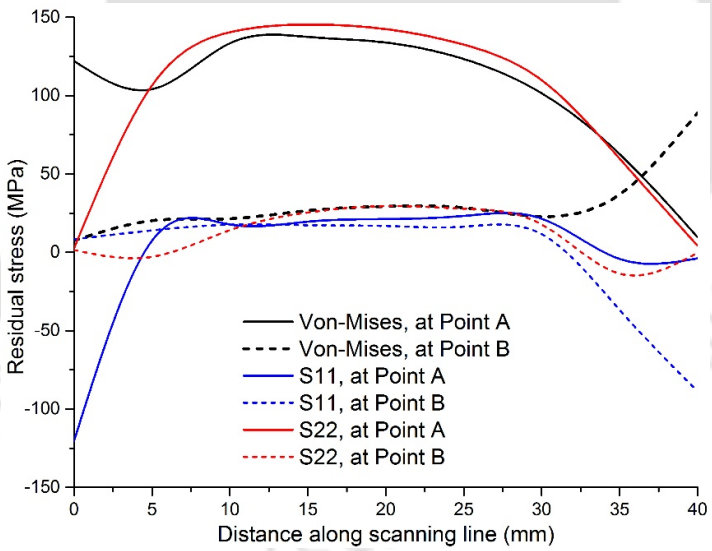

Figure 5.13. Distribution of residual stresses at top and bottom surfaces (based on numerical results).

5.4 Effect of Process Parameters on Bend Angle

In this section, the effects of energy (laser) parameters such as laser power, scan speed and beam diameter on bend angle are presented. The bend angle is measured at the middle of the scanning path. Based on the numerical and experimental analysis, the bend angle are also compared.

5.4.1 Effect of laser power

Laser power directly controls the input energy into the worksheet. The input energy is more at a higher laser power. Figure 5.14 to Figure 5.16 show the effect of laser power on bend angle. It can be observed that at a scan speed of 2000 mm/min and 3000 mm/min, the bend angle increases with the increase in laser power. It is because the heat energy absorbed by the worksheet is more at higher laser power. This results in the increase in peak temperatures, which leads to the higher plastic deformation and larger bend angle.

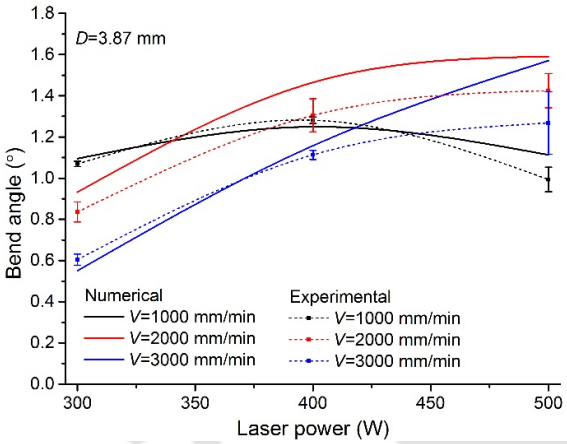

Figure 5.14. Effect of laser power on bend angle at small beam diameter.

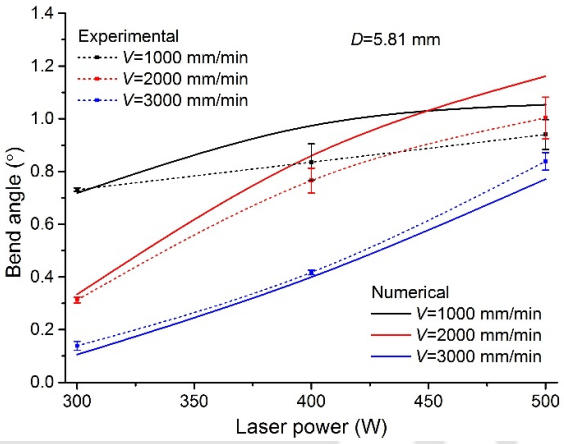

Figure 5.15. Effect of laser power on bend angle at medium beam diameter.

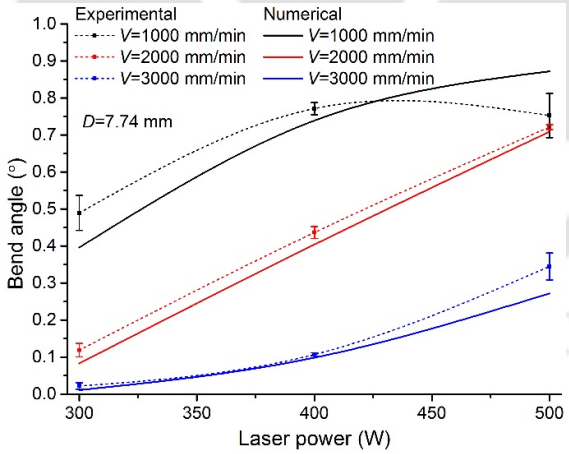

Figure 5.16. Effect of laser power on bend angle at large beam diameter.

At a slow scan speed of 1000 mm/min, the effect of laser power interacts with the beam diameter. At large beam diameter, the bend angle increases with the increase in laser power as a result of high energy input. At small beam diameter, the bend angle increases with the increase in laser power, attains a peak, and then decreases with further increase in the laser

power as shown in Figure 5.14. It is because the peak temperature at the bottom surface is high enough to generate the plastic deformation, which reduces the difference between plastic deformations at the top and bottom surfaces. The increase in compressive deformation at the bottom surface results in the decrease of bend angle at higher laser power.

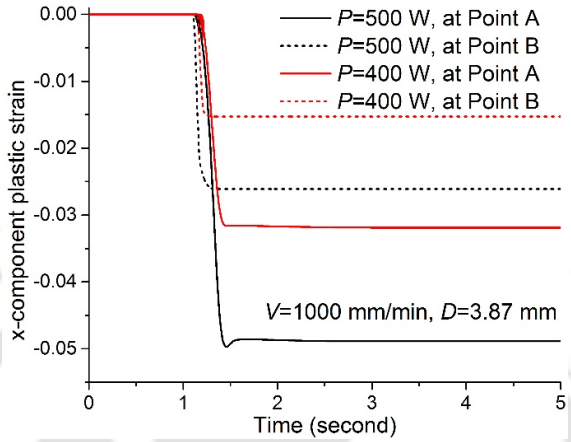

Figure 5.17. Plastic strains at Point A and Point B at different power levels.

Figure 5.17 shows the comparison between plastic deformation at top (Point A) and bottom (Point B) surfaces for two different levels of laser power. The process conditions used are:

1. High power: P=500 W, V=1000 mm/min, D=3.87 mm
2. Medium power: P=400 W, V=1000 mm/min, D=3.87 mm

It can be seen that the x-component of plastic strain at the top and bottom surfaces are -0.03189 and -0.01527 respectively for the process condition with medium laser power, while it is -0.04887 and -0.0261 respectively for the high laser power. Due to the increase in laser power, the percentage increase in plastic deformation at the top and bottom surfaces is about 53.2% and 70.9%, respectively. Therefore, the percentage increase in plastic deformation is more at the bottom surface as compare with that of the top surface. This leads to the decrease in bend angle with increase in the laser power at slow scan speed and small beam diameter.

5.4.2 Effect of scan speed

Scan speed controls the input energy into the worksheet by changing heat input per unit length. Figure 5.18 to Figure 5.20 show the effect of scan speed on bend angle. It can be seen that in general the bend angle reduces with the increase in scan speed. This is mainly due to the fact that the contact time between laser beam and worksheet surface decreases with the increase in scan speed. Thus, the energy absorption per unit length decreases at faster scan speed. This

results in the decrease in peak temperature, which leads to the reduction in plastic deformation in the heated region.

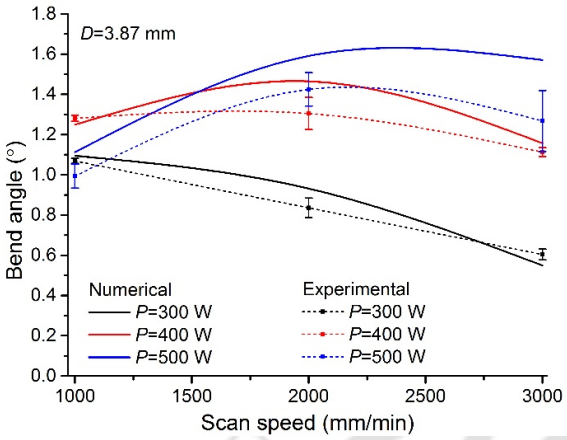

Figure 5.18. Effect of scan speed on bend angle at small beam diameter.

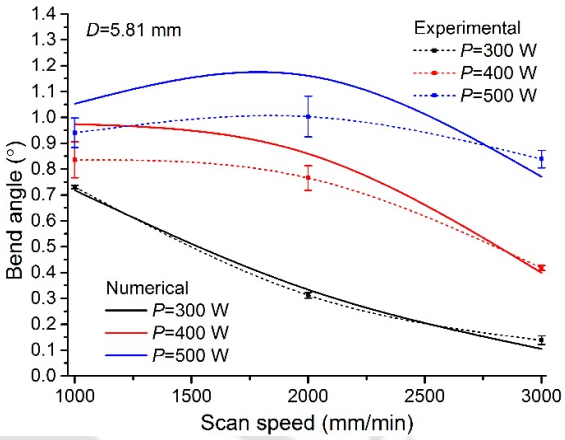

Figure 5.19. Effect of scan speed on bend angle at medium beam diameter.

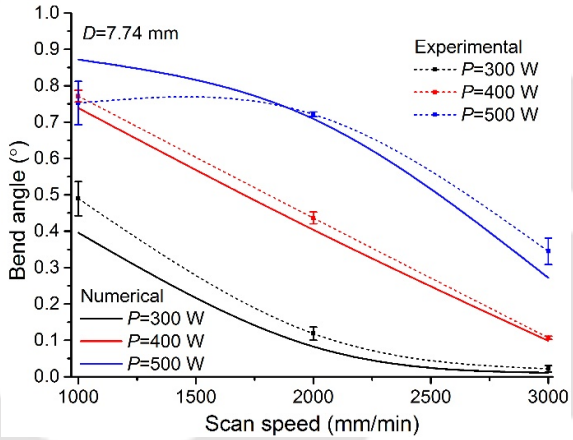

Figure 5.20. Effect of scan speed on bend angle at large beam diameter.

At small beam diameter and high laser power, the bend angle first increases with scan speed, attains a peak, and then decreases with further increase in the scan speed as shown in Figure 5.18 and Figure 5.19. It is because the peak temperature and the resulting plastic deformation at the bottom surface is high enough to reduce the bend angle at high laser power and small beam diameter. The higher plastic deformation at the bottom surface reduces the bend angle at slower scan speed, when worksheet is irradiated with higher laser power. In that case, the temperature gradient between top and bottom surfaces increases with the increase in scan speed. The magnesium alloys have high thermal conductivity, and significant temperature gradient cannot be maintained at slow scan speed. The increase in scan speed leads to a lower

peak temperature at the bottom surface, which may increase the bend angle when plastic deformation at the bottom surface is significantly high.

5.4.3 Effect of beam diameter

Figure 5.21 to Figure 5.23 show that the bend angle decreases with the increase in beam diameter. The beam diameter controls the heat flux density. The heat flux density decreases with the increase in beam diameter. It results in the decrease in peak temperature and temperature gradient between top and bottom surfaces as shown in Figure 5.5. This leads to the decrease in bend angle. It can be observed that the rate of decrease in bend angle is more, when laser power is less. It is because the peak temperature at lower laser power is too less to create a significant plastic deformation. Comparing the Figure 5.21 to Figure 5.23, it can also be observed that the rate of decrease in bend angle with increase in beam diameter is more at faster scan speed.

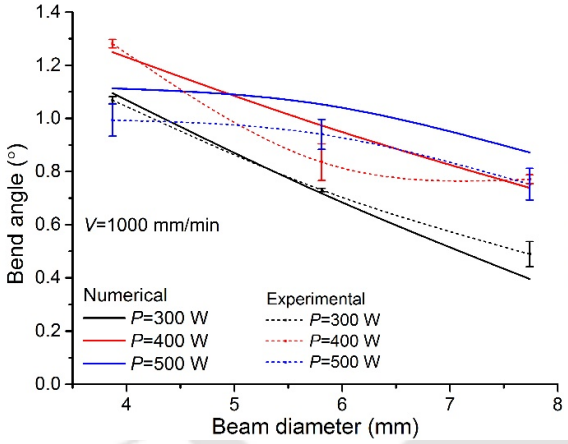

Figure 5.21. Effect of beam diameter on bend angle at slow scan speed.

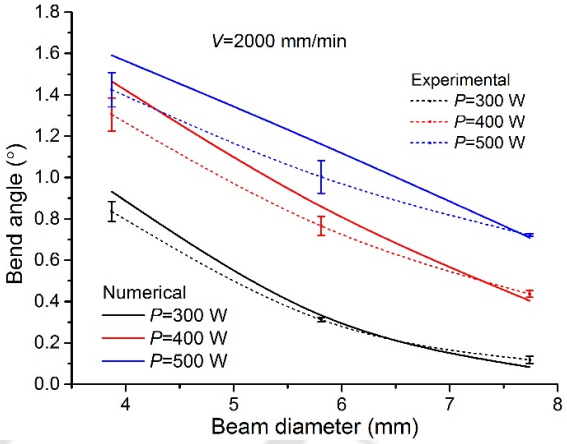

Figure 5.22. Effect of beam diameter on bend angle at medium scan speed.

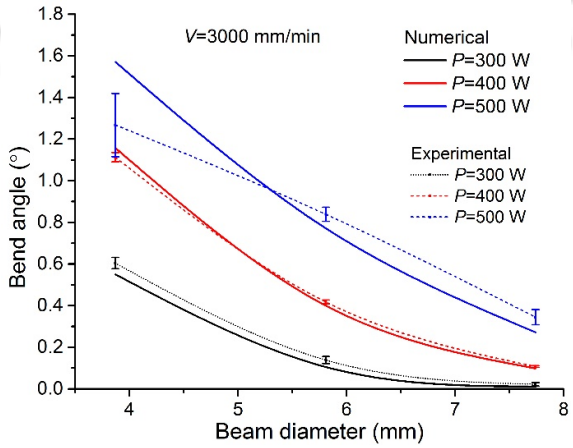

Figure 5.23. Effect of beam diameter on bend angle at fast scan speed.

5.5 Effect of Process Parameters on Edge Effect

In laser bending process, the bend angle is not uniform along the scanning path and it varies from one end to the other end. Figure 5.24 shows the variation in bend angle along the scanning path for a typical process condition P=300 W, V=1000 mm/min and D=3.87 mm. It can be seen that the bend angle is maximum near the middle and reduces towards the free ends. It is called as edge effect. The variation in bend angle is a result of non-uniform thermal and mechanical boundaries along the scanning path as shown in Figure 5.25. It can be seen that the thermal conduction does not occur (towards outside) along free sides of the worksheet, and it is uniform at the middle of the irradiation line. This variation results in a higher peak temperature near the edges, and a lower peak temperature at the middle of the scanning path. The mechanical constraint provided by the surrounding cooler region varies from one end to the other end of the scanning line. It is due to the increase in heated region as the laser beam moves forward from its present position. The heated material has less stiffness to resist the thermal expansion (Dieter and Bacon 1988). This leads to a non-uniform bend angle along the scanning path.

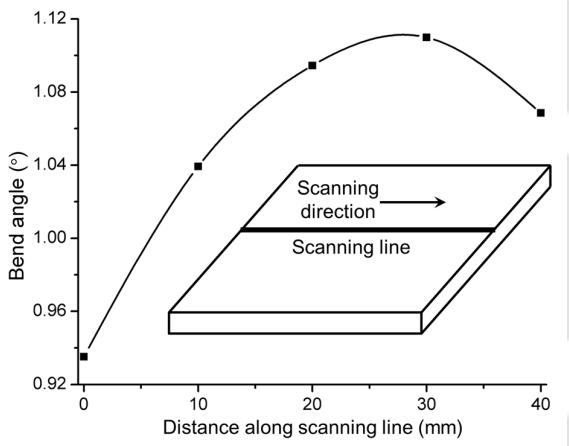

Figure 5.24. Distribution of bend angle along the scanning line.

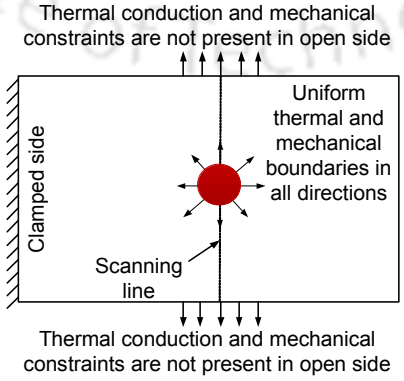

Figure 5.25. Schematic of non-uniform thermal and mechanical boundaries along the scanning path.

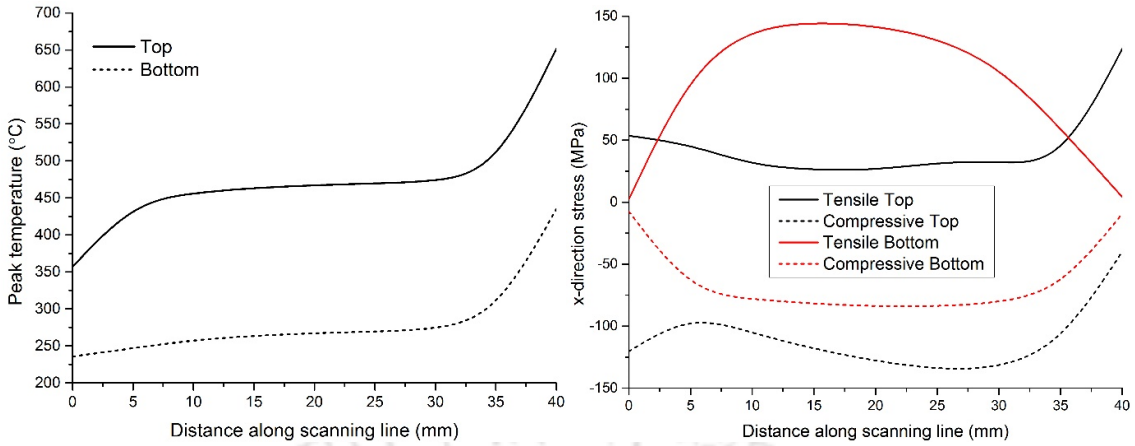

(a) (b)

Figure 5.26. Distribution of peak (a) temperature along the scanning line, (b) thermal stresses along the scanning line.

The variations in temperature distribution and stress distribution along the scanning path are shown in Figure 5.26 (a) and Figure 5.26 (b). Figure 5.26 (a) shows the peak temperature along the scanning path at top and bottom surfaces. It can be seen that the peak temperature is not uniform, and it increases along the scanning line. The peak temperature rapidly increases when the laser beam is about to leave the worksheet. It is because, towards the free side (edge) of the worksheet, material volume for the conduction of heat is very less. Figure 5.26 (b) shows the distribution of peak thermal stresses along the scanning path at top and bottom surfaces. The distribution of peak thermal stresses are not uniform, and varies from one end to another end of the worksheet. It is due to the non-uniform temperature distribution and surrounding material distribution along the scanning line. The variations in temperature distribution and stress distribution along the scanning path result in the variation of bend angle along the scanning line. This generates edge effect during laser bending process.

The edge effect is quantified as the relative variation in bend angle per unit length along the scanning line. In the present work, the bend angle is measured at five equidistant locations. The relative variation in bend angle (*RVBA*) at these five locations was calculated as per Equation (4.29) of Chapter 4. Higher value of *RVBA* represents a larger variation in bend angle or edge effect, and vice-versa.

5.5.1 Effect of laser power

Figure 5.27 to Figure 5.29 show the effect laser power on edge effect at various scan speeds and beam diameters. It can be seen that the edge effect decreases with the increase in laser power for all sets of process conditions. It is because the bend angle increases with laser power

which reduces the percentage variation in bend angle along the scanning line. The peak temperature along the scanning line increases with laser power. It reduces percentage variation of temperature along the scanning line, which leads to the decrease in edge effect. The effect of laser power on the rate of change in edge effect is more when beam diameter is larger. It is due to low heat flux density at larger beam diameter, which leads to the lower peak temperature. At low temperature range, a small variation in temperature may lead to the high variation in the bend angle.

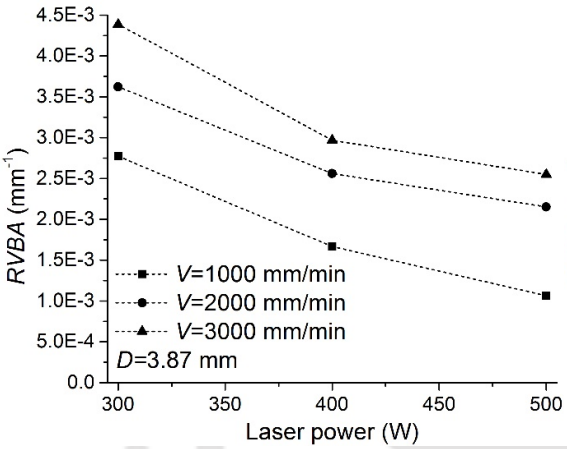

Figure 5.27. Effect of laser power on edge effect at small beam diameter.

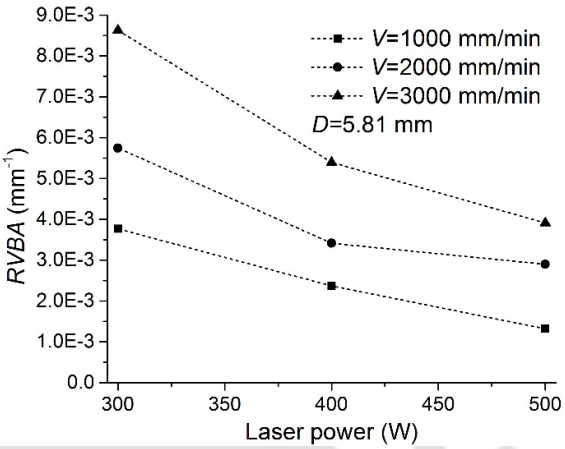

Figure 5.28. Effect of laser power on edge effect at medium beam diameter.

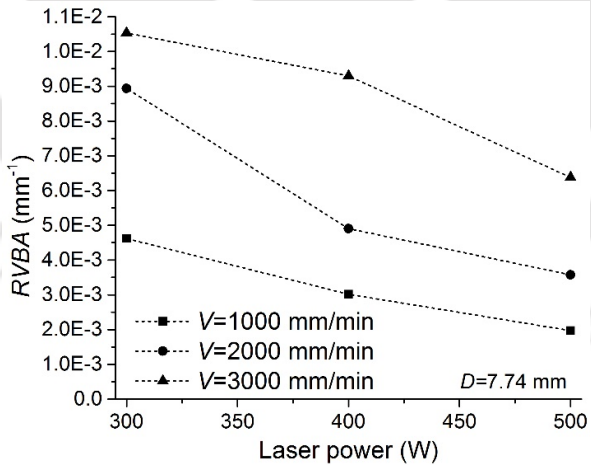

Figure 5.29. Effect of laser power on edge effect at large beam diameter.

5.5.2 Effect of scan speed

Figure 5.30 to Figure 5.32 show the effect of variation in scan speed on the edge effect. It can be seen that the edge effect increases with the increase in scan speed for all sets of process conditions. It may be due to the fact that the peak temperature and bend angle decrease with

the increase in scan speed. It results in the increase of percentage variation in peak temperature and bend angle along the scanning path, and hence the edge effect increases with the increase in scan speed. The rate of increase in edge effect is more at larger beam diameter due to less heat flux density.

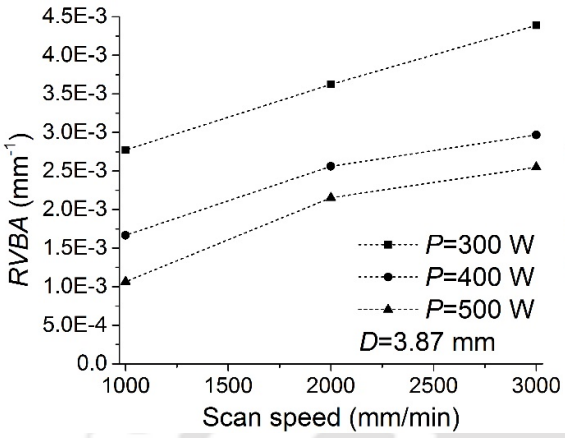

Figure 5.30. Effect of scan speed on edge effect at small beam diameter.

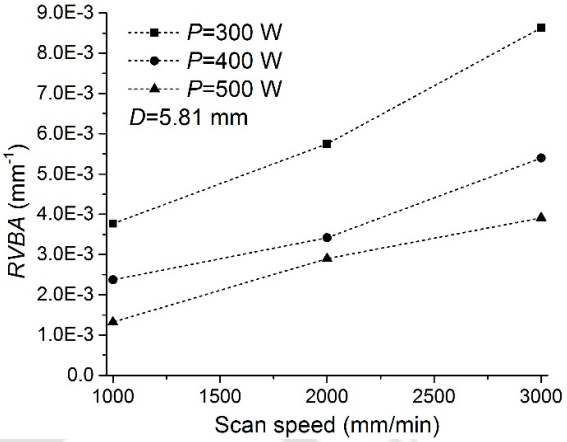

Figure 5.31. Effect of scan speed on edge effect at medium beam diameter.

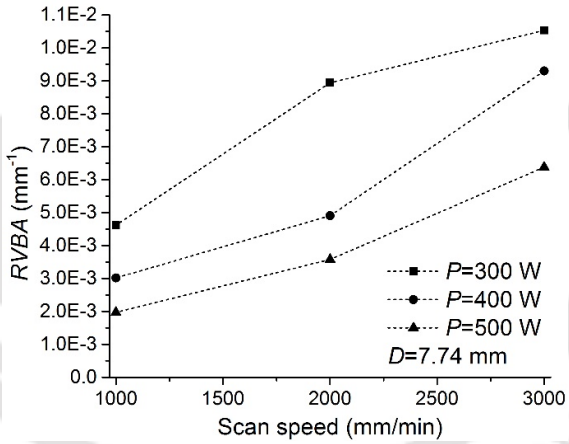

Figure 5.32. Effect of scan speed on edge effect at large beam diameter.

5.5.3 Effect of beam diameter

Figure 5.33 to Figure 5.35 show the effect of variation in beam diameter on the edge effect. Unlike scan speed, the edge effect increases with the increase in beam diameter for all sets of process condition. It is because the peak temperature and bend angle decrease with the increase in beam diameter. This results in the increase of percentage variation in peak temperature and bend angle along the scanning path, and hence the edge effect increases with the increase in beam diameter.

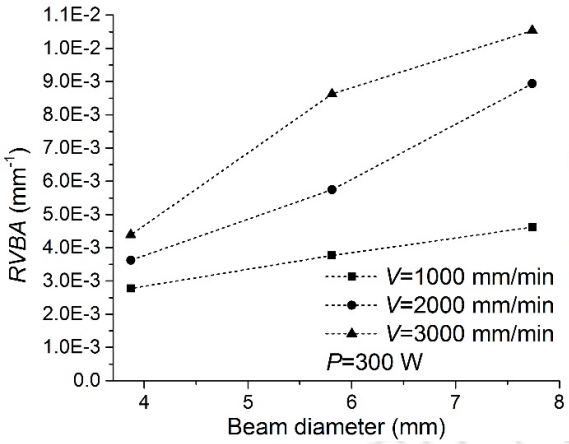

Figure 5.33. Effect of beam diameter on edge effect at low laser power.

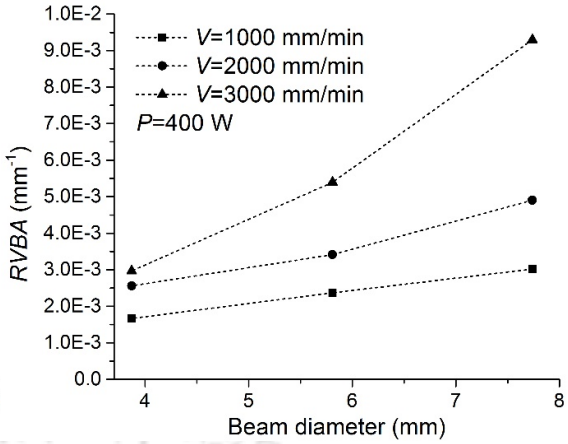

Figure 5.34. Effect of beam diameter on edge effect at medium laser power.

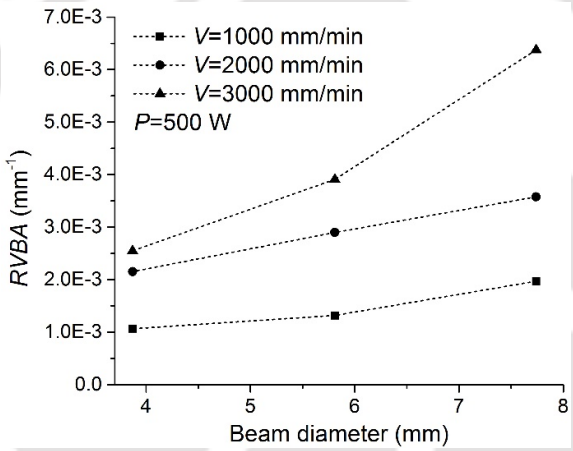

Figure 5.35. Effect of beam diameter on edge effect at high laser power.

5.6 Summary

This chapter presented numerical studies on the straight line laser bending of magnesium alloy M1A sheets. The finite element based numerical model presented in Chapter 4, was validated with the experimental results for the single scan laser bending operation. The numerical model was found to be in good agreement with the experimental results. The absolute average error of prediction in the bend angle was about 10.88%. The developed model was used to explain the laser bending mechanism for magnesium alloys, and to study the effects of process parameters on temperature distribution, stress-strain distribution, bend angle and edge effect for laser bending of the magnesium alloy M1A. The process was found to be TGM dominated, and the worksheet was bent towards the laser source. It was observed that the bend angle increases with the increase in laser power at fast scan speed, while at slow scan speed, the bend

angle first increases with laser power, and after attaining a peak, it decreases. At low laser power, the bend angle decreases with the increase in scan speed, while at high laser power, it increases, and then decreases with the increase in scan speed. The bend angle decreases with the increase in beam diameter. The effects of laser power, scan speed and beam diameter were also analyzed in terms of temperature and plastic deformation.

The edge effect was explained and analyzed in detail. It was observed that the edge effect decreases with the increase in laser power, and increases with the increase in scan speed and beam diameter. Laser power, scan speed and beam diameter were found to have non-linear effects on the bend angle and edge effect. It was observed that the effects of process parameters are difficult to generalize, however a combination of high laser power, fast scan speed and small beam diameter produces a large bend angle. However, it was noted that these parameters lead to the melting and higher edge effect on the worksheet surface. Therefore, a study on the variation in shape of the scanning pattern (curvilinear irradiation) to reduce the melting and edge effect was carried out. Details of the numerical and experimental investigations on the curvilinear laser bending process are presented in the next chapter.

CHAPTER 6: CURVILINEAR LASER BENDING OF MAGNESIUM M1A ALLOY SHEETS

6.0 Scope

This chapter presents numerical investigations on the curvilinear laser bending of magnesium alloy M1A. The need to investigate the curvilinear laser bending is defined. The modified numerical model with curvilinear scanning is presented. The experimental validation of the results predicted by the modified numerical model is also discussed. The deformation behavior of curvilinear laser bending process is investigated and compared with the straight line laser bending process. Effects of various process parameters on the bend angle, edge effect and deformation behavior have been studied for various scanning path curvatures, and compared with those obtained for the straight line laser bending process.

6.1 The Need

Scanning path curvature is an important parameter that affects the laser bending process. It controls the deformation profile of the worksheet and the displacement at the edges. Simple shapes or distortions can be generated with straight line laser bending process. However, complex shapes or curved parts can be produced by employing curved irradiation instead of the linear irradiation. The process of worksheet bending by applying curved irradiation is called curvilinear laser bending process. It can be used to compensate the deformation non-uniformity generated due to the edge effect.

Literature reveals very scant research on the curvilinear laser bending process. It is observed that the effects of curvilinear irradiation parameters such as scanning path curvature on the deformation behavior, temperature distribution, and warping of the worksheet are not explored. Thus, a need is identified to investigate the effect of scanning path curvature on the bending profile, bend angle, and edge displacements for the effective use of curvilinear laser bending process in real practice.

6.2 Numerical Simulation of Curvilinear Laser Bending Process

In this part of work, the already developed three-dimensional non-linear thermo-mechanical FEM based numerical model was modified for the curvilinear laser bending of magnesium alloy M1A. The model considered that the laser beam is irradiated along a circular arc as shown in Figure 6.1. The scanning path curvature was controlled by changing the arc height (A_H).

The laser scan start and finish points were taken at the middle of the Edge S and Edge F, respectively. The scanning path curvature increases with the increase in arc height. The arc height is related to the scanning path radius (R_{SP}) as

$$R_{SP} = \frac{4A_H{}^2 + W^2}{8A_H}, \tag{6.1}$$

where W is the arc width, and A_H is the arc height. The length of scanning path (L) was calculated as

$$L = 2 \times sin^{-1}\left(\frac{W}{2R_{SP}}\right) \times R_{SP}. \tag{6.2}$$

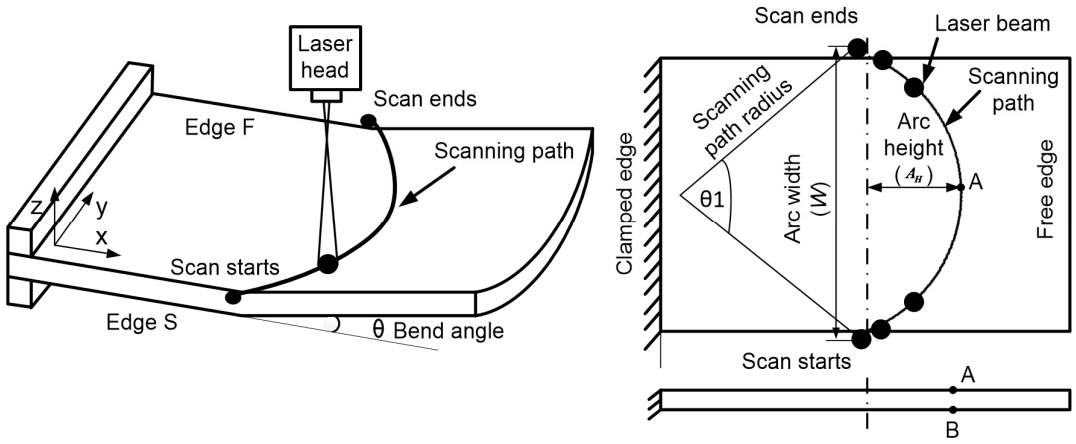

Figure 6.1. Schematic and terminology of curvilinear laser irradiation.

The laser beam moves along a curvilinear scanning path, and therefore, instantaneous positions of x and y coordinates of the center of the laser beam moving along the scanning path with a scan speed V is given as

$$\mathrm{x} = R_{SP}\mathrm{Sin}\theta - (R_{SP} - A_H), \tag{6.3}$$

$$\mathrm{y} = R_{SP}\mathrm{Cos}\theta, \tag{6.4}$$

where θ is the instantaneous angle of movement by which laser beam moved along the scanning path at some time instant T_{inst}. The value of θ varies from zero (when scan starts) to the maximum value (when scan ends) as shown in Figure 6.1. The instantaneous angular movement θ is given as

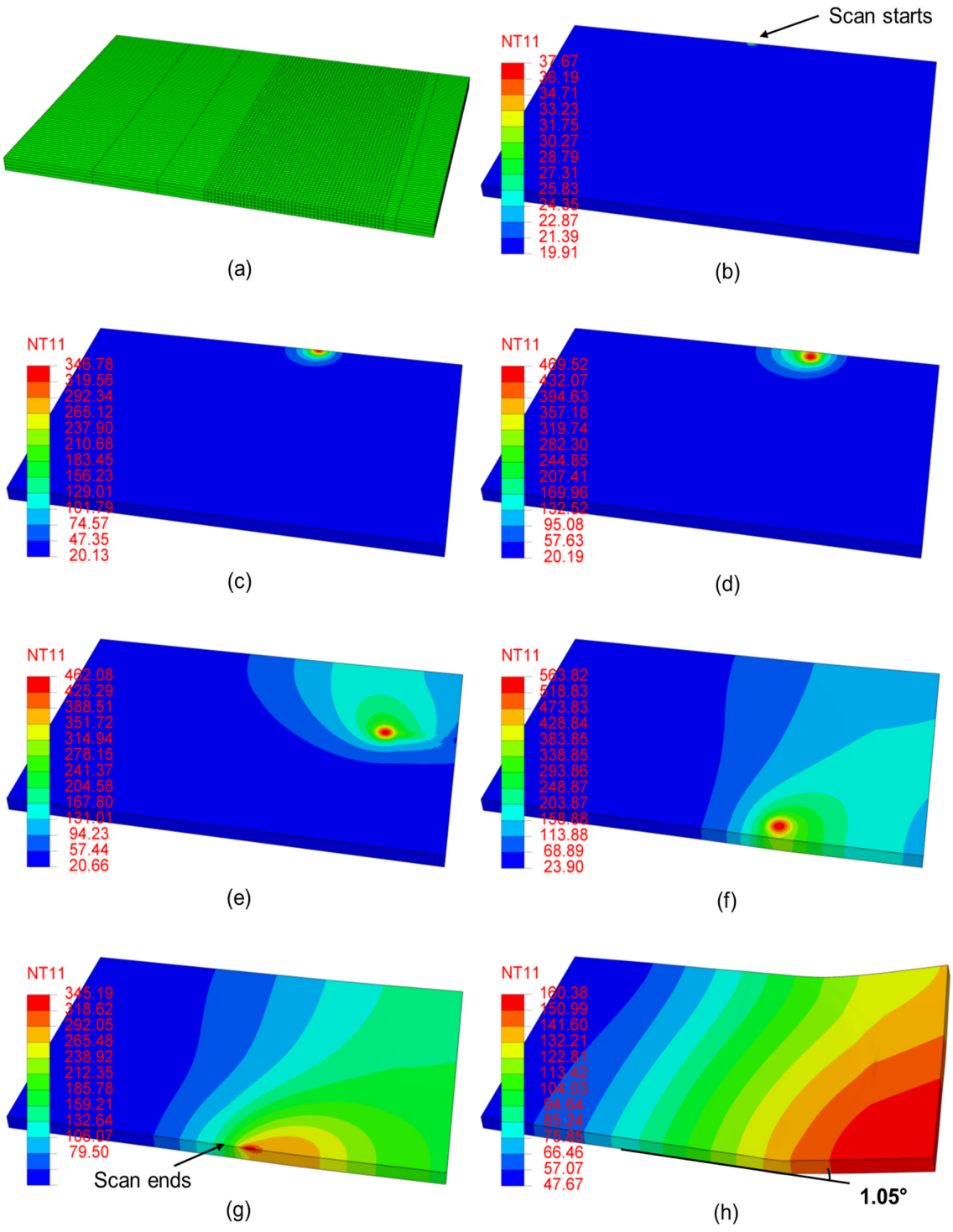

Process conditions: *P*=300 W, *V*=1000 mm/min, *D*=3.87 mm, Arc height=20 mm.

Figure 6.2. Various stages of the curvilinear irradiation (a) Meshed worksheet (b) Laser beam enters in to the worksheet (c) At start, laser beam is partially out of the worksheet (d) Laser beam completely enters in to the worksheet (e) Laser beam is at middle of the scanning path (f) Laser beam is near to the irradiation finish edge (g) Before leaving laser is partially out of the worksheet (h) Final bent worksheet with curvilinear laser bending process (scaled deformation with a factor of 15).

$$\theta = \left(\frac{\pi}{2} - \theta_1\right) + \left(\frac{2\theta_1 \times T_{inst}}{L/V}\right), \tag{6.5}$$

where θ_1 is the maximum angle of rotation required to complete the irradiation along the scanning path shown in Figure 6.1. The maximum angle of rotation θ_1 is given as

$$\theta_1 = \mathrm{Sin}^{-1}\left(W/R_{SP}\right). \tag{6.6}$$

Laser irradiation along the curvilinear scanning path was modeled by the mathematical Equation (6.1) to Equation (6.6). Various details of the thermo-mechanical finite element numerical model including boundary conditions, governing equations and solution methodology have already been presented in Chapter 4. Discretization of the worksheet is shown in Figure 6.2 (a). The fine mesh was used near to the scanning path and course biased mesh was used in the rest of the region. Four elements were taken along the thickness of the worksheet.

Various stages of the curvilinear irradiation are shown in Figure 6.2. Initially, the worksheet is clamped over the laser machine bed and does not have any applied thermal load or mechanical load. The worksheet is under normal room temperature condition which is shown in Figure 6.2 (a). Laser irradiation starts with a point contact with the worksheet as shown in Figure 6.2 (b), and then moves along the curvilinear scanning path. The deformation of the worksheet changes with the movement of the laser beam as shown in Figure 6.2 (c) to Figure 6.2 (g). Finally, the laser beam comes out of the worksheet completely and the worksheet gets deformed due to the laser beam irradiation. Final bending of the worksheet is shown in Figure 6.2 (h).

6.3 Experimental Validation of Numerical Simulations

The developed numerical model was validated with the experimental results obtained for the maximum scanning path curvature (arc height 20 mm). Details regarding the specimen preparation, laser machine, work holding are similar to those used for the straight line irradiation scheme, and have already been presented in Chapter 3. The experiments were carried out on the curvilinear laser bending of magnesium alloy M1A worksheets. Each experiment was repeated thrice, and the variation was calculated as the ratio of standard deviation to the mean of three trials. It is called coefficient of variation (*CV*). Figure 6.3 (a) to Figure 6.3 (d) show some of the laser bent specimens irradiated with the curvilinear laser

bending process. The experimental results were used to validate the developed numerical model.

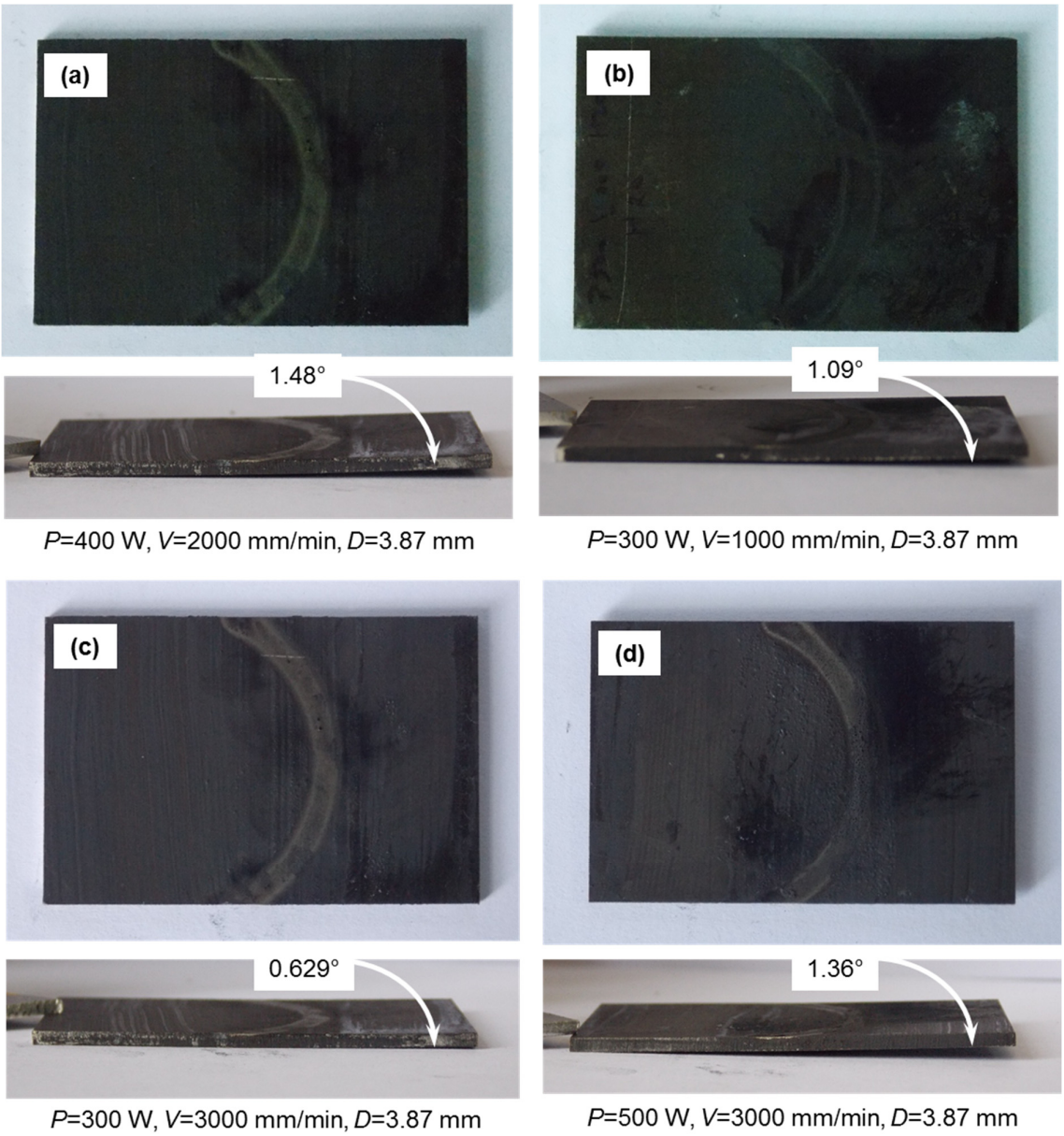

Figure 6.3. Laser bent specimens with curvilinear irradiations.

A comparison between numerical and experimental results (bend angle) obtained during the curvilinear laser bending of magnesium alloy M1A is shown in Table 6.1. The comparison results show that the numerical results are in good agreement with the experimental results. The numerical model predicted the bend angle within an error band of 0.04–16.15% during the curvilinear laser bending process. The average absolute error was about 4.71%, which was considered to be very good for the further analysis of the process using this

numerical model. For better visualization, the percentage of absolute error between numerical and experimental results for various sets of process conditions is also shown in Figure 6.4. The experimental validation for the minimum scanning path curvature (arc height is zero), *i.e.* straight line laser bending process has already been presented in Chapter 5.

Table 6.1. Experimental validation of the numerical model for curvilinear laser bending process.

S. No.	*P* (W)	*V* (mm/min)	*D* (mm)	Average Experimental Bend Angle (°)	*CV* (%)	Numerical Bend Angle (°)	Absolute Error
1	300	1000	3.87	1.080	2.273	1.050	2.78
2	300	1000	5.81	0.714	8.065	0.720	0.93
3	300	1000	7.74	0.381	21.642	0.379	0.31
4	300	2000	3.87	0.872	9.212	1.013	16.15
5	300	2000	5.81	0.350	11.523	0.336	4.04
6	300	2000	7.74	*	*	0.053	*
7	300	3000	3.87	0.570	12.742	0.615	7.83
8	300	3000	5.81	0.110	27.693	0.097	11.86
9	300	3000	7.74	*	*	0.003	*
10	400	1000	3.87	1.031	13.833	1.014	1.61
11	400	1000	5.81	0.893	6.952	0.904	1.24
12	400	1000	7.74	0.739	5.888	0.713	3.53
13	400	2000	3.87	1.522	7.023	1.473	3.23
14	400	2000	5.81	0.855	11.453	0.919	7.44
15	400	2000	7.74	0.407	17.026	0.407	0.04
16	400	3000	3.87	1.330	4.698	1.250	5.98
17	400	3000	5.81	0.379	15.309	0.421	11.01
18	400	3000	7.74	*	*	0.075	*
19	500	1000	3.87	0.742	13.721	0.772	4.01
20	500	1000	5.81	0.804	4.736	0.791	1.58
21	500	1000	7.74	0.746	4.451	0.722	3.22
22	500	2000	3.87	1.489	7.173	1.488	0.03
23	500	2000	5.81	1.178	7.707	1.196	1.53
24	500	2000	7.74	0.796	3.002	0.737	7.42
25	500	3000	3.87	1.624	4.059	1.622	0.14
26	500	3000	5.81	0.904	7.546	0.830	8.15
27	500	3000	7.74	0.228	24.108	0.249	8.94
***=insignificant bend angle (<0.1°)**						**Average absolute error = 4.71%**	

Based on the validation studies, the developed model was used to investigate the curvilinear laser bending process. The effect of scanning path curvature on the bend angle, edge effect and edge displacement are analyzed in terms of the temperature distribution, stress-strain distributions and distortions. The predicted results for curvilinear laser bending have also been compared with those obtained for the straight line laser bending process. These are presented in the following sections.

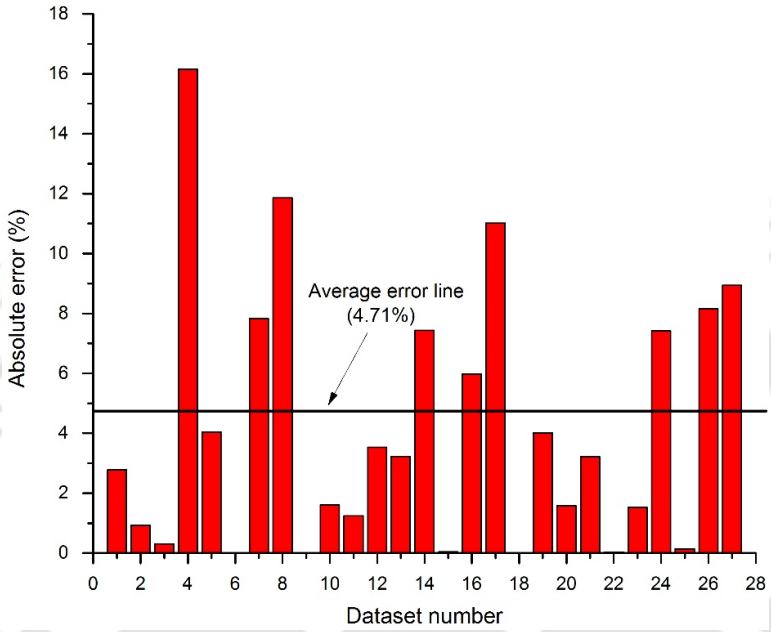

Figure 6.4. Absolute error between numerical and experimental bend angle.

6.4 Effect of Arc Height on Edge Effect

The effect of arc height on edge effect is shown in Figure 6.5 to Figure 6.13. The edge effect is presented in terms of '*RVBA*' as given in Equation (4.29). It can be seen that as compared with the straight line laser bending process (arc height=0 mm), the edge effect is less in curvilinear laser bending when arc height is small (10 mm). It may be due to the fact that a small enhancement in the arc height leads to the increase in scanning path, which preheats the work surface more. This helps to reduce the relative variation in bend angle (edge effect). However, the edge effect was found to be increased with further increase in the arc height from 10 mm to 20 mm. It may be due to the fact that higher arc height (20 mm) results in longer interaction time between the laser beam and worksheet material. This heats up the work surface substantially, which results in the generation of non-uniform thermal boundaries along the curvilinear scanning path. Thus, the mechanism of bending may change and affect the quality of sheet bending in terms of relative variation in bend angle (edge effect).

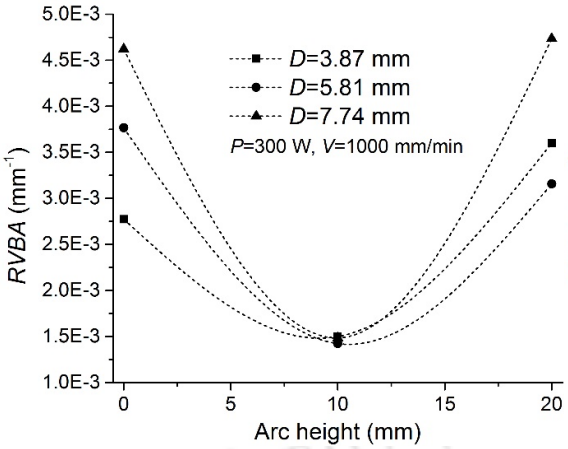

Figure 6.5. Effect of arc height on edge effect at *P*=300 W, *V*=1000 mm/min.

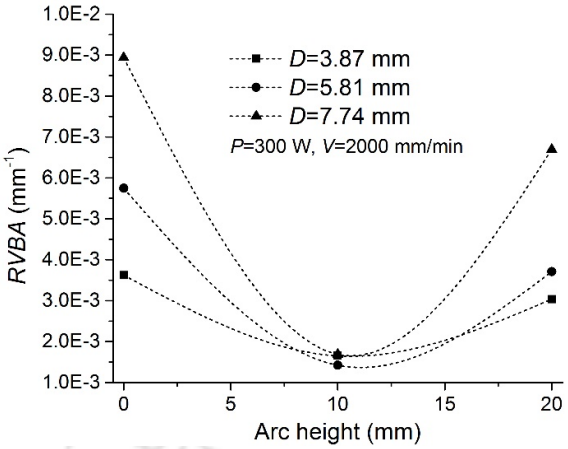

Figure 6.6. Effect of arc height on edge effect at *P*=300 W, *V*=2000 mm/min.

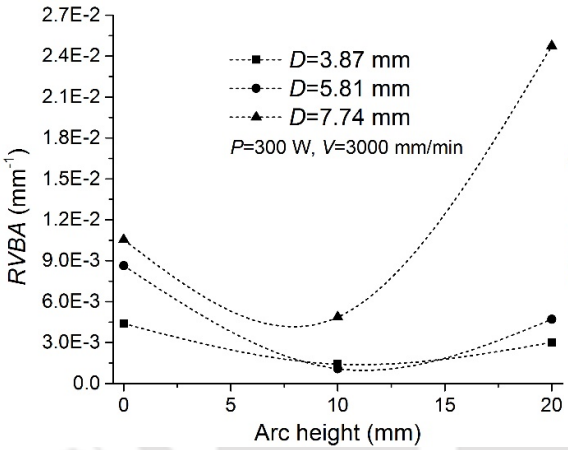

Figure 6.7. Effect of arc height on edge effect at *P*=300 W, *V*=3000 mm/min.

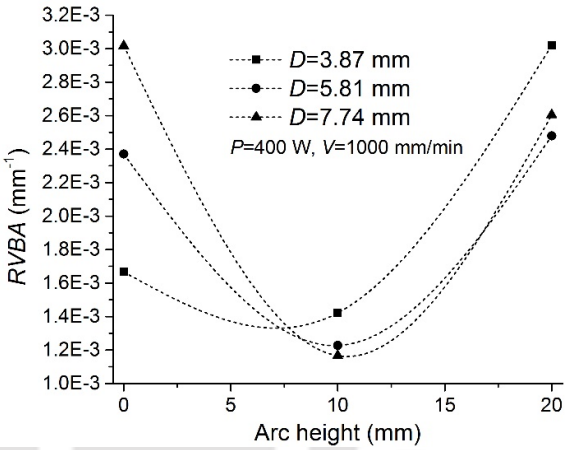

Figure 6.8. Effect of arc height on edge effect at *P*=400 W, *V*=1000 mm/min.

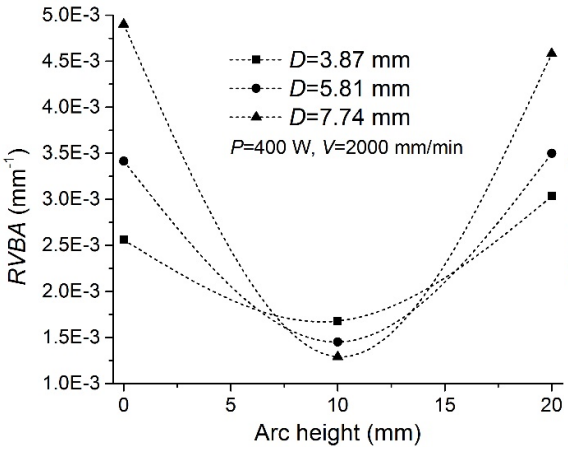

Figure 6.9. Effect of arc height on edge effect at *P*=400 W, *V*=2000 mm/min.

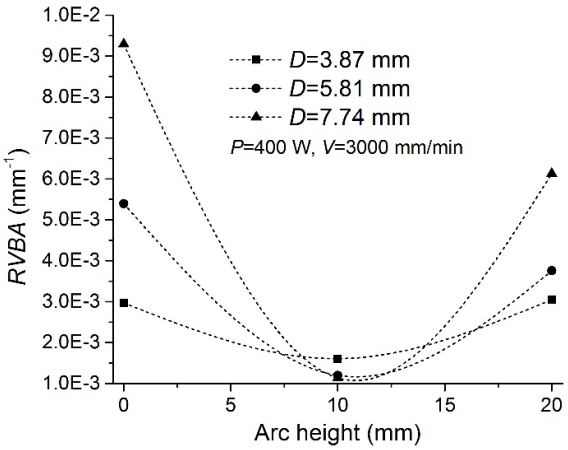

Figure 6.10. Effect of arc height on edge effect at *P*=400 W, *V*=3000 mm/min.

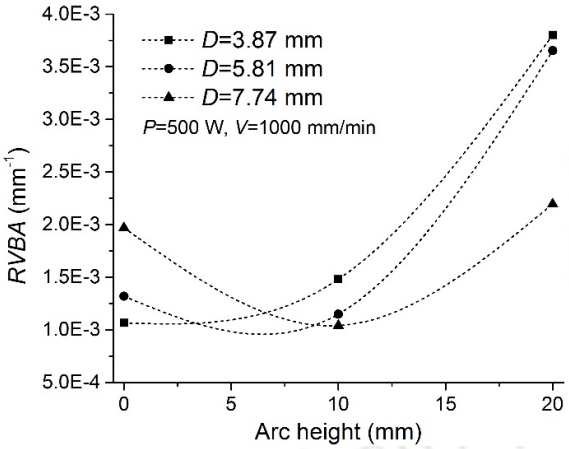

Figure 6.11. Effect of arc height on edge effect at *P*=500 W, *V*=1000 mm/min.

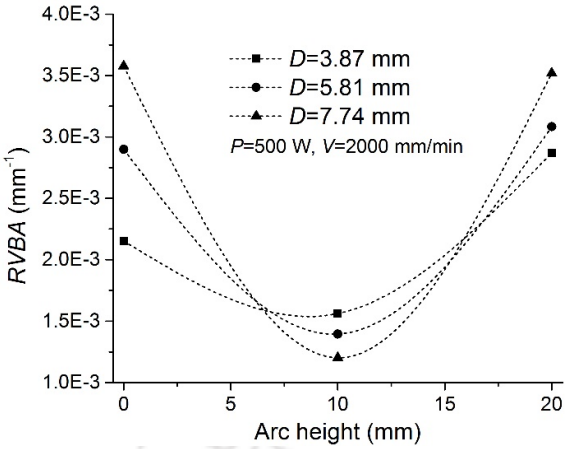

Figure 6.12. Effect of arc height on edge effect at *P*=500 W, *V*=2000 mm/min.

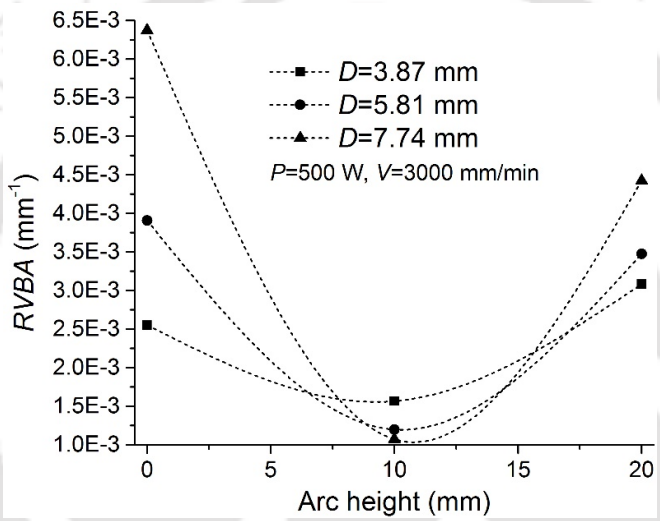

Figure 6.13. Effect of arc height on edge effect at *P*=500 W, *V*=3000 mm/min.

For a set of process condition: *P*=500 W, *V*=1000 mm/min and *D*=3.87 mm (Figure 6.11), the trend is different from other sets of process conditions. In this process condition, the edge effect is more in the curvilinear laser bending process as compared with that of the straight line laser bending process. It may be due to the effect of melting occurred during this process condition of high laser power, slow scan speed and small beam diameter.

6.5 Effect of Arc Height on Bend Angle

Figure 6.14 to Figure 6.22 show the effect of arc height on bend angle. It can be seen that for a variety of process conditions the increase in arc height does not have significant effect on the bend angle except for the process conditions shown for Figure 6.15 and Figure 6.16.

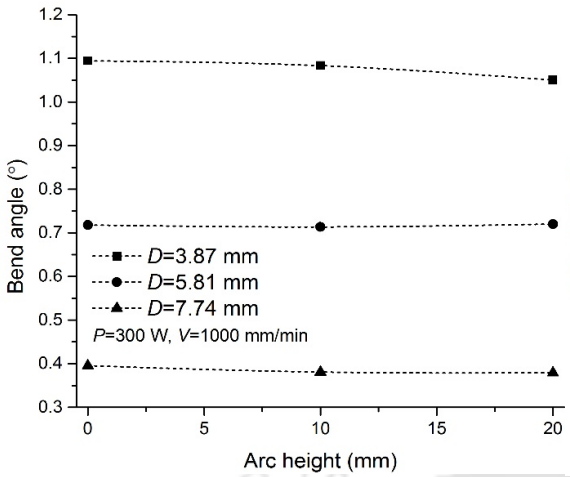

Figure 6.14. Effect of arc height on bend angle at *P*=300 W, *V*=1000 mm/min.

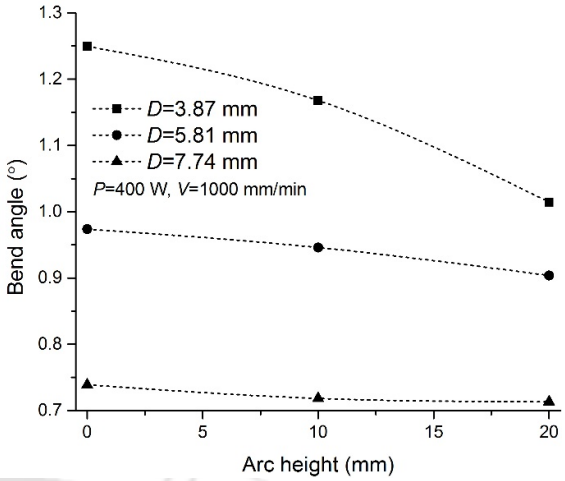

Figure 6.15. Effect of arc height on bend angle at *P*=400 W, *V*=1000 mm/min.

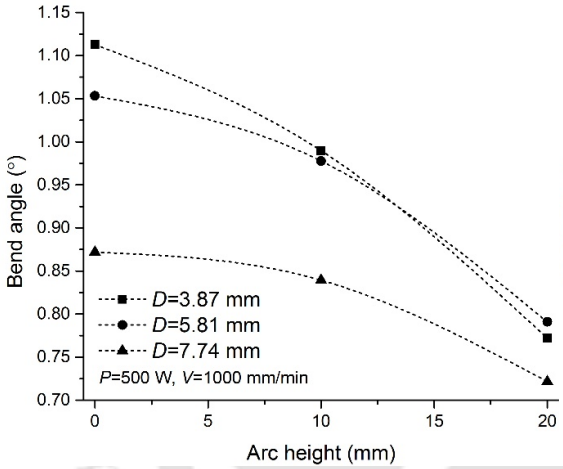

Figure 6.16. Effect of arc height on bend angle at *P*=500 W, *V*=1000 mm/min.

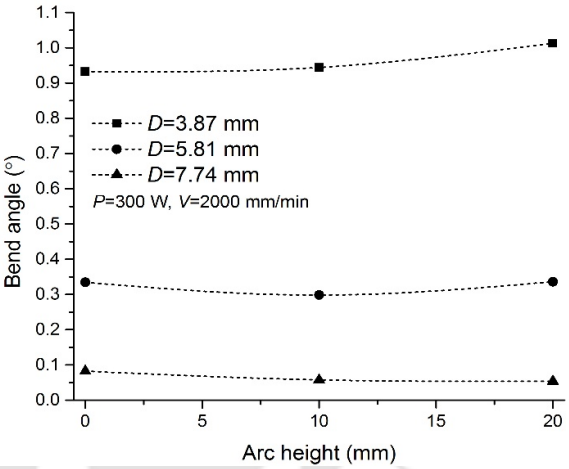

Figure 6.17. Effect of arc height on bend angle at *P*=300 W, *V*=2000 mm/min.

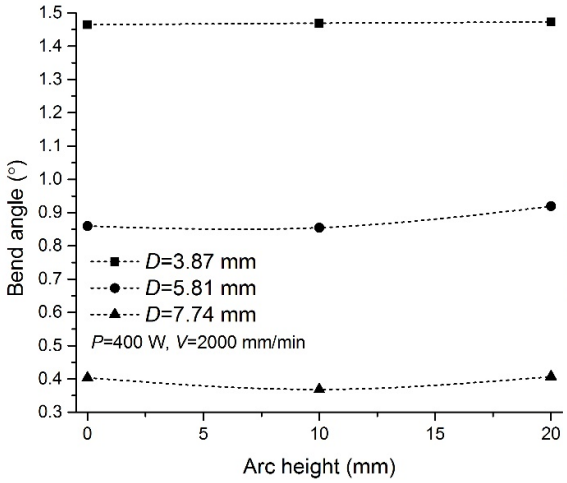

Figure 6.18. Effect of arc height on bend angle at *P*=400 W, *V*=2000 mm/min.

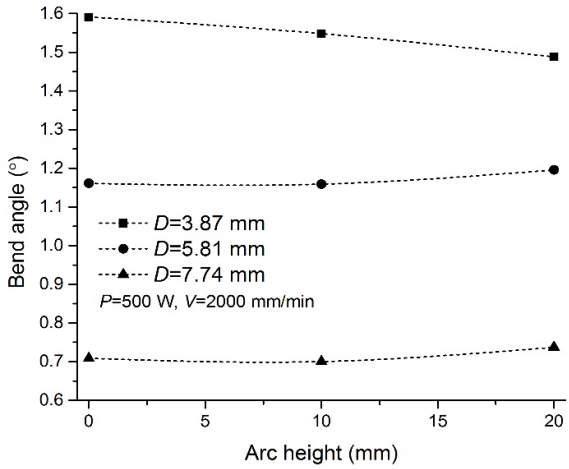

Figure 6.19. Effect of arc height on bend angle at *P*=500 W, *V*=2000 mm/min.

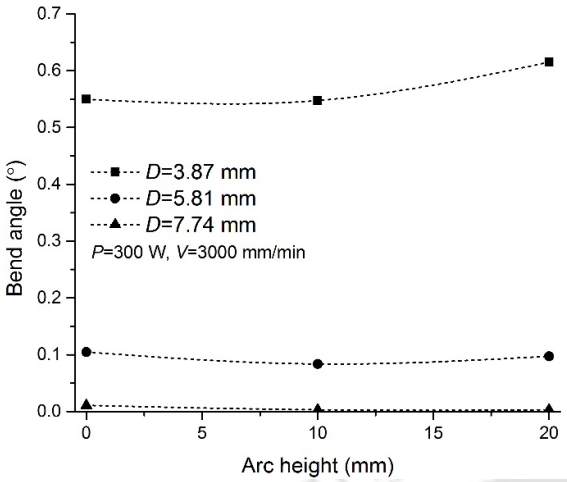

Figure 6.20. Effect of arc height on bend angle at *P*=300 W, *V*=3000 mm/min.

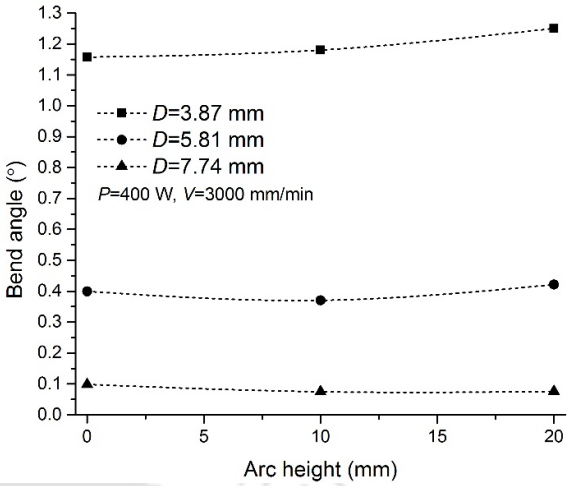

Figure 6.21. Effect of arc height on bend angle at *P*=400 W, *V*=3000 mm/min.

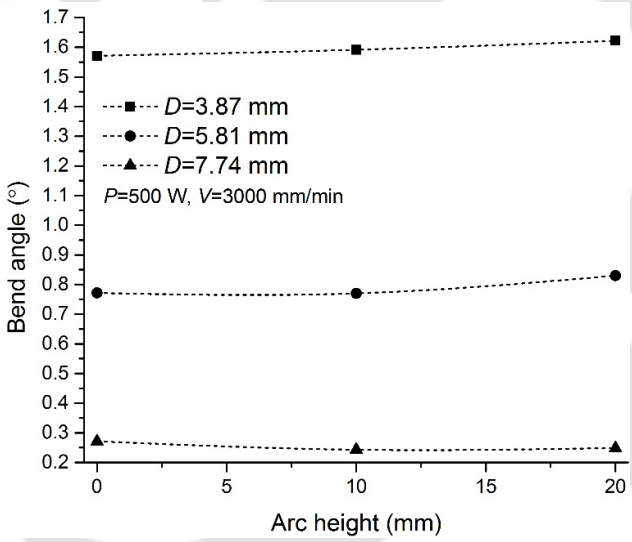

Figure 6.22. Effect of arc height on bend angle at *P*=500 W, *V*=3000 mm/min.

For the combination of slow scan speed (1000 mm/min) with medium (400 W) and high level (500 W) laser power, the bend angle decreases with the increase in arc height (Figure 6.15 and Figure 6.16). This may be due to the fact that these process conditions generate higher heat densities and higher peak temperatures. It was also observed that for these process conditions, the peak temperature at bottom surface also increases. This results in the plastic deformation at the bottom surface, and thus the bend angle decreases. The rate of decrease in bend angle with the increase in arc height is more at the high level of laser power (500 W). It is because the temperature at bottom surface is high, which generates a significant plastic deformation at the bottom surface. It leads to the significant decrease in bend angle at a high level of laser power.

The increase in arc height increases the contact time between laser beam and worksheet surface. This results in more preheating of the succeeding work material that reduces the temperature gradient in the worksheet. Thus, the bend angle decreases for higher levels of arc height.

6.6 Analysis of the Deformation Behavior: Bending Offset and Edge Displacement

Based on the studies reported in the earlier chapter, it was found that the worksheet bends along the scanning line during the straight line laser bending operation. However, in case of curvilinear irradiation, it is observed that the worksheet does not bend along the scanning path, and it has some offset away from the scanning path. The offset is always outside of the scanning path curvature. Figure 6.23 shows a three dimensional model of the bent worksheet with laser scanning start and bending start positions. It can be clearly seen that the bending occurs outside of the scanning path curvature, and the difference between laser scanning start and bending start positions is termed as the bending offset.

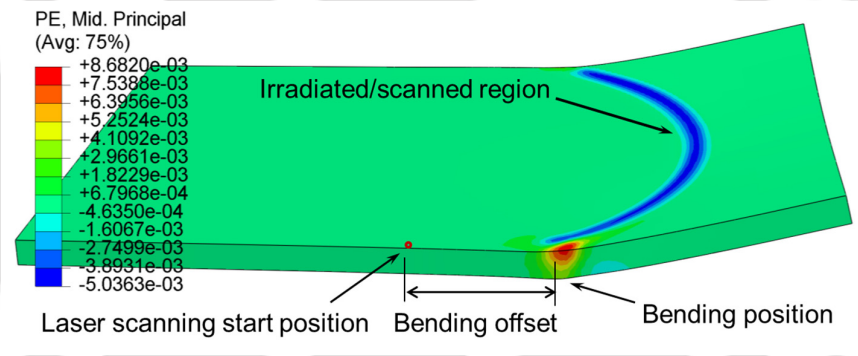

Figure 6.23. Bending offset observed in curvilinear laser bending process.

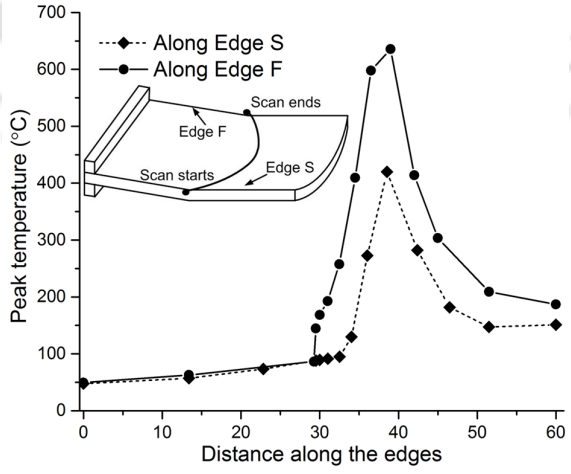

Figure 6.24. Distribution of the peak temperature along scan start and scan finish edges (P=300 W, V=1000 mm/min and D=3.87 mm).

The bending offset occurs mainly for two reasons, first is, the focus of the laser beam on the worksheet surface is partially outside of the worksheet near the Edge S and Edge F as shown in Figure 6.1 and Figure 6.2. It results in the offset of peak temperature outside the scanning path as shown in Figure 6.24. It can be seen that the peak temperature is far away from the scan start and scan finish positions. Scan started and finished at the middle of Edge S and Edge F, respectively, which is at 30 mm distance from the clamped side. The peak temperature occurred at a distance of about 40 mm from the clamped side, and therefore, the peak temperature has an offset of about 10 mm from the scan start and scan finish position. This leads to the offset in plastic deformation into the worksheet. Second reason is that the bending at middle of the scanning path tries to bend the worksheet away from the scanning path. For example, the bending about Point A (shown in Figure 6.1) tries to bend the worksheet about a y-axis passing through Point A. Therefore, the worksheet has a tendency to bend away from the scanning path. However, at the middle of the scanning path, the bending occurred over the scanning path.

The bending offset for all sets of process conditions are presented in Appendix 6.1. The effects of process parameters, *viz.* laser power, scan speed, beam diameter and arc height are studied on the bending offset. These are presented as follows.

6.6.1 Effect of laser power on bending offset

Figure 6.25 shows the comparison between scanning path profile and worksheet bending profile at laser power of 300 W and 500 W for a scan speed of 1000 mm/min and beam diameter of 3.87 mm. It can be observed that the bending path is offset by about 9.5 mm and 8.5 mm from the scan start position for 300 W and 500 W laser power, respectively. The bending offset is about 11 and 10.5 mm respectively at the end of the scanning path. The bending offset at both scan start and scan end points decrease with the increase in laser power. It may be due to the fact that the plastic deformation generated near the scanning path increases with the increase in laser power. It is because of larger thermal expansion in the heated region, and lower flow stress at higher temperature. As shown in Figure 6.24, the peak temperature is less at the scan start point and scan end point of the irradiation. The peak temperature has some offset from the scan start and scan end points. Therefore, the peak temperature near the scan start position and scan end position is too less to generate the plastic deformation, and hence the plastic deformation at middle of the scanning path dominates that leads to the higher bending offset. Similarly, when laser power is higher, the peak temperature at both scan start and scan end point is also higher. It generates comparatively larger plastic deformation near to the scan start

and scan end positions. This reduces overall tendency of the worksheet to bend away from the worksheet caused by the plastic deformation at middle of the scanning path. Therefore, the bending offset decreases with the increase in laser power.

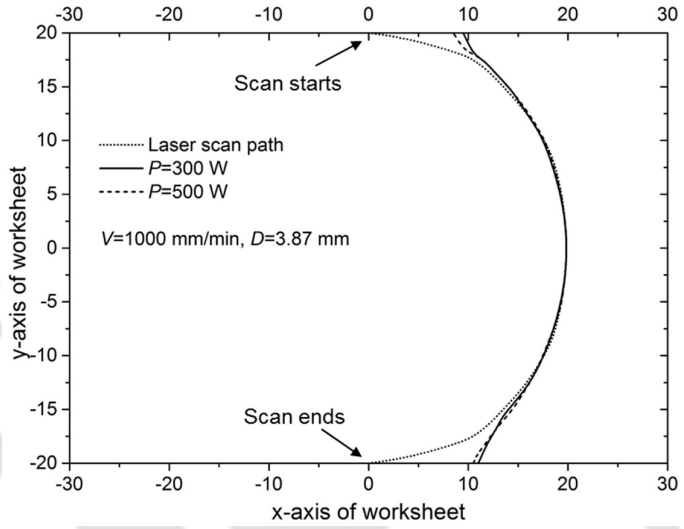

Figure 6.25. Effect of laser power on bending path profile.

The bending offset is more at the end of irradiation. It is because near to the scan start position, the plastic deformation starts as the irradiation starts, and the effect of plastic deformation at the middle of the scanning path (which is responsible for the increases in the bending offset) starts later. It reduces the bending offset. However, near to the scan finish position, the laser beam reaches later while the effect of plastic deformation at the middle of the scanning path starts earlier. As the plastic deformation at middle of the scanning path has a tendency to generate a bending offset, which is more near to the scan finish position.

6.6.2 Effect of scan speed on bending offset

Effect of scan speed on bending profile is shown in Figure 6.26. It shows a comparison between scanning profile (path) and worksheet bending profile for two levels of scan speed, *viz*. 1000 mm/min and 3000 mm/min for a laser power of 500 W and beam diameter of 3.87 mm. It can be seen that the bending offsets are about 7.5 mm and 8.5 mm at the scan start for a scan speed of 1000 mm/min and 3000 mm/min, respectively. The offset values of about 10.5 mm and 9.5 mm are noted at the scan finish position for a scan speed of 1000 mm/min and 3000 mm/min, respectively. The bending offset decreases with the increase in scan speed. It is due to the decrease in peak temperature at a faster scan speed as shown in Figure 6.27. The plastic deformation decreases at faster scan speed as a result of lower peak temperature. Also, the

effect of material preheating is less at a faster scan speed as the heating time is less. The bending offset is more near to the laser beam exit edge (Edge F), which is due to higher peak temperature at this edge as compared to that of the scan start edge (Edge S) (Figure 6.27).

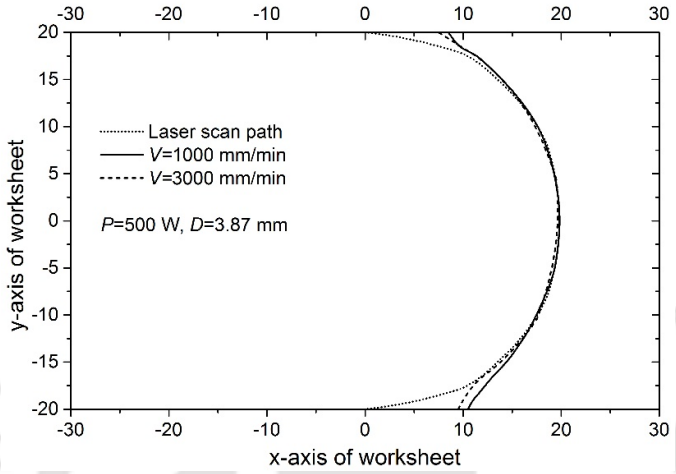

Figure 6.26. Effect of scan speed on bending path profile.

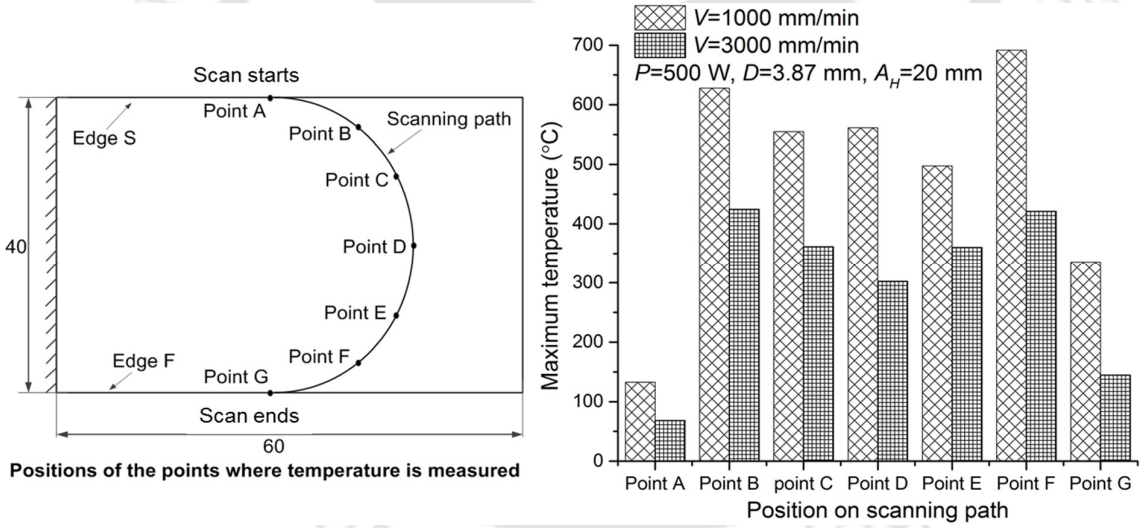

(a) (b)

Figure 6.27. (a) Positions of points where temperature data are extracted (b) Distribution of the peak temperature along the scanning path.

6.6.3 Effect of beam diameter on bending offset

Figure 6.28 shows the effect of laser beam diameter on the worksheet bending profile. For beam diameter of 3.87 mm and 7.74 mm, at the scan start (Edge S), the bending offset of about 9.5 mm and 12.5 mm were observed, respectively. At the end of irradiation, the bending offsets were 8.5 mm and 11 mm for beam diameter of 3.87 mm and 7.74 mm, respectively. At both, scan start and scan end points, the bending offsets increase with the increase in beam diameter.

It is because the peak temperature offset increases with beam diameter as shown in Figure 6.29. It can be seen that the peak temperature occurs at a distance of about 37 mm (7 mm offset from scan start) and 42 mm (12 mm offset from scan start) from the clamped edge along the Edge S for a beam diameter of 3.87 mm and 7.74 mm, respectively. The offset in peak temperature occurs because the complete laser beam does not enter at the starting and end time of the irradiation. Initially, it has a point contact at the Edge S. As the irradiation starts, the laser beam enters gradually into the worksheet as shown in Figure 6.1 and Figure 6.2. Relatively higher temperature occurs near the position when a complete laser beam just enters into the worksheet. As the scanning path is curvilinear, and therefore the peak temperature has some offset towards the free edge. The increase in peak temperature offset with beam diameter leads to the increase in bending offset at a larger beam diameter.

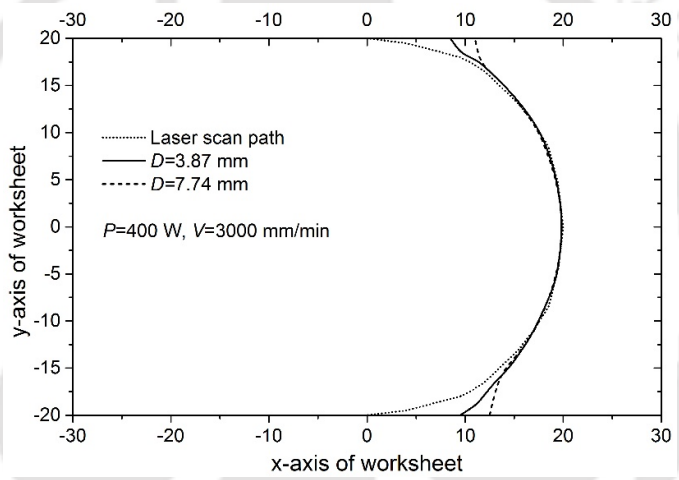

Figure 6.28. Effect of laser beam diameter on bending path profile.

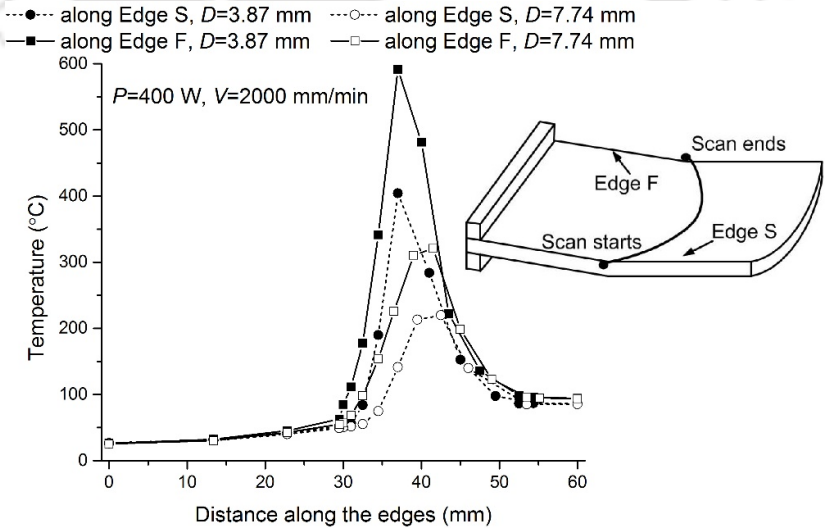

Figure 6.29. Effect of beam diameter on peak temperature distribution along Edge S and Edge F.

6.6.4 Effect of arc height on bending offset

Figure 6.30 and Figure 6.31 show the effect of arc height on the bending offset at Edge S and at Edge F, respectively. It can be seen that the bending offset increases with the increase in arc height at both the edges. The same trends were observed for all sets of processing conditions. It is mainly due to two reasons; first the peak temperature offset increases with the increase in arc height as shown in Figure 6.32, and second, the distance of outer most point at the scanning path (Point A, see Figure 6.1) from straight line axis increases with the increase in arc height. As discussed earlier, the plastic deformation at the middle of the scanning path (for example Point A) tends to bend the worksheet away from the scanning path, and therefore the bending offset increases with the increase in arc height.

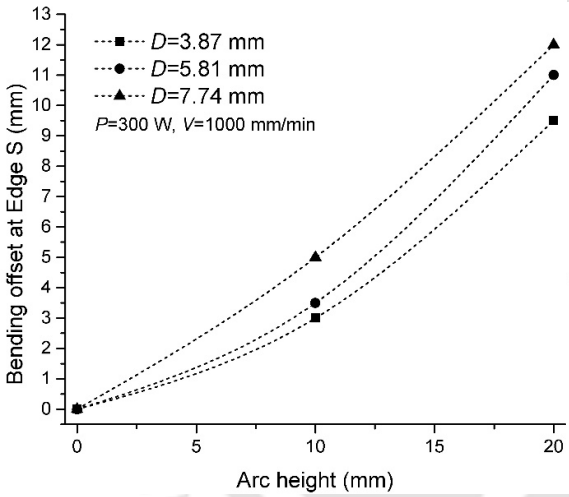

Figure 6.30. Effect of arc height on bending offset at Edge S.

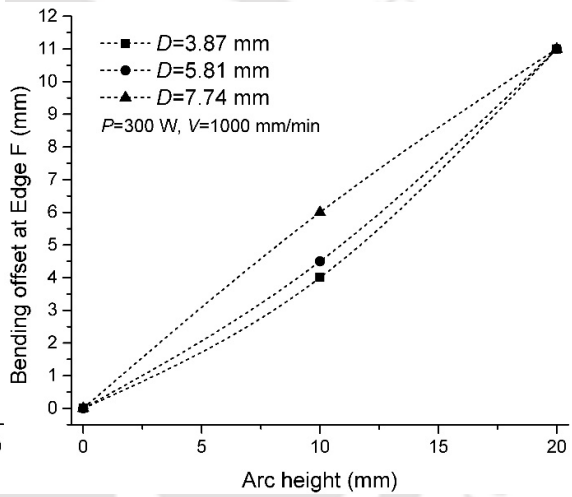

Figure 6.31. Effect of arc height on bending offset at Edge F.

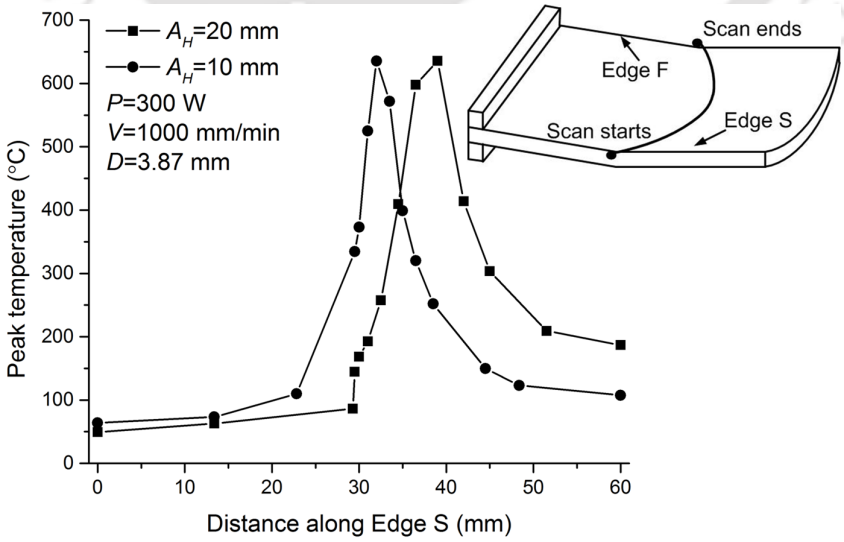

Figure 6.32. Effect of arc height on peak temperature offset.

6.6.5 Effect of arc height on edge displacement

Scanning path curvature affects the edge displacement induced by the laser beam irradiation. Figure 6.33 and Figure 6.34 show the vertical displacement produced by the laser beam irradiation along Edge S and Edge F respectively at various arc heights. It can be seen that the bending occurs at the middle of the edge (at 30 mm), when laser is irradiated along a straight line (arc height is zero). As the arc height increases, the bending moves away from the mid-point. It is due to the curvilinear irradiation which creates bending offset. The bending offset increases with the increase in arc height as discussed in Section 6.6.4. It can be seen that in case of curvilinear irradiation, the bending does not occur along a single line axis, however the bending occurs in a curved profile as shown in Figure 6.33 and Figure 6.34. It is also observed that in case of the curvilinear irradiation, the Edge S and Edge F move in downward direction near to the worksheet bending position. It is due to the curvilinear irradiation, which generates three dimensional deformation along the scanning path.

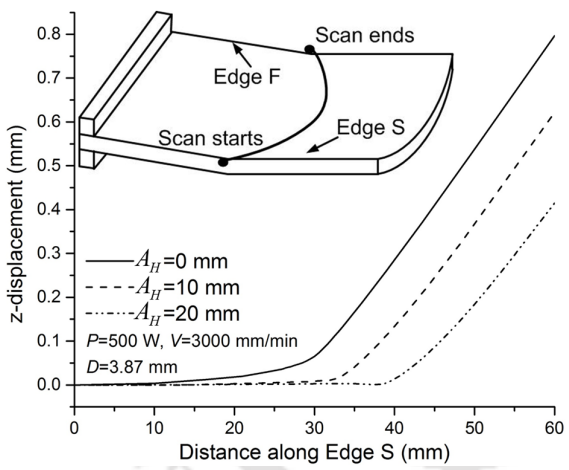

Figure 6.33. Effect of arc height on z-displacement along Edge S.

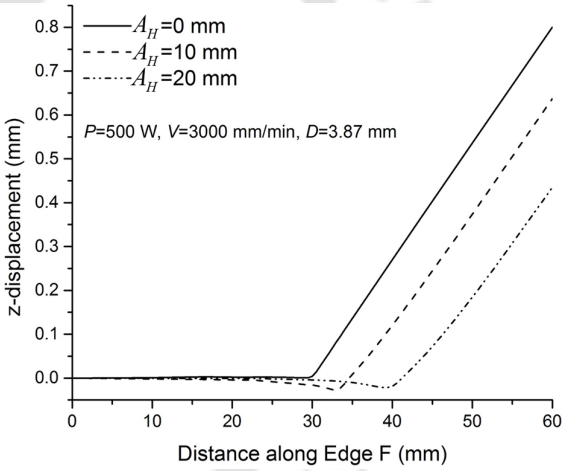

Figure 6.34. Effect of arc height on z-displacement along Edge F.

Figure 6.35 shows the z-displacement (vertically upward) along the free edge of the worksheet. The study of z-displacement along the free edge is important to investigate the effect of arc height on warping. It may be a helpful guideline for the use of laser in sheet alignment applications. It can be observed that the z-displacement along the free edge decreases with the increase in arc height. It is due to the fact that the bending occurs near to the free edge when arc height is more, and similarly, it occurs at a larger distance when arc height is less. Therefore, for the same bend angle, the z-displacement is less, when arc height is more. It is also observed that the warping is less at the free edge when arc height is less. It is due to less

scanning path curvature at a smaller arc height. The mechanical constraint (clamping) may also have significant role in warping. The clamping is closer to the scanning path when arc height is less, and therefore it resists the curved deformation along the y-axis more effectively. Hence, the warping decreases with the decrease in arc height.

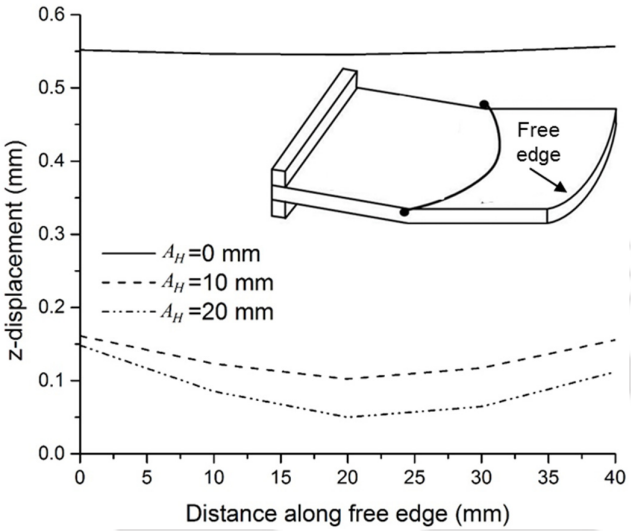

Figure 6.35. Effect of arc height along the free edge.

For all sets of process conditions, warping at the free edge was found to be more for higher arc height, and a bowl shape is observed as shown in Figure 6.35. Therefore, the curvilinear laser bending process can be used to generate complex shapes and for the alignment of sheets with complex geometries by controlling the arc height or laser scanning path. The presented results may be important guidelines in such applications.

6.7 Summary

This chapter presented numerical simulation and experimental validation of curvilinear laser bending of magnesium alloy M1A sheet. A three-dimensional non-linear coupled thermo-mechanical numerical model has been developed for the curvilinear laser bending process, and validated with the experimental results. The numerical results and their trends were found to be in good agreement with the experimental results.

Developed model was used to study the effect of scanning path curvature on the edge displacement, bend angle, and the deformation behavior. The deformation behavior of the curvilinear laser bending process was found to be different from that of the straight line laser bending process. The results showed that in curvilinear laser bending process, the bending does not occur over the scanning path. The bending was occurred outside of the scanning path

curvature. Effects of process parameters on bending offset were studied, and it was observed that the bending offset decreases with the increase in laser power and scan speed and increases with the increase in beam diameter. Beam diameter was the most effective parameter which influenced the bending offset.

The effect of variation in scanning path curvature on the edge displacement was also studied. It was found that the z-displacement decreases with the increase in arc height. The warping at the free edge decreased as the scanning path moved towards the clamped edge (less arc height). It was observed that in curvilinear laser bending, the sheet bends along a curved profile.

The bend angle was found to be affected by the scanning path curvature. It was observed that depending on the set of process condition, the bend angle may increase or decrease with the change in scanning path curvature. It was also observed that the edge effect is less for the curvilinear laser bending process in comparison with that obtained in straight line laser bending process. However, for curvilinear laser bending, the edge effect was increased with the increase in arc height. In general, the edge effect was less for the curvilinear laser bending with 10 mm of arc height.

CHAPTER 7: MULTI-SCAN LASER BENDING OF MAGNESIUM M1A ALLOY SHEETS

7.0 Scope

This chapter presents numerical studies on multi-scan laser bending of magnesium alloy M1A sheets. The need to carry out the numerical simulations is defined. Initially the methodology for numerical simulations using finite element method is presented. Then, the validation of the predictions by numerical model using experimental results is presented. Further detailed analysis of the effects of process parameters on bending mechanism and deformation behavior for multi-scan mode of operation is presented. The chapter concludes with discussion on the parametric studies in a view of improvement in the productivity of laser bending process using multi-scan approach.

7.1 The Need

Single scan laser bending produces small bend angles of the order of 1º. However, in real life industrial applications, large bend angles (of the order of 10º) are required, which may not be possible to obtain using single laser scan. To overcome this limitation, experimental studies have been attempted by employing multiple scans during laser bending process (Cheng and Yao 2001, Edwardson et al. 2006, Edwardson et al. 2010). However, numerical studies are important to explore the insight of the process in terms of the bending mechanism, bend angle, edge effect and temperature distribution during each laser scan of the multi-scanning mode of operation. The investigation on these aspects may help to improve the product quality and process efficiency of the process. A need, thus, exists to carry out the numerical simulations of the multi-scan laser bending process to study the bending mechanism and the effects of process parameters on bend angle and edge effect. This forms the basis of the present work.

7.2 Numerical Simulations of Multi-scan Laser Bending

The laser beam scans over the worksheet surface from its start position to the end position along a straight line and returns to its start position. This complete cycle is called one laser scan/irradiation. In this work, total 10 number of laser scans have been employed to investigate the effect of various process parameters on the performance parameters. After each scan, the laser machine takes about 5 seconds to return to the laser start position. Therefore, in the present numerical simulations, a natural cooling is applied to the worksheet for 5 seconds in between

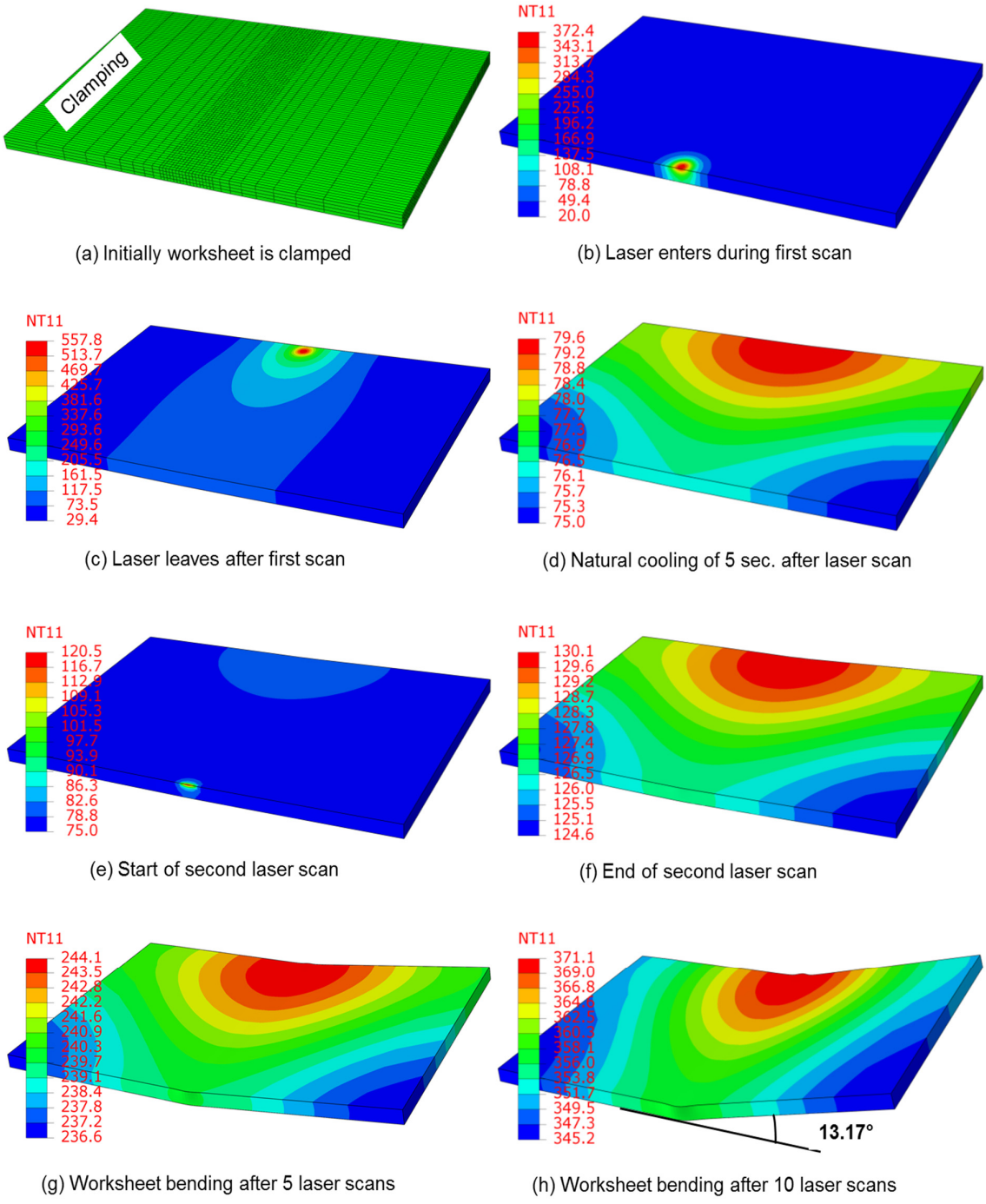

Figure 7.1. Steps in multi-scan laser bending of the worksheet (P=300 W, V=1000 mm/min and D=3.87 mm).

two successive laser scans. Details regarding the thermal analysis and mechanical analysis in terms of the governing equations, boundary conditions; geometric modeling of worksheet; material modeling; meshing; and solution methodology are presented in Chapter 4. Figure 7.1 shows various steps involved in the multi-scan laser bending process. It can be seen that

initially, the worksheet do not have any thermal load (Figure 7.1 (a)), and the worksheet is at room temperature condition. The laser beam starts heating the worksheet surface from the laser start position, scans along a pre-defined straight line path and after completing the scan, the laser returns to its start position as shown in Figure 7.1 (b) to Figure 7.1 (d). This repeats for a number of times as shown in Figure 7.1 (e) to Figure 7.1 (h). Figure 7.1(h) shows a typical bend angle of about 13.17º obtained at the end of 10 number of scans.

7.3 Experimental Validation of Numerical Simulations

In the present work, experiments have been carried out to validate the results predicted by the developed numerical model. During the experiments, ten number of scans were applied over the worksheet surface. Each laser scan was followed by a natural cooling of about 5 seconds. In this duration, the laser source moved from laser end to the laser start position, and prepared itself to start the next irradiation. The size of specimen was 70 mm length, 40 mm width and 1.9 mm thickness. Graphite spray coating was applied over the worksheet surface. It was applied only once before the start of the first laser scan even though it ablates due to the laser beam irradiations. After ten laser scans, the bend angle was measured over the coordinate measuring machine (CMM). Details of specimen preparation, application of coating and measurement of the bend angle are presented in Chapter 3.

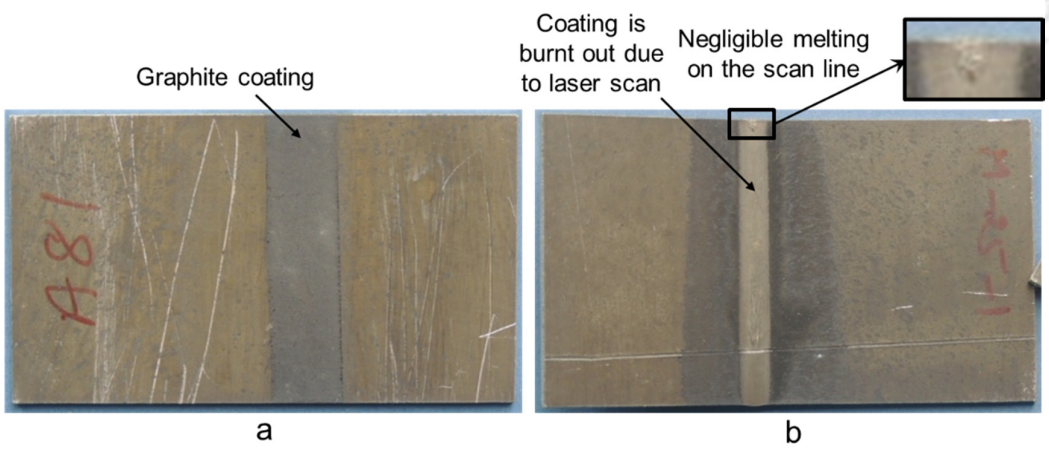

Figure 7.2. Graphite spray coated and laser beam irradiated bent specimen.

Figure 7.2 shows magnesium alloy worksheet specimens undergone multi-scan laser bending process. Figure 7.2 (a) shows graphite spray coated specimen. The coating was found to be damaged due to the laser heating as shown in Figure 7.2 (b). Figure 7.3 shows the bent specimens for various process conditions. It can be observed that a significantly large bend angle up to 15.50º was achieved with multi-scan laser bending process.

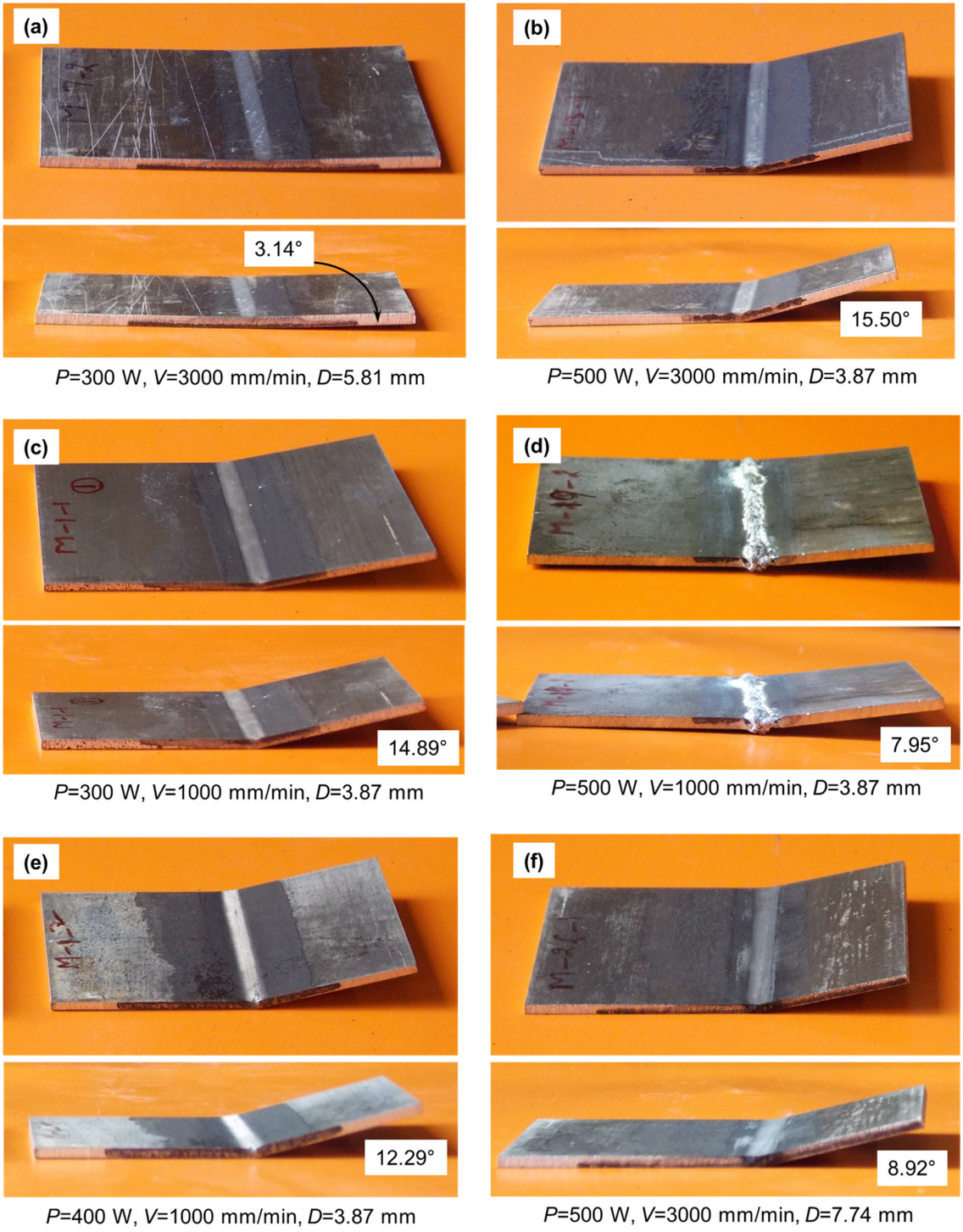

Figure 7.3. Laser bent specimens with multiple scans.

The experimental results were used to validate the developed numerical model for the multi-scan laser bending of magnesium alloy M1A sheets. A comparison between bend angle obtained from the numerical model and experimental studies is given in Table 7.1. The

percentage of the absolute error between numerical and experimental results is shown in Table 7.1 and Figure 7.4. It can be observed that the numerical model is able to predict the bend angle with an acceptable average absolute error of about 12.41%. The minimum absolute error is 2.97% while the maximum is about 22.7%. From the prediction error, it can be concluded that the numerical model predicts the process responses well for the chosen ranges of process conditions. It can also be observed that the bend angle is increased by 9.29–24.05 times for various process conditions, when the number of scans increased from one to ten. In multi-scan laser bending, a significant bend angle was obtained for some sets of process conditions, when the noticeable bending was not observed with the single scan laser bending process.

Table 7.1. Comparison between numerical and experimental results of single and multi-scan laser bending of magnesium alloy M1A.

Data-set No.	*P* (W)	*V* (mm/min)	*D* (mm)	Multi-scan laser bending with 10 laser scans				Performance enhancement during multi-scan mode in comparison with that of single scan mode	
				Num.	Exp.	*CV* (%)	Error (%)	Bend angle in single scan (Exp.)	Enhancement in bend angle after 10 scans (No. of times)
1	300	1000	3.87	13.17	13.58	7.01	2.97	1.069	12.70
2	300	1000	5.81	10.99	11.49	4.22	4.37	0.731	15.71
3	300	1000	7.74	8.64	9.07	0.81	4.72	0.490	18.50
4	300	2000	3.87	13.16	10.89	1.94	20.85	0.836	13.02
5	300	2000	5.81	8.05	7.06	11.28	13.94	0.312	22.63
6	300	2000	7.74	4.22	3.54	9.69	19.23	*	-
7	300	3000	3.87	9.48	7.73	7.47	22.66	0.604	12.80
8	300	3000	5.81	3.55	3.01	3.19	17.96	0.139	21.68
9	300	3000	7.74	1.06	0.86	6.56	22.70	*	-
10	400	1000	3.87	12.99	11.90	2.37	9.14	1.281	9.29
11	400	1000	5.81	11.84	10.49	1.99	12.83	0.836	12.55
12	400	1000	7.74	10.93	9.33	0.99	17.18	0.771	12.10
13	400	2000	3.87	16.07	14.49	0.37	10.94	1.305	11.10
14	400	2000	5.81	13.13	11.96	3.22	9.80	0.766	15.62
15	400	2000	7.74	9.29	8.33	13.33	11.50	0.437	19.07
16	400	3000	3.87	14.98	12.81	4.44	16.95	1.113	11.51
17	400	3000	5.81	8.92	7.69	15.17	15.96	0.418	18.40
18	400	3000	7.74	4.18	3.50	17.28	19.46	*	-
19	500	1000	3.87	9.04	7.79	2.49	16.07	0.993	7.85
20	500	1000	5.81	9.35	8.86	0.65	5.50	0.940	9.43
21	500	1000	7.74	9.38	8.83	3.38	6.17	0.753	11.73
22	500	2000	3.87	16.37	15.39	1.11	6.36	1.425	10.80
23	500	2000	5.81	15.35	13.42	0.47	14.37	1.003	13.38
24	500	2000	7.74	12.51	11.45	4.66	9.24	0.721	15.88
25	500	3000	3.87	17.09	15.25	1.53	12.09	1.268	12.03
26	500	3000	5.81	12.72	12.20	7.12	4.27	0.838	14.56
27	500	3000	7.74	7.64	8.30	13.53	7.91	0.345	24.05

*** insignificant bend angle (<0.1º), Num.=Numerical bend angle (º) Exp.=Experimental bend angle (º), *CV*=Coefficient of variation**

Average prediction (absolute) error = 12.41%

Average Enhancement in bend angle = 14.43 times more than the single scan

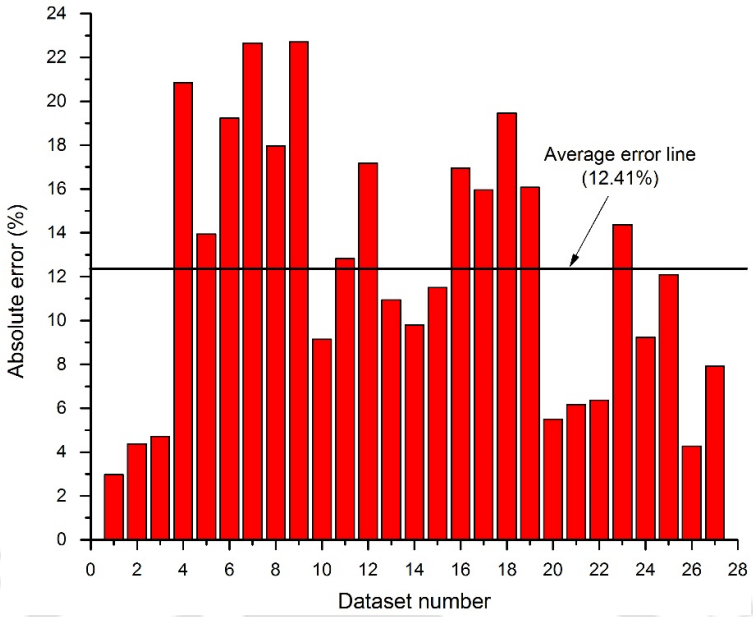

Figure 7.4. Absolute prediction error between numerical and experimental bend angle.

During experimental studies, it was noticed that for some of the process conditions such as P=500 W, V=1000 mm/min and D=3.87 mm, the work surface melts. Figure 7.3 (d) shows the bent specimen with a melted work surface. During melting, the applied energy is utilized for the phase transformation, which affects the plastic deformation of the worksheet. For an efficient bending operation, melting is not desired. Melting is generally governed by many random parameters, such as surface conditions, thickness of the coating, damage of the coating in preceding scans, and surrounding conditions. These parameters are difficult to control. Also, it is very difficult to model the effects of such random parameters in the numerical model. However, the present numerical model considers the effect of melting by taking into account the latent heat (Section 4.2.2).

The validated numerical model was further used to investigate the multi-scan laser bending of magnesium alloy M1A. Simulations were carried out to study the effect of process parameters such as laser power, scan speed, beam diameter on the performance parameters, *viz*. temperature, stress, strain, bend angle and edge effect during multi-scan laser bending process.

7.4 Bending Mechanism: Effect of the Number of Scans

In this section, effects of the number of scans on the temperature distribution, stress-strain distribution and distortions are presented for a typical process condition of P=300 W, V=1000 mm/min and D=3.87 mm. The results are presented based on the numerical simulations for a typical process condition of P=300 W, V=1000 mm/min and D=3.87 mm.

7.4.1 Temperature distribution

Figure 7.5 shows temperature history at Point A (top) and Point B (bottom) for multi-scan laser bending of magnesium alloy M1A for a typical process condition of P=300 W, V=1000 mm/min and D=3.87 mm. It can be observed that a steep temperature gradient occurs between top and bottom surfaces of the worksheet. In each successive scan, peak temperature at both top and bottom surfaces is higher than the previous laser scan as the worksheet is preheated. The peak temperature and percentage change in the peak temperature at top and bottom surfaces after each laser scans are shown in Figure 7.6. It can be seen that the percentage change in temperature at the bottom surface is more than the top surface. It is due to the continuous heat flow from the top to the bottom surface as a result of temperature gradient. The peak temperature increases due to the preheating of worksheet in each successive scan, and exceeds the melting temperature (649 °C) in sixth laser scan. The similar observation was also made during the experimental study on multi-scan laser bending of magnesium alloy (see Figure 7.2 and Figure 7.3). This verifies the need for the consideration of the melting phenomenon in the numerical model, which makes the model more realistic.

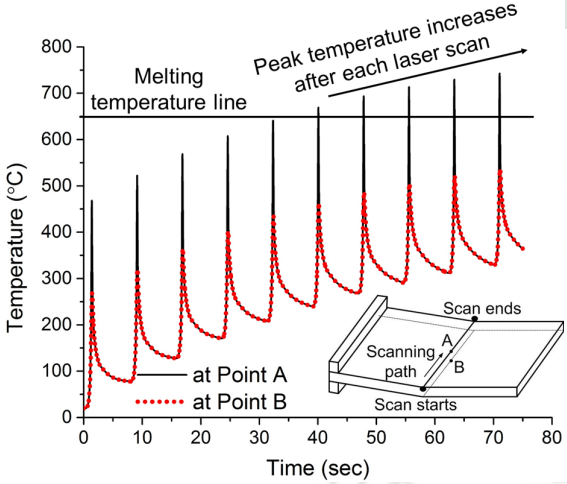

Figure 7.5. Temperature history at top and bottom surfaces.

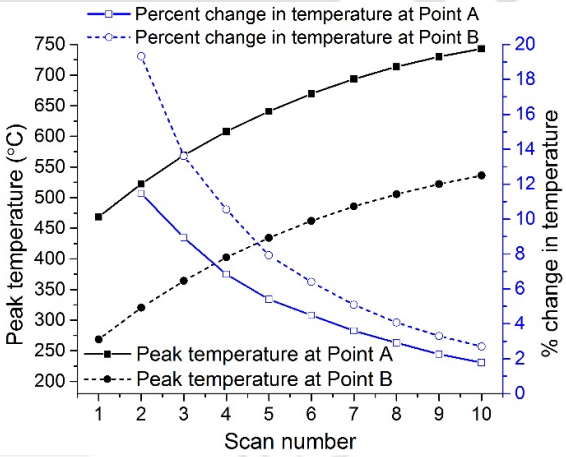

Figure 7.6. Change in temperature at top and bottom surfaces with number of scans.

7.4.2 Stress distribution

During laser bending, as the temperature increases, thermal expansion occurs in the heated region. The surrounding material at relatively low temperature resists the expansion of the heated region. This results in the generation of compressive stresses in the heated region and tensile stresses in the surrounding region.

Figure 7.7 shows x-direction stress history at Point A and Point B. It can be observed that as the laser beam reaches over Point A, compressive stresses are induced. It is because the temperature at Point A becomes higher compared to the surrounding material, and hence the expansion at Point A is resisted by the surrounding cooler materials. When the laser beam moves away, the temperature at Point A decreases, and therefore the thermal expansion at Point A is less as compared to the nearby heated region. This induces tensile stresses at Point A. In the worksheet the heat flows in the thickness direction quickly, which leads to the increase in temperature at Point B. This generates compressive stresses at Point B. These tensile and compressive stresses are induced during each laser scan (Figure 7.7). It can also be observed that the induced stresses decrease with the successive laser scans. It is because the worksheet temperature increases in each scan, and the heated material provides less restriction to the thermal expansion. This results in the decrease in thermal stresses after each scan.

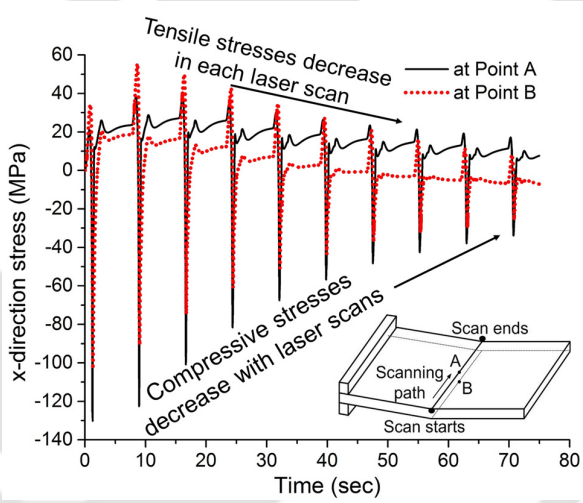

Figure 7.7. x-direction stress history at top and bottom surfaces.

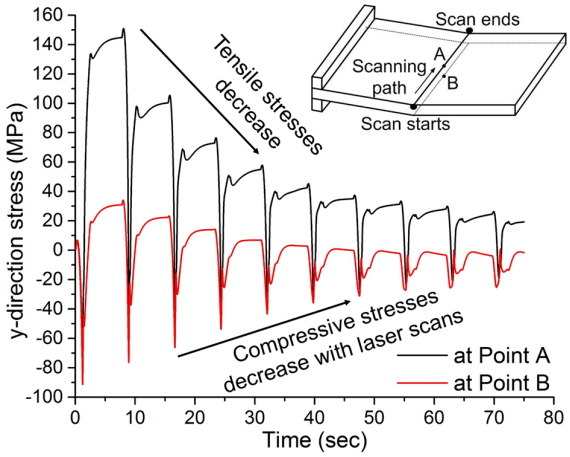

Figure 7.8. y-direction stress history at top and bottom surfaces.

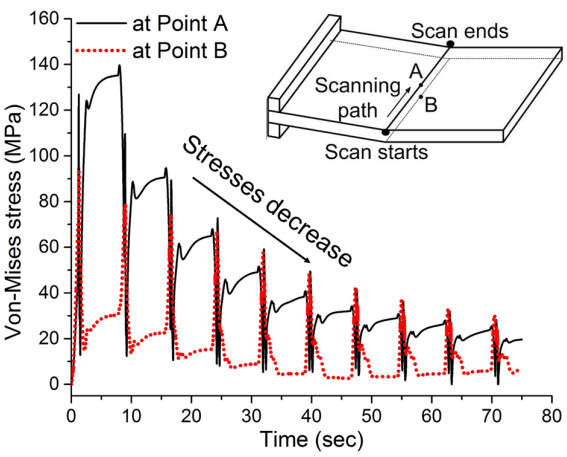

Figure 7.9. Von-Mises stress history at top and bottom surfaces.

Figure 7.8 shows y-direction stress history at Point A and Point B. Stresses induced in y-direction result in the worksheet bending along the scanning path. It can be seen that the components of induced stresses decrease in each consecutive scan. It is due to the softening of material at the elevated worksheet temperature during each scan, which results in less resistance of material to the thermal expansion in the heated region. The decrease in the magnitude of induced thermal stresses components results in the decrease of von-Mises stresses as shown in Figure 7.9.

7.4.3 Plastic strains and distortions

During the laser bending operation, when the induced thermal stresses exceed the temperature dependent flow stress, the plastic deformation occurs in the worksheet. The x-direction plastic strain history at Point A and Point B is shown in Figure 7.10. It can be observed that the plastic deformation is compressive at both Points A and Point B. It may be attributed to the fact that the temperature at Point B is high enough to generate the plastic deformation. The plastic compressive deformation at Points A and Point B increases with increase in the number of scans. The difference between plastic deformation at Point A and Point B also increases with increase in the number of scans. This leads to the increase in bend angle after each scan. Thus, the worksheet bends mainly due to the difference between plastic deformations at the top and bottom surfaces. The history of worksheet bending during multi-scan laser bending process is shown in Figure 7.11. It shows that the bend angle linearly increases during the laser heating phase, and it is almost constant during the cooling phase. The bend angle increases with increase in the number of scans.

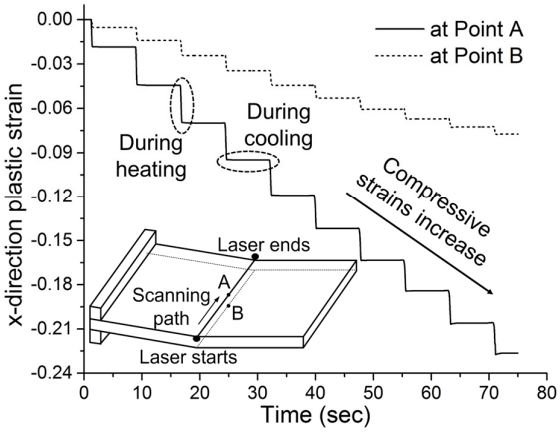

Figure 7.10. x-direction plastic strain history at top and bottom surfaces.

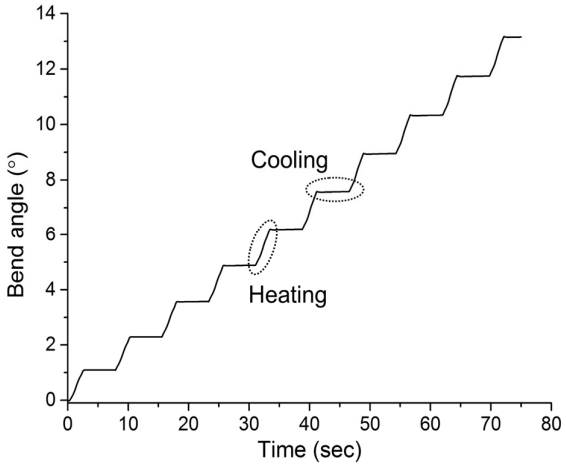

Figure 7.11. Worksheet bending history at middle of scanning path.

7.5 Bend Angle: Effect of Process Parameters

In this work, the effects of various process parameters such as laser power, scan speed and beam diameter on bend angle were studied for ten numbers of scans. The bend angle was measured at the middle of the scanning path as shown in Figure 3.10 (Chapter 3).

7.5.1 Effect of laser power

Figures 7.12 to Figure 7.14 show the effect of laser power on total bend angle after ten laser scans. It can be observed that the numerical results are in good agreement with the experimental results. The trends of variation of bend angle predicted by the developed numerical model are similar to those obtained in experiments. For all levels of beam diameter, the bend angle increases with the increase in laser power at scan speed of 2000 mm/min and 3000 mm/min. It is due to more energy input at the higher laser power, which leads to the higher plastic deformation and larger bend angle.

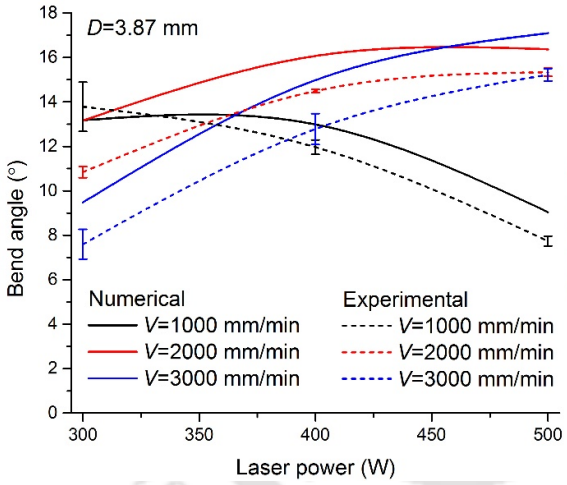

Figure 7.12. Effect of laser power on total bend angle at small beam diameter after 10 laser scans.

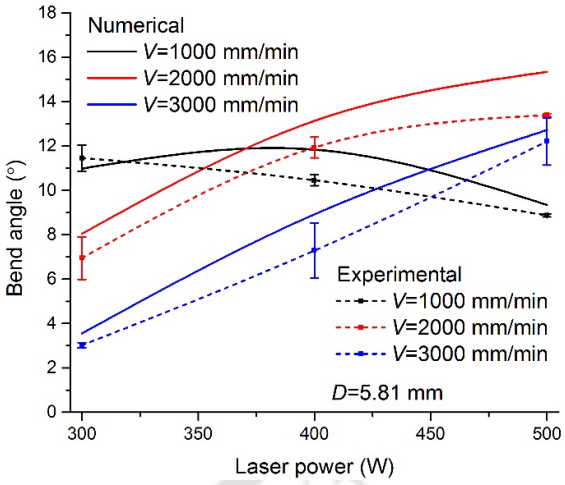

Figure 7.13. Effect of laser power on total bend angle at medium beam diameter after 10 laser scans.

At a scan speed of 1000 mm/min, the effect of laser power on the bend angle was found to be different than that observed with a scan speed of 2000 mm/min and 3000 mm/min. At a small beam diameter of 3.87 mm, the bend angle decreases with the increase in laser power. It may be due to two reasons, first, the significant melting occurs at high laser power as shown in Figure 7.3, and the energy is consumed into the phase transformation instead of the worksheet bending. The second reason may be that due to a slow scan speed and small beam diameter, the peak temperature is high at the bottom surface, and consequently the plastic deformation is also high.

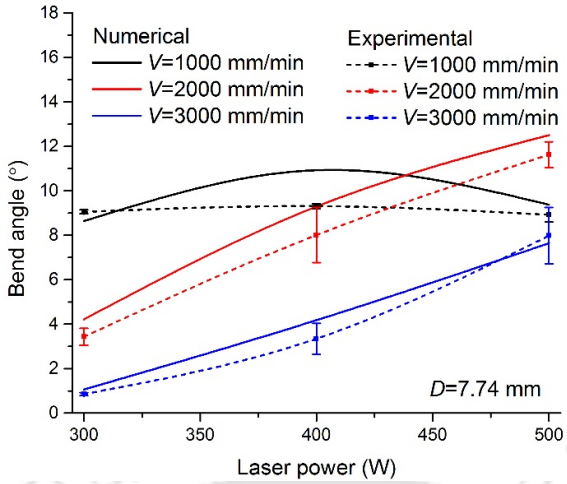

Figure 7.14. Effect of laser power on total bend angle at large beam diameter after 10 laser scans.

The plastic deformation at bottom surface increases with the increase in laser power. It results in the decrease of bend angle at higher laser power. At larger beam diameters of 5.81 mm and 7.74 mm, the bend angle first increases and then decreases with the increase in laser power. It is because the heat flux density is less at larger beam diameter and the increase in laser power leads to a higher peak temperature at both top and bottom surfaces. The peak temperature at the bottom surface is not enough to generate a significant plastic deformation. Therefore, the bend angle increases with the increase in laser power, however, further increase in the laser power, leads to a significant plastic deformation at the bottom surface, which results in the decrease in bend angle.

7.5.2 Effect of scan speed

Figure 7.15 to Figure 7.17 show the effect of scan speed on total bend angle after ten laser scans. It can be seen that the numerical results are in good agreement with the experimental studies. The trends of variation of bend angle predicted by the developed numerical model are similar to those obtained in experiments. From the figures, it can be seen that at low laser power of 300 W, the bend angle decreases with the increase in scan speed for all levels of beam diameter. It is because the energy absorption per unit length decreases with the increase in scan speed. This results in the decrease in peak temperature and plastic deformation, and hence the bend angle reduces at faster scan speed. For a combination of high laser power and small beam diameter, the bend angle increases with the increase in scan speed as shown in Figure 7.15. It is because at a slower scan speed, the peak temperature and plastic deformation at the bottom surface are significantly high, which reduces the bend angle. The increase in scan speed

decreases the plastic deformation at the bottom surface, and hence the bend angle increases with the increase in scan speed.

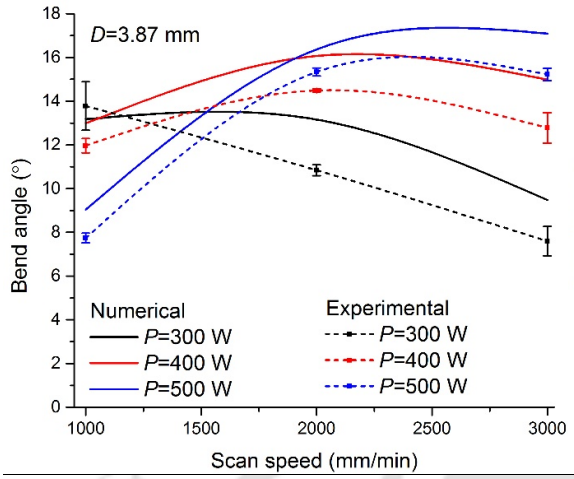

Figure 7.15. Effect of scan speed on total bend angle at small beam diameter after 10 laser scans.

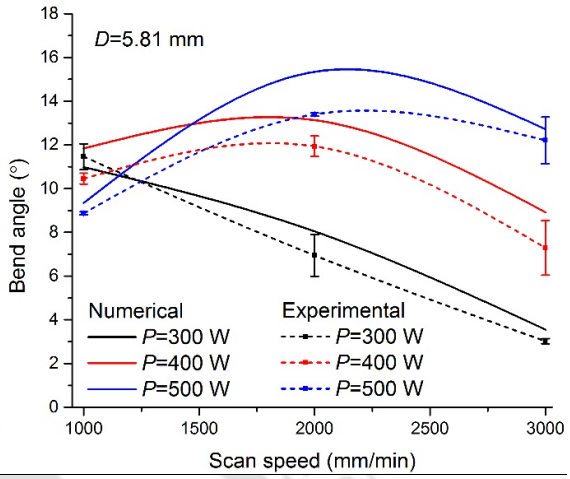

Figure 7.16. Effect of scan speed on total bend angle at medium beam diameter after 10 laser scans.

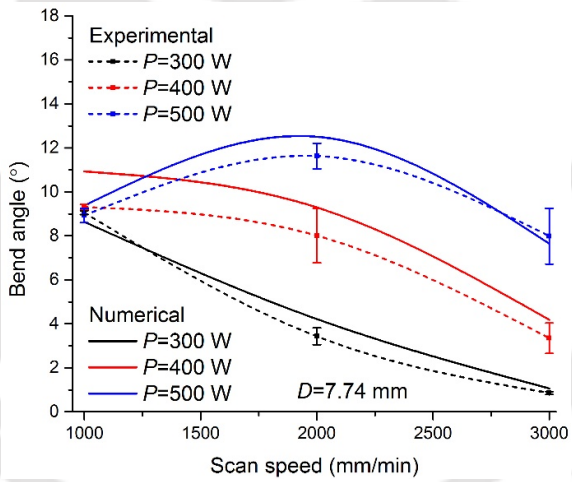

Figure 7.17. Effect of scan speed on total bend angle at large beam diameter after 10 laser scans.

For some sets of the process conditions: (1) *P*=400 W (Figure 7.15), (2) *P*=400 W & 500 W (Figure 7.16) and (3) *P*=500 W (Figure 7.17), it was observed that, the bend angle first increases, attains a peak, and then decreases with the increase in scan speed as shown in Figure 7.15 to Figure 7.17. It is due to the fact that with increase in the scan speed, the peak temperature decreases and temperature gradient increases. This results in the decrease in plastic deformation at both top and bottom surfaces. The bend angle increases with scan speed until the plastic deformation at the bottom surface reduces to a negligible value and further increase in the scan speed leads to the decrease in bend angle.

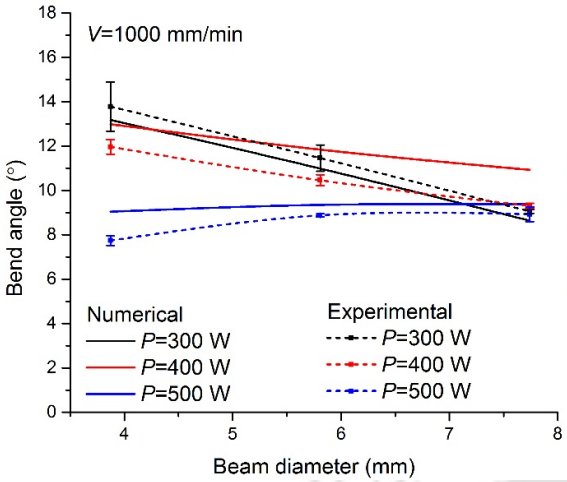

Figure 7.18. Effect of beam diameter on total bend angle at slow scan speed after 10 laser scans.

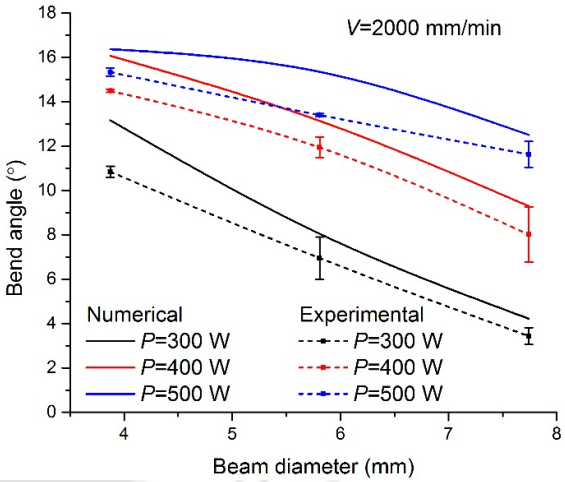

Figure 7.19. Effect of beam diameter on total bend angle at medium scan speed after 10 laser scans.

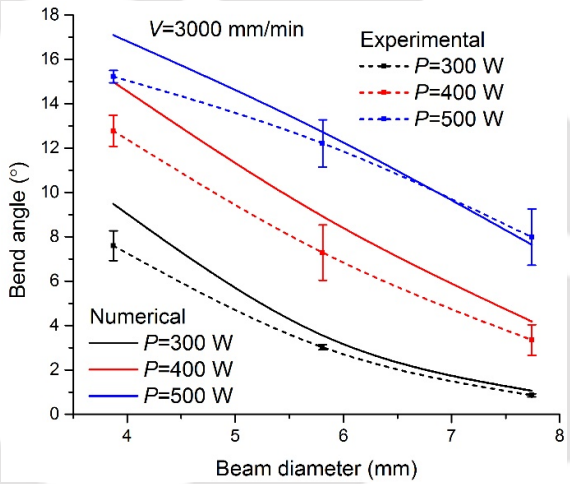

Figure 7.20. Effect of beam diameter on total bend angle at fast scan speed after 10 laser scans.

7.5.3 Effect of beam diameter

Figures 7.18 to Figure 7.20 show the effect of beam diameter on bend angle after ten laser scans. It is noted that the numerical results are in good agreement with the experimental studies. The trends of variation of bend angle predicted by the developed numerical model are similar to those obtained in experiments. From Figures 7.18 to Figure 7.20, it can be seen that the bend angle decreases with the increase in beam diameter for all sets of process conditions except for P=500 W, V=1000 mm/min, D=3.87 mm. It is because the heat flux density and the temperature gradient along the thickness direction both decreases with the increase in beam diameter. The effect of decrease in peak temperature and lower temperature gradient results in the decrease in bend angle at larger beam diameter.

For the process condition of laser power 500 W, scan speed 1000 mm/min and beam diameter 3.87 mm, the bend angle marginally increases with the increase in beam diameter as shown in Figure 7.18. It is because at high laser power and slow scan speed, high temperature occurs at the bottom surface. Increase in beam diameter reduces the temperature at the bottom surface, which dominates over the effect of heat flux density and temperature gradient along the thickness direction, and subsequently, the bend angle marginally increases with the increase in beam diameter.

7.6 Variation in Bend Angle

In this section, a study on the effect of process parameters on the variation in increment in the bend angle after each scan is presented. It is envisaged that this information may be useful in deciding the number of scans to be employed to obtain the desired bend angle for a chosen set of process condition.

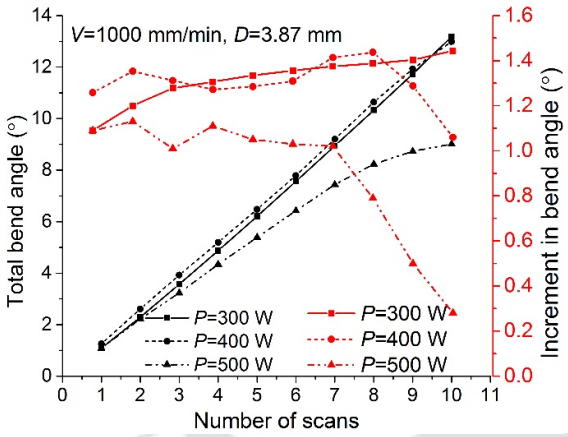

Figure 7.21. Variation in bend angle with number of scans at slow scan speed.

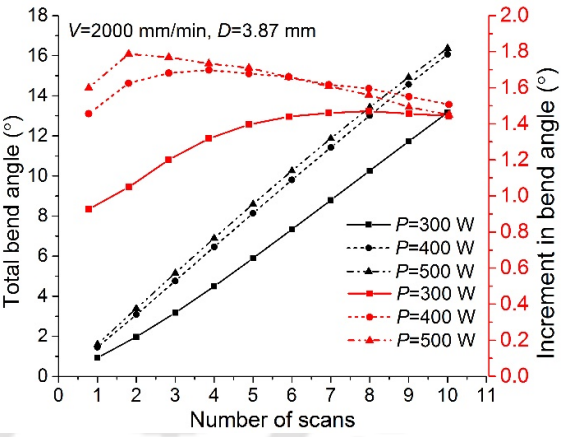

Figure 7.22. Variation in bend angle with number of scans at medium scan speed.

Figures 7.21 to Figure 7.23 show the variation in increment in bend angle and total bend angle with number of scans for various levels of laser power and scan speed at constant beam diameter of 3.87 mm. It can be observed that, in general, the bend angle linearly increases with increase in the number of scans. The increment in bend angle was found to be uniform for lower and medium level of laser power, however the increment in the bend angle was noted to be decreased with the number of scans for higher laser power of 500 W. It may be due to the fact that the high laser power excessively heats up the top and bottom surfaces of the worksheet resulting into a low temperature gradient along the thickness direction. This increases the plastic deformation at the bottom surface reduces the bend angle. Similar observations were

made for the variations in laser power and scan speed at beam diameter of 5.81 mm and 7.74 mm.

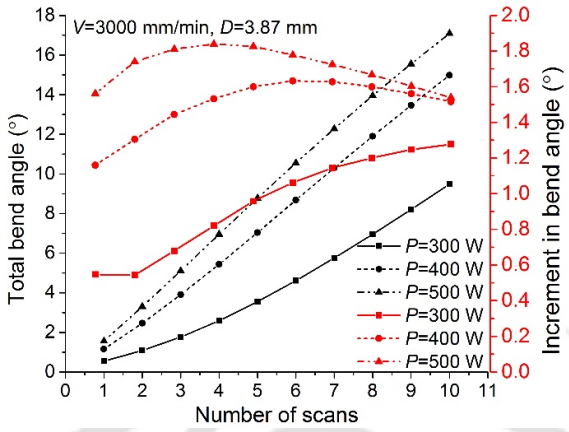

Figure 7.23. Variation in bend angle with number of scans at fast scan speed.

For an efficient multi-scan laser bending operation, the bend angle in a laser scan should be more as compared with the previous scan. These simulation results may be helpful in prediction of bend angle after each laser scan for chosen set of process conditions and may be useful in selecting suitable process conditions for obtaining the desired process performance.

7.7 Edge Effect

In multi-scan laser bending, the bend angle is not uniform along the scanning line and it varies from one end to another end of the scanning line which is called edge effect. The variation in bend angle is due to non-uniform temperature and stress distribution along the scanning line. The edge effect is quantified by using bend angle measured at five equidistant locations along the scanning line as shown in Figure 4.11. The edge effect is computed as the relative variation in bend angle per unit length (*RVBA*) along the scanning line as given in Equation (4.29). The results in terms of *RVBA* for various sets of process condition during multi-scan laser bending of magnesium alloy M1A are presented in Appendix 7.1.

Figure 7.24 to Figure 7.26 show the relative variation in bend angle values with the number of scans for varying scan speeds at a beam diameter of 3.87 mm. It can be seen that in general the edge effect exponentially decreases with increase in the number of scans for all process conditions except the condition: P= 500W, V=1000 mm/min. It is because the worksheet is preheated during each successive scan that reduces the effect of uneven mechanical constraint along the scanning path.

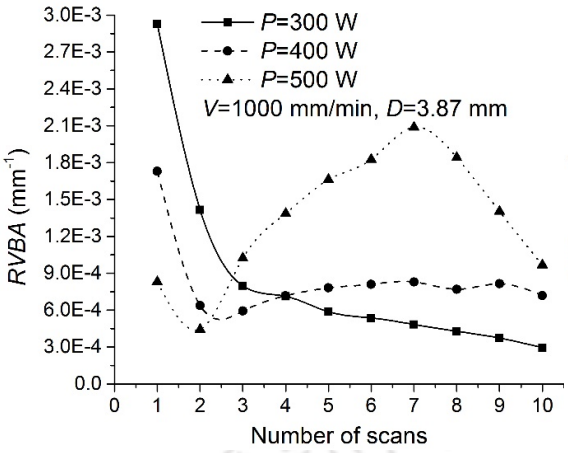

Figure 7.24. Effect of number of scans on edge effect at slow scan speed and small beam diameter.

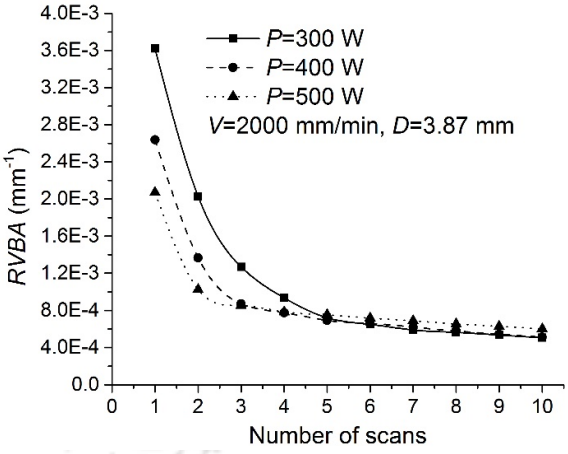

Figure 7.25. Effect of number of scans on edge effect at slow scan speed and large beam diameter.

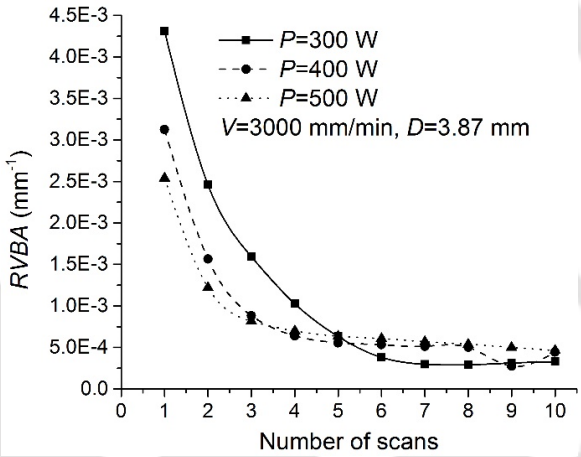

Figure 7.26. Effect of number of scans on edge effect at fast scan speed and small beam diameter.

At medium level of laser power and slow scan speed, the edge effect initially decreases; and then increases slightly as shown in Figure 7.24. However, at a high level of laser power the edge effect first decreases; then increases and further decreases with increase in the number of scans. It may be due to two reasons, first the melting occurs in the irradiated region of the worksheet after a few laser scans. The melting reduces the stiffness of material which leads to the uneven expansion of the heated region. Another reason is the change in worksheet thickness in the scanned region. The worksheet thickness increases in the scanned region due to the compressive deformation along the thickness direction (Figure 7.10). Figure 7.27 shows the change in thickness along the scanning line with number of scans. It can be seen that the change in thickness is not uniform along the scanning line. The change in thickness leads to the variation in constraint to the heated region by the surrounding cooler material and temperature

gradient along the thickness direction. It results in the increase of edge effect. For higher laser power, the edge effect decreases after attaining a peak. This may be due to the fact that higher laser power produces a large bend angle in comparison with that of the medium and low levels of power. For the large bend angle, the relative variation along the scanning line may be less.

It is also observed that the edge effect decreases with the increase in scan speed. The bend angles obtained at medium to higher levels of scan speed are less in comparison with those obtained at slower scan speed. Less bend angle has higher relative variation along the scanning line. From Figure 7.24 to Figure 7.26, it is noted that with the increase in laser power, the edge effect reduces. This may be attributed to the fact that medium to high laser power levels produce larger bend angles which leads to the less relative variation in bend angle.

In case of other two levels of beam diameter, 5.81 and 7.74 mm, similar observations (as discussed in this section) were noted for the variation in edge effect with the increase in laser power and scan speed. Graphs related to these comparisons are presented in Appendix 7.1.

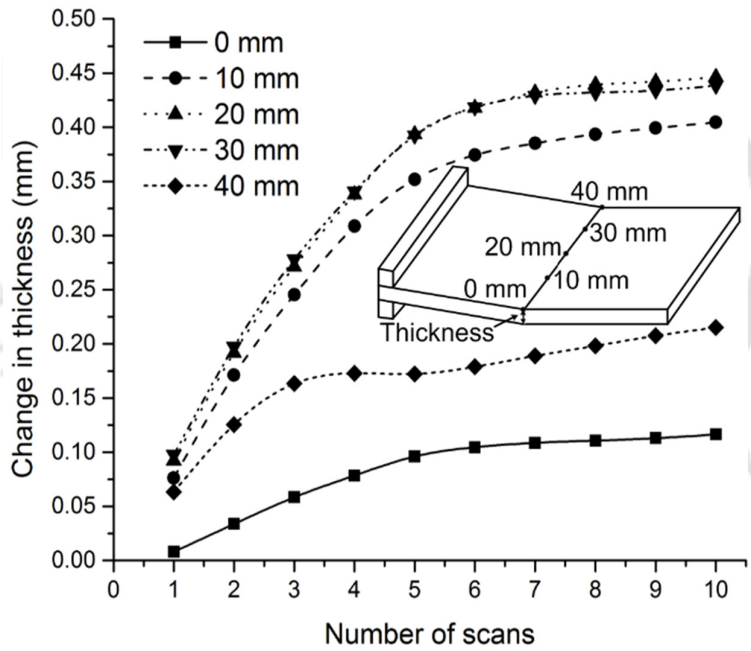

Figure 7.27. Effect of number of scans on change in thickness in the laser scanned region (P=500 W, V=1000 mm/min and D=3.87 mm).

7.8 Summary

This chapter presented numerical investigations on the multi-scan laser bending of magnesium alloy M1A by using a thermo-mechanical numerical model. Initially, the need of the work was

defined in terms of manufacture of large bend angles (of the order of 10º) by applying multiple laser irradiations. In view of this, numerical simulations were carried out by using the developed FEM based three-dimensional thermo-mechanical numerical model (Chapter 4). Experimental studies on multi-scan laser bending of magnesium alloy M1A were conducted to validate the results predicted by the developed numerical model. The developed model was found to be in good agreement with the experiments. The validated numerical model was used to investigate the multi-scan laser bending process. Effects of laser power, scan speed, beam diameter and number of scans on the bending mechanism, bend angle, variation in bend angle after each laser scan and the edge effect were studied in detail. The important conclusions of this work as follows:

- The temperature and stress-strain distribution was significantly affected by the number of laser scans. It was observed that due to pre-heating, the peak temperature increases and tensile and compressive stresses at various points of the worksheet decrease in each successive laser scan. The increase of temperature in each successive laser scan results in the melting of worksheet surface. It was also noted that the plastic deformation at the bottom surface increases with the number of scans which reduces the efficiency of the multi-scan laser bending process.
- It was seen that the bend angle increases with increase in the number of laser scans. The multi-scan laser bending process was found to be suitable for obtaining large bend angles of the order of 18° in the difficult-to-form material such as magnesium alloy. It was concluded that a combination of high laser power, fast scan speed and small beam diameter produces a larger bend angle.
- From the studies it was observed that, the edge effect decreases with increase in the number of scans, laser power and scan speed, while it increases with the increase in beam diameter. However, at slow scan speed and medium to high level of laser power, the edge effect first decreases; then increases and further decreases with increase in the number of scans.
- From the experiments it was observed that the multiple scans result in melting of the irradiated region. The melting can be avoided either by providing significant cooling time or by applying forced cooling between two consecutive scans. However, this may result in longer processing time and higher cost for the development of a set up for forced cooling. It was also observed that the application of multiple scans consume a lot of laser energy. The laser machines have less efficiency which further increases the cost of

production of a product on such machines. These factors limit the application of multi-scan laser bending process in real practice. A need, thus, exists to develop a simple and efficient methodology to produce large bend angles in difficult-to-form material such as magnesium alloy.

The next chapter presents the details regarding the design and development of such an approach.

CHAPTER 8: LASER ASSISTED BENDING WITH MOVING PRE-DISPLACEMENT

8.0 Scope

This chapter presents a simple and efficient methodology to obtain large bend angles in difficult-to-form material such as magnesium alloy by using laser assisted bending with moving pre-displacement. The need to design and develop the proposed methodology is defined. Based on the derived objectives, an experimental setup is fabricated, and details are presented. Initially, a performance comparative study among the two variants of laser bending, *viz*. single scan bending, and laser assisted bending has been presented. Then, the numerical investigations on laser assisted bending with moving pre-displacement in terms of the effect of laser power, scan speed, beam diameter and pre-displacement on bending mechanism, bend angle, edge effect and spring-back angle are presented in detail. The chapter concludes with a discussion on the effectiveness of the proposed approach in the productivity improvement of laser bending.

8.1 The Need

As mentioned in the earlier chapters, the single scan laser bending produces a small angle (of the order of 1º) which may not be useful in real life applications such as automobile and ship building. However, it was seen that a larger bend angle can easily be obtained with multiple scans (Chapter 7). From the experimental studies presented in the Chapter 3 and Chapter 7, it was observed that some of the process conditions caused melting in the irradiated region during multiple scanning of the laser beam. The remedy to this problem is to choose lower laser power, however that may produce a very small bend angle. Alternatively, one can employ forced cooling to control the temperature at the irradiated surface below the melting temperature. But, this may require the development of a dedicated experimental setup comprising of the cooling gas and controlled environment chamber. These factors limit the employment of multi-scan laser bending process to achieve large bend angles with minimum degradation of the work surface. Also, the energy consumption in multi-scan laser bending is quiet high. A need was thus identified to develop a simple and efficient methodology to produce large bend angles in difficult-to-form materials such as magnesium alloys. This formed the basis of the present work.

8.2 Proposed Methodology for Laser Bending with Moving Pre-displacement

To satisfy the need identified, one probable solution was envisaged the use of external mechanical load along with the laser beam irradiation. It is called as laser assisted bending or external load assisted laser bending. In laser assisted bending both thermal and mechanical stresses are responsible for the worksheet bending. Laser beam irradiation increases temperature of the worksheet which enhances formability in terms of low yield strength and low hardening coefficient (Hsieh and Lin, 2005; Yao et al., 2007).

Review of literature reveals a few attempts on the laser assisted bending for TGM (Yanjin et al. 2003, Yao et al. 2007) and BM (Hsieh and Lin 2005, Liu et al. 2010) dominated process conditions. However, the presented works are mainly focused on the point load or the distributed mechanical load, which may not be suitable for the practical applications. Especially, in case of the laser assisted bending of large sized sheets (size of the order of meters) used in the shipbuilding, aerospace and automobile industries, application of distributed load is quiet difficult due to the requirement of large force application system. A large size sheet with a uniformly distributed load along an edge of the worksheet is difficult and inconvenient to process. Therefore, in the present work, it is proposed to employ a moving pre-displacement in conjunction with the laser beam radiation to obtain a desired bend angle in the magnesium alloy worksheet.

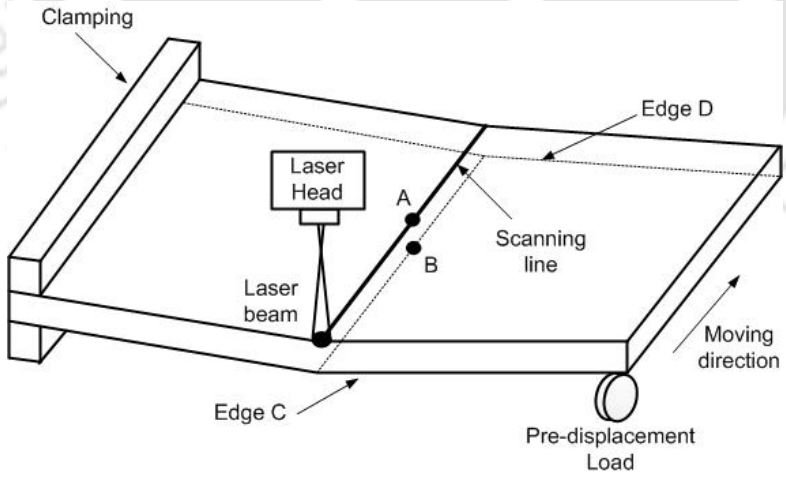

Figure 8.1. Schematic of laser assisted bending.

In the proposed methodology, a moving pre-displacement is applied along the free edge of the worksheet. The schematic of the proposed methodology is shown in Figure 8.1. The sheet is rigidly clamped at one side and an external mechanical load is applied on another free

side of the worksheet. The external load is applied in terms of the pre-displacement. The external moving load (pre-displacement) has a rolling contact with the worksheet, which prevents wear and tear during application of the moving pre-displacement. First, a pre-displacement is applied at one corner of the free side, and then the laser scans over the worksheet surface along a pre-defined straight line. The pre-displacement moves along the free edge in conjunction with laser scan.

The experimental setup was developed for the proposed moving pre-displacement methodology. The worksheet was needed to be clamped rigidly as the application of pre-displacement could dislocate it from the original position. Therefore, both the load application setup and sheet holding setup were designed and fabricated accordingly. Figure 8.2 shows a schematic of the method adopted to incorporate the moving pre-displacement. The synchronization between laser beam and moving pre-displacement was achieved by making the laser source and pre-displacement setup stationary and providing pre-defined motion to the worksheet. The pre-displacement was applied by height adjustment screw. Each rotation of the screw changed the pre-displacement equal to the pitch of the thread. For this methodology, an arrangement was designed and developed. Part drawings of the developed experimental setup along with the dimensional details are presented in Appendix 8.1.

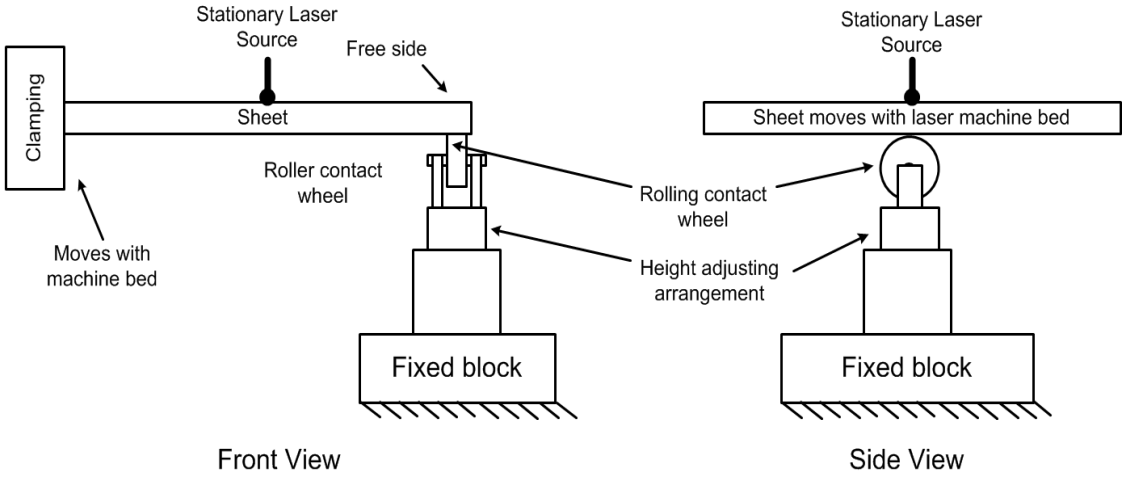

Figure 8.2. Schematic of experimental setup for laser assisted bending with moving pre-displacement.

8.3. Development of Experimental Setup

Three dimensional model of the experimental setup is shown in Figure 8.3. The experimental setup mainly includes two units: sheet holding unit and mechanical load (pre-displacement) application unit. In sheet holding unit, the worksheet is clamped by using the screw and nut

arrangement. The moving load setup and clamping setup are rigidly fixed on the laser machine bed. The laser source is stationary and the laser machine bed moves with a predefined scan speed. The worksheet clamping unit moves with the predefined scan speed as it is fixed to the laser machine bed.

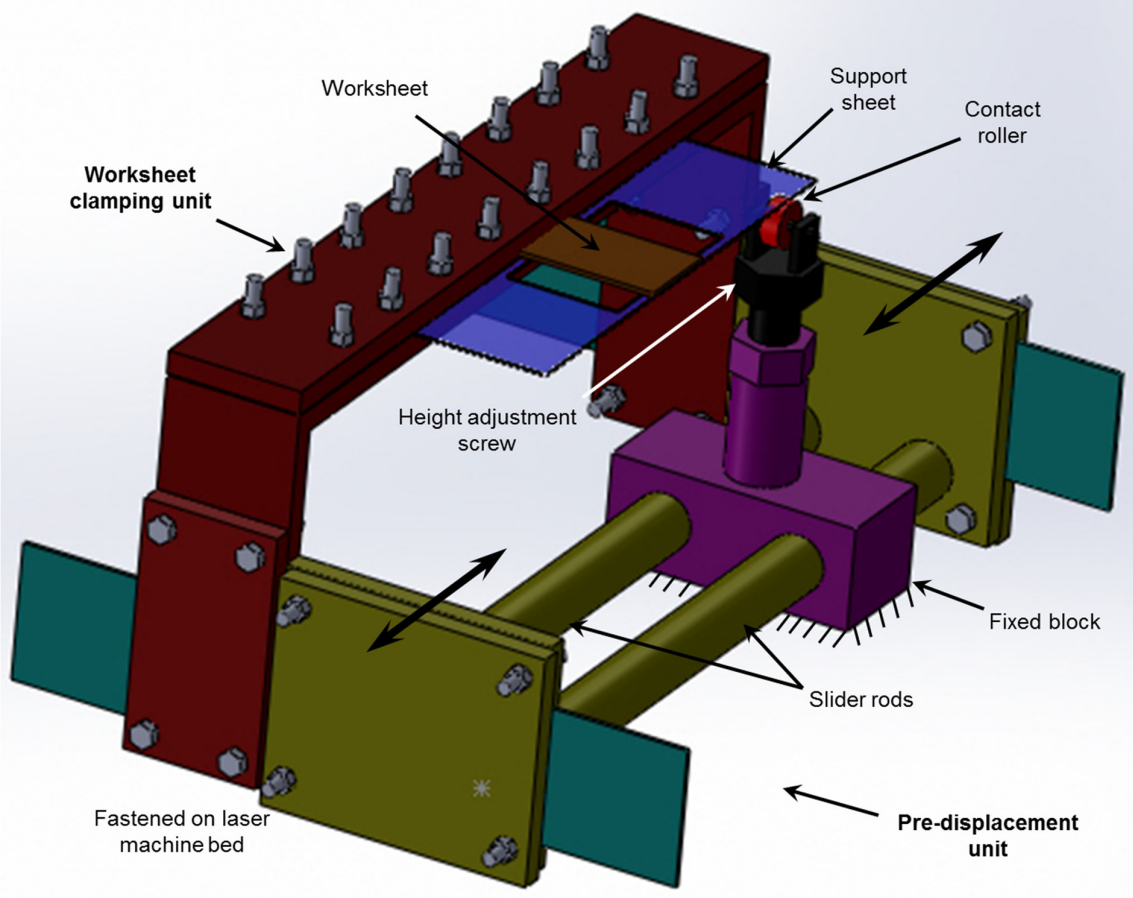

Figure 8.3. The moving load setup and clamping arrangement.

The pre-displacement unit in terms of the height adjustment screw and the contact roller is fastened to a rigid part of the laser machine. This part is labelled as 'Fixed block'. Figure 8.3 shows the fabricated setup for laser assisted bending with pre-displacement unit. During the movement of the laser machine bed, the worksheet moves, but the fixed block does not move because the slider rods slide through the holes of the fixed block. The load is applied in terms of the pre-displacement using a height adjustment screw. This arrangement has a rolling contact with the worksheet through a contact wheel. Roller is provided to reduce the friction and wear during the application of moving pre-displacement. A supportive thin sheet is placed below the worksheet to avoid sudden jerk during the initial contact between the worksheet and roller. It helped to obtain smooth engagement of the pre-displacement to the worksheet.

The designed setup for the moving pre-displacement load was developed at central workshop of Indian Institute of Technology Guwahati. The developed setup is shown in Figure 8.4. All parts are made up of mild steel. The slider rods are lubricated with an oil to reduce the friction. Pitch of the height adjustment screw is 2 mm, which means that a rotation of the height adjustment screw increases/decreases the pre-displacement by 2 mm.

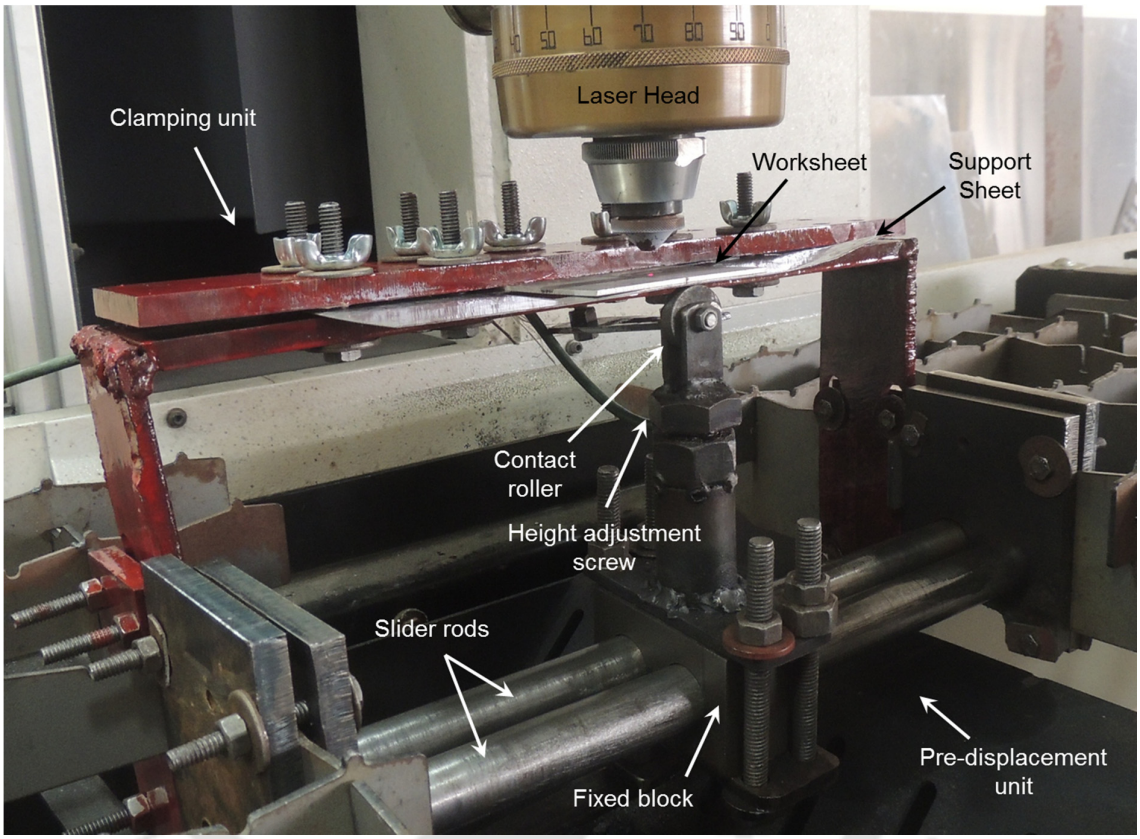

Figure 8.4. Experimental setup for the laser assisted bending with moving pre-displacement.

8.4. Preliminary Experimental Work

After the fabrication, the experimental setup was tested by carrying out preliminary experiments. The moving pre-displacement unit and worksheet clamping unit were assembled to the laser machine bed. The fabricated setup assembled over the laser machine bed is shown in Figure 8.5. The magnesium alloy M1A worksheet of 1.9 mm thickness was cut in the size of 70 mm length and 40 mm width. The length 70 mm was taken along the rolling direction. The specimens were coated with graphite spray to increase the absorptivity and also to ensure uniform absorptivity along the scanning line. Details of the specimen preparation and laser irradiation are already presented in Chapter 3.

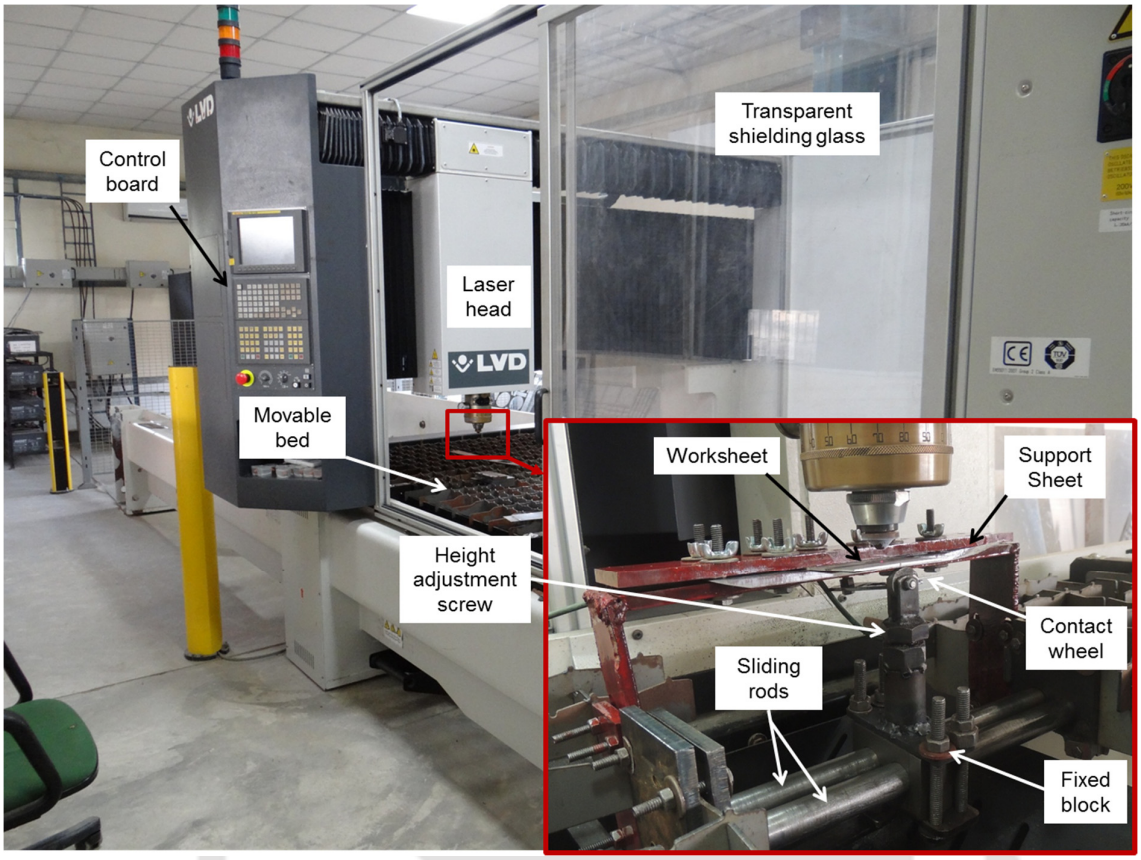

Figure 8.5. Details of the experimental setup.

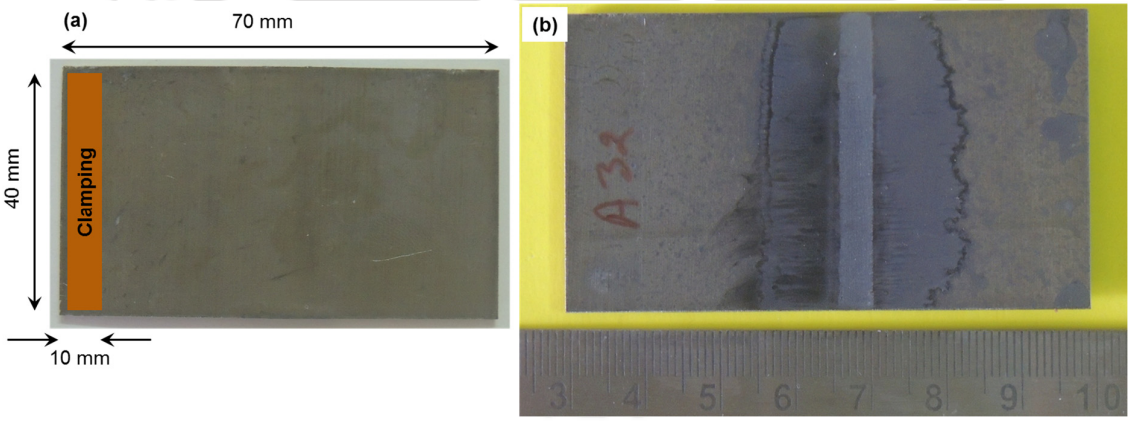

Figure 8.6. (a) Dimensions of the worksheet (b) laser irradiated worksheet.

The worksheet was held in the clamping setup by inserting about 10 mm portion of the worksheet. The remaining 60 mm portion was freely hanging. The worksheet specimen with geometric details is shown in Figure 8.6 (a). The worksheet was clamped and the laser beam was irradiated over the specimen in conjunction with a moving pre-displacement. A laser irradiated specimen is shown in Figure 8.6 (b). It can be observed that due to laser heating, the

coating was damaged and the worksheet was bent during laser assisted bending operation. The experiments were carried out by applying 5 mm pre-displacement. Figure 8.7 shows some of the laser assisted bent specimens. The experiments successfully demonstrated that by using the laser assisted bending with moving pre-displacement, a significantly large bend angle can be obtained in difficult-to-form material such as magnesium alloys.

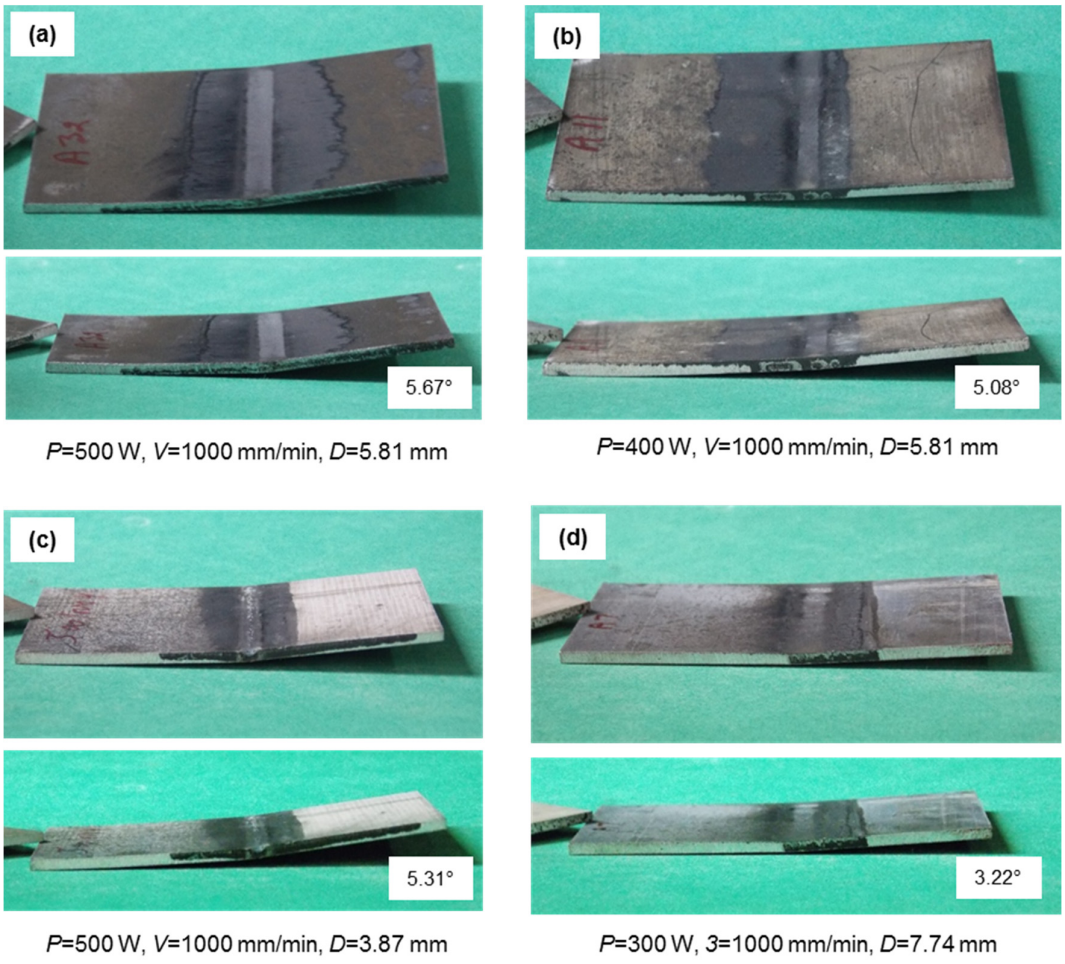

Figure 8.7. Bent specimens with laser assisted bending.

Figure 8.8 (a) shows the bottom surface of the bent specimen with assisted bending process. It can be observed that the bending radius is small in the laser assisted bent specimen as compared with that obtained in the mechanically bent specimen (see Figure 1.2). The laser assisted bent specimen has a sharp edge on the bending line. The laser bent specimen was seen under the optical magnification using ZEISS made optical microscope. The magnified image of the bottom surface of the laser bent specimen is shown in Figure 8.8 (b). It can be observed that the cracks are not generated during laser assisted bending of the magnesium alloy M1A

worksheet. Thus, the experimental study revealed that the laser assisted bending is suitable for producing a crack-free large bend angle in magnesium alloy worksheets.

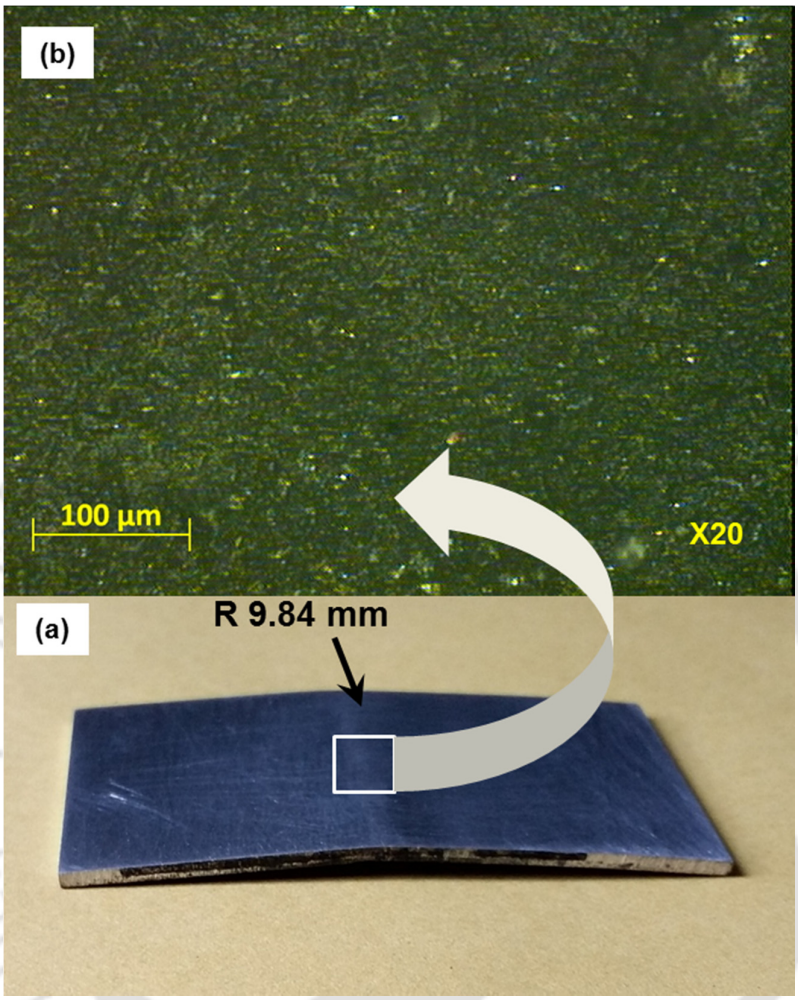

Figure 8.8. Laser bending of magnesium alloys (a) bent specimen and (b) magnified image.

Based on the encouraging results obtained during the preliminary experiments, numerical studies on the bending mechanism, bend angle, edge effect and spring-back were planned. To achieve this, numerical simulations have been carried out to obtain the temperature distribution, stress-strain histories, and distortions at various points. Before that, a comparative analysis of the performance of the proposed methodology with that of single scan laser bending was carried out. This is presented in the following section.

8.5 Performance Study of the Proposed Methodology

The performance of the proposed approach was studied by comparing the bend angle obtained during the laser assisted bending with that produced in the single scan laser bending of the magnesium alloys for similar sets of process conditions. Table 8.1 shows the comparison

between bend angles obtained in single scan laser bending and bending with moving pre-displacement. It can be seen that the bend angle obtained in laser assisted bending is more in many folds as compared with that of the single scan laser bending for all sets of process conditions. The bend angle increased by 2.05–10.91 times with an average of 4.49 times for the laser assisted bending with 5 mm pre-displacement. For 10 mm pre-displacement, the bend angle increased by 5.69–48.55 times with an average value of 12.35 times.

Table 8.1. Comparison between bend angles obtained in laser assisted bending with single scan laser bending process.

S. No.	*P* (W)	*V* (mm/min)	*D* (mm)	Bend angle (º)			Increment in bend angle (number of times)	
				Single scan	with pre-displacement		with 5 mm pre-displacement	with 10 mm pre-displacement
					of 5 mm	of 10 mm		
1	300	1000	3.87	1.09	3.63	9.9	3.33	9.08
2	300	1000	5.81	0.72	3.31	9.09	4.60	12.63
3	300	1000	7.74	0.4	2.90	8.23	7.25	20.58
4	300	2000	3.87	0.93	2.39	7.78	2.57	8.37
5	300	2000	5.81	0.33	1.71	6.66	5.18	20.18
6	300	2000	7.74	*	0.99	5.8	-	-
7	300	3000	3.87	0.55	1.60	6.56	2.91	11.93
8	300	3000	5.81	0.11	1.20	5.34	10.91	48.55
9	300	3000	7.74	*	0.58	4.54	-	-
10	400	1000	3.872	1.25	4.78	12.19	3.82	9.75
11	400	1000	5.807	0.97	5.02	10.98	5.18	11.32
12	400	1000	7.743	0.74	4.56	10.92	6.16	14.76
13	400	2000	3.872	1.46	3.49	9.52	2.39	6.52
14	400	2000	5.807	0.86	2.82	8.47	3.28	9.85
15	400	2000	7.743	0.4	1.88	7.5	4.70	18.75
16	400	3000	3.872	1.16	2.38	7.92	2.05	6.83
17	400	3000	5.807	0.4	2.13	6.63	5.33	16.58
18	400	3000	7.743	*	1.04	5.61	-	-
19	500	1000	3.87	1.11	5.28	13.67	4.76	12.32
20	500	1000	5.81	1.05	5.55	13.35	5.29	12.71
21	500	1000	7.74	0.87	5.13	12.9	5.90	14.83
22	500	2000	3.87	1.59	4.18	10.78	2.63	6.78
23	500	2000	5.81	1.16	4.20	9.87	3.62	8.51
24	500	2000	7.74	0.71	2.81	8.91	3.96	12.55
25	500	3000	3.87	1.57	3.28	8.94	2.09	5.69
26	500	3000	5.81	0.77	2.95	7.7	3.83	10.00
27	500	3000	7.74	0.27	1.63	6.6	6.04	24.44
***insignificant bend angle (<0.1º)**				**Average increment in bend angle = 4.49**				**12.35**

***P*=Laser power, *V*=scan speed, *D*=Beam diameter**

Overall, it can be concluded that the laser assisted bending increased the bend angles by many folds in comparison with that obtained in a single scan. However, this methodology was noted to have a limitation of spring back effect during the bending operation. A detailed study on the spring-back effect is presented in the later sections of this chapter.

8.6. Numerical Simulations of Laser Assisted Bending with Moving Pre-Displacement

As mentioned in Section 8.4, numerical simulations of laser assisted bending have been carried out by using finite element method. Geometric models of the worksheet and the roller were developed. A model of the meshed worksheet and roller is shown in Figure 8.9. A frictionless surface contact was defined between the roller and the worksheet. The worksheet was clamped at one of its sides while the other side had a contact with the roller. Zero displacement and zero rotation constraints were applied to the clamped face.

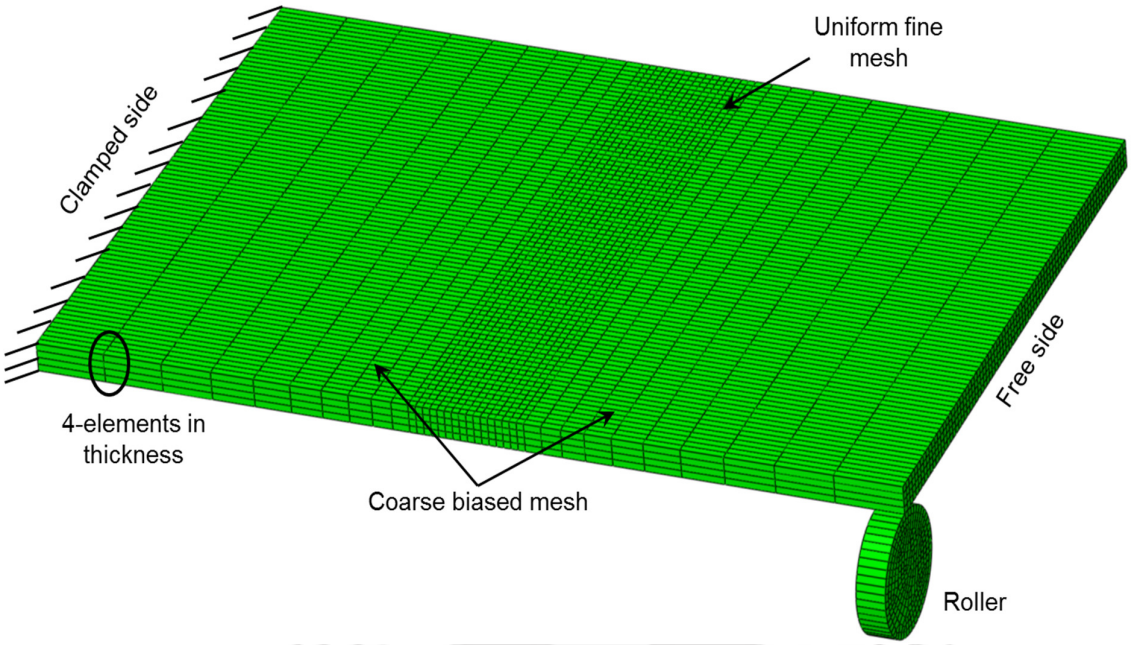

Figure 8.9. Meshed model of the laser assisted bending with moving pre-displacement.

Details of the worksheet material modeling, governing equations, discretization of the worksheet (meshing) and the solution methodology of the numerical model are presented at length in Chapter 4. An automatic time step increment was selected for solving the governing equations and boundary conditions. The maximum change in temperature in a time step was used to define the time step increment. It was taken as 10–50 °C.

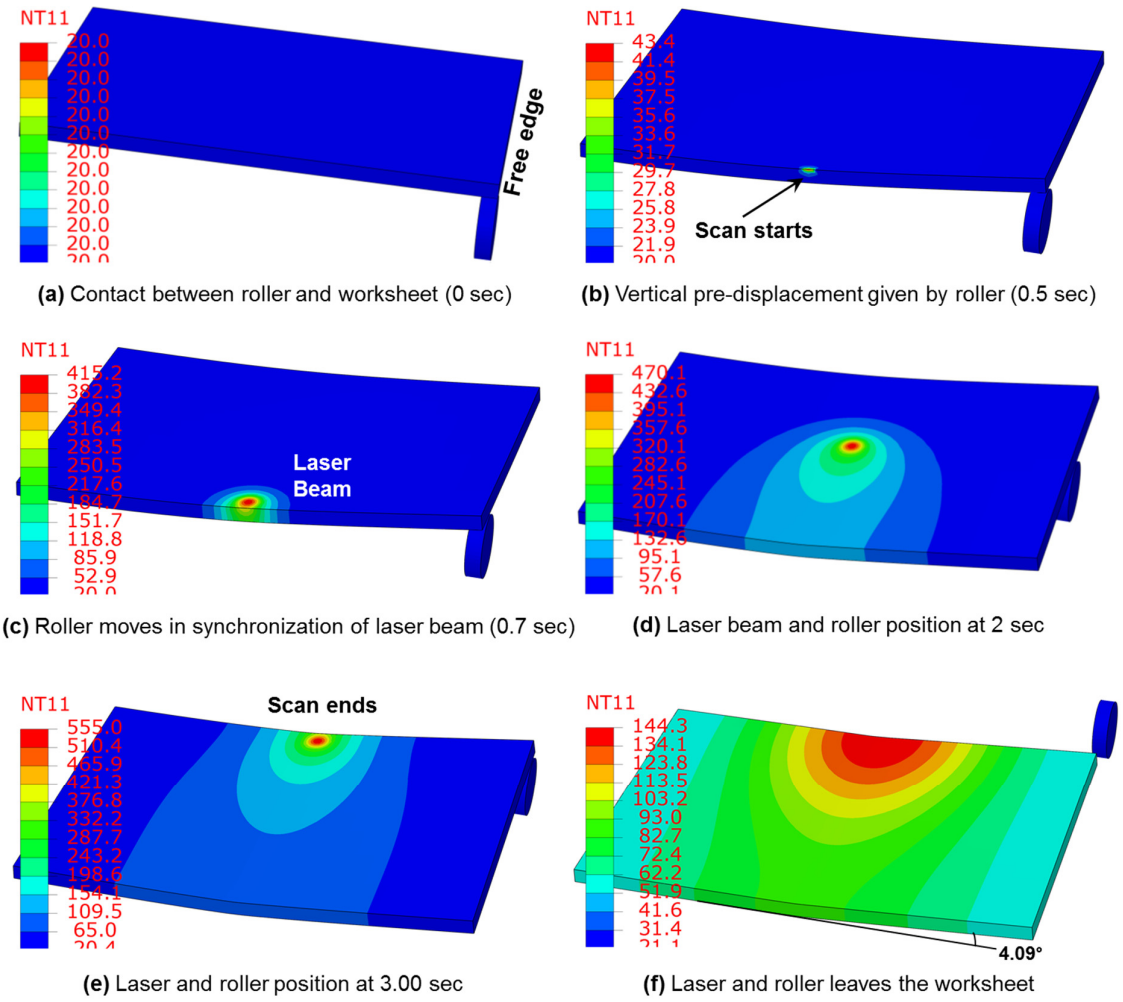

Figure 8.10. Movement of the laser beam and pre-displacement during numerical simulations.

A pre-displacement was applied using the roller. Initially, the roller was at free side of the starting edge of the irradiation path (Figure 8.10 (a)). The roller was moved in the upward direction during first 0.5 second. In this duration, a defined vertical pre-displacement was applied at the starting point (Figure 8.10 (b)). After obtaining the defined pre-displacement, roller maintained the vertical displacement and moved along the free edge in conjunction with laser beam irradiation as shown in Figure 8.10 (b) to Figure 8.10 (e). Finally, both the laser beam and the roller left the worksheet and the worksheet was bent due to the combined effect of laser beam irradiation and the moving pre-displacement (Figure 8.10 (f)). After the laser irradiation with moving pre-displacement, the worksheet was bent. The bent worksheet along with distorted mesh is shown in Figure 8.11. It is a scaled (by factor five) image of the deformed worksheet. It can be seen that the plastic deformation occurred only in the irradiated region

which justifies the use of fine mesh in the heated region and coarse biased mesh in the outer region. Then the bend angle was measured and used for further study.

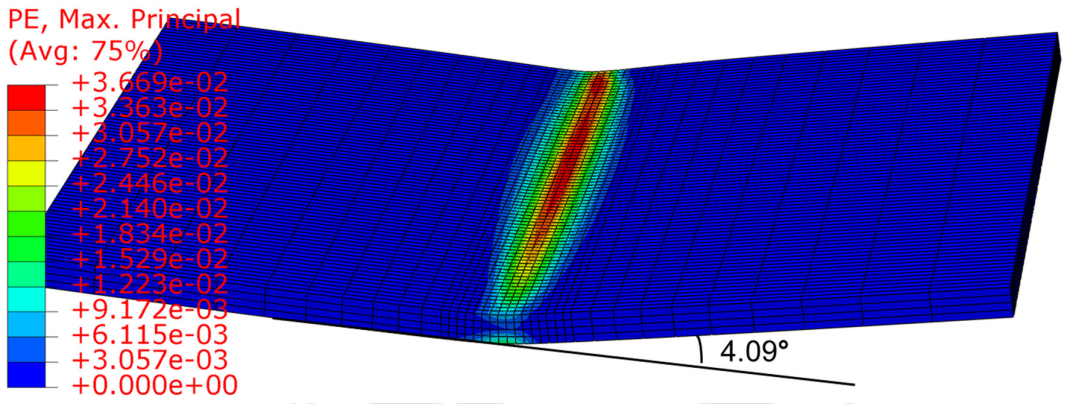

Figure 8.11. Deformed worksheet with plastic strain contour.

Table 8.2. Comparison between numerical and experimental results.

Data-set No.	Process parameters			Bend angle (°) with 5 mm pre-displacement			
	P (W)	*V* (mm/min)	*D* (mm)	Numerical bend angle (°)	Experimental bend angle (°)	*CV* (%)	Absolute Error (%)
1	300	1000	3.87	4.09	3.63	5.44	12.45
2	300	1000	5.81	3.40	3.31	5.83	2.78
3	300	1000	7.74	2.80	2.90	13.65	3.41
4	300	2000	3.87	2.75	2.39	9.36	14.99
5	300	2000	5.81	1.88	1.71	6.88	10.17
6	300	2000	7.74	1.24	0.99	3.99	25.36
7	300	3000	3.87	1.99	1.60	17.45	24.11
8	300	3000	5.81	1.20	1.20	9.60	0.05
9	300	3000	7.74	0.56	0.58	20.15	3.12
10	400	1000	3.87	5.69	4.78	5.08	19.14
11	400	1000	5.81	5.26	5.02	0.98	4.83
12	400	1000	7.74	4.79	4.56	6.55	5.01
13	400	2000	3.87	4.07	3.49	4.30	16.69
14	400	2000	5.81	3.18	2.82	12.26	12.62
15	400	2000	7.74	2.40	1.88	2.53	27.35
16	400	3000	3.87	2.97	2.38	2.29	24.77
17	400	3000	5.81	2.63	2.13	2.49	23.95
18	400	3000	7.74	1.20	1.04	4.48	15.79
19	500	1000	3.87	6.63	5.28	0.62	25.61
20	500	1000	5.81	6.58	5.55	2.64	18.46
21	500	1000	7.74	6.21	5.13	4.89	21.09
22	500	2000	3.87	4.96	4.18	1.91	18.76
23	500	2000	5.81	4.24	4.20	17.42	1.02
24	500	2000	7.74	3.45	2.81	4.07	23.00
25	500	3000	3.87	3.76	3.28	4.32	14.54
26	500	3000	5.81	3.92	2.95	0.93	32.86
27	500	3000	7.74	1.85	1.63	10.27	13.87
						Average error =	**15.40**

***CV*=Coefficient of variation, *P*=Laser power, *V*=Scan speed, *D*=Beam diameter**

8.6.1 Experimental validation of the numerical simulations

The developed numerical model was validated with the experimental results. Each experiment was repeated thrice. The average of responses recorded for three trials was considered as the experimental value. A comparison between numerical and experimental results of the laser assisted bending with 5 mm pre-displacement is presented in Table 8.2. The coefficient of variation (*CV*) was calculated as the ratio of standard deviation to the mean of three trials. The numerical bend angles were found to be in good agreement with those obtained during the experiments. The mean absolute prediction error was about 15.40% for laser assisted bending with moving pre-displacement. The percentage absolute errors between numerical and experimental results for various sets of process conditions are also shown Figure 8.12.

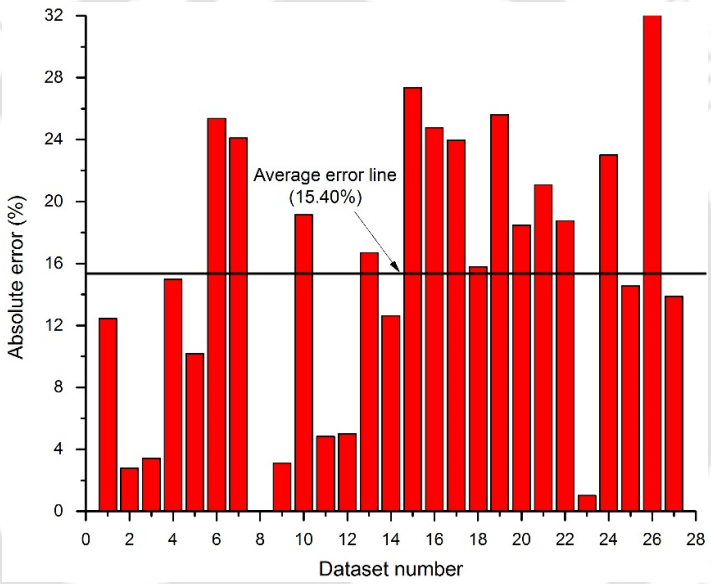

Figure 8.12. Absolute error between numerical and experimental bend angle for laser assisted bending with a moving 5 mm pre-displacement load.

Prediction accuracy of the numerical model was found to be reasonably good, and therefore, the numerical was further used to investigate the effect of moving pre-displacement on the bending mechanism and deformation behavior during laser assisted bending. The effects of pre-displacement on the temperature distribution, stress-strain distribution, bend angle, edge effect and spring-back effect are presented in the following sections.

8.7 Effect of Process Parameters on Bend Angle

Effect of laser power, scan speed and beam diameter on bend angle is studied for the proposed methodology. Also, the effects of pre-displacement on bending mechanism, bend angle, edge effect and spring-back effect are studied and presented in the following sections.

Figure 8.13 to Figure 8.15 show the effect of process parameters, *viz*. laser power, scan speed and beam diameter on the bend angle obtained during the laser assisted bending with moving pre-displacement of 5 mm.

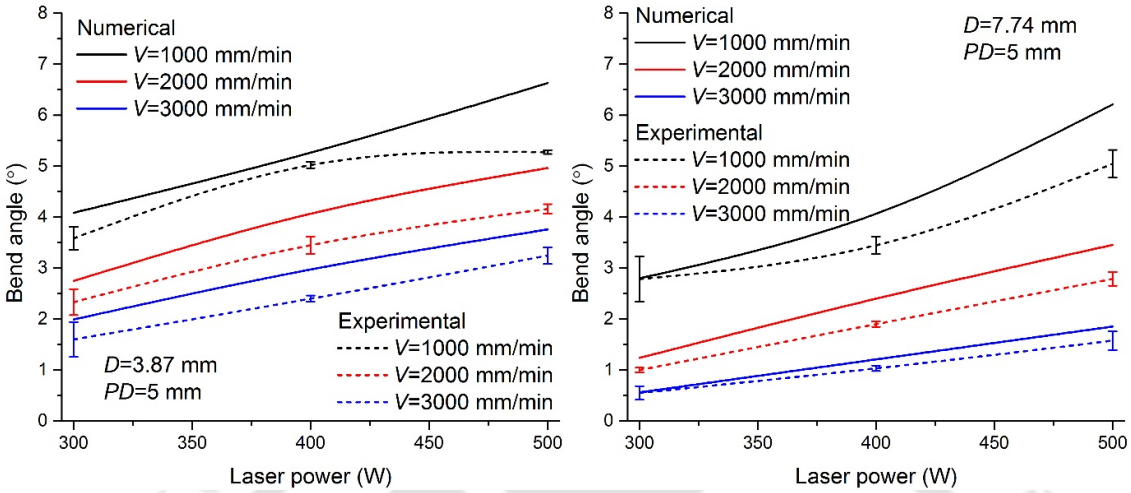

(a) (b)

Figure 8.13. Effect of laser power on bend angle for laser assisted bending with moving pre-displacement (a) at small beam diameter (b) at large beam diameter.

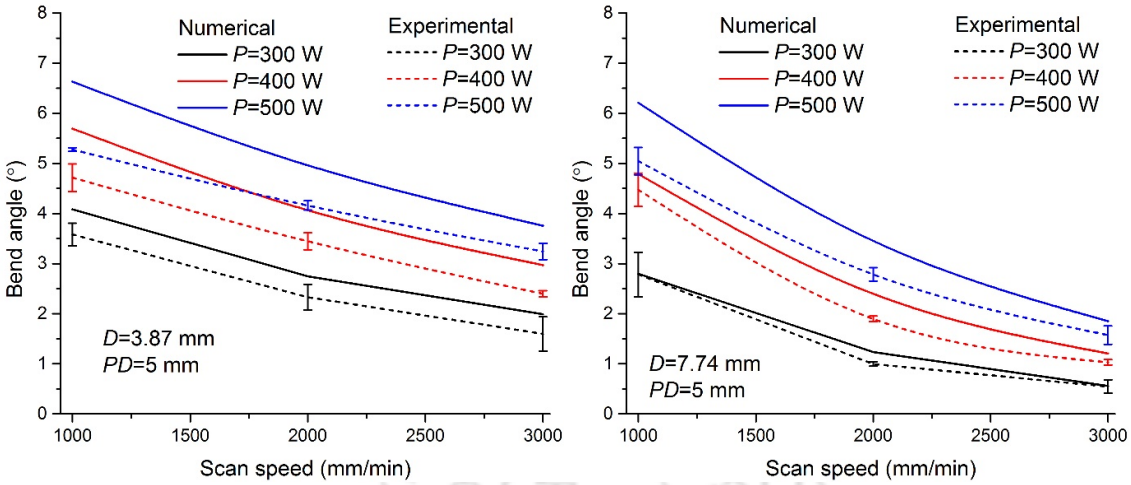

(a) (b)

Figure 8.14. Effect of scan speed on bend angle for laser assisted bending with moving pre-displacement (a) at small beam diameter (b) at large beam diameter.

Figure 8.13 (a) and Figure 8.13 (b) show the effect of laser power on bend angle at a small and large beam diameter, respectively. It can be observed that the bend angle increases with the increase in laser power. It is because the peak temperature in the irradiated region increases with the increase in laser power. It reduces the yield strength and results in a higher

plastic deformation, and hence the bend angle increases. For medium level of beam diameter, similar trends were observed which are presented in Appendix 8.2.

Figure 8.14 (a) and Figure 8.14 (b) show the effect of scan speed on bend angle at a small and large beam diameter, respectively. It can be observed that the bend angle decreases with the increase in scan speed. It is because the energy absorbed by the worksheet surface reduces at a faster scan speed that results in a lower peak temperature. This leads to higher yield strength and low bend angle. For medium level of beam diameter, similar trends were observed which are presented in Appendix 8.2.

Figure 8.15 (a) and Figure 8.15 (b) show the effect of beam diameter on bend angle at slow and fast scan speed, respectively. It can be seen that the bend angle decreases with the increase in beam diameter. It is due to the decrease in heat flux density at a larger beam diameter, which reduces the peak temperature at the scanning surface. For medium level of scan speed (2000 mm/min), similar trends were observed which are presented in Appendix 8.2.

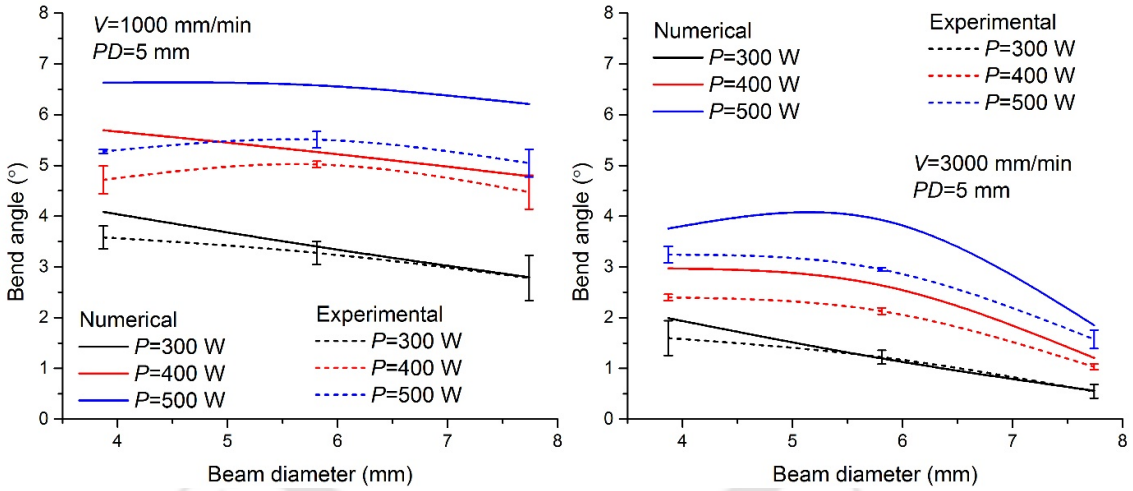

Figure 8.15. Effect of beam diameter on bend angle for laser assisted bending with moving pre-displacement (a) at slow scan speed (b) at fast scan speed

From Figure 8.13 to Figure 8.15, it can be observed that the trends of variation of bend angle predicted by the numerical model are well matching with those obtained during the experiments. This provided a confidence in the numerical model for its further use in the study of the effect of pre-displacement on the bending mechanism, distortion behavior, edge effect and spring-back effect during laser assisted bending with moving pre-displacement. These are presented in the following sections.

8.8 Effect of Pre-displacement

8.8.1 Bending mechanism

Due to the presence of mechanical stresses, the bending mechanism of laser assisted bending is different from that of the laser bending process. The mechanical stresses may affect the deformation behavior during the process. In view of this, numerical simulations have been carried out on the bending mechanism of laser assisted bending with moving pre-displacement. The effect of moving pre-displacement on the temperature distribution, stress-strain distribution, deformation behavior, residual stresses, and elastic recovery are also presented in detail. For the present study, a typical process condition: P=300 W, V=1000 mm/min and D=3.87 mm was chosen which facilitates melting free bending of the worksheet.

A. Temperature distribution

Figure 8.16 shows a comparison between temperature histories at Point A and Point B for the laser bending and laser assisted bending process. The laser assisted bending is considered for a pre-displacement (*PD*) of 10 mm. It can be seen that the peak temperatures at the top and bottom surfaces are almost equal in both the cases, *i.e*. laser bending and laser bending with 10 mm pre-displacement. That means, the mechanical load does not have any influence on the temperature distribution. The temperature profile of laser assisted bending has an offset delay of 0.5 second as compared with that of the laser bending process. It is because the developed pre-displacement unit gives a vertical movement to the worksheet for 0.5 second at start of the laser scan.

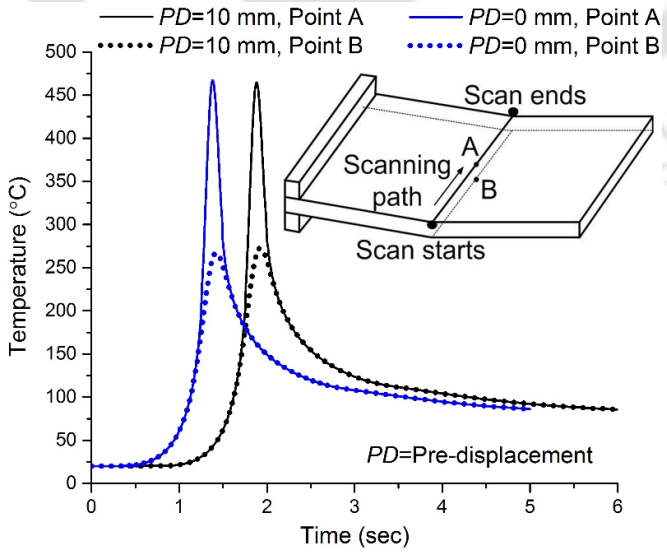

Figure 8.16. Temperature history for laser assisted and laser bending process.

B. Stress distribution

As discussed in earlier chapters, for TGM, the increase in temperature causes a thermal expansion in the heated region that is restricted by the surrounding material, which is at relatively low temperature. This induces compressive stresses in the heated region and tensile stresses in the surrounding region. Figure 8.17 shows the x-direction stress histories at Point A and Point B for laser bending and laser assisted bending process. The stress distribution in laser bending and laser assisted bending is quite different.

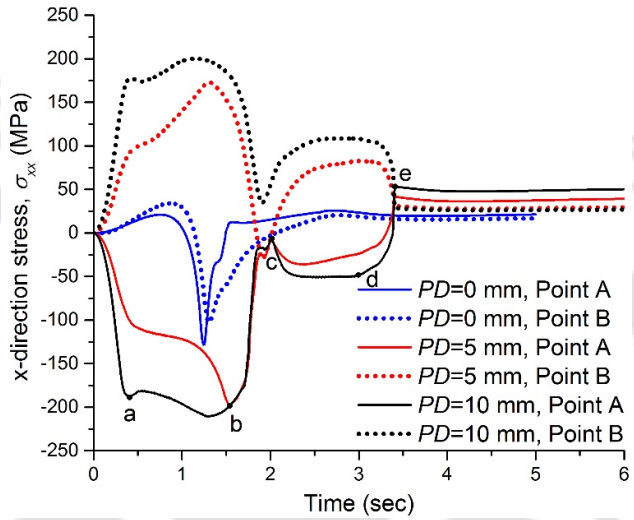

Figure 8.17. Comparison of x-direction stress histories for laser and laser assisted bending.

From Figure 8.17, it can be observed that the tensile stresses at bottom (Point B) and compressive stresses at top (Point A) surfaces increase gradually from time 0 to 0.5 second (Point *a*). During this period (0 to *a*) the initial pre-displacement (*PD*) is applied at the corner of the worksheet. Once the desired pre-displacement is achieved, the laser beam irradiates and the mechanical load moves along the free edge simultaneously with the laser beam. The tensile and compressive stresses at the top and bottom surfaces increase slightly from *a* to *b*. It is because as the moving pre-displacement reaches near to Point A, the vertical displacement increases at Point A. The stresses at both top and bottom surfaces decrease gradually due to heating of the material (*b* to c). When the laser beam reaches at Point A, the temperature of the material is high, and hence stiffness of the material reduces to a very low value. Therefore, the stresses are very less at '*c*'. As the laser beam moves forward, stresses increase at Point A and Point B as shown between *c* and *d*. At the end, on removal of laser energy and mechanical pre-displacement, the stresses at top and bottom surfaces (from *d* and *e*) reduce. Laser beam and mechanical load have completely been removed from the worksheet at *e*. It can be seen that

residual stresses remain in the worksheet material at the end of the process. Residual stresses are minimum when the pre-displacement is not applied and they increase with the increase in applied pre-displacement.

From Figure 8.17, it can also be observed that significant tensile stresses are generated at the bottom surface due to the application of pre-displacement. However, in case of pure laser bending, compressive stresses are induced at the bottom surface. Thus, the mechanism of laser assisted bending differs from that of laser bending.

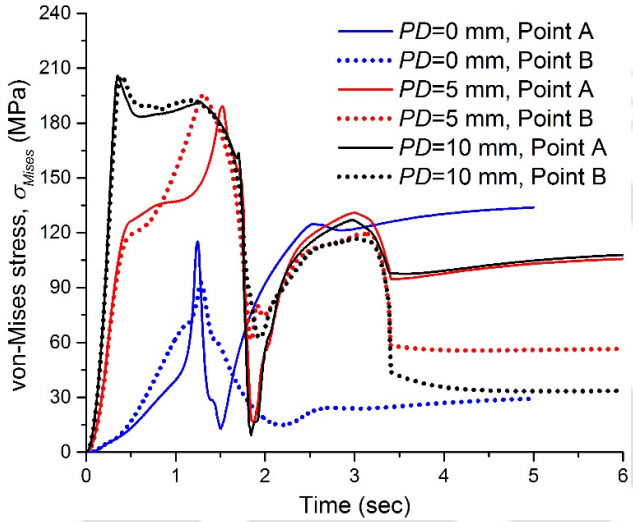

Figure 8.18. Comparison of von-Mises stress histories for laser and laser assisted bending.

Figure 8.18 shows the von-Mises stress histories at Point A and Point B for laser bending and laser assisted bending of magnesium alloy. It can be seen that the peak stresses are quite high in laser assisted bending. In case of laser bending without pre-displacement, von-Mises residual stresses are higher at the top and lower at the bottom surface. The peak residual stress increases with the increase in pre-displacement. It can also be observed that after the irradiation, the residual von-Mises stresses in the worksheet are almost similar at the top surface for both 5 mm and 10 mm pre-displacements. At the bottom surface, the von-Mises stresses are low for the case of 5 mm pre-displacement in comparison with those of 10 mm pre-displacement. The von-Mises stress is the highest at the top surface and the lowest at the bottom surface, when pre-displacement is not applied.

Figure 8.19 shows x-directional components of the residual stresses along the scanning line for chosen process conditions. It can be seen that the residual stresses are compressive at start of the scanning line. The residual stresses decrease along the scanning line and finally become tensile. The tensile stresses attain a peak and then slightly decrease towards the end of

scanning line. At bottom surface, stresses increase slightly along the scanning line, and then decrease to become compressive in nature. The compressive stresses increase towards the end of the scanning line. At bottom surface, the compressive stresses are the highest at the end of scanning line, while at the top surface, these are the highest at the start of scanning line.

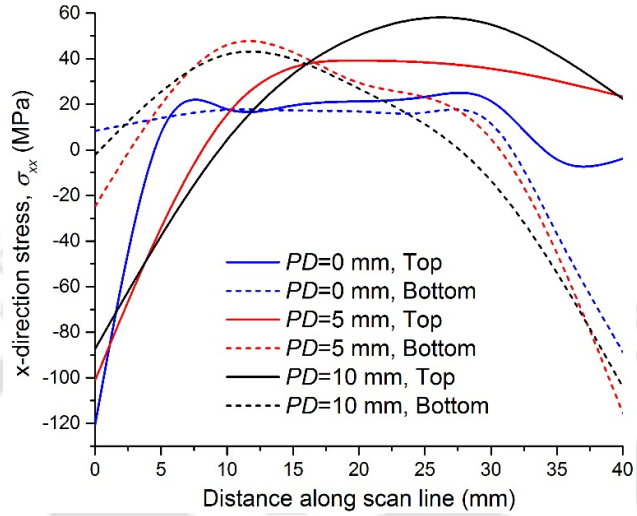

Figure 8.19. Residual stresses along the scanning line.

The trends of residual stress distribution along the scanning line is different for laser bending with and without application of the pre-displacement. For laser bending without pre-displacement, the residual stresses are near to zero all along the scanning line except at the edges. During laser assisted bending with both 5 mm and 10 mm pre-displacement, the residual stresses are compressive at start, then become tensile. They attain a peak at middle of the scanning line, and then decrease towards the end of the scanning line.

C. Strain distribution

When induced thermal stresses exceed temperature dependent flow stress, the plastic deformation occurs. The x-direction plastic strain histories for laser bending and laser assisted bending with 5 mm and 10 mm pre-displacements are shown in Figure 8.20. In laser bending, compressive deformation occurs at both top and bottom surfaces and the worksheet bends due to the difference between plastic deformation at top and bottom surfaces. However, in laser assisted bending, the deformation behavior is different. In laser assisted bending, the tensile deformation occurs at the bottom surface while the compressive deformation occurs at the top surface. This results in a large difference between plastic deformations at the top and bottom surfaces, which leads to a significant increase in the bend angle. The magnitude of compressive deformation at the top surface increases due to the application of external mechanical load. The

tensile deformation at the bottom surface and compressive deformation at the top surface increases with the increase in pre-displacement. This leads to the increase in bend angle with the increase in pre-displacement as shown in Figure 8.21.

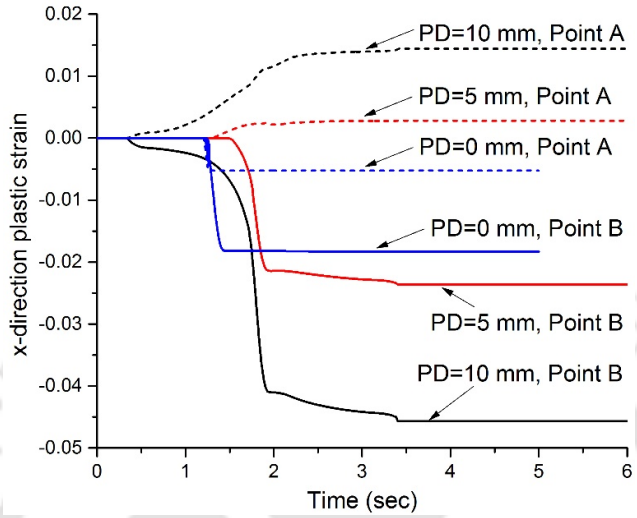

Figure 8.20. Comparison of x-direction strain histories for laser and laser assisted bending.

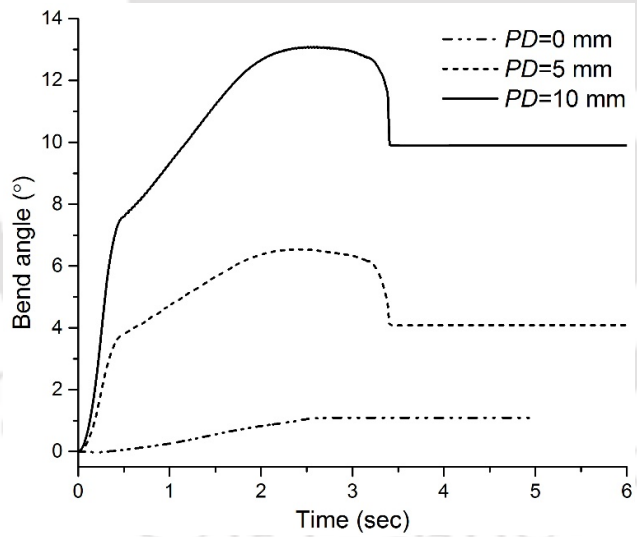

Figure 8.21. Comparison of bending histories for laser and laser assisted bending.

Figure 8.21 shows a comparison between bending histories at the middle of the scanning line for the laser bending and laser assisted bending. It can be seen that on employing the pre-displacements, larger bend angles are obtained. The bend angle increases with the increase in pre-displacement. It is because the pre-displacement is applied towards the bending direction (laser source), and hence the mechanical stresses support the thermal stresses to bend the worksheet. It can also be seen that an elastic recovery of the bend angle occurs when the

pre-displacement is removed from the worksheet. This elastic recovery is called spring-back effect, and it increases with the increase in pre-displacement. In laser bending, the elastic recovery does not exist. It is because the mechanical stresses are not present.

8.8.2 Bend angle

The pre-displacement bends the worksheet in the upward (towards laser head) direction. Due to this, compressive stresses induce on the top surface and tensile stresses on the bottom surface. These mechanical stresses induced along with thermal stresses bend the worksheet. Effects of pre-displacement on the bend angle are shown in Figure 8.22 to Figure 8.25. The bend angle increases with the increase in pre-displacement. It is because the pre-displacement generates large plastic compressive deformation at the top surface and tensile deformation at the bottom surface (see Figure 8.20). The bend angle is a result of the difference between plastic deformation at the top and bottom surfaces. Thus, a larger bend angle is obtained when a higher pre-displacement is applied.

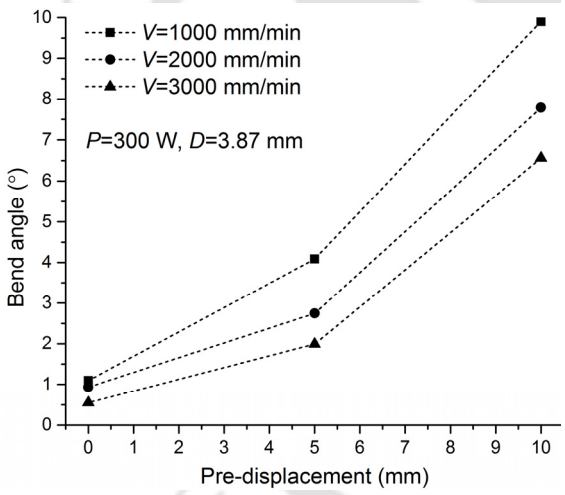

Figure 8.22. Effect of pre-displacement on bend angle at *P*=300 W and *D*=3.87 mm.

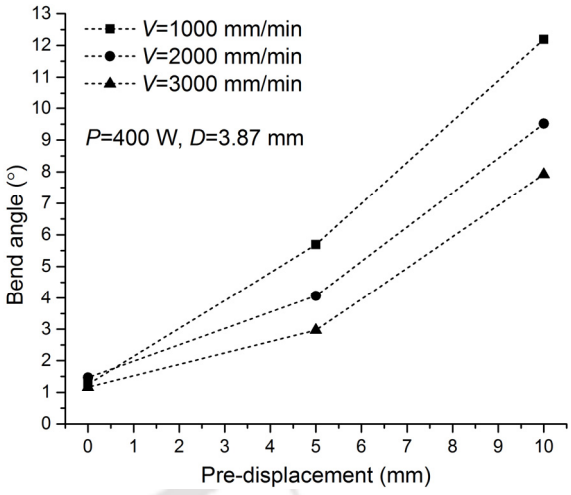

Figure 8.23. Effect of pre-displacement on bend angle at *P*=400 W and *D*=3.87 mm.

From Figure 8.22 to Figure 8.24, it can be observed that the bend angle decreases with the increase in scan speed. It is because the energy absorbed by the worksheet surface is less at a faster scan speed. It results in a lower peak temperature, and relatively higher yield strength. The rate of increase in the bend angle with pre-displacement is more at a slower scan speed in comparison with that observed for medium to fast scan speeds. It is because the pre-displacement produces a higher plastic deformation when the temperature of the scanning surface is more.

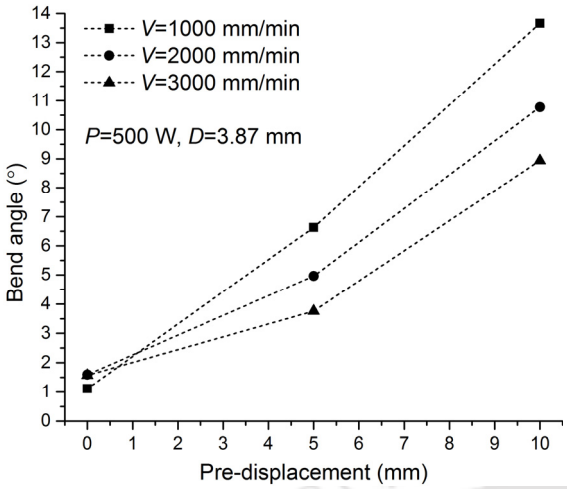

Figure 8.24. Effect of pre-displacement on bend angle at *P*=500 W and *D*=3.87 mm.

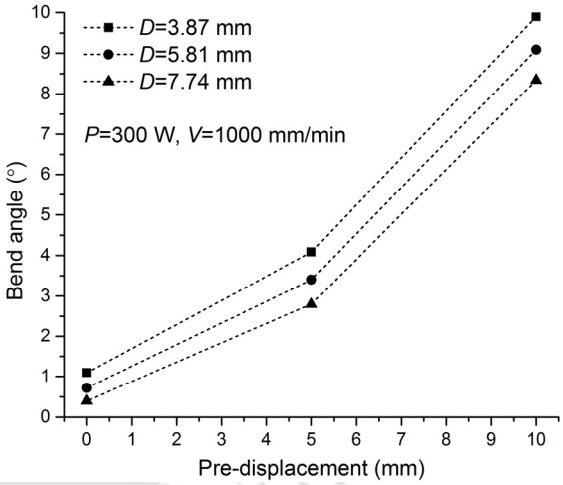

Figure 8.25. Effect of pre-displacement on bend angle at *P*=300 W and *V*=1000 mm/min.

From Figure 8.22 to Figure 8.24, it can also be seen that the bend angle increases with the increase in laser power. It is because the peak temperature in the irradiated region is more at higher laser power. It reduces the yield strength and results in a higher plastic deformation when the pre-displacement is applied. Figure 8.25 shows that the bend angle decreases with the increase in beam diameter. It is due to decrease in the heat flux density at a larger beam diameter, which reduces the peak temperature at the scanning surface.

It is to be noted that in this section the effects of variation in the laser power and scan speed on the bend angle are discussed for the beam diameter of 3.87 mm. However, a full factorial study was carried out with the other two levels of beam diameters (*viz*., 5.81 mm and 7.74 mm). During this study, similar trends were observed for medium and large beam diameters. These are reported in the Appendix 8.3.

8.8.3 Spring-back effect

The induced stresses in the worksheet varies from the tensile stresses at the bottom surface to the compressive stresses at the top surface. This variation in stresses results in the spring-back during laser assisted bending process. The highest tensile stresses occur at the bottom surface of the worksheet. These stresses decrease along the worksheet thickness and become zero at the neutral axis. The neutral axis is stressed to a value below the elastic limit which creates a narrow elastic band on both sides of the neutral axis. The metal away from the neutral axis is stressed beyond the yield strength, and is plastically deformed. When external pre-displacement is removed, the elastically deformed material at the neutral axis tries to return to the original flat condition. However, it could not come to the original condition due to

restrictions provided by the plastically deformed surrounding material. Elastic recovery occurs up to the equilibrium of elastic and plastic zones. This elastic recovery is called spring-back.

The spring-back effect is a limitation of laser assisted bending. The information of the spring-back angle is important to produce accurate bend angles in laser assisted bending. The spring-back is quantified in terms of elastic recovery of bend angle and calculated as a difference of the maximum bend angle observed during laser scanning and the final bend angle obtained after completion of the process.

Figure 8.26 to Figure 8.29 show the effect of various process parameters on spring-back angle and percentage spring-back angle. The percentage spring-back angle is calculated as

$$\% \text{ Spring-back angle} = \frac{\text{Spring-back angle}}{\text{Final bend angle}} \times 100. \quad (8.1)$$

The spring-back does not occur in the laser bending process as mechanical stresses are not present. Figure 8.26 to Figure 8.29 show the variation of spring back and % spring back angle with the increase in pre-displacement for various laser conditions. It can be observed that the spring-back angle increases with the increase in pre-displacement. It is because the higher pre-displacement results in higher elastic and plastic deformation. The elastic deformation recovers in the form of spring-back angle, and therefore the spring-back angle increases with the pre-displacement. The rate of increase in spring-back angle is less at higher pre-displacement (10 mm). It may be due to the fact that the percentage spring-back angle decreases with the increase in pre-displacement. The plastic deformation is more as compared with the elastic deformation when a higher pre-displacement is applied. Also in case of higher pre-displacement, the induced stresses are higher those deform the worksheet material plastically.

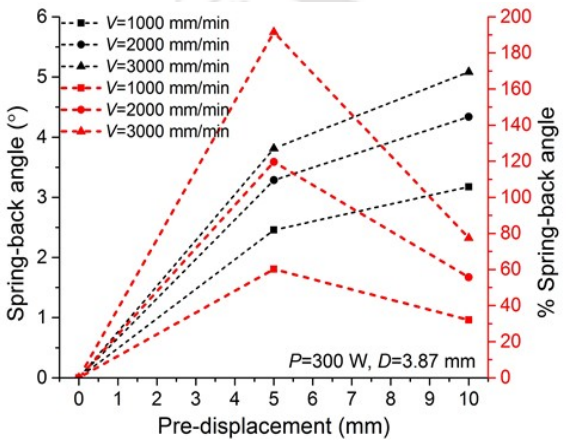

Figure 8.26. Effect of pre-displacement on spring-back effect at *P*=300 W and *D*=3.87 mm.

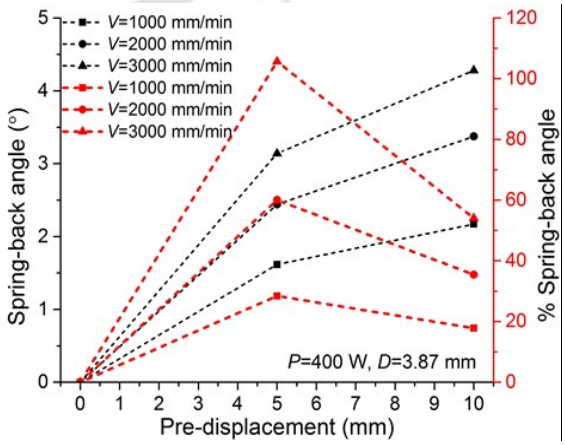

Figure 8.27. Effect of pre-displacement on spring-back effect at *P*=400 W and *D*=3.87 mm.

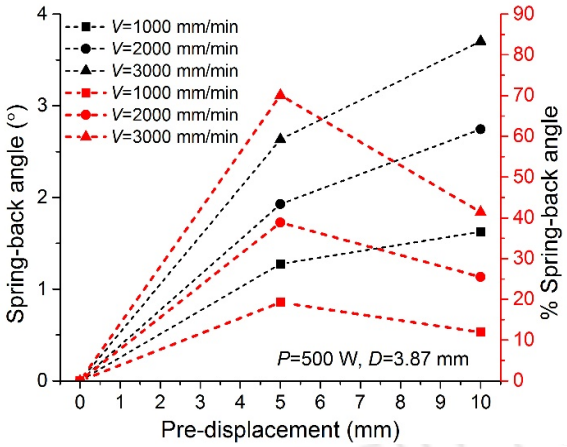

Figure 8.28. Effect of pre-displacement on spring-back effect at *P*=500 W and *D*=3.87 mm.

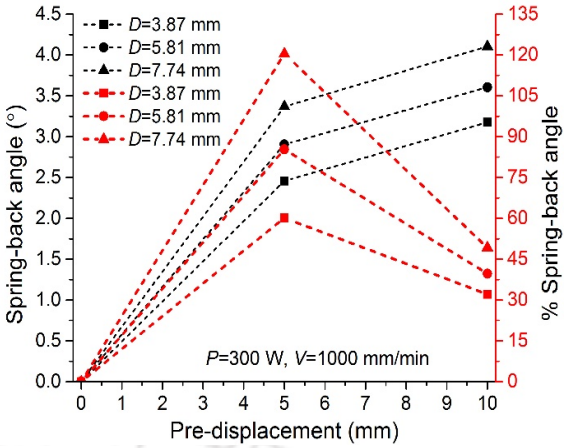

Figure 8.29. Effect of pre-displacement on spring-back effect at *P*=300 W and *V*=1000 mm/min.

The spring-back angle increases with the increase in scan speed, beam diameter and decreases with the increase in laser power. The increase in scan speed and beam diameter reduces the peak temperature of the worksheet while the increase in laser power increases the peak temperature. Therefore, it can be concluded that the spring-back angle decreases with the increase in peak temperature. It is because the yield strength decreases at higher temperature which leads to a higher plastic deformation in the heated region.

The percentage of spring-back angle is also affected by the laser process parameters. It increases with the increase in scan speed and beam diameter and decreases with the increase in laser power. It is because when energy input or heat flux density increases, the peak temperature in the heated region increases. It reduces the yield strength and a larger amount of material undergoes the plastic deformation. This decreases the ratio of elastic deformation to the plastic deformation, and hence the percentage of spring-back angle increases with the increase in scan speed and beam diameter, and decreases with the increase in laser power.

Figure 8.26 to Figure 8.28 are plotted for the chosen process parameters for beam diameter of 3.87 mm. However, a full factorial study was carried out with the other two levels of beam diameters (*viz*., 5.81 mm and 7.74 mm) also. During this study, similar trends of were observed for medium and large beam diameters. These are reported in the Appendix 8.4.

8.8.4 Edge effect

Edge effect is a performance parameter which is quantified in terms of the relative variation in bend angle per unit length (*RVBA*) as given in Equation (4.29). The effect of pre-displacement on *RVBA* is discussed in detail in this section.

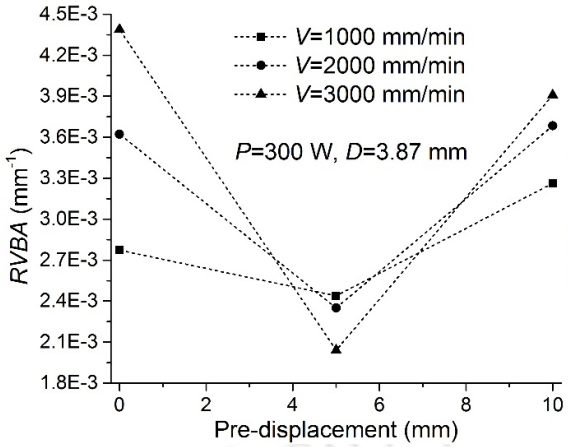

Figure 8.30. Effect of pre-displacement on edge effect at *P*=300 W and *D*=3.87 mm.

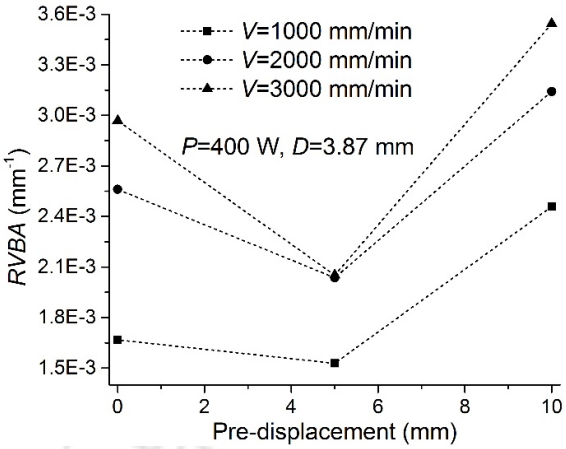

Figure 8.31. Effect of pre-displacement on edge effect at *P*=400 W and *D*=3.87 mm.

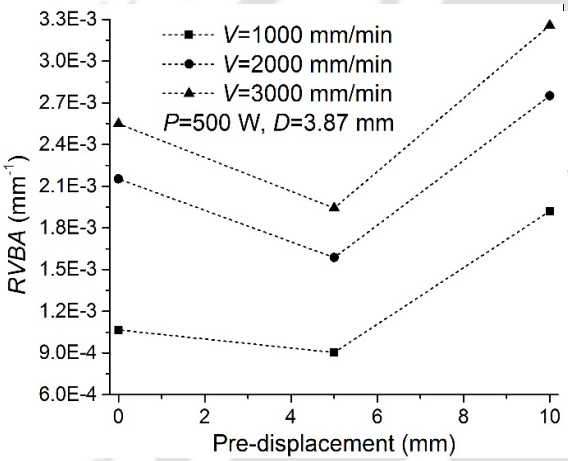

Figure 8.32. Effect of pre-displacement on edge effect at *P*=500 W and *D*=3.87 mm.

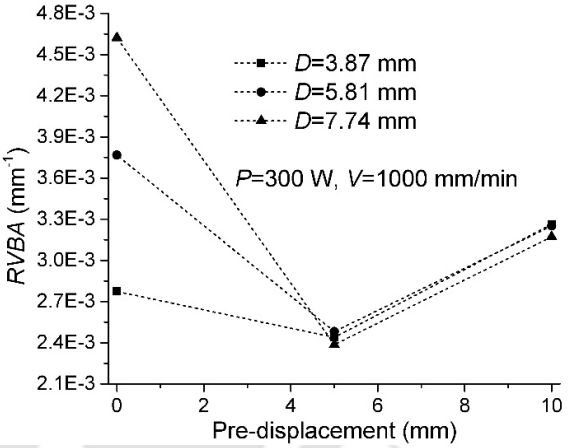

Figure 8.33. Effect of pre-displacement on edge effect at *P*=300 W and *V*=1000 mm/min.

Figure 8.30 to Figure 8.33 show the effect of pre-displacement on the edge effect. It can be seen that the edge effect is less when 5 mm pre-displacement is applied as compared to that obtained in the cases of no external mechanical load (pre-displacement=0 mm) and pre-displacement of 10 mm. It may be due to the fact that the applied pre-displacement is uniform along the irradiation line that tends to obtain uniform bending of the worksheet along the scanning line. However, due to elastic recovery, the required bend angle cannot be achieved. The elastic recovery (spring-back) is not uniform along the scanning line. It is because when scanning starts, heated region is small, and hence the restriction to the pre-displacement is more. When the laser beam is about to leave the worksheet, the heated region is large, and therefore the mechanical constraint provided by the worksheet material is negligible. This non-uniform distribution of the temperature and the mechanical constraint provided by the

worksheet material results in a non-uniform elastic recovery along the scanning line. When pre-displacement is small, the propagated displacement (generated due to moving pre-displacement load) along the free edge is small and its contribution to the heated region is limited. The effect of the restriction provided by the surrounding material is small, and hence the edge effect is less in case of 5 mm of pre-displacement. When a large pre-displacement of 10 mm is applied, the edge effect increases. It is because the restriction provided by the surrounding material has significant variation along the scanning line. The restriction is maximum at start of the laser scan when the heated region is negligible and it is minimum when the laser beam is about to leave the worksheet.

The effect of process parameters on laser assisted bending with 5 mm pre-displacement is different in comparison with the cases of laser bending without pre-displacement and pre-displacement of 10 mm. In case of 5 mm pre-displacement, the edge effect decreases with the increase in scan speed at low laser power, It may be due to the fact that at low laser power, the peak temperature is less, and therefore a faster scan speed provides nearly equal temperature distribution and mechanical constraint by the pre-displacement along the scanning line. At medium and high laser power, the edge effect increases with the increase in scan speed. It is because the peak temperature is high and the worksheet can be deformed easily. The plastic deformation is more near the edges as the temperature is more, and therefore the edge effect increases with the increase in scan speed at a medium and high level of laser power. Also, in case of 5 mm pre-displacement, the edge effect decreases with the increase in laser power and beam diameter. From Figure 8.33, it can be observed that the beam diameter has a significant influence on the edge effect when pre-displacement is not applied while it has a negligible effect on the laser assisted bending with a moving pre-displacement.

Figure 8.30 to Figure 8.33 are plotted for the chosen process parameters. However, a full factorial study was carried out with the other process conditions also. During this study, similar trends of the results were observed for other process conditions. These are reported in the Appendix 8.5.

8.8.5 Edge displacement

Study on the edge displacement is important to know the deformation behavior of the process. Figure 8.34 and Figure 8.35 show the effect of pre-displacement on the bent profiles of Edge C and Edge D, respectively. Bent profiles are obtained after the completion of the laser scan. It can be seen that in both laser bending and laser assisted bending, the worksheet bends about

the scanning line. The displacement at free edge increases with the increase in pre-displacement. It is due to the increase in bend angle with pre-displacement.

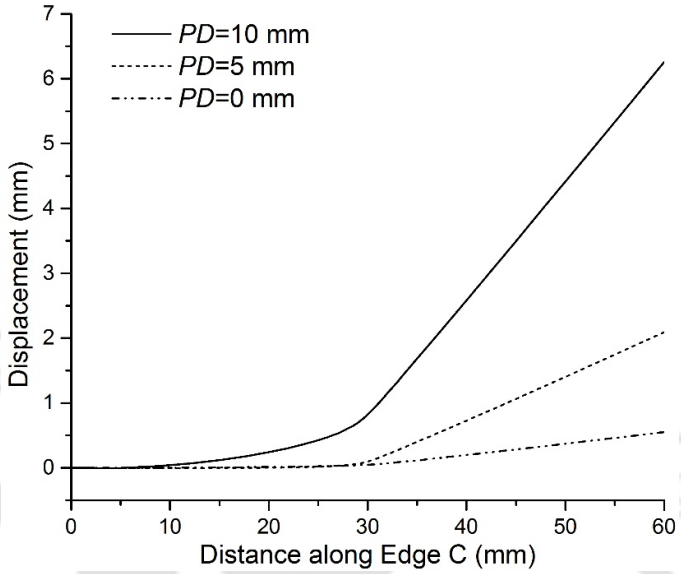

Figure 8.34. Profile of the Edge C after bending.

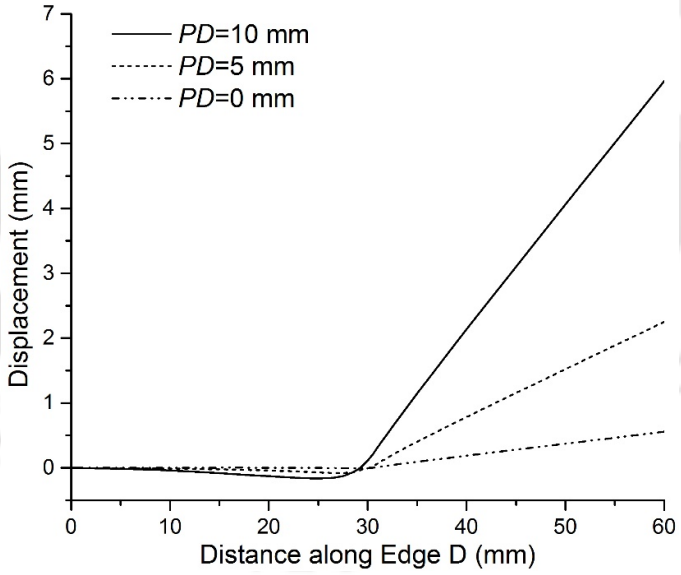

Figure 8.35. Profile of the Edge D after bending.

The pre-displacement induces bending moment along length of the worksheet. The magnitude of bending moment increases towards the fixed edge due to increase in its distance from the location of the applied load. The bending moment may cause curved bending along the length of the worksheet. Therefore, it is expected that instead of the bending about scanning line axis the worksheet may bend in a curvilinear direction. In the present work, the curved

bending is not observed for a lower pre-displacement (5 mm). For a higher pre-displacement (10 mm), a slight curved bending is observed along the Edge C between scanning line and clamping (Figure 8.34). It is because the pre-displacement is applied first, and then the laser scanning is started. At start of the process, since the worksheet is at room temperature, which do not deform the scanning region plastically even though the pre-displacement is employed. When the laser heating starts, the deformation occurs in the heated region, as the yield strength of the material reduces at an elevated temperature. As the load moves near to Edge D, the laser pre-heat the material near to the Edge D, and therefore the curved bending does not occur along Edge D.

It can be seen that the application of pre-displacement twists the worksheet. When the roller is near to Edge C, it moves the worksheet in clockwise direction and when it is near to Edge D, it bends the worksheet in anti-clockwise direction. The effect of clockwise motion is more because it starts when worksheet is at room temperature. As laser beam moves along the scanning line, area of the heated region increases. It results in the plastic deformation in the heated region which reduces the torsional effect induced by the moving pre-displacement. The effect of torsion can be analyzed by studying edge displacements along Edge C and Edge D shown in Figure 8.34 and Figure 8.35, respectively. It can be seen that the effect of torsion moment on edge displacement is less when a pre-displacement of 5 mm is applied, while it has a significant effect for 10 mm of pre-displacement.

8.9 Summary

In this work an integrated, simple and efficient technique – the laser assisted bending with moving pre-displacement has been developed. It combines together the advantages of thermal and mechanical bending operations. In this method, the mechanical load moves along the free edge of the worksheet simultaneously with the moving laser heat source. The moving mechanical load was applied in terms of the moving pre-displacement. An experimental setup was designed and developed to achieve the defined objectives. Initially, preliminary experiments were carried out to check the feasibility of proposed technique. It was found that the proposed technique can generate a large bend angle in a single laser scan. Three dimensional non-linear thermo-mechanical FEM based model was developed to carry out the numerical simulations of the proposed methodology. The model was validated with the experimental results and was found to be in good agreement with the experimental results. The average prediction error of the numerical model was about 15.4%. The validated numerical model was further used to investigate the effects of laser power, scan speed, beam diameter

and pre-displacement on the bending mechanism, edge displacement, residual stresses, bend angle, edge effect and spring-back effect during the laser assisted bending with moving pre-displacement. Important conclusions of the work are as follows:

- The bending mechanism was found to be significantly affected by the application of external mechanical load. It was observed that the moving pre-displacement does not affect the temperature distribution, however it significantly affects the stress-strain distribution. During the operation, the compressive stresses and tensile stresses were found to be generated at top surface and bottom surfaces, respectively. It was seen that the difference between the compressive and tensile stresses significantly increased the bend angle.
- The simulation studies revealed that the residual stresses and vertical displacement at the free end increase with the increase in pre-displacement. The pre-displacement also affects the distortions into the worksheet. It was also observed that the bend angle increases (1) with the increase in pre-displacement and laser power, and (2) decreases with the increase in scan speed and beam diameter. The bend angle was found to be increased up to 48 times due to the application of pre-displacement.
- The studies also concluded that the application of pre-displacement significantly affects the quality of bend, *i.e*. the edge effect. Smaller pre-displacement (5 mm) produces less edge effect in comparison with that of the higher pre-displacement. It was observed that for 10 mm of pre-displacement, the edge effect increases (1) with the increase in scan speed and beam diameter, and (2) decreases with the increase in laser power. In case of 5 mm pre-displacement, the edge effect decreases with the increase in scan speed at low laser power while at a higher laser power, the edge effect increases with the increase in scan speed. The edge effect decreases with the increase in laser power and beam diameter.
- A parametric study on the spring-back effect was also carried out. It was seen that with the increase in pre-displacement, the spring-back angle increases, but its rate of variation decreases. The spring-back angle increases with the increase in scan speed and beam diameter and it decreases with the increase in laser power. The percentage of spring-back angle was found to be affected by the laser process parameters. It increased with the increase in scan speed and beam diameter and decreased with the increase in laser power.

Overall it can be said that the proposed methodology may be suitable for the laser assisted bending of medium to large sized sheets used in the aerospace, automobile and shipbuilding industries at mass scale. One of the important advantages of the proposed methodology is that the laser beam irradiates away from the mechanical tool that does not affect the tool (roller) life.

CHAPTER 9: CONCLUSIONS AND FUTURE SCOPE

9.0 Overview

The primary objective of the present research work was to assess the feasibility of the laser bending of difficult-to-form materials such as magnesium alloys, and further to improve the process productivity and product quality by conducting systematic numerical and experimental studies on laser bending of magnesium alloy M1A. The work reported herein was carried out in the following stages:

- Feasibility study of the laser bending of magnesium alloy M1A sheets by carrying out systematic experiments. Comparative study of the mechanical properties of laser bent specimens with those of the parent material.
- Development of a finite element based three-dimensional non-linear coupled thermo-mechanical numerical model by considering realistic assumptions for the laser bending of magnesium alloy M1A and the experimental validation of developed numerical model.
- Simulations of single scan laser bending of magnesium alloy using the developed numerical model and its experimental validation. Parametric studies on the performance of the process.
- Study on the effect of curvilinear scanning path on the control of edge effect during laser bending process by using modified numerical model.
- Numerical simulations of multi-scan laser bending of magnesium alloy using the developed numerical model and its experimental validation. Investigations on the bending mechanism, edge effect and bend increment per scan during multi-scan laser bending process by using the developed numerical model.
- Design and development of an experimental set up for a simple integrated and efficient variant of the laser forming technique ─ laser assisted bending process with moving pre-displacement
- A study on the bending mechanism, edge effect and efficiency of the proposed technique, and its performance comparison with that of the laser bending process.

Important observations and research contributions from the present work are summarized in the following section.

9.1 Conclusions and Research Contributions

Literature reports that a variety of materials such as metals, non-metals, ceramics, glass, plastics have been bent using lasers successfully. However, the laser bending of magnesium alloys is not yet explored systematically. The magnesium alloys are important due to their highest strength to weight ratio among all structural metals. They are widely used in the automobile, electronics, medical, aviation and aerospace industries. The studies on magnesium alloy M1A are important for the practical implementation of the process. The present work contributes comprehensive experimental and numerical studies to assess the feasibility, productivity and product quality of laser bending of magnesium alloy M1A. Based on the research gaps identified in the literature, the present work is carried out. Specific contributions of the current research work are presented below.

Experimental studies on laser bending of magnesium alloy M1A

- At start of this research work, experimental studies were carried out to assess the feasibility of laser bending of magnesium alloy M1A. These studies revealed that difficult-to-form magnesium alloys can successfully be bent with laser beam irradiations. It was observed that the specimen did not catch the fire for any set of the process condition. Some process conditions resulted in a significant melting over the irradiated region, however burning of the specimen was not observed.
- Experimental studies revealed that the single scan laser bending can be suitable for micro-bending applications. In general a bend angle of about 1.5° was obtained in a single laser scan. However, in multi-scan laser bending, a large bend angle (up to 16°) was obtained with ten laser scans. The bending radius of the laser bent specimen was found to be very small as compared with that obtained by using the mechanical bending operation. During laser bending, cracks were not observed on the bottom surface of the irradiated specimen. Based on this study it was concluded that the laser bending can be used for precise and crack-free micro as well as macro bending of the magnesium alloys.
- Mechanical properties of the laser irradiated region was studied. Along the scanning direction, the tensile strength of base material and laser scanned material was found to be about 250.9 MPa and 239.7 MPa, respectively, and the elongation at break was about 22.6% and 19.1%, respectively. Perpendicular to the laser scan, the tensile strength of the base and laser scanned specimens was about 240 MPa and 228 MPa, respectively, and the elongation at break was about 22% and 17.7%, respectively. The specimen was

found to be broken in the heated region. Overall the yield strength and tensile strength the laser irradiated specimen were decreased by about 4–5%. The hardness of the heated region was found to be slightly more (50.05 HV) than that of the base material (48.2 HV). The tensile properties of the magnesium alloy was deteriorated due to laser beam irradiation, however deterioration was very less, and was limited to the irradiated region only. Overall it was concluded that the magnesium alloys can easily be bent with the laser bending process without much deterioration in the mechanical properties of the heated region.

3-D thermo-mechanical numerical simulation of laser bending process using finite element method

- A three-dimensional non-linear thermo-mechanical numerical model was developed for laser bending process using finite element method. The convection and radiation boundary conditions were implemented for the heat loss to the surroundings. The temperature and strain rate dependent material properties of magnesium alloy M1A were employed. The effect of melting was incorporated which made the developed model suitable for a wide range of process conditions. The mesh sensitivity analysis was carried out to obtain optimum mesh parameters.
- A formulation to calculate the beam diameter from stand-off distance between the laser head nozzle and worksheet surface was developed. The formulation was validated by taking burn prints on the photographic paper using a defocused laser beam at various stand-off distances. The beam diameter model was found to be in good agreement with the experimental results. Incorporation of this module made the developed numerical process model more realistic.
- Using DFLUX subroutine, a Gaussian distributed source of heat, moving with a predefined scan speed along a predefined scanning path was modeled and applied over the worksheet surface. The subroutine was used to define the distribution of heat flux, laser power, scan speed, beam shape, beam size, number of scans, cooling time between two consecutive scans, and scanning path during laser beam irradiation over the worksheet surface.
- A case study was carried out to assess the prediction capability of the developed numerical model. It was found that the developed model can successfully simulate the laser bending process. It was capable of predicting the temperature distribution, stress-strain distribution and distortions generated by the laser beam irradiations. The predicted

bend angle was compared with the experimental bend angle and was found to be in good agreement. The prediction error of the developed numerical angle was about 2.4% for the chosen process condition.

Single scan straight line laser bending of magnesium M1A alloy sheets

- The straight line laser bending of magnesium alloy M1A sheet was investigated by using developed finite element based numerical model. The numerical model was first validated with experimental results and found to be in good agreement. The numerical model was able to predict the bend angle with an average absolute error of about 10.88%.
- The bending mechanism was studied in terms of temperature and stress-strain distributions. The process was found to be temperature gradient mechanism (TGM) dominated and the worksheet was bent towards the laser head. The effects of laser power, scan speed and beam diameter were studied on the bending mechanism. It was observed that the peak temperature and plastic deformation at both top and bottom surfaces increase with the increase in laser power and decrease with the increase in scan speed and beam diameter. The peak compressive stresses induced at the top and bottom surfaces increase with the increase in laser power and decrease with the increase in scan speed and beam diameter. The peak tensile stresses at both top and bottom surfaces increase with the increase in laser power, scan speed and beam diameter. The transition of bending mechanism was observed with the increase in the laser power and beam diameter and decrease in the scan speed. It resulted in a relatively higher plastic deformation at the bottom surface which reduced the bend angle.
- Effects of process parameters, *viz*. laser power, scan speed and beam diameter on the bend angle and edge effect were studied. Results showed that the laser power, scan speed and beam diameter have a non-linear effect on the bend angle and edge effect. At faster scan speed of 2000 and 3000 mm/min, the bend angle increased with the increase in laser power due to a higher energy input. At a slow scan speed of 1000 mm/min with the increase in laser power, the bend angle was first increased, attained a peak and then decreased. Literature reports that it may be due to melting occurred on the irradiation path. However, based on the analysis carried out in the present work, it was observed that the increase in plastic deformation at the bottom surface is the main reason for the decrease in bend angle when irradiated with a high laser power and slow scan speed.
- Literature reports that the bend angle decreases with the increase in scan speed. In present work, it was observed that the bend angle may increase with the increase in scan speed.

It is due to the high thermal conductivity of magnesium material which helps to achieve a sufficient temperature gradient at a faster scan speeds. The bend angle was found to be decreased with the increase in laser beam diameter. It was observed that, in general, a combination of high laser power, fast scan speed and a small beam diameter produces a large bend angle.

- The quality of laser bent worksheet was analyzed by studying the edge effect. The edge effect is a non-uniform distribution of the bend angle along the scanning path. The edge effect was quantified in terms of the relative variation in bend angle per unit length (*RVBA*). It was noted to be decreased with the increase in laser power and increased with the increase in scan speed and beam diameter. It was observed that a combination of high laser power, slow scan speed and small beam diameter produced the minimum edge effect of about 1.06×10^{-3} mm^{-1} in relative variation of bend angle (*RVBA*).

Curvilinear laser bending of magnesium M1A alloy sheets

- In this work, the numerical analysis of curvilinear laser bending process was carried out. The laser beam was irradiated along a circular arc. The numerical model was validated with experimental results in terms of the bend angle and found to be in good agreement with the experimental results. The numerical model predicted the bend angle with an absolute average error of about 4.71%. The validated numerical model was used to study the effect of scanning path curvature on the edge effect, bend angle and the deformation behavior during laser bending of magnesium alloy.
- Results showed that the scanning path can significantly reduce the edge effect. It was observed that the edge effect is less for the curvilinear laser bending process in comparison with the straight line laser bending process. However, for curvilinear laser bending, the edge effect was increased with the increase in arc height. In general, the edge effect was less for the curvilinear laser bending with 10 mm of arc height. However it was seen that, in general, the increase in arc height does not have any significant effect on the bend angle except for some selected process conditions
- Results showed that in a curvilinear laser bending, the deformation does not occur over the laser scanning path. The deformation was occurred outside of the scanning path curvature. The bending was offset near the edges, while it was on the scanning path at the middle of the scanning path. This behavior is quite different from the straight line laser bending process, where the bending occurs exactly over the scanning line. It was an important finding, which can play an important role in the complex shape generation

using curvilinear laser bending process. The bending offset decreased with the increase in laser power and scan speed and increased with the increase in beam diameter. The beam diameter was found to be the most effective parameter to influence the bending offset.

- In this research work, the edge displacement which is an important bend quality parameter was studied. The effect of change in scanning path curvature on the edge displacement was observed. It was found that the z-displacement decreases with the increase in arc height. The warping at free edge was found to be decreased with the reduction in arc height.

Multi-scan laser bending of magnesium M1A alloy sheets

- Single scan laser bending produced small bend angles of the order of 1º. In view of the requirement of large bend angles (of the order of 10º) in the industrial applications, systematic experimental studies have been carried out by employing multiple scans during the laser bending process.
- Initially, the developed numerical model was validated with the experimental results. It was able to predict the bend angle after tenth laser scan with an average prediction error of about 12.41%. A series of numerical simulations were carried out to explore the change in bending mechanism, bend angle, edge effect and temperature distribution during each laser scan of multi-scan laser bending operation.
- The temperature and stress-strain distribution were observed to be significantly affected by the number of laser scans. It was found that due to pre-heating, the peak temperature increases, while induced stresses in the worksheet decrease in each successive laser scan. It was also seen that the increase in temperature during each successive laser scans results in the worksheet melting after a few laser scans. The plastic deformation at the bottom surface increases with the number of scans which reduces the efficiency of the multi-scan laser bending process.
- The bend angle was found to be increased with increase in the number of laser scans. The multi-scan laser bending process was found to be suitable for obtaining the large bend angle of the order of 10° in difficult-to-form material such as magnesium alloy. In general, a combination of high laser power, fast scan speed and small beam diameter produced a large bend angle.
- The quality of the bend angle was observed to be improved in terms of less edge effect with increase in the number of scans, laser power and scan speed. While it was

deteriorated with the increase in beam diameter. However, at slow scan speed, for medium and high levels of laser power, the edge effect first decreased; then increased and further decreased with increase in the number of scans.

- It can be concluded that these simulation results will be helpful in the prediction of bend angle after each laser scan for a chosen set of process conditions and may be useful in selecting suitable process conditions for obtaining the desired process performance.
- It was observed that the multiple scans result in melting of the irradiated region when processed with high energy density parameters. The melting can be avoided either by providing significant cooling time or by applying forced cooling between two consecutive scans. However, this may result in longer processing time and higher cost for the development of a set up for the forced cooling. It was also observed that the application of multiple scans consume a lot of laser energy. The laser machines have less efficiency which further increases the cost of production of a product on such machines. These factors limit the application of multi-scan laser bending process in real practice.

Laser assisted bending with moving pre-displacement

- In this work, an integrated simple and efficient methodology – the laser assisted bending with moving pre-displacement was developed. It combines together the advantages of thermal and mechanical bending operations. The moving mechanical load was applied in terms of the moving pre-displacement. One of the important advantages of the proposed methodology is that the laser beam irradiates away from the mechanical tool that does not affect the tool (roller) life
- An experimental setup was designed and developed to achieve the defined objectives. Initially, preliminary experiments were carried out to check the feasibility of the process. The proposed methodology was found to be well suited to generate a large bend angle in a single laser scan.
- Three dimensional non-linear thermo-mechanical FEM based model was developed to carry out the numerical simulations of the proposed methodology. The model was validated with the experimental results and was found to be in good agreement with the experimental results. The average prediction error of the numerical model was about 15.4%. The validated numerical model was used to investigate the effect of laser power, scan speed, beam diameter and pre-displacement on the bending mechanism, edge

displacement, residual stresses, bend angle, edge effect and spring-back effect during laser assisted bending with moving pre-displacement.

- The bending mechanism was found to be significantly affected by the application of external mechanical load. The temperature distribution was not affected, but the stress-strain distribution was significantly changed when external load (pre-displacement) was applied. In laser assisted bending, the compressive stresses were generated at the top surface while the tensile stresses were produced at the bottom surface, which significantly increased the bend angle.
- The residual stresses and vertical displacement at the free edge were observed to be increased with pre-displacement. It was noted that the pre-displacement also affects the distortions into the worksheet. The bend angle increases (1) with the increase in pre-displacement and laser power, and (2) decreases with the increase in scan speed and beam diameter. The bend angle was noted to be increased by 12 times (average) due to the application of pre-displacement.
- It was also observed that the application of pre-displacement affects the edge effect. For a small pre-displacement (5 mm), the edge effect is less as compared with the laser bending process and it increases with the increase in pre-displacement. For 10 mm of pre-displacement, the edge effect increases (1) with the increase in scan speed and beam diameter, and (2) decreases with the increase in laser power. In case of 5 mm pre-displacement, the edge effect decreases with the increase in scan speed at low laser power while at a higher laser power, the edge effect increases with the increase in scan speed. The edge effect decreases with the increase in laser power and beam diameter.
- During this work, a study on the effects of process parameters on spring-back effect was carried out. It was seen that with the increase in pre-displacement, the spring-back angle increases but its rate of variation decreases. The spring-back angle increases with the increase in scan speed and beam diameter and decreases with the increase in laser power. The percentage of spring-back angle was found to be affected by the laser process parameters. It was increased with the increase in scan speed and beam diameter, and decreased with the increase in laser power.

In conclusion, the present research work has contributed systematic and extensive numerical as well as experimental studies on the laser bending of magnesium alloy M1A. This study covered important variants of the laser bending process, *viz*. straight line, curvilinear, multi-scan and laser assisted bending processes. Numerical simulations of all variants were

validated with the experimental results. Experimental studies also confirm the feasibility of the employment of laser to generate bend angles in the range of about $0.1–16^0$ in magnesium alloy sheets. Effects of various process parameters on the performance of the process in terms of bend angle, edge effect, edge displacement were studied. The efficiency of the process was improved by developing a simple laser based bending technique with the assistance of moving pre-displacement. The developed methodology of the moving pre-displacement can be employed in confidence to enhance the productivity and product quality of the laser bending process.

9.2 Scope for Future Work

The present research work can be extended on the following fronts.

- Development of numerical model for buckling mechanism dominated laser bending process.
- Development of the feedback based control system to get a desired shape of the worksheet.
- Experimental study on the multi-scan laser bending with forced cooling.
- Development of a three-dimensional laser forming system for manufacturing of micro-sized components of magnesium alloys.

REFERENCES

Abed, E., Edwardson, S. P., Bartkowiak, K., Dearden, G., & Watkins, K. G. (2007). Control method for 3D laser forming based on geometrical data. In *Laser Materials Processing Conference*, (pp. 200–205).

Akinlabi, S. A., & Akinlabi, E. T. (2013). Experimental investigation of laser beam forming of titanium and statistical analysis of the effects of parameters on curvature. *Proceedings of the International Multi-Conference of Engineers and Computer Scientists*, Vol II, IMECS 2013, March 13–15, 2013, Hong Kong.

Akinlabi, S. A., Pietra, F., & Akinlabi, E. T. (2014). Experimental and numerical investigation on laser beam forming of steel sheets. *Proceedings of the Institution of Mechanical Engineers, Part L*: *Journal of Materials Design and Applications*, DOI: 10.1177/1464420714526864.

Alexander, K. (2007). Laser Assisted Forming Techniques. *Proceedings of SPIE*, Vol. 6346, p. 634615.

Arnet, H., & Vollertsen, F. (1995). Extending laser bending for the generation of convex shapes. *Proceedings of the Institution of Mechanical Engineers, Part B*: *Journal of Engineering Manufacture*, *209*(6), 433–442.

Avedesian, M.M. & Baker, H. (1999). Magnesium and magnesium alloys. 2nd edition *ASM International*, Materials Park, USA

Bammer, F., Schuöcker, D., Schumi, T., Holzinger, B., & Humenberger, G., 2011, A diode-laser-system for laser-assisted bending of brittle materials. *Advances in Optical Technologies*, *2011*, p. 321807.

Bao, J., & Yao, Y. L. (2001). Analysis and prediction of edge effects in laser bending. *Journal of manufacturing science and engineering*, *123*(1), 53–61.

Barletta, M., Casamichele, L., & Tagliaferri, V. (2006). Line bending of Al_2O_3 coated and uncoated aluminium thin sheets. *Surface and Coatings Technology*, *201*(3), 660–673.

Barletta, M., Gisario, A., & Guarino, S. (2009). Hybrid forming process of AA 6108 T4 thin sheets: modelling by neural network solutions. *Proceedings of the Institution of Mechanical Engineers, Part B*: *Journal of Engineering Manufacture*, *223*(5), 535–545.

Bartkowiak, K., Dearden, G., & Watkins, K. G. (2004). 2-D laser forming comparative study on Nd: Yag of titanium alloy Ti-6Al-4V,". In *23rd International Congress on Applications of Lasers and Electro-optics (ICALEO 2004) San Franscisco*, Vol. 97, p. 528.

Bejan, A., & Kraus, A. D. (Eds.). (2003). Heat transfer handbook. (Vol. 1), *John Wiley & Sons*, New Jersey, USA.

Birnbaum, A. J., Cheng, P., & Yao, Y. L. (2007). Effects of clamping on the laser forming process. *Journal of Manufacturing Science and Engineering*, *129*(6), 1035–1044.

Carey, C., Cantwell, W. J., Dearden, G., Edwards, K. R., Edwardson, S. P., Mullett, J. D., Williams, C. J., & Watkins, K. G. (2007). Effects of laser interaction with graphite coatings. In *Proceedings of the Laser Assisted Net Shape Engineering*, Vol. 5, pp. 673–686.

Carey, C., Cantwell, W. J., Dearden, G., Edwards, K. R., Edwardson, S. P., & Watkins, K. G. (2010). Towards a rapid, non-contact shaping method for fibre metal laminates using a laser source. *The International Journal of Advanced Manufacturing Technology*, *47*(5–8), 557–565.

Carlone, P., Palazzo, G. S., & Pasquino, R. (2008). Inverse analysis of the laser forming process by computational modelling and methods. *Computers & Mathematics with Applications*, *55*(9), 2018–2032.

Casalino, G., & Ludovico, A. D. (2002). Parameter selection by an artificial neural network for a laser bending process. *Proceedings of the Institution of Mechanical Engineers, Part B*: *Journal of Engineering Manufacture*, *216*(11), 1517–1520.

Casamichele, L., Quadrini, F., & Tagliaferri, V. (2007). Process-efficiency prediction in high power diode laser forming. *Journal of Manufacturing Science and Engineering*, *129*(5), 868–873.

Chakraborty, S. S., Maji, K., Racherla, V., & Nath, A. K. (2015). Investigation on laser forming of stainless steel sheets under coupling mechanism. *Optics & Laser Technology*, *71*, 29–44.

Chakraborty, S. S., Racherla, V., & Nath, A. K. (2012). Parametric study on bending and thickening in laser forming of a bowl shaped surface. *Optics and Lasers in Engineering*, *50*(11), 1548–1558.

Chan K.C., & Liang J. (2000a). Effect of microstructures on deformation behaviour of aluminium matrix composites in laser bending, *Textures and Microstructures*, *34*(1), pp. 43–54.

Chan, K. C., & Liang, J. (2000b). Laser bending of an Al6013/SiC_p aluminium matrix composite sheet. *Journal of Materials Processing Technology*, *100*(1), 214–218.

Chan, K. C., & Liang, J. (2001). Thermal expansion and deformation behaviour of aluminium-matrix composites in laser forming. *Composites science and technology*, *61*(9), 1265–1270.

Chehrghani, A., Torkamany, M. J., Hamedi, M. J., & Sabbaghzadeh, J. (2012). Numerical modeling and experimental investigation of TiC formation on titanium surface pre-coated by graphite under pulsed laser irradiation. *Applied Surface Science*, *258*(6), 2068–2076.

Chen, D. J., Wu, S. C., & Li, M. Q. (2004a). Studies on laser forming of Ti–6Al–4V alloy sheet. *Journal of Materials Processing Technology*, *152*(1), 62–65.

Chen, D. J., Xiang, Y. B., Wu, S. C., & Li, M. Q. (2002). Simulation and experiment of curve irradiated laser bending process of titanium alloy sheet. *Materials science and technology*, *18*(6), 673–676.

Chen, D., Wu, S., & Li, M. (2004b). Deformation behaviours of laser curve bending of sheet metals. *Journal of materials processing technology*, *148*(1), 30–34.

Chen, G., & Xu, X. (2001). Experimental and 3D finite element studies of CW laser forming of thin stainless steel sheets. *Journal of Manufacturing science and Engineering*, *123*(1), 66–73.

Chen, G., Xu, X., Poon, C. C., & Tam, A. C. (1998). Laser-assisted microscale deformation of stainless steels and ceramics. *Optical Engineering*, *37*(10), 2837–2842.

Chen, G., Xu, X., Poon, C. C., & Tam, A. C. (1999). Experimental and numerical studies on microscale bending of stainless steel with pulsed laser. *Journal of Applied Mechanics*, *66*(3), 772–779.

Chen, J., Qi, Y., Shi, Y., & Bi, Z. (2010). An analytical model to predict bending angles in high-frequency induction heat forming. *Proceedings of the Institution of Mechanical Engineers, Part C*: *Journal of Mechanical Engineering Science*, *224*(3), 655–660.

Chen, M. L., Jeswiet, J., Bates, P. J., & Zak, G. (2008). Experimental study on sheet metal bending with medium-power diode laser. *Proceedings of the Institution of Mechanical Engineers, Part B*: *Journal of Engineering Manufacture*, *222*(3), 381–389.

Cheng, J. G., & Yao, Y. L. (2004a). Process synthesis of laser forming by genetic algorithm. *International Journal of Machine Tools and Manufacture*, *44*(15), 1619–1628.

Cheng, J., & Yao, Y. L. (2001). Cooling effects in multiscan laser forming. *Journal of Manufacturing processes*, *3*(1), 60–72.

Cheng, J., & Yao, Y. L. (2002). Microstructure integrated modeling of multiscan laser forming. *Journal of manufacturing science and engineering*, *124*(2), 379–388.

Cheng, J., & Yao, Y. L. (2004b). Process design of laser forming for three-dimensional thin plates. *Journal of Manufacturing Science and Engineering*, *126*(2), 217–225.

Cheng, P. J., & Lin, S. C. (2000a). An analytical model for the temperature field in the laser forming of sheet metal. *Journal of Materials Processing Technology*, *101*(1), 260–267.

Cheng, P. J., & Lin, S. C. (2000b). Using neural networks to predict bending angle of sheet metal formed by laser. *International Journal of Machine Tools and Manufacture*, *40*(8), 1185–1197.

Cheng, P. J., & Lin, S. C. (2001). An analytical model to estimate angle formed by laser. *Journal of Materials Processing Technology*, *108*(3), 314–319.

Cheng, P., & Yao, Y. L. (2005). The influence of sheet metal anisotropy on laser forming process. *Journal of Manufacturing Science and Engineering*, *127*(3), 572–582.

Cheng, P., Fan, Y., Zhang, J., Yao, Y. L., Mika, D. P., Zhang, W., Graham M., Marte J., & Jones, M. (2006a). Laser forming of varying thickness plate—Part I: Process analysis. *Journal of Manufacturing Science and Engineering*, *128*(3), 634–641.

Cheng, P., Fan, Y., Zhang, J., Yao, Y. L., Mika, D. P., Zhang, W., W., Graham M., Marte J., & Jones, M. (2006b). Laser forming of varying thickness plate—Part II: process synthesis. *Journal of Manufacturing Science and Engineering*, *128*(3), 642–650.

Cheng, P., Mika, D., Graham, M., Yao, Y. L., & Jones, M. (2005a). Laser forming of complex structures. In *The 1st International Workshop on Thermal Forming (IWOTF'05)*.

Cheng, P., Yao, Y. L., Liu, C., Pratt, D., & Fan, Y. (2005b). Analysis and prediction of size effect on laser forming of sheet metal. *Journal of Manufacturing Processes*, *7*(1), 28–41.

Dearden, G., & Edwardson, S. P. (2003). Some recent developments in two-and three-dimensional laser forming for 'macro' and 'micro' applications. *Journal of Optics A*: *Pure and Applied Optics*, *5*(4), S8.

Dearden, G., Edwardson, S. P., Abed, E., Bartkowiak, K., & Watkins, K. G. (2006). Correction of distortion and design shape in aluminium structures using laser forming. In *25th*

International Congress on Applications of Lasers and Electro Optics (*ICALEO 2006*), pp. 813–817.

Dearden, G., Taylor, C., Bartkowiak, K., Edwardson, S. P., & Watkins, K. G. (2003). An experimental study of laser micro-forming using a pulsed Nd: YAG laser and scanning optics. In *Proceeding of the 21st International Congress on Applications of Laser & Electro-Optics*, Vol. 409, pp. 1–10.

Dickey F. M., & Holswade S. C., 2005, Beam shaping: a review, *Laser Beam Shaping Applications edited by Dickey F. M., Holswade S.C. and Shealy D. L.*, CRC Press, pp. 269–305.

Dieter, G. E., & Bacon, D. (1988). Elements of the theory of plasticity. *Mechanical metallurgy*, 76–79. McGraw-Hill Publications, New York.

Dirscherl, M., Esser, G., & Schmidt, M. (2006). Ultrashort pulse laser bending. *Journal of Laser Micro/Nanoengineering*, *1*(1), 54–60.

Dragos, V., Dan, V., & Kovacevic, R. (2000). Prediction of the laser sheet bending using neural network. In *Circuits and Systems, 2000. Proceedings. ISCAS 2000 Geneva. The 2000 IEEE International Symposium on* (Vol. 3, pp. 686–689). IEEE.

Du, Y., Wang, X., & Silvanus, J. (2010). Improved BP network to predict bending angle in the laser bending process for sheet metal. In *Intelligent System Design and Engineering Application (ISDEA), 2010 International Conference on* (Vol. 1, pp. 839–843). IEEE.

Dutta P. P., Kalita K., & Dixit U. S., 2013, Experimental investigation on laser bending of mild steel coated with black enamel paint, In *Proceedings of National Conference on Manufacturing*: *Vision for Future*, pp. 198–203.

Edwardson S.P., French P., Dearden G., Watkins K.G., & Cantwell W.J. (2005a) 'Laser forming of fibre metal laminates', *Lasers in Engineering*, *15*(3–4), pp. 233–255.

Edwardson, S. P., Abed, E., Bartkowiak, K., Dearden, G., & Watkins, K. G. (2006). Geometrical influences on multi-pass laser forming. *Journal of Physics D*: *Applied Physics*, *39*(2), 382.

Edwardson, S. P., Abed, E., French, P., Dearden, G., Watkins, K. G., McBride, R., Hand, D. P., Jones, J. D. C. & Moore, A. J. (2005b). Developments towards controlled three-dimensional laser forming of continuous surfaces. *Journal of Laser Applications*, *17*(4), 247–255.

Edwardson, S. P., Griffiths, J., Dearden, G., & Watkins, K. G. (2010a). Temperature gradient mechanism: Overview of the multiple pass controlling factors. *Physics Procedia*, *5*(A), 53–63.

Edwardson, S. P., Griffiths, J., Edwards, K. R., Dearden, G., & Watkins, K. G. (2010b). Laser forming: overview of the controlling factors in the temperature gradient mechanism. *Proceedings of the Institution of Mechanical Engineers, Part C*: *Journal of Mechanical Engineering Science*, *224*(5), 1031–1040.

Edwardson, S. P., Watkins, K. G., Dearden, G., & Magee, J. (2001). 3D laser forming of saddle shapes. *Proceedings of Laser Assisted Net Shaping*, 559–568.

Eideh A., & Dixit U. S., 2013, "A robust and efficient inverse method for determining the thermal parameters during laser forming", *Proceedings of National Conference of Recent Advancements in Mechnical Engineering*, November 8–9, NERIST, Nirjuli, India, pp. 38–43.

Eideh A., 2014, Determination of parameters during laser bending by inverse analysis, *M.Tech. Thesis*, Department of Mechanical Engineering, IIT Guwahati, India.

Eideh A., Dixit, U. S., & Echempati, R. (2015). A Simple Analytical Model of Laser Bending Process, *Laser Based Manufacturing*: *5th International and 26th National All India Manufacturing Technology, Design and Research AIMTDR 2014*, edited by Shrikrishna N. Joshi and Uday S. Dixit, pp. 1–15, Chapter 1.

Fan, Y., Cheng, P., Yao, Y. L., Yang, Z., & Egland, K. (2005). Effect of phase transformations on laser forming of Ti–6Al–4V alloy. *Journal of Applied Physics*, *98*(1), 013518.

Fan, Y., Yang, Z., Cheng, P., Egland, K., & Yao, L. (2007). Investigation of effect of phase transformations on mechanical behavior of AISI 1010 steel in laser forming. *Journal of Manufacturing Science and Engineering*, *129*(1), 110–116.

Gärtner, E., Frühauf, J., Löschner, U., & Exner, H. (2001). Laser bending of etched silicon microstructures. *Microsystem Technologies*, *7*(1), 23–26.

Geiger, M. (1994). Synergy of laser material processing and metal forming. *CIRP Annals-Manufacturing Technology*, *43*(2), 563–570.

Geiger, M., & Vollertsen, F. (1993). The mechanisms of laser forming. *CIRP Annals-Manufacturing Technology*, *42*(1), 301–304.

Geiger, M., Merklein, M., & Pitz, M. (2004). Laser and forming technology—an idea and the way of implementation. *Journal of Materials Processing Technology*, *151*(1), 3–11.

Geiger, M., Vollertsen, F., & Deinzer, G. (1993). Flexible straightening of car body shells by laser forming. *SAE Technical Paper*, (No. 930279).

Gisario, A., Barletta, M., Conti, C., & Guarino, S. (2011). Springback control in sheet metal bending by laser-assisted bending: Experimental analysis, empirical and neural network modelling. *Optics & Lasers in Engineering*, *49*(12), 1372–1383.

Gollo, M. H., Mahdavian, S. M., & Naeini, H. M. (2011). Statistical analysis of parameter effects on bending angle in laser forming process by pulsed Nd: YAG laser. *Optics & Laser Technology*, *43*(3), 475–482.

Gollo, M. H., Naeini, H. M., Liaghat, G. H., Torkamany, M. J., Jelvani, S., & Panahizade, V. (2008). An experimental study of sheet metal bending by pulsed Nd: YAG laser with DOE method. *International Journal of Material Forming*, *1*(1), 137–140.

Griffiths, J., Edwardson, S. P., Dearden, G., & Watkins, K. G. (2010). Finite element modelling of laser forming at macro and micro scales. *Physics Procedia*, *5*(B), 371–380.

Guan, Y., Sun, S., Zhao, G., & Luan, Y. (2005). Influence of material properties on the laser-forming process of sheet metals. *Journal of Materials Processing Technology*, *167*(1), 124–131.

Hennige, T. (2000). Development of irradiation strategies for 3D-laser forming. *Journal of Materials Processing Technology*, *103*(1), 102–108.

Hennige, T., Holzer, S., Vollertsen, F., & Geiger, M. (1997). On the working accuracy of laser bending. *Journal of Materials Processing Technology*, *71*(3), 422–432.

Holzer, H., Arnet, M., Geiger, M., 1994, "Physical and numerical modeling of the buckling mechanism". *Proceedings of Laser assisted net shape engineering*, Vol. 1, pp. 379–386.

Hsieh, H. S., & Lin, J. (2004a). Laser-induced vibration during pulsed laser forming. *Optics & Laser Technology*, *36*(6), 431–439.

Hsieh, H. S., & Lin, J. (2004b). Thermal–mechanical analysis on the transient deformation during pulsed laser forming. *International Journal of Machine Tools and Manufacture*, *44*(2), 191–199.

Hsieh, H. S., & Lin, J. (2005). Study of the buckling mechanism in laser tube forming with axial preloads. *International Journal of Machine Tools and Manufacture*, *45*(12), 1368–1374.

Hu, J., Dang, D., Shen, H., & Zhang, Z. (2012). A finite element model using multi-layered shell element in laser forming. *Optics & Laser Technology*, *44*(4), 1148–1155.

Hu, J., Xu, H., & Dang, D. (2013). Modeling and reducing edge effects in laser bending. *Journal of Materials Processing Technology*, *213*(11), 1989–1996.

Hu, Y., Xu, X., Yao, Z., & Hu, J. (2010). Laser peen forming induced two way bending of thin sheet metals and its mechanisms. *Journal of Applied Physics*, *108*(7), 073117.

Hu, Z., Kovacevic, R., & Labudovic, M. (2002). Experimental and numerical modeling of buckling instability of laser sheet forming. *International Journal of Machine Tools and Manufacture*, *42*(13), 1427–1439.

Hu, Z., Labudovic, M., Wang, H., & Kovacevic, R. (2001). Computer simulation and experimental investigation of sheet metal bending using laser beam scanning. *International Journal of Machine Tools and Manufacture*, *41*(4), 589–607.

Jamil, M. C., Sheikh, M. A., & Li, L. (2011a). A study of the effect of laser beam geometries on laser bending of sheet metal by buckling mechanism. *Optics & Laser Technology*, *43*(1), 183–193.

Jamil, M. S. C., Sheikh, M. A., & Li L. (2011b). A numerical study of the temperature gradient mechanism in laser forming using different laser beam geometries, *Lasers in Engineering*, *22*(5–6), pp. 413–428.

Jha, G. C., Nath, A. K., & Roy, S. K. (2008). Study of edge effect and multi-curvature in laser bending of AISI 304 stainless steel. *Journal of Materials Processing Technology*, *197*(1), 434–438.

Ji, Z., & Wu, S. (1998). FEM simulation of the temperature field during the laser forming of sheet metal. *Journal of Materials Processing Technology*, *74*(1), 89–95.

Kannatey-Asibu Jr, E. (2009). Principles of laser materials processing. (Vol. 4). *John Wiley & Sons*, Hoboken, New Jersey, USA.

Kgomari, L. C., & Mbaya, R. K. K. (2010). Metallographic Analysis of Laser and Mechanically Formed HSLA Steel. *World Academy of Science, Engineering and Technology*, *46*, 267–272.

Kim, J., & Na, S. J. (2003). Development of irradiation strategies for free curve laser forming. *Optics & Laser Technology*, *35*(8), 605–611.

Kim, J., & Na, S. J. (2005). Feedback control for 2D free curve laser forming. *Optics & Laser Technology*, *37*(2), 139–146.

Kim, J., & Na, S. J. (2009). 3D laser-forming strategies for sheet metal by geometrical information. *Optics & Laser Technology*, *41*(6), 843–852.

Kitamura, K. (1983). Materials processing by high powered laser, *Japan Welding Engineering Society*, Technical report JWESTP-8302, pp 359–371.

Knupfer, S. M., & Moore, A. J. (2010). The effects of laser forming on the mechanical and metallurgical properties of low carbon steel and aluminium alloy samples. *Materials Science and Engineering*: *A*, *527*(16), 4347–4359.

Knupfer, S. M., Paradowska, A. M., Kirstein, O., & Moore, A. J. (2012). Characterization of the residual strains in iterative laser forming. *Journal of Materials Processing Technology*, *212*(1), 90–99.

Kraus, J. (1997). Basic processes in laser bending of extrusions using the upsetting mechanism. *Laser Assisted Net shape Engineering 2*, Proceedings of the LANE'97, Meisenbach, Bamberg.

Kumar, G. R. S., & Dixit, U. S. (2008). Determination of traverse speed in the laser forming by using FEM with online learning. In *Proceeding of the 2nd International & 23rd All India Manufacturing Technology, Design and Research Conference*, IIT Madras, Chennai, December 15–17.

Kyrsanidi, A. K., Kermanidis, T. B., & Pantelakis, S. G. (1999). Numerical and experimental investigation of the laser forming process. *Journal of Materials Processing Technology*, *87*(1), 281–290.

Kyrsanidi, A. K., Kermanidis, T. B., & Pantelakis, S. G. (2000). An analytical model for the prediction of distortions caused by the laser forming process. *Journal of Materials Processing Technology*, *104*(1), 94–102.

Labeas, G. N. (2008). Development of a local three-dimensional numerical simulation model for the laser forming process of aluminium components. *Journal of Materials Processing Technology*, *207*(1), 248–257.

Laeng, J., Stewart, J. G., & Liou, F. W. (2000). Laser metal forming processes for rapid prototyping–A review. *International Journal of Production Research*, *38*(16), 3973–3996.

Lambiase F. (2012). An analytical model for evaluation of bending angle in laser forming of metal sheets. *Journal of Materials Engineering and Performance*, *21*(10), pp. 2044–2052.

Lambiase, F., & Di Ilio, A. (2013). A closed-form solution for thermal and deformation fields in laser bending process of different materials. *The International Journal of Advanced Manufacturing Technology*, *69*(1–4), 849–861.

Lambiase, F., Di Ilio, A., & Paoletti, A. (2013). An experimental investigation on passive water cooling in laser forming process. *The International Journal of Advanced Manufacturing Technology*, *64*(5–8), 829–840.

Lawrence, J. (2002). A comparative investigation of the efficacy of CO_2 and high-power diode lasers for the forming of EN3 mild steel sheets. *Proceedings of the Institution of Mechanical Engineers, Part B*: *Journal of Engineering Manufacture*, *216*(11), 1481–1491.

Lawrence, J., Schmidt, M. J., & Li, L. (2001). The forming of mild steel plates with a 2.5 kW high power diode laser. *International Journal of Machine Tools and Manufacture*, *41*(7), 967–977.

Lee, K. C., & Lin, J. (2002). Transient deformation of thin metal sheets during pulsed laser forming. *Optics & Laser Technology*, *34*(8), 639–648.

Li, W., & Yao, Y. L. (2000). Numerical and experimental study of strain rate effects in laser forming. *Journal of Manufacturing Science and Engineering*, *122*(3), 445–451.

Li, W., & Yao, Y. L. (2001a). Laser bending of tubes: mechanism, analysis, and prediction. *Journal of Manufacturing Science and Engineering*, *123*(4), 674–681.

Li, W., & Yao, Y. L. (2001b). Numerical and experimental investigation of convex laser forming process. *Journal of Manufacturing Processes*, *3*(2), 73–81.

Liu, C., & Yao, Y. L. (2002). Optimal and robust design of the laser forming process. *Journal of Manufacturing Processes*, *4*(1), 52–66.

Liu, C., & Yao, Y. L. (2005). FEM-based process design for laser forming of doubly curved shapes. *Journal of Manufacturing Processes*, *7*(2), 109–121.

Liu, C., Yao, Y. L., & Srinivasan, V. (2004). Optimal process planning for laser forming of doubly curved shapes. *Journal of Manufacturing Science and Engineering*, *126*(1), 1–9.

Liu, F. R., Chan, K. C., & Tang, C. Y. (2005). Theoretical analysis of deformation behavior of aluminum matrix composites in laser forming. *Materials Science and Engineering*: *A*, *396*(1), 172–180.

Liu, F. R., Chan, K. C., & Tang, C. Y. (2007). Numerical simulation of laser forming of aluminum matrix composites with different volume fractions of reinforcement. *Materials Science and Engineering*: *A*, *458*(1), 48–57.

Liu, F. R., Chan, K. C., & Tang, C. Y. (2008). Numerical modeling of the thermo-mechanical behavior of particle reinforced metal matrix composites in laser forming by using a multi-particle cell model. *Composites Science and Technology*, *68*(9), 1943–1953.

Liu, J., Sun, S., & Guan, Y. (2009). Numerical investigation on the laser bending of stainless steel foil with pre-stresses. *Journal of Materials Processing Technology*, *209*(3), 1580–1587.

Liu, J., Sun, S., Guan, Y., & Ji, Z. (2010). Experimental study on negative laser bending process of steel foils. *Optics & Lasers in Engineering*, *48*(1), 83–88.

Magee, J., & De Vin, L. J. (2002). Process planning for laser-assisted forming. *Journal of Materials Processing Technology*, *120*(1), 322–326.

Magee, J., Sidhu, J., & Cooke, R. L. (2000). A prototype laser forming system. *Optics & lasers in engineering*, *34*(4), 339–353.

Magee, J., Watkins, K. G., Steen, W. T., Calder, N. J., & Sidhu, J. K. J. (1997). Laser forming of aerospace alloys. *ICALEO'97*, 156–165.

Maji, K., Pratihar, D. K., & Nath, A. K. (2013b). Experimental investigations and statistical analysis of pulsed laser bending of AISI 304 stainless steel sheet. *Optics & Laser Technology*, *49*, 18–27.

Maji, K., Pratihar, D. K., & Nath, A. K. (2014a). Analysis of pulsed laser bending of sheet metal using neural networks and neuro-fuzzy system. *Proceedings of the Institution of Mechanical Engineers, Part B*: *Journal of Engineering Manufacture*, 0954405414522212.

Maji, K., Pratihar, D. K., & Nath, A. K. (2014b). Laser forming of a dome shaped surface: experimental investigations, statistical analysis and neural network modeling. *Optics & Lasers in Engineering*, *53*, 31–42.

Maji, K., Pratihar, D. K., &Nath, A. K. (2013a). Analysis and synthesis of laser forming process using neural networks and neuro-fuzzy inference system. *Soft Computing*, *17*(5), 849–865.

Majumdar, J. D., & Manna, I. (2011). Laser material processing. *International Materials Reviews*, *56*(5/6), 341–388.

Majumdar, J. D., Nath, A. K., & Manna, I. (2004). Studies on laser bending of stainless steel. *Materials Science and Engineering*: *A*, *385*(1), 113–122.

Martin R., 1979, Automated adjusting in precision engineering (German patent: Automatisiertesjustieren in der feinwerktechnik), DeutschesPatentamt, Offenlegungsschrift, 29 (18), 100.

Matsushita, N. (2003). Laser micro-bending for precise micro-fabrication of magnetic disk drive components. In *Fourth International Symposium on laser Precision Microfabrication* (pp. 24–29). International Society for Optics and Photonics.

Mazhukin, V. I., Lobok, M. G., & Smurov, I. (2007). Transient effects in pulsed laser irradiation. *Applied Surface Science*, *253*(19), 7744–7748.

McBride, R., Bardin, F., Gross, M., Hand, D. P., Jones, J. D. C., & Moore, A. J. (2005). Modelling and calibration of bending strains for iterative laser forming. *Journal of Physics D*: *Applied Physics*, *38*(22), 4027.

McBride, R., Gross, M., Moore, A. J., Hand, D. P., & Jones, J. D. C. (2004). Calibration of bending and membrane strains for iterative laser forming of non-developable surfaces. *Proceedings of ICALEO 2004*, 71–80.

McGrath, P. J., & Hughes, C. J. (2007). Experimental fatigue performance of laser-formed components. *Optics & Lasers in Engineering*, *45*(3), 423–430.

Merklein, M., Hennige, T., & Geiger, M. (2001). Laser forming of aluminium and aluminium alloys—microstructural investigation. *Journal of Materials Processing Technology*, *115*(1), 159–165.

Ming, Z., Guo-Huan, Z., Tao, H., Hua, D., & Lan, C. (2010). Characterizations of stress and strain variation in three-dimensional forming of laser micro-manufacturing. *Chinese Physics Letters*, *27*(2), 024202.

Mishra, A., & Dixit, U.S. (2013). Determination of thermal diffusivity of the material, absorptivity of the material and laser beam radius during laser forming by inverse heat transfer. *Journal of Machining and Forming Technologies*, 5, 207–226.

Ocaña, J. L., Morales, M., Molpeceres, C., García, O., Porro, J. A., & García-Ballesteros, J. J. (2007). Short pulse laser microforming of thin metal sheets for MEMS manufacturing. *Applied Surface Science*, *254*(4), 997–1001.

Ocaña, J., Morales, M., Molpeceres, C., Garcıa, O., Porro, J., & Garcıa-Ballesteros, J. (2008). Numerical modelling and experimental characterization of short pulse laser microforming of thin metal sheets. In *Proc. of the 4M2008 Conference Multi-Material Micro Manufacture, Cardiff, UK, September* (pp. 9–11).

Okamoto, Y., Miyamoto, I., Uno, Y., & Takenaka, T. (2004). Deformation characteristics of plastics in YAG laser forming. In *Fifth International Symposium on Laser Precision Microfabrication* (pp. 576–581). International Society for Optics and Photonics.

Palani, I. A., Subbu, S. K., Vasa, N. J., Ramkumar, J., & Singaperumal, M. (2008). Laser based surface processing of engineering materials- State of the art. *International Journal on Design and Manufacturing Technologies*, *2*(1), 1–9.

Pallav, K., Han, P., Ramkumar, J., & Ehmann, K. F. (2011). Comparative assessment of the laser induced plasma micro-machining (LIP-MM) and the Micro-EDM Processes, *ASME 2011 International Manufacturing Science and Engineering Conference*, Vol. 2.

Pallav, K., Ramkumar, J., Nagahanumaiah, & Ehmann, K. F. (2010). Numerical simulation of the laser induced plsma micro-machining process (LIP-MM). *7th International Workshop on Microfactories, Daejeon Convention Centre*, Korea, 24–27 October 2010.

Pandey, N. D., Arora, N., Bharti, A., & Chakravorty, P. (2002). Dissimilar Metal Welding Using Nd: Yag Pulsed Laser. *Indian Welding Journal*, *35*(3), 37–48.

Paramasivan, K., Das, S., & Misra, D. (2014). A study on the effect of rectangular cut out on laser forming of AISI 304 plates. *The International Journal of Advanced Manufacturing Technology*, *72*(9–12), 1513–1525.

Paunoiu, V., Squeo, E. A., Quadrini, F., Gheorghies, C., & Nicoara, D. (2008). Laser bending of stainless steel sheet metals. *International Journal of Material Forming*, *1*(1), 1371–1374.

Pitz, I., Otto, A., & Schmidt, M. (2010). Simulation of the laser beam forming process with moving meshes for large aluminium plates. *Physics Procedia*, *5*(B), 363–369.

Qi, L., & Namba, Y. (2011). Precision laser adjustment using CW diode laser. *Precision Engineering*, *35*(1), 126–132.

Rao, S.S., (1984). Optimization: theory and applications. 2nd ed., *Wiley Eastern Ltd*, New York.

Ravindra, D., & Patten, J. (2014). Micro-Laser-Assisted Machining: The Future of Manufacturing Ceramics and Semiconductors. *Sensors and Materials*, *26*(6), 417–427.

Reutzel, E. W., Zhang, L., & Michaleris, P. (2006). A differential geometry approach to analysis of thermal forming. *International Journal of Mechanical Sciences*, *48*(10), 1046–1062.

Safari, M., & Farzin, M. (2013). Experimental and numerical investigation of laser bending of tailor machined blanks. *Optics & Laser Technology*, *48*, 513–522.

Safdar, S., Li, L., Sheikh, M. A., & Liu, Z. (2007). The effect of nonconventional laser beam geometries on stress distribution and distortions in laser bending of tubes. *Journal of Manufacturing Science and Engineering*, *129*(3), 592–600.

Safdar, S., Li, L., Sheikh, M. A., & Schmidt, M. J. (2006). Thermal history analysis of surface heating of mild steel with different laser beam geometries. *Proceedings of the Institution of Mechanical Engineers, Part C*: *Journal of Mechanical Engineering Science*, *220*(10), 1549–1557.

Santo L., Trovalusci F., & Davim J. P. (2014). Laser applications in field of plastics, Chapter 12, (Vol. 9, pp. 243–260) in Comprehensive Materials Processing, edited by B. Yilbas and M. S. Hashmi, *Elsevier Science*, London.

Santo, L., & Davim, J. P. (2011). Laser cladding: an overview, Chapter 10 (pp. 367–382), in Laser Beams: Theory, Properties and Applications, edited by Maxim Thys and Eugene Desmet, *NOVA Publishers*, New York.

Santos, E. C., Shiomi, M., Osakada, K., & Laoui, T. (2006). Rapid manufacturing of metal components by laser forming. *International Journal of Machine Tools and Manufacture*, *46*(12), 1459–1468.

Schuöcker D., (2000). Laser assisted forming, *Proceedings of SPIE*, *4065*, 117–127.In High-Power Laser Ablation Ill, Claude R. Phipps, Editor, Proceedings of SPIE

Shealy D. L. (2005). History of beam shaping, *Laser Beam Shaping Applications edited by Dickey F. M., Holswade S.C. and Shealy D. L.*, *CRC Press*, pp. 307–348.

Sheikh, M. A., & Li, L. (2010). Understanding the effect of non-conventional laser beam geometry on material processing by finite-element modelling. *Proceedings of the Institution of Mechanical Engineers, Part C*: *Journal of Mechanical Engineering Science*, *224*(5), 1061–1072.

Shen, H. (2008). Mechanism of laser micro-adjustment. *Journal of Physics D*: *Applied Physics*, *41*(24), 245106.

Shen, H., & Vollertsen, F. (2009). Modelling of laser forming–An review. *Computational Materials Science*, *46*(4), 834–840.

Shen, H., & Yao, Z. (2009). Study on mechanical properties after laser forming. *Optics & Lasers in Engineering*, *47*(1), 111–117.

Shen, H., Hu, J., & Yao, Z. (2010). Analysis and control of edge effects in laser bending. *Optics & Lasers in Engineering*, *48*(3), 305–315.

Shen, H., Hu, J., & Yao, Z. Q. (2011). Cooling effects in laser forming. *Materials Science Forum*, *663*, 58–63.

Shen, H., Ran, M., Hu, J., & Yao, Z. (2014). An experimental investigation of underwater pulsed laser forming. *Optics & Lasers in Engineering*, *62*, 1–8.

Shen, H., Shi, Y., & Yao, Z. (2006a). Laser forming of plates using two sequent scans of different intervals. *Proceedings of the Institution of Mechanical Engineers, Part C*: *Journal of Mechanical Engineering Science*, *220*(4), 507–511.

Shen, H., Shi, Y., & Yao, Z. (2006b). Numerical simulation of the laser forming of plates using two simultaneous scans. *Computational Materials Science*, *37*(3), 239–245.

Shen, H., Shi, Y., Yao, Z., & Hu, J. (2006c). An analytical model for estimating deformation in laser forming. *Computational Materials Science*, *37*(4), 593–598.

Shen, H., Yao, Z., & Hu, J. (2008). An analytical model for bending angle in metal/ceramic bilayer system of laser forming. *Journal of Applied Physics*, *104*(11), 113531.

Shen, H., Yao, Z., & Hu, J. (2009). Numerical analysis of metal/ceramic bilayer materials systems in laser forming. *Computational Materials Science*, *45*(2), 439–442.

Shen, H., Zhou, J., & Yao, Z. Q. (2007). Study on overlapping of two sequential scans in laser forming. *Proceedings of the Institution of Mechanical Engineers, Part C*: *Journal of Mechanical Engineering Science*, *221*(9), 993–997.

Shi, Y. J., Shen, H., Yao, Z. Q., & Hu, J. (2006a). Numerical investigation of straight-line laser forming under the temperature gradient mechanism. *Acta Metallurgica Sinica (English Letters)*, *19*(2), 144–150.

Shi, Y., Hu, J., & Dong, C. (2011). Analysis of the geometric effect on the forming accuracy in laser forming. *Proceedings of the Institution of Mechanical Engineers, Part B*: *Journal of Engineering Manufacture*, *225*(10), 1792–1800.

Shi, Y., Liu, Y., Yao, Z., & Shen, H. (2008). A study on bending direction of sheet metal in laser forming. *Journal of Applied Physics*, *103*(5), 053101.

Shi, Y., Liu, Y., Yi, P., & Hu, J. (2012a). Effect of different heating methods on deformation of metal plate under upsetting mechanism in laser forming. *Optics & Laser Technology*, *44*(2), 486–491.

Shi, Y., Lu, X., Liu, Y., & Yi, P. (2013). Forming accuracy analysis of plate in multi-scanning laser bending process. *Proceedings of the Institution of Mechanical Engineers, Part E*: *Journal of Process Mechanical Engineering*, *227*(3), 225–228.

Shi, Y., Shen, H., Yao, Z., & Hu, J. (2007a). Temperature gradient mechanism in laser forming of thin plates. *Optics & Laser Technology*, *39*(4), 858–863.

Shi, Y., Shen, H., Yao, Z., & Hu, J. (2007b). An analytical model based on the similarity in temperature distributions in laser forming. *Optics & Lasers in Engineering*, *45*(1), 83–87.

Shi, Y., Shen, H., Yao, Z., Hu, J., & Xia, L. (2006b). Application of similarity theory in the laser forming process. *Computational Materials Science*, *37*(3), 323–327.

Shi, Y., Yao, Z., Shen, H., & Hu, J. (2006c). Research on the mechanisms of laser forming for the metal plate. *International Journal of Machine Tools and Manufacture*, *46*(12), 1689–1697.

Shi, Y., Yi, P., & Liu, Y. (2012b). Numerical investigation of temperature field of different mechanisms in laser forming. *Proceedings of the Institution of Mechanical Engineers, Part C*: *Journal of Mechanical Engineering Science*, *226*(8), 2118–2125.

Shichun, W., & Jinsong, Z. (2001). An experimental study of laser bending for sheet metals. *Journal of Materials Processing Technology*, *110*(2), 160–163.

Shichun, W., & Zhong, J. (2002). FEM simulation of the deformation field during the laser forming of sheet metal. *Journal of Materials Processing Technology*, *121*(2), 269–272.

Shidid, D. P., Gollo, M. H., Brandt, M., & Mahdavian, M. (2013). Study of effect of process parameters on titanium sheet metal bending using Nd: YAG laser. *Optics & Laser Technology*, *47*, 242–247.

Shim, H. B., & Kim, K. H. (2011). Springback correction of stamped, curved U-channel part by laser bending. *Proceedings of the Institution of Mechanical Engineers, Part B*: *Journal of Engineering Manufacture*, *225*(3), 367–376.

Singh K., Joshi S.N., Ray A.K. & Dixit U.S. (2013a), A comparison of bend quality of mechanical and laser bending of mild steel. *Proceedings of National Symposium on Miniature Manufacturing in 21st Century (NSMMIC–2013)*, August 16–18, 2013, IIT (BHU), Varanasi, India.

Singh K., Ray A.K., Joshi S.N., Dixit U.S. (2013b). Effect of lime and graphite grease coatings on the absorptivity of mild steel sheet in line heating by CO_2 laser. *Proceedings of National Conference of Recent Advancements in Mechanical Engineering*, November 8–9, 2013, NERIST, Nirjuli, India.

Singh, G., Teli, M., Samanta, A., & Singh, R. (2013). Finite Element Modeling of Laser-Assisted Machining of AISI D2 Tool Steel. *Materials and Manufacturing Processes*, *28*(4), 443–448.

Singh, R., & Melkote, S. N. (2009). Force Modeling in Laser-Assisted Microgrooving Including the Effect of Machine Deflection. *Journal of Manufacturing Science and Engineering*, *131*(1), 011013.

Sowdari, D., & Majumdar, P. (2010). Finite element analysis of laser irradiated metal heating and melting processes. *Optics & Laser Technology*, *42*(6), 855–865.

Stevens, V., Celentano, D., Ramos-Grez, J., & Walczak, M. (2012). Experimental and numerical analysis of low output power laser bending of thin steel sheets. *Journal of Manufacturing Science and Engineering*, *134*(3), 031010.

Subbu, S. K., Ramkumar, J., Vasa, N. J., (2009). Investigation on laser shot peening (LSP) of Ti alloys. *International Conference on Emerging Research and Advances in Mechanical Engineering*, *ERA-2009*, Chennai, India.

Sun, H. (1998). Thin lens equation for a real laser beam with weak lens aperture truncation. *Optical Engineering*, *37*(11), 2906–2913.

Tam, A. C., Poon, C. C., & Crawforth, L. (2001). Laser bending of ceramics and application to manufacture magnetic head sliders in disk drives. *Analytical Sciences/Supplements*, *17*(0), s419–s421.

Thomson, G., & Pridham, M. (1997). A feedback control system for laser forming. *Mechatronics*, *7*(5), 429–441.

Thomson, G., & Pridham, M. (1998). Improvements to laser forming through process control refinements. *Optics & Laser Technology*, *30*(2), 141–146.

Thomson, G., & Pridham, M. (2001). Material property changes associated with laser forming of mild steel components. *Journal of Materials Processing Technology*, *118*(1), 40–44.

Topić, M. N., McGrath, P., Vorster, W. J., Zhang, S. Y., Bucher, R., Venter, A., & Korsunsky, A. M. (2007). Multi-scan laser forming: Synchrotron strain scanning and microstructure evolution. *The Journal of Strain Analysis for Engineering Design*, *42*(7), 497–504.

Ueda, T., Sentoku, E., Wakimura, Y., & Hosokawa, A. (2009). Flattening of sheet metal by laser forming. *Optics & Lasers in Engineering*, *47*(11), 1097–1102.

Ueda, T., Sentoku, E., Yamada, K., & Hosokawa, A. (2005). Temperature measurement in laser forming of sheet metal. *CIRP Annals-Manufacturing Technology*, 54(1), 179–182.

Ueda, T., Wakimura, Y., Furumoto, T., Hosokawa, A., & Tanaka, R. (2011). Experimental investigation on laser flattening of sheet metal. *Optics & Lasers in Engineering*, *49*(1), 137–144.

Vásquez-Ojeda, C., & Ramos-Grez, J. (2009). Bending of stainless steel thin sheets by a raster scanned low power CO_2 laser. *Journal of Materials Processing Technology*, *209*(5), 2641–2647.

Venkadeshwaran, K., Das, S., & Misra, D. (2010). Finite element simulation of 3-D laser forming by discrete section circle line heating. *International Journal of Engineering, Science and Technology*, *2*(4), 163–175.

Vollertsen, F. (1994). An analytical model for laser bending. *Lasers in Engineering*, *2*(1), 261–276.

Vollertsen, F., & Rödel, M. (1994). Model for the temperature gradient mechanism of laser bending. In *Proceeding of the LANE'94*, pp. 371–378.

Vollertsen, F., & Sakkiettibutra, J. (2010). Different types to use laser as a forming tool. *Physics Procedia*, *5*(B), 193–203.

Vollertsen, F., Geiger, M., & Li, W. (1993). FDM and FEM simulation of laser forming: a comparative study. In *Proceeding of the Forth International Conference on Technology of Plasticity*, *4*, 1793–1798.

Vollertsen, F., Komel, I., & Kals, R. (1995). The laser bending of steel foils for microparts by the buckling mechanism-A model. *Modelling and Simulation in Materials Science and Engineering*, *3*(1), 107.

Walczyk, D. F., & Vittal, S. (2000). Bending of titanium sheet using laser forming. *Journal of Manufacturing Processes*, *2*(4), 258–269.

Wang, X. F., Takacs, J., Krallics, G., Szilagyi, A., & Markovits, T. (2002). Research on the thermo-physical process of laser bending. *Journal of Materials Processing Technology*, *127*(3), 388–391.

Wang, X. Y., Xu, W. X., Xu, W. J., Hu, Y. F., Liang, Y. D., & Wang, L. J. (2011). Simulation and prediction in laser bending of silicon sheet. *Transactions of Nonferrous Metals Society of China*, *21*(1), s188–s193.

Watkins, K. G., Edwardson, S. P., Magee, J., Dearden, G., French, P., Cooke, R. L., Sidhu, J., & Calder, N. J. (2001). Laser forming of aerospace alloys. *SAE Technical Paper*, (No. 2001–01–2610).

Wu, D. J., Ma, G. Y., Liu, S., Wang, X. Y., & Guo, D. M. (2010a). Experiments and simulation on laser bending of silicon sheet with different thicknesses. *Applied Physics A*, *101*(3), 517–521.

Wu, D., Zhang, Q., Ma, G., Guo, Y., & Guo, D. (2010b). Laser bending of brittle materials. *Optics & Lasers in Engineering*, *48*(4), 405–410.

Xu, W., Zhang, L. C., & Wang, X. (2013). Laser bending of silicon sheet: Absorption factor and mechanisms. *Journal of Manufacturing Science and Engineering*, *135*(6), 061005.

Xu, X., Lin, X., Yang, M., Chen, J., & Huang, W. (2009). Microstructure evolution in laser solid forming of Ti–50wt% Ni alloy. *Journal of Alloys and Compounds*, *480*(2), 782–787.

Yang, L. J., Tang, J., Wang, M. L., Wang, Y., & Chen, Y. B. (2010). Surface characteristic of stainless steel sheet after pulsed laser forming. *Applied Surface Science*, *256*(23), 7018–7026.

Yanjin, G., Sheng, S., Guoqun, Z., & Yiguo, L. (2003). Finite element modeling of laser bending of pre-loaded sheet metals. *Journal of Materials Processing Technology*, *142*(2), 400–407.

Yao, Z., Shen, H., Shi, Y., & Hu, J. (2007). Numerical study on laser forming of metal plates with pre-loads. *Computational Materials Science*, *40*(1), 27–32.

Yau, C. L., Chan, K. C., & Lee, W. B. (1998). Laser bending of leadframe materials. *Journal of Materials Processing Technology*, *82*(1), 117–121.

Yilbas, B. S., Arif, A. F. M., & Aleem, B. A. (2012). Laser bending of AISI 304 steel sheets: Thermal stress analysis. *Optics & Laser Technology*, *44*(2), 303–309.

Yu, G., Masubuchi, K., Maekawa, T., & Patrikalakis, N. M. (2001). FEM simulation of laser forming of metal plates. *Journal of Manufacturing Science and Engineering*, *123*(3), 405–410.

Yu, G., Patrikalakis, N. M., & Maekawa, T. (2000). Optimal development of doubly curved surfaces. *Computer Aided Geometric Design*, *17*(6), 545–577.

Zahrani, E. G., & Marasi, A. (2013a). Modeling and optimization of laser bending parameters via response surface methodology. *Proceedings of the Institution of Mechanical Engineers, Part C*: *Journal of Mechanical Engineering Science*, *227*(7), 1577–1584.

Zahrani, E. G., & Marasi, A. (2013b). Experimental investigation of edge effect and longitudinal distortion in laser bending process. *Optics & Laser Technology*, *45*, 301–307.

Zhang, L., & Michaleris, P. (2004). Investigation of Lagrangian and Eulerian finite element methods for modeling the laser forming process. *Finite Elements in Analysis and Design*, *40*(4), 383–405.

Zhang, L., Reutzel, E. W., & Michaleris, P. (2004). Finite element modeling discretization requirements for the laser forming process. *International Journal of Mechanical Sciences*, *46*(4), 623–637.

Zhang, P., Guo, B., Shan, D. B., & Ji, Z. (2007). FE simulation of laser curve bending of sheet metals. *Journal of Materials Processing Technology*, *184*(1), 157–162.

Zhang, P., Yu, J., & Zheng, X. (2009). Deformation behaviors of laser forming of ring sheet metals. *Tsinghua Science & Technology*, *14*(1), 132–136.

Zhang, X. R., & Xu, X. (2005a). Laser bending for adjusting curvatures of hard disk suspensions. *Microsystem Technologies*, *11*(11), 1197–1203.

Zhang, X. R., & Xu, X. (2005b). Laser bending for high-precision curvature adjustment of microcantilevers. *Applied Physics Letters*, *86*(2), 021114.

Zhang, X. R., Chen, G., & Xu, X. (2002). Numerical simulation of pulsed laser bending. *Transactions-American Society of Mechanical Engineers Journal of Applied Mechanics*, *69*(3), 254–260.

Zhang, X. R., Xu, X., & Tam, A. C. (2001). Microscale bending using pulsed and CW laser. In *Photonics West 2001–LASE* (pp. 58–65). International Society for Optics and Photonics.

Zhou, J., Shen, H., Yu, X., Hu, J., & Yao, Z. (2013). On the competition between in-plane and out-of-plane deformations in laser thermal adjustment. *Optics & Laser Technology*, *45*, 689–696.

Appendix 2.1

PERMISSIONS FOR FIGURE 2.3 (only first page of the license agreement)

ELSEVIER LICENSE
TERMS AND CONDITIONS

Aug 22, 2015

This is a License Agreement between Ravi Kant ("You") and Elsevier ("Elsevier") provided by Copyright Clearance Center ("CCC"). The license consists of your order details, the terms and conditions provided by Elsevier, and the payment terms and conditions.

All payments must be made in full to CCC. For payment instructions, please see information listed at the bottom of this form.

Supplier	Elsevier Limited The Boulevard,Langford Lane Kidlington,Oxford,OX5 1GB,UK
Registered Company Number	1982084
Customer name	Ravi Kant
Customer address	Department of Mechanical Engineering
	Guwahati, Assam 781039
License number	3694530430506
License date	Aug 22, 2015
Licensed content publisher	Elsevier
Licensed content publication	Journal of Manufacturing Processes
Licensed content title	Numerical and Experimental Investigation of Convex Laser Forming Process
Licensed content author	Wenchuan Li,Y. Lawrence Yao
Licensed content date	2001
Licensed content volume number	3
Licensed content issue number	2
Number of pages	9
Start Page	73
End Page	81
Type of Use	reuse in a thesis/dissertation
Portion	figures/tables/illustrations
Number of figures/tables /illustrations	1
Format	both print and electronic
Are you the author of this Elsevier article?	No
Will you be translating?	No
Original figure numbers	Figure 2
Title of your thesis/dissertation	Assessment of Feasibility, Productivity and Product Quality during Laser Based Bending of Magnesium Alloy Sheets
Expected completion date	Feb 2016
Estimated size (number of pages)	300

PERMISSIONS FOR FIGURE 2.5 (only first page of the license agreement)

ELSEVIER LICENSE
TERMS AND CONDITIONS

Aug 22, 2015

This is a License Agreement between Ravi Kant ("You") and Elsevier ("Elsevier") provided by Copyright Clearance Center ("CCC"). The license consists of your order details, the terms and conditions provided by Elsevier, and the payment terms and conditions.

All payments must be made in full to CCC. For payment instructions, please see information listed at the bottom of this form.

Supplier	Elsevier Limited The Boulevard,Langford Lane Kidlington,Oxford,OX5 1GB,UK
Registered Company Number	1982084
Customer name	Ravi Kant
Customer address	Department of Mechanical Engineering Guwahati, Assam 781039
License number	3694530654693
License date	Aug 22, 2015
Licensed content publisher	Elsevier
Licensed content publication	Optics and Lasers in Engineering
Licensed content title	Analysis and control of edge effects in laser bending
Licensed content author	Hong Shen,Jun Hu,Zhenqiang Yao
Licensed content date	March 2010
Licensed content volume number	48
Licensed content issue number	3
Number of pages	11
Start Page	305
End Page	315
Type of Use	reuse in a thesis/dissertation
Intended publisher of new work	other
Portion	figures/tables/illustrations
Number of figures/tables /illustrations	1
Format	both print and electronic
Are you the author of this Elsevier article?	No
Will you be translating?	No
Original figure numbers	Figure 3
Title of your thesis/dissertation	Assessment of Feasibility, Productivity and Product Quality during Laser Based Bending of Magnesium Alloy Sheets
Expected completion date	Feb 2016

PERMISSIONS FOR FIGURE 2.6 (only first page of the license agreement)

ELSEVIER LICENSE
TERMS AND CONDITIONS

Aug 22, 2015

This is a License Agreement between Ravi Kant ("You") and Elsevier ("Elsevier") provided by Copyright Clearance Center ("CCC"). The license consists of your order details, the terms and conditions provided by Elsevier, and the payment terms and conditions.

All payments must be made in full to CCC. For payment instructions, please see information listed at the bottom of this form.

Supplier	Elsevier Limited The Boulevard,Langford Lane Kidlington,Oxford,OX5 1GB,UK
Registered Company Number	1982084
Customer name	Ravi Kant
Customer address	Department of Mechanical Engineering Guwahati, Assam 781039
License number	3694530821916
License date	Aug 22, 2015
Licensed content publisher	Elsevier
Licensed content publication	Journal of Materials Processing Technology
Licensed content title	Bending of stainless steel thin sheets by a raster scanned low power CO2 laser
Licensed content author	Carlos Vásquez-Ojeda,Jorge Ramos-Grez
Licensed content date	1 March 2009
Licensed content volume number	209
Licensed content issue number	5
Number of pages	7
Start Page	2641
End Page	2647
Type of Use	reuse in a thesis/dissertation
Intended publisher of new work	other
Portion	figures/tables/illustrations
Number of figures/tables /illustrations	1
Format	both print and electronic
Are you the author of this Elsevier article?	No
Will you be translating?	No
Original figure numbers	Figure 2
Title of your thesis/dissertation	Assessment of Feasibility, Productivity and Product Quality during Laser Based Bending of Magnesium Alloy Sheets
Expected completion date	Feb 2016

PERMISSIONS FOR FIGURE 2.7

https://s100.copyright.com/AppDispatchServlet#formTop

Copyright Clearance Center RightsLink®

Home | Create Account | Help

SAGE

Title: Forming accuracy analysis of plate in multi-scanning laser bending process:

Author: Yongjun Shi, Xianfa Lu, Yancong Liu, Peng Yi

Publication: Proceedings of the Institution of Mechanical Engineers, Part E: Journal of Process Mechanical Engineering

Publisher: SAGE Publications

Date: 08/01/2013

Copyright © 2013, © SAGE Publications

LOGIN

If you're a copyright.com user, you can login to RightsLink using your copyright.com credentials. Already **a RightsLink user** or want to learn more?

Gratis Reuse

Permission is granted at no cost for use of content in a Master's Thesis and/or Doctoral Dissertation. If you intend to distribute or sell your Master's Thesis/Doctoral Dissertation to the general public through print or website publication, please return to the previous page and select 'Republish in a Book/Journal' or 'Post on intranet/password-protected website' to complete your request.

BACK | CLOSE WINDOW

Copyright © 2015 Copyright Clearance Center, Inc. All Rights Reserved. Privacy statement. Terms and Conditions.

Comments? We would like to hear from you. E-mail us at customercare@copyright.com

Appendix 3.1

COMPOSITIONS TEST REPORT OF THE MATERIAL USED

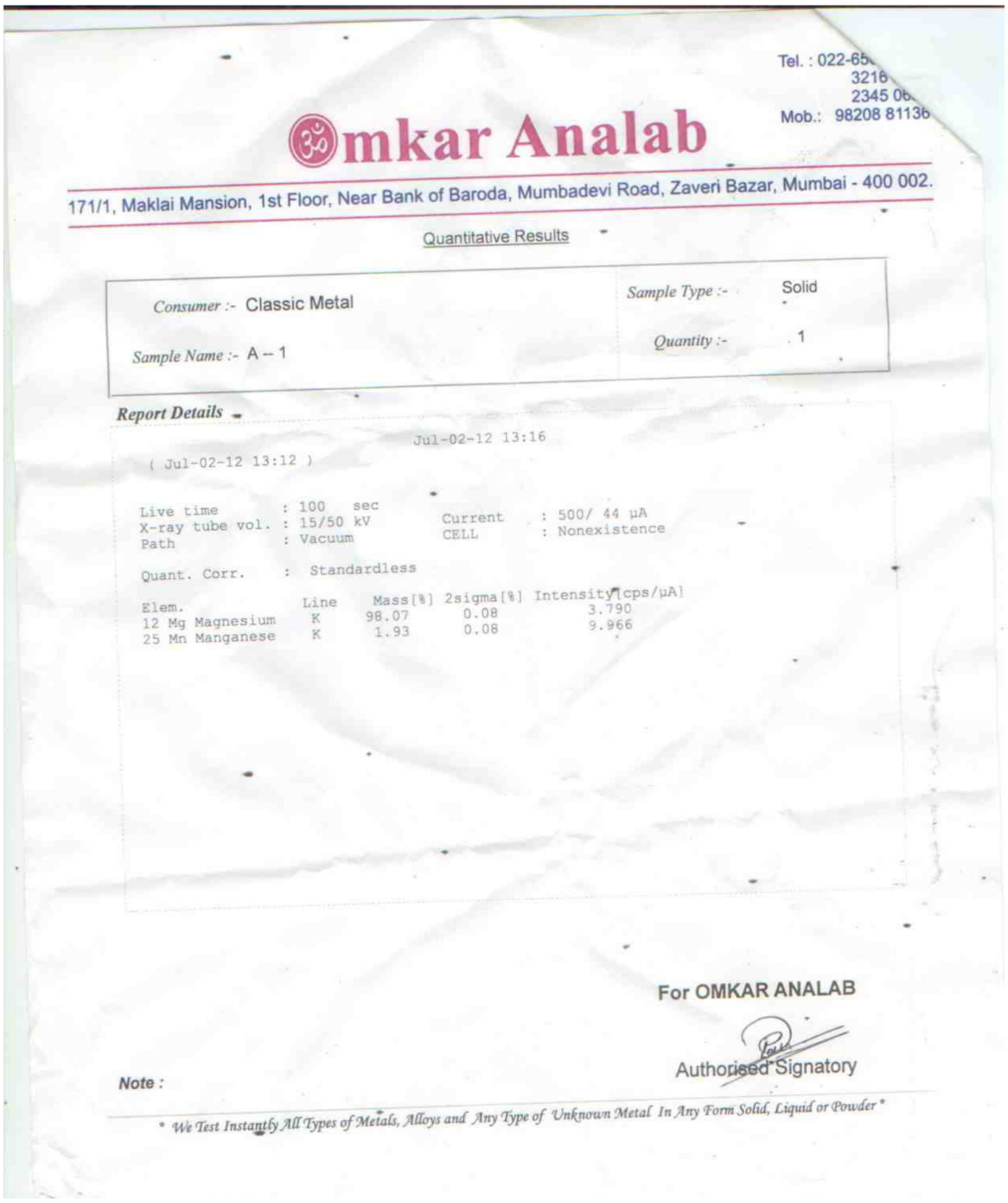

Tel. : 022-65
3216
2345 06
Mob.: 98208 81136

Omkar Analab

171/1, Maklai Mansion, 1st Floor, Near Bank of Baroda, Mumbadevi Road, Zaveri Bazar, Mumbai - 400 002.

Quantitative Results

Consumer :- Classic Metal — *Sample Type :-* Solid

Sample Name :- A – 1 — *Quantity :-* 1

Report Details

Jul-02-12 13:16

(Jul-02-12 13:12)

Live time : 100 sec
X-ray tube vol. : 15/50 kV — Current : 500/ 44 µA
Path : Vacuum — CELL : Nonexistence

Quant. Corr. : Standardless

Elem.	Line	Mass[%]	2sigma[%]	Intensity[cps/µA]
12 Mg Magnesium	K	98.07	0.08	3.790
25 Mn Manganese	K	1.93	0.08	9.966

For OMKAR ANALAB

Authorised Signatory

Note :

** We Test Instantly All Types of Metals, Alloys and Any Type of Unknown Metal In Any Form Solid, Liquid or Powder **

Appendix 3.2

LASER MACHINE SPECIFICATIONS

CO_2 laser machine (Orion 3015 2.5 kW industrial LVD-type) was used in this work. It is a gantry type machine with so-called 'flying optics': The cutting head moves along Y-axis and work table moves along X-axis to define irradiation path. The workpiece is fixed on the work table which has a working area of 2000 × 1000 mm. The movements in X, Y and Z axis is accomplished by the servo motor units, from which the rotary motion is converted into a linear motion by a rack and pinion transmission. The important specifications of the laser machine are given below;

Make	: Orion 3015 from LVD
Type	: GE FANUC HF excited CO_2 laser
Capacity	: 2.5 kW
Wavelength	: 10.6 μm
Sheet size	: 3000 × 1500 mm
Maximum sheet weight	: 570 kg
Axis travel X-axis	: 3080 mm
Axis travel Y-axis	: 1555 mm
Axis travel Z-axis	: 290 mm
Machine dimensions	: Length 7975 mm × Width 2825 mm × Height 2200 mm
Total weight of installation	: 11500 kg
Maximum positioning speed	
X-Y axis	: 100 m/min
Z-axis	: 15 m/min
Repetitive accuracy	: ± 0·02 mm
Positioning accuracy	: ± 0·05 mm/m
Controlling parameters	
CNC control	: GE FANUC 16 iLB with Pentium processor
Software	: CADMAN-L3D
Laser power	: 50 to 2500 W
Output stability	: ± 1% ± 2%
Focal lens	: 5 and 7.5 inches focal length
Duty cycle	: 5 to 100%

Frequency : Continuous wave, Pulsed (1 to 2000)

Laser gas : Composition of He (60%), N_2 (35%) and CO_2 (5%) with 99.99% purity

Laser gas flow rate : 10 liter/hour (for maximum power)

Assisted gas : Oxygen and nitrogen

Appendix 3.3

COORDINATE MEASURING MACHINE SPECIFICATIONS

Make	: Carl –Zeiss
Measuring range (mm)	: 400 × 500 × 350
Overall dimensions (mm)	: 1415 × 1780 × 2470
Resolution (μm)	: 0.5
Maximum velocity (mm/sec)	: 400
Air requirements (kg/cm^2)	: 5.35
Machine weight (kg)	: 1540

Appendix 3.4

EXPERIMENTAL RESULTS OF STRAIGHT LINE SINGLE SCAN LASER BENDING OF MAGNESIUM ALLOY M1A SHEETS

S. No.	*P* (W)	*V* (mm/min)	*D* (mm)	Experimental bend angle (°)				*CV* (%)
				Trial 1	Trial 2	Trial 3	Average	
1	300	1000	3.87	1.007	1.106	1.094	1.069	4.11
2	300	1000	5.81	0.762	0.723	0.708	0.731	3.14
3	300	1000	7.74	0.464	0.519	0.486	0.490	4.60
4	300	2000	3.87	0.881	0.825	0.802	0.836	3.96
5	300	2000	5.81	0.309	0.328	0.300	0.312	3.77
6	300	2000	7.74	0.149	0.108	0.099	0.119	18.09
7	300	3000	3.87	0.629	0.450	0.733	0.604	19.31
8	300	3000	5.81	0.145	0.104	0.167	0.139	18.62
9	300	3000	7.74	0.014	0.031	0.021	*	*
10	400	1000	3.87	1.167	1.327	1.350	1.281	6.37
11	400	1000	5.81	0.719	0.801	0.987	0.836	13.40
12	400	1000	7.74	0.695	0.820	0.800	0.771	7.10
13	400	2000	3.87	1.484	1.209	1.222	1.305	9.69
14	400	2000	5.81	0.802	0.767	0.728	0.766	3.91
15	400	2000	7.74	0.569	0.401	0.340	0.437	22.17
16	400	3000	3.87	0.964	1.263	1.112	1.113	10.99
17	400	3000	5.81	0.482	0.408	0.363	0.418	11.78
18	400	3000	7.74	0.122	0.064	0.135	0.107	28.65
19	500	1000	3.87	0.911	1.088	0.981	0.993	7.31
20	500	1000	5.81	0.956	0.923	0.941	0.940	1.44
21	500	1000	7.74	0.567	0.783	0.908	0.753	18.69
22	500	2000	3.87	1.265	1.736	1.273	1.425	15.45
23	500	2000	5.81	0.923	1.105	0.981	1.003	7.58
24	500	2000	7.74	0.833	0.742	0.589	0.721	13.98
25	500	3000	3.87	1.273	1.162	1.368	1.268	6.63
26	500	3000	5.81	0.659	0.979	0.878	0.838	15.93
27	500	3000	7.74	0.337	0.297	0.400	0.345	12.29

***P*=Laser power, *V*=Scan speed, *D*=Beam diameter, *CV*=Coefficient of variation**

Appendix 3.5

EXPERIMENTAL RESULTS OF MULTI-SCAN LASER BENDING OF MAGNESIUM ALLOY M1A

S. No.	*P* (W)	*V* (mm/min)	*D* (mm)	Experimental bend angle (°)				*CV* (%)
				Trial 1	Trial 2	Trial 3	Average	
1	300	1000	3.87	14.89	12.67	13.17	13.58	7.01
2	300	1000	5.81	12.05	10.87	11.54	11.49	4.22
3	300	1000	7.74	8.97	9.14	9.09	9.07	0.81
4	300	2000	3.87	10.60	10.98	11.09	10.89	1.94
5	300	2000	5.81	5.99	7.90	7.29	7.06	11.28
6	300	2000	7.74	3.81	3.05	3.74	3.54	9.69
7	300	3000	3.87	6.93	8.27	7.99	7.73	7.47
8	300	3000	5.81	2.90	3.00	3.14	3.01	3.19
9	300	3000	7.74	0.79	0.89	0.92	0.86	6.56
10	400	1000	3.87	11.64	12.29	11.77	11.90	2.37
11	400	1000	5.81	10.21	10.71	10.56	10.49	1.99
12	400	1000	7.74	9.42	9.20	9.35	9.33	0.99
13	400	2000	3.87	14.43	14.56	14.48	14.49	0.37
14	400	2000	5.81	11.47	12.41	12.01	11.96	3.22
15	400	2000	7.74	6.77	9.25	8.98	8.33	13.33
16	400	3000	3.87	12.09	13.47	12.87	12.81	4.44
17	400	3000	5.81	8.50	6.04	8.54	7.69	15.17
18	400	3000	7.74	2.66	3.82	4.03	3.50	17.28
19	500	1000	3.87	7.96	7.52	7.90	7.79	2.49
20	500	1000	5.81	8.84	8.94	8.81	8.86	0.65
21	500	1000	7.74	9.25	8.60	8.65	8.83	3.38
22	500	2000	3.87	15.15	15.52	15.50	15.39	1.11
23	500	2000	5.81	13.33	13.47	13.46	13.42	0.47
24	500	2000	7.74	11.05	12.20	11.09	11.45	4.66
25	500	3000	3.87	15.50	14.94	15.30	15.25	1.53
26	500	3000	5.81	11.14	13.27	12.19	12.20	7.12
27	500	3000	7.74	6.72	9.25	8.92	8.30	13.53

***P*=Laser power, *V*=Scan speed, *D*=Beam diameter, *CV*=Coefficient of variation**

Appendix 4.1

FORTRAN CODE TO DEFINE LASER INPUT PARAMETERS, BEAM SHAPE, HEAT FLUX DISTRIBUTION, SCANNING PATH AND NUMBER OF SCANS

Subroutine For Single Scan and Multi-Scan Laser Bending Process

```
      SUBROUTINE DFLUX(FLUX,SOL,KSTEP,KINC,TIME,NOEL,NPT,COORDS,
     1 JLTYP,TEMP,PRESS,SNAME)

       INCLUDE 'ABA_PARAM.INC'

        DIMENSION FLUX(2), TIME(2), COORDS(3)
         CHARACTER*80 SNAME
         integer rem
          real x,y,xa,ya,xc,yc,r,pi
          real Power,Velocity,Height,Absorption,CoolingTime,TotalTime
          real BeamRadius,Mean,Gaussian
          real Length,Width,Thickness
          real FocalLength,MSquare,RadiusLens,BeamWaist,Wavelength

!~~~~~~~~~~~~~~~~~~     INITIALIZATION  ~~~~~~~~~~~~~~~~~~~~~~~~

!       #### sheet dimensions in mm ####
          Length=60
          Width=40
          Thickness=1.9

!  ##### Laser Bending Energy Parameters in mm, mm/sec, mW and sec #####
          Height=20                %stand-off distance
          Velocity=1000/60         %scan speed
          Power=1000*300           %laser power
          Absorption=0.80          %absorptivity
          CoolingTime=5            %idle time between two scans

!         #### Laser beam/machine parameters ####
             Wavelength=0.0106     %wavelength of CO2 laser beam
             Focallength=127       %focal length of lens
             MSquare=1.4
             RadiusLens=12         %beam radius before lens
!
!~~~~~~~~~~~~~ Formulation for laser beam spot radius (Ra) ~~~~~~~~~~~~
!
!    #### Beam Waist and Beam Radius in mm ####
!
       BeamWaist=(MSquare*Wavelength*FocalLength)/(pi*RadiusLens)

       BeamRadius=BeamWaist*(sqrt(1+(((MSquare*Wavelength*Height)
     1          /(pi*(BeamWaist**2)))**2)))
!
! Formulations for Circular Beam, Moving Flux and Multi-scan Scanning
!
!     #### Total time in one scan (scanning time + cooling time) ####
      TotalTime=((Width+(2*BeamRadius))/Velocity)+CoolingTime
!
```

```
!~~~~~~~ Fomulation for Multi-scan and y-coordinate moving ~~~~~~~~~
!
                    rem=TIME(1)/TotalTime
!
!     ### Moving y-coordinate relation for multi-scan ####
        y=-(Width+(2*BeamRadius))/2+((TIME(1)-rem*TotalTime)*Velocity)
!
!     #### instantaneous coordinate values ####
       yc=y-COORDS(2)
       xc=COORDS(1)
!
!~~~~~~~~~~~~~~~~ Shape of Laser Beam (Circular) ~~~~~~~~~~~~~~~~~~
                     r=sqrt(xc**2 + yc**2)
!
!~~~~~~~~~~~~~~  Formulation for Distributions of Heat Flux  ~~~~~~~~~~~~~~~

!           ### uniform ###
            Mean=Absorption*Power/(pi*(BeamRadius**2))
!           ### Gaussian ###
            Gaussian=2*Mean*exp(-2*(r**2)/BeamRadius**2)
!
!~~~~~~~~~~~~     FLUX Implimentation ~~~~~~~~~~~~~~~~~~~~
             if(r.LE.BeamRadius) then
             FLUX(1)=Gaussian
             end if
             FLUX(2)=0
             RETURN

             END
```

Subroutine For Curvilinear Laser Bending Process

```
      SUBROUTINE DFLUX(FLUX,SOL,KSTEP,KINC,TIME,NOEL,NPT,COORDS,
     1  JLTYP,TEMP,PRESS,SNAME)

       INCLUDE 'ABA_PARAM.INC'

         DIMENSION FLUX(2), TIME(2), COORDS(3)
          CHARACTER*80 SNAME
          integer rem
          real x, y, xc, yc, Ra, r, q, G, K, P, D, TP, Height, H, W, Rb,
          real L, theta, theta1, ST, N,Length,Width,Thickness,v,CT,pi
```

```
% Definition of sheet parameters, laser parameters, beam diameter
calculation are given above. The method to irradiate along a circular arc
is given below

W=Width+(2*Ra)          %Arc Width or Straight line scanning length
Rb=(H/2)+(W**2/(8*H))   %Arc radius
theta=ASIN(W/(2*Rb))
L=2*theta*Rb            %Scanning arc length
ST=L/v                  %Scanning time
TP=ST+CT                %Total time one scan including cooling
theta1=(pi/2-theta)+(2*theta*time(1)/ST)
rem=time(1)/TP
x=Rb*sin(theta1)-(Rb-H)       %Moving x coordinate relation
y=Rb*cos(theta1)              %moving y coordinate relation
yc=y-coords(2)                %y instantaneous value
```

```
xc=x-coords(1)                  %x instantaneous value
r=sqrt(xc**2 + yc**2)           %circular beam definition

### uniform ###
      Mean=Absorption*Power/(pi*(BeamRadius**2))
      ### Gaussian ###
      Gaussian=2*Mean*exp(-2*(r**2)/BeamRadius**2)

!~~~~~~~~~~~~~     FLUX Implimentation ~~~~~~~~~~~~~~~~~~~~
       if(r.LE.BeamRadius) then
       FLUX(1)=Gaussian
       end if
       FLUX(2)=0
       RETURN

       END
```

Appendix 6.1

BENDING OFFSET FOR ALL SETS OF PROCESS CONDITIONS DURING CURVILINEAR LASER BENDING PROCESS

S. No.	*P*	*V*	*D*	Bending offset at			
				Scan start	Scan end	Scan start	Scan end
				Arc height=10 mm		Arc height=20 mm	
1	300	1000	20	3	4	9.5	11
2	300	1000	30	3.5	4.5	11	11
3	300	1000	40	5	6	12	11
4	300	2000	20	2	3	9.5	9
5	300	2000	30	4	3.5	11.5	11
6	300	2000	40	8	8	12	11
7	300	3000	20	2.5	2	9	8
8	300	3000	30	6.5	6	11.5	11
9	300	3000	40	7.5	7	12	11
10	400	1000	20	2.5	3.5	8.5	11
11	400	1000	30	3	4.5	9.5	12
12	400	1000	40	4	5	12	13
13	400	2000	20	2	3.5	8.5	10
14	400	2000	30	4	4.5	10	11
15	400	2000	40	4.5	6	12	12.5
16	400	3000	20	2	2.5	8.5	9.5
17	400	3000	30	3	3	11	9.5
18	400	3000	40	5	5.5	11	12.5
19	500	1000	20	2.5	3.5	7.5	10.5
20	500	1000	30	3.5	4.5	9.5	11.5
21	500	1000	40	4	5.5	11	12.5
22	500	2000	20	2.5	3.5	8.5	10.5
23	500	2000	30	3	4	9.5	11
24	500	2000	40	4	4.5	10.5	11.5
25	500	3000	20	2	2	8.5	9.5
26	500	3000	30	3	3	9.5	9.5
27	500	3000	40	5	3.5	10	11

Appendix 7.1

VARIATION IN BEND ANGLE FOR VARIOUS SETS OF PROCESS CONDITION DURING MULTI-SCAN LASER BENDING OF MAGNESIUM ALLOY M1A

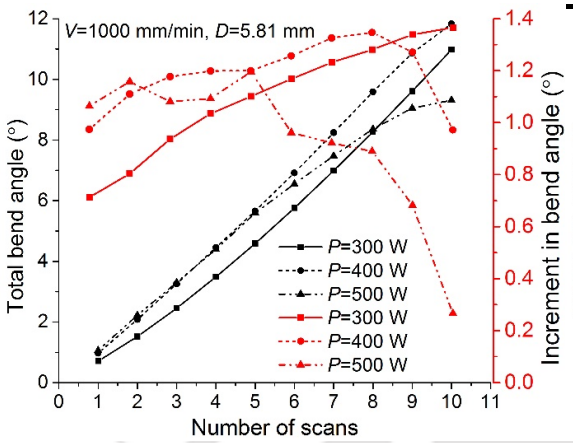

Variation in bend angle with number of scans at slow scan speed and medium beam diameter

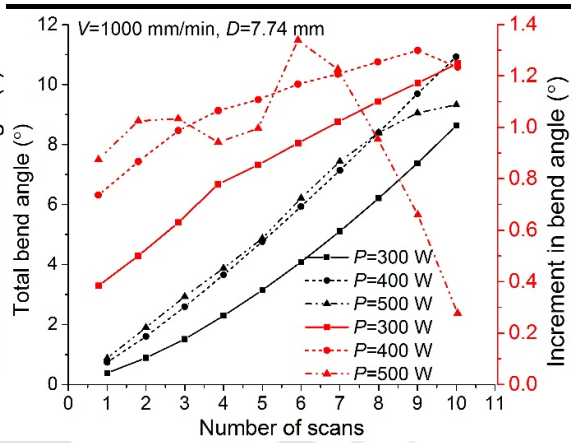

Variation in bend angle with number of scans at slow scan speed and large beam diameter

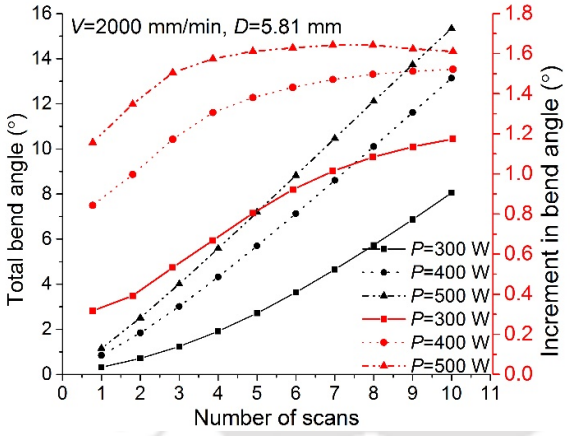

Variation in bend angle with number of scans at medium scan speed and medium beam diameter

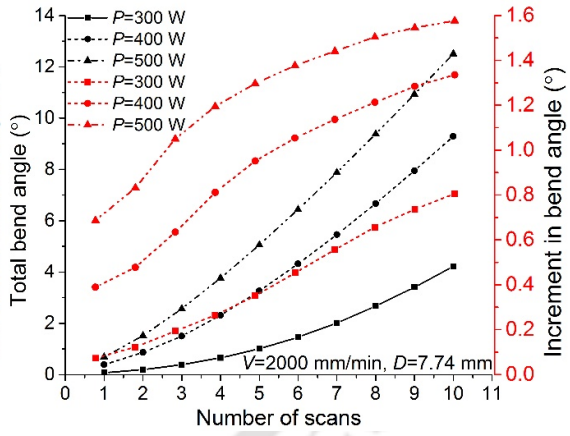

Variation in bend angle with number of scans at medium scan speed and large beam diameter

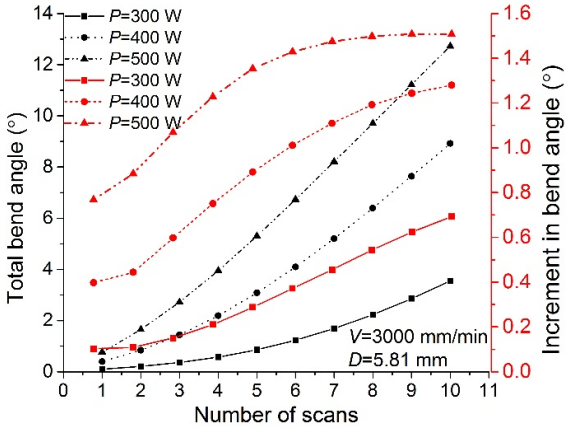

Variation in bend angle with number of scans at fast scan speed and medium beam diameter

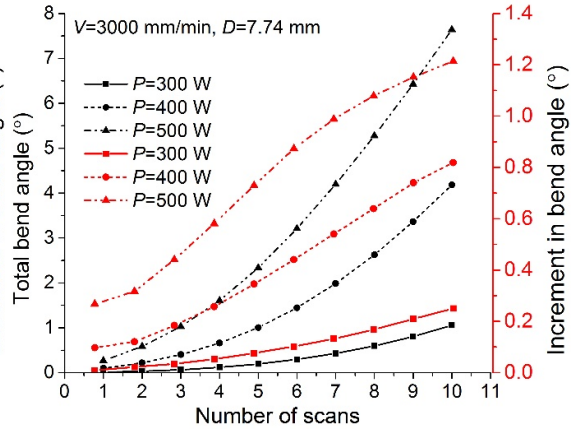

Variation in bend angle with number of scans at fast scan speed and large beam diameter

Appendix 7.2

RVBA VALUES FOR VARIOUS SETS OF PROCESS CONDITION DURING MULTI-SCAN LASER BENDING OF MAGNESIUM ALLOY M1A

S. No.	*P*	*V*	*D*	*RVBA* in during each scan (multiplied by 100)									
				Number of laser scans									
				1	2	3	4	5	6	7	8	9	10
1	300	1000	3.87	0.293	0.142	0.080	0.071	0.059	0.054	0.048	0.043	0.037	0.030
2	400	1000	3.87	0.173	0.064	0.059	0.072	0.078	0.081	0.083	0.077	0.082	0.072
3	500	1000	3.87	0.083	0.044	0.102	0.139	0.166	0.183	0.209	0.184	0.140	0.097
4	300	2000	3.87	0.362	0.203	0.127	0.094	0.072	0.065	0.059	0.056	0.054	0.051
5	400	2000	3.87	0.264	0.137	0.087	0.078	0.069	0.066	0.062	0.058	0.054	0.051
6	500	2000	3.87	0.207	0.103	0.085	0.078	0.075	0.072	0.069	0.065	0.063	0.060
7	300	3000	3.87	0.431	0.246	0.160	0.103	0.063	0.038	0.030	0.029	0.031	0.033
8	400	3000	3.87	0.313	0.157	0.088	0.064	0.056	0.053	0.051	0.050	0.028	0.045
9	500	3000	3.87	0.254	0.122	0.082	0.070	0.064	0.061	0.057	0.054	0.050	0.046
10	300	1000	5.81	0.390	0.208	0.115	0.079	0.070	0.064	0.061	0.059	0.056	0.038
11	400	1000	5.81	0.240	0.091	0.069	0.070	0.068	0.073	0.073	0.072	0.070	0.054
12	500	1000	5.81	0.130	0.055	0.087	0.114	0.141	0.154	0.161	0.164	0.139	0.080
13	300	2000	5.81	0.598	0.343	0.198	0.108	0.064	0.055	0.061	0.064	0.064	0.061
14	400	2000	5.81	0.346	0.169	0.094	0.067	0.058	0.052	0.048	0.044	0.041	0.038
15	500	2000	5.81	0.291	0.139	0.098	0.092	0.088	0.083	0.079	0.074	0.070	0.064
16	300	3000	5.81	0.873	0.707	0.500	0.353	0.246	0.153	0.095	0.053	0.024	0.024
17	400	3000	5.81	0.535	0.288	0.161	0.076	0.026	0.027	0.042	0.050	0.054	0.054
18	500	3000	5.81	0.395	0.162	0.072	0.052	0.059	0.065	0.066	0.065	0.063	0.060
19	300	1000	7.74	0.490	0.271	0.150	0.085	0.073	0.071	0.071	0.070	0.068	0.064
20	400	1000	7.74	0.313	0.123	0.080	0.078	0.081	0.083	0.082	0.079	0.076	0.073
21	500	1000	7.74	0.190	0.071	0.094	0.122	0.156	0.173	0.181	0.173	0.149	0.090
22	300	2000	7.74	0.977	0.649	0.424	0.258	0.137	0.047	0.020	0.042	0.053	0.056
23	400	2000	7.74	0.513	0.236	0.111	0.064	0.074	0.079	0.080	0.079	0.077	0.073
24	500	2000	7.74	0.354	0.150	0.090	0.093	0.093	0.092	0.091	0.089	0.085	0.079
25	300	3000	7.74	1.103	1.017	0.872	0.746	0.556	0.432	0.330	0.245	0.181	0.132
26	400	3000	7.74	0.928	0.606	0.400	0.251	0.147	0.074	0.031	0.043	0.055	0.060
27	500	3000	7.74	0.623	0.329	0.165	0.060	0.008	0.043	0.058	0.064	0.068	0.068

Effect of the number of scans on edge effect at *D*=5.81 mm, and *D*=7.74 mm

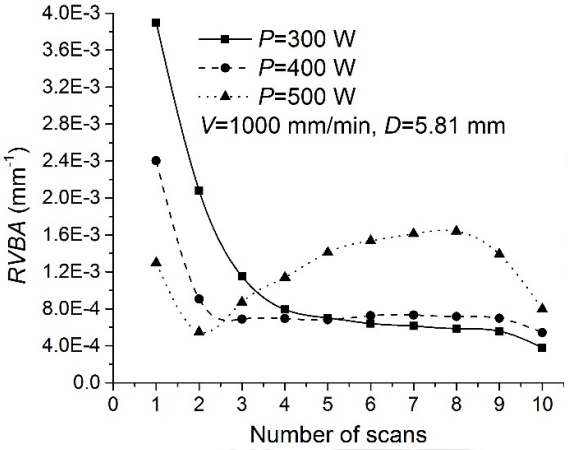

Effect of number of scans on edge effect at slow scan speed and medium beam diameter

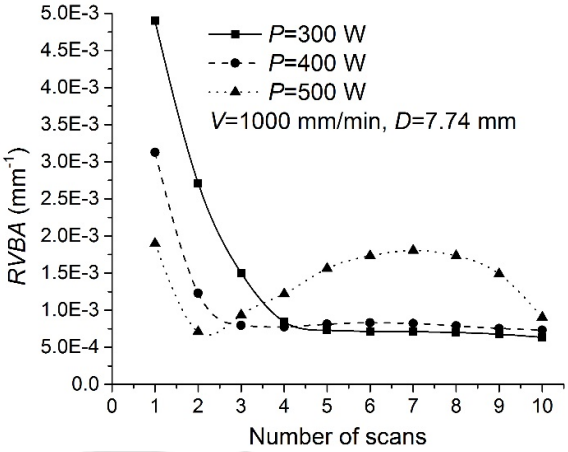

Effect of number of scans on edge effect at slow scan speed and large beam diameter

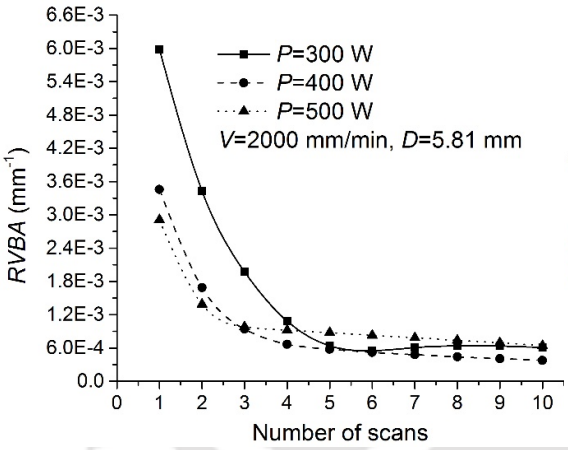

Effect of number of scans on edge effect at medium scan speed and medium beam diameter

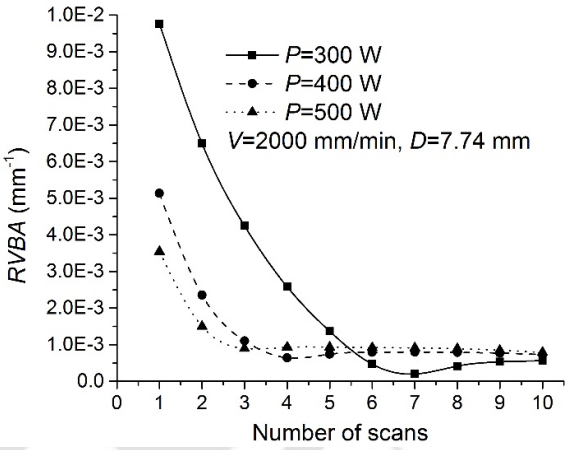

Effect of number of scans on edge effect at medium scan speed and large beam diameter

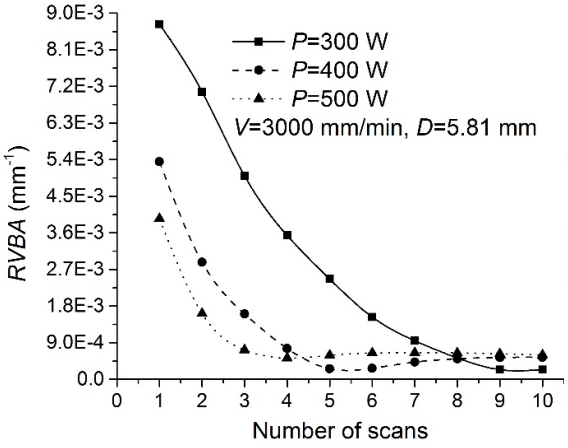

Effect of number of scans on edge effect at fast scan speed and medium beam diameter

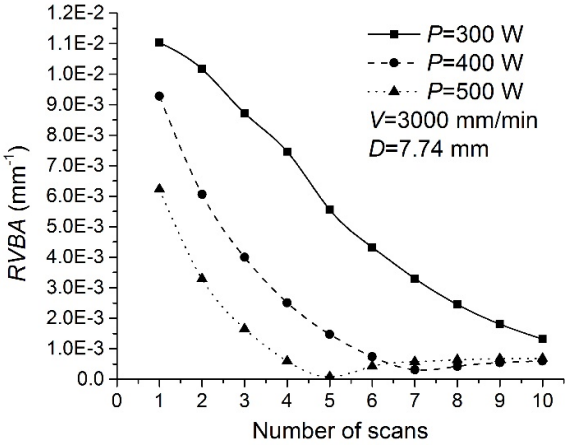

Effect of number of scans on edge effect at fast scan speed and large beam diameter

Appendix 8.1

PART DRAWINGS OF THE MOVING PRE-DISPLACEMENT SETUP

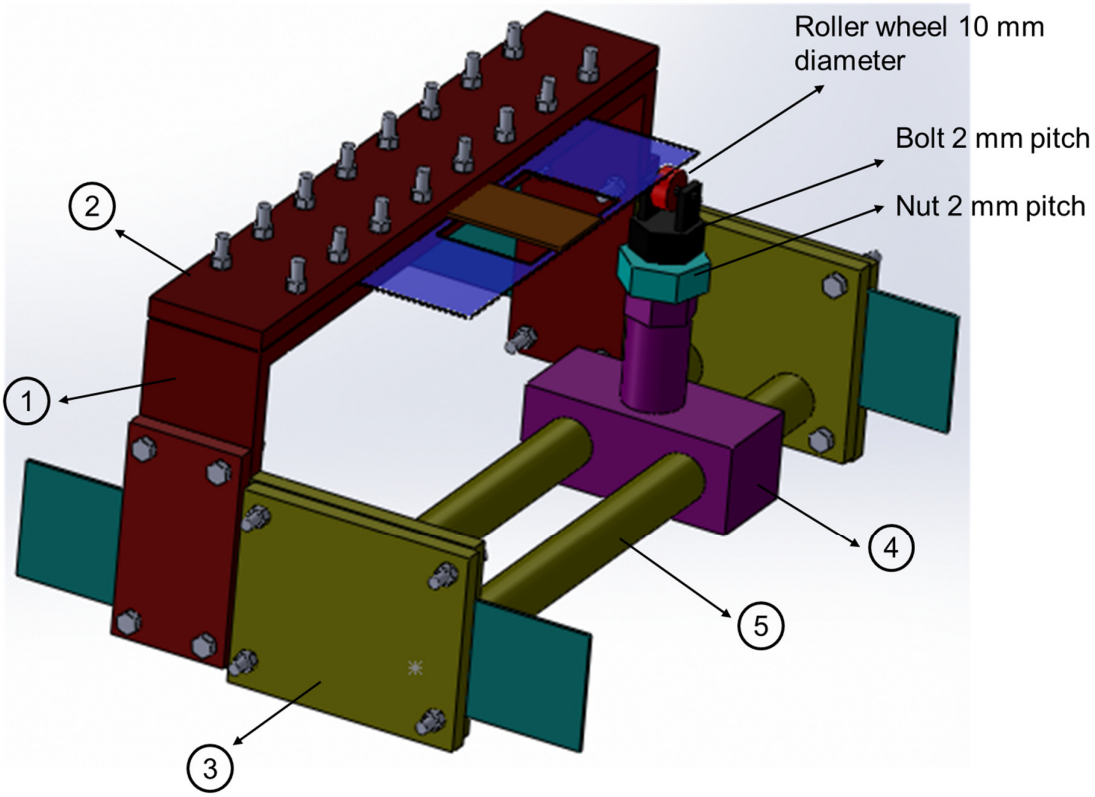

All dimensions are in mm

1. Sheet Clamping Base

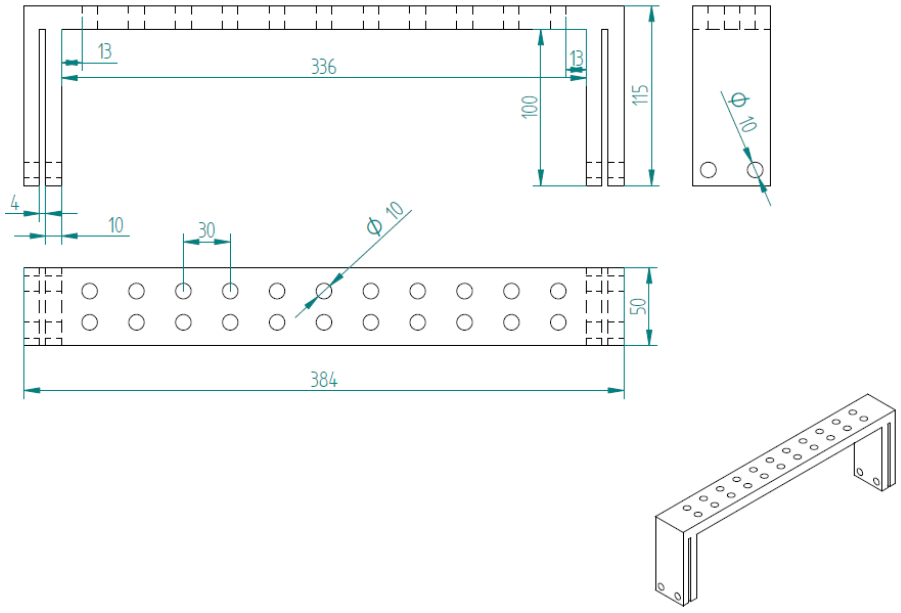

2. **Sheet Clamping and Tightening Plate**

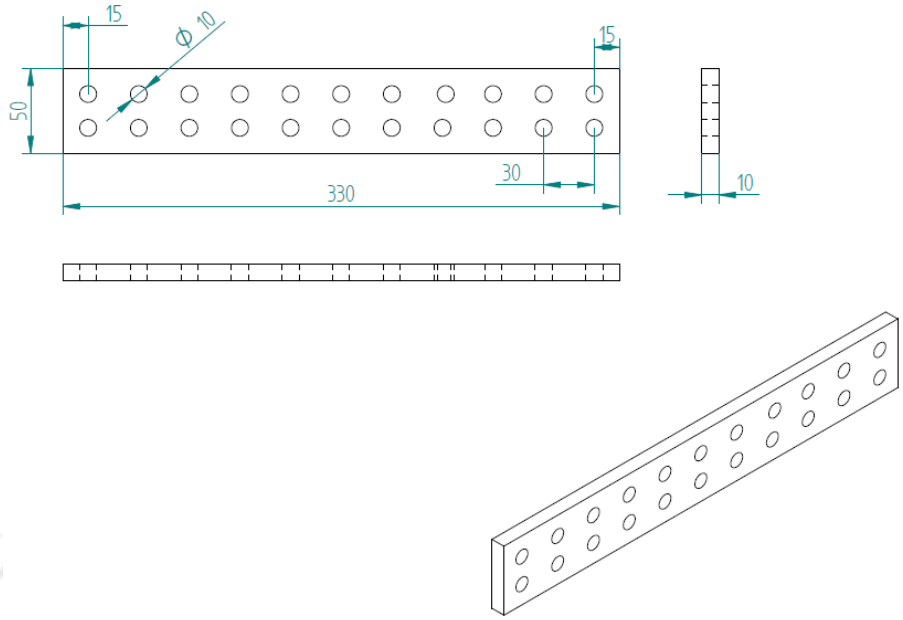

3. **Moving Pre-displacement Tightening Plate**

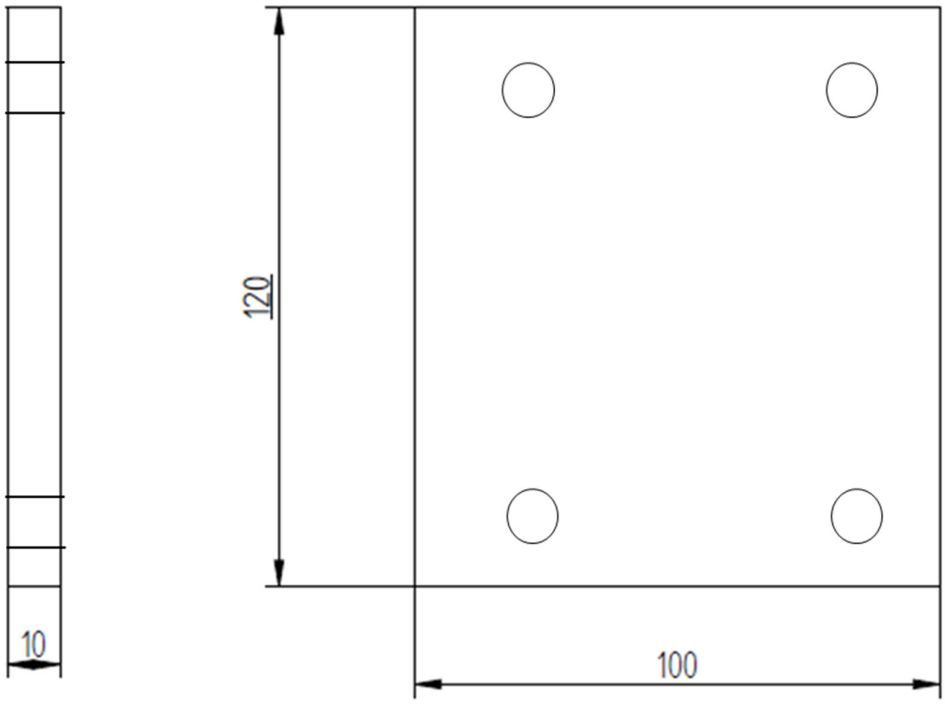

4. Fixed Block

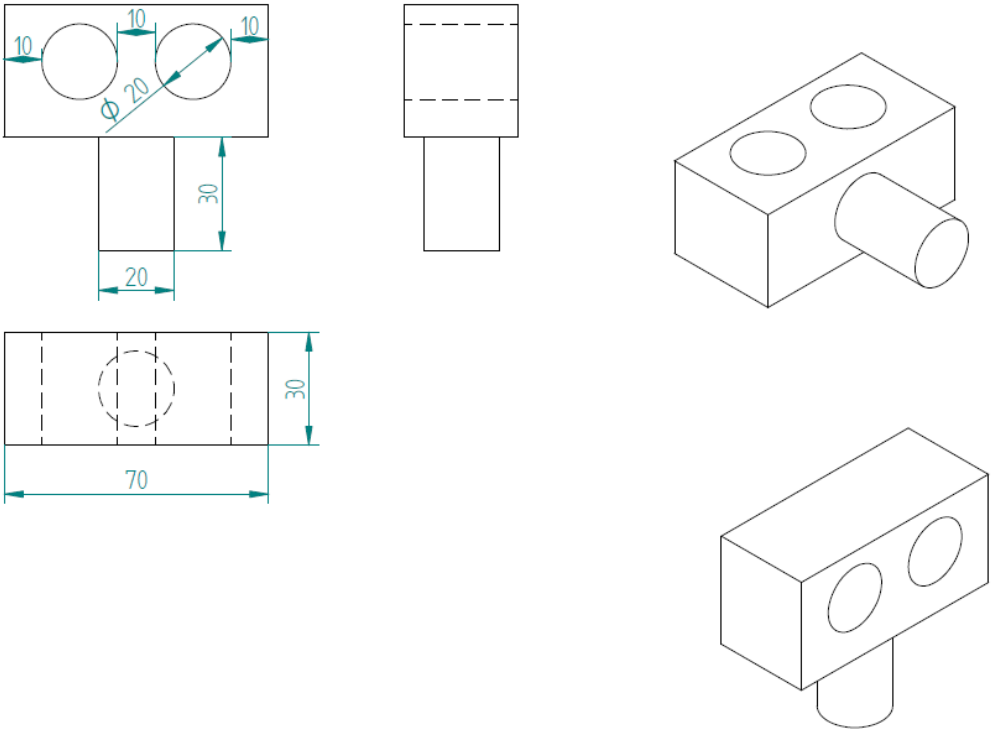

5. Sliding Rods

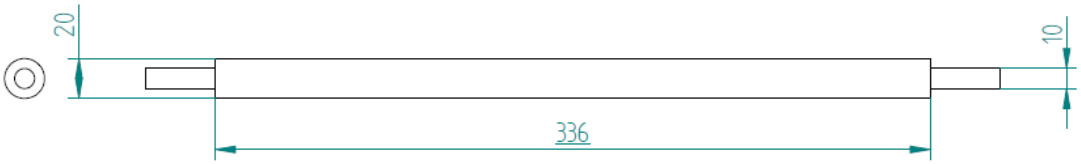

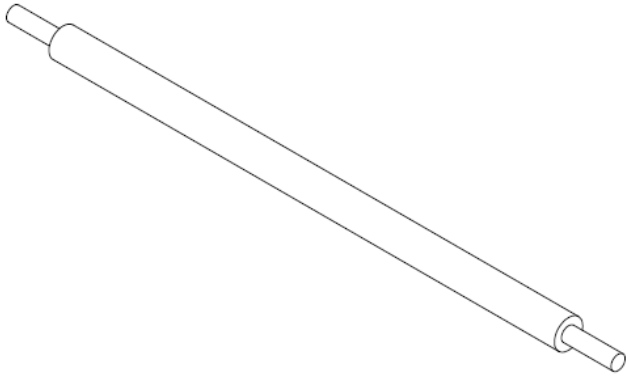

Appendix 8.2

EFFECT OF LASER PROCESS PARAMETERS ON BEND ANGLE

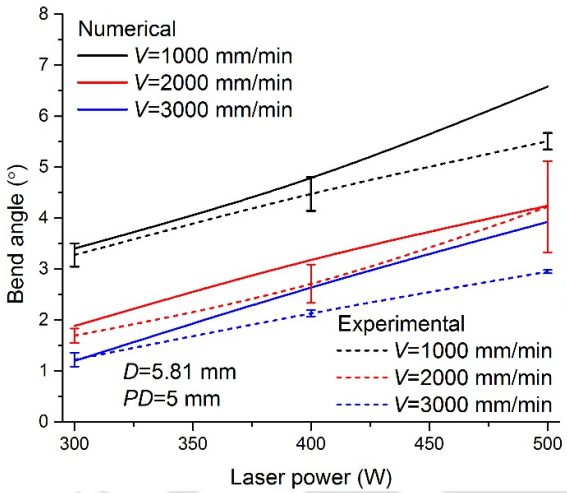

Effect of laser power on bend angle for laser assisted bending with moving pre-displacement at D=5.81 mm.

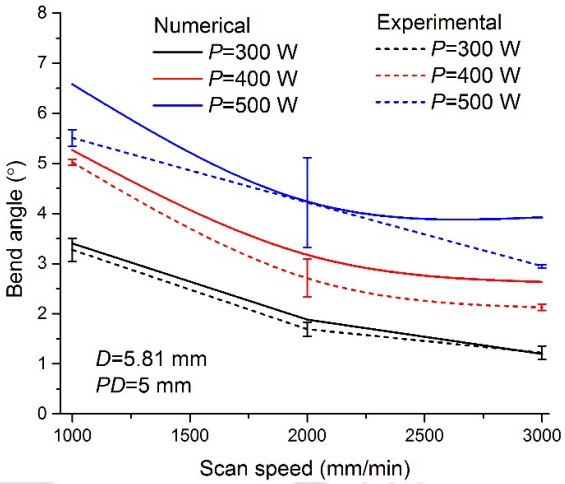

Effect of scan speed on bend angle for laser assisted bending with moving pre-displacement at D=5.81 mm.

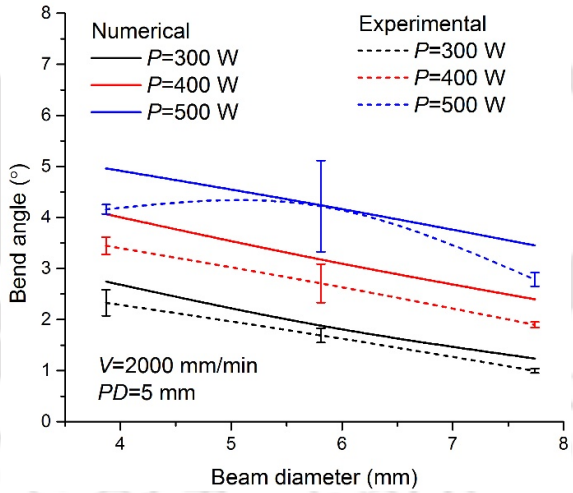

Effect of beam diameter on bend angle for laser assisted bending with moving pre-displacement at V=2000 mm/min.

Appendix 8.3

EFFECT OF PRE-DISPLACEMENT ON BEND ANGLE

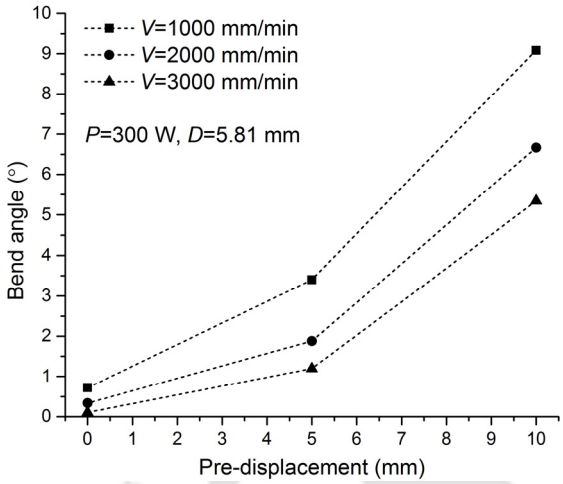

Effect of pre-displacement on bend angle at P=300 W and D=5.81 mm.

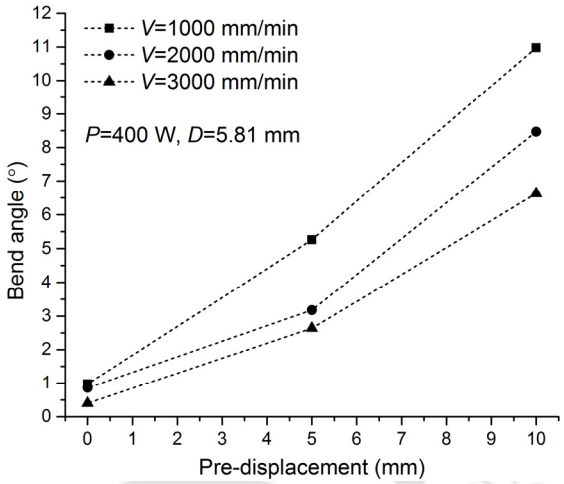

Effect of pre-displacement on bend angle at P=400 W and D=5.81 mm.

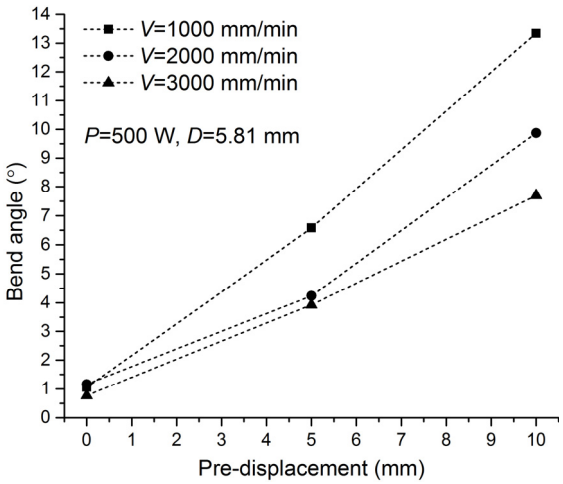

Effect of pre-displacement on bend angle at P=500 W and D=5.81 mm.

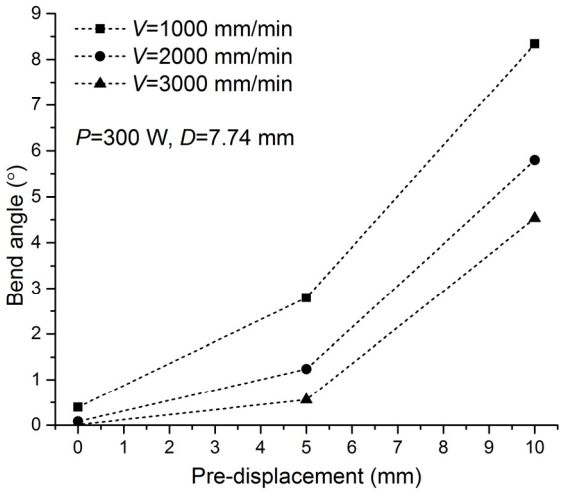

Effect of pre-displacement on bend angle at P=300 W and D=7.74 mm.

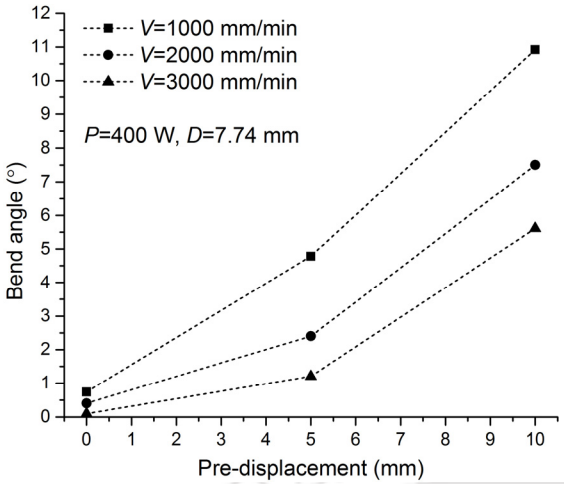

Effect of pre-displacement on bend angle at *P*=400 W and *D*=7.74 mm.

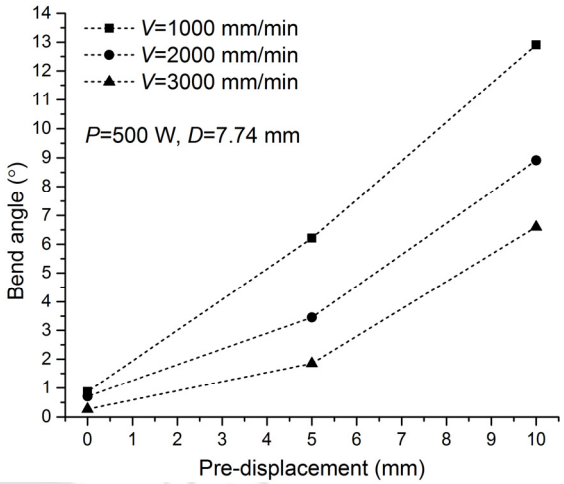

Effect of pre-displacement on bend angle at *P*=500 W and *D*=7.74 mm.

Appendix 8.4

EFFECT OF PRE-DISPLACEMENT ON SPRING-BACK ANGLE

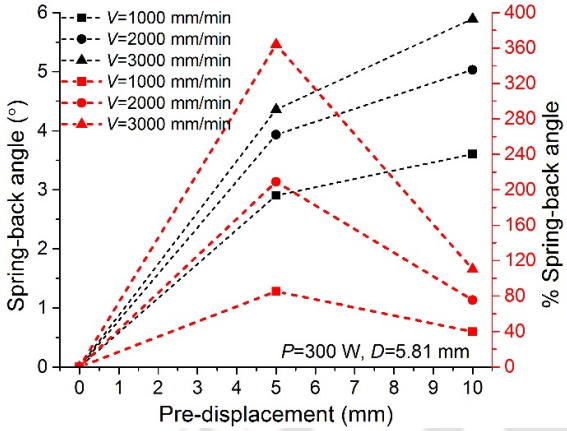

Effect of pre-displacement on spring-back effect at P=300 W and D=5.81 mm.

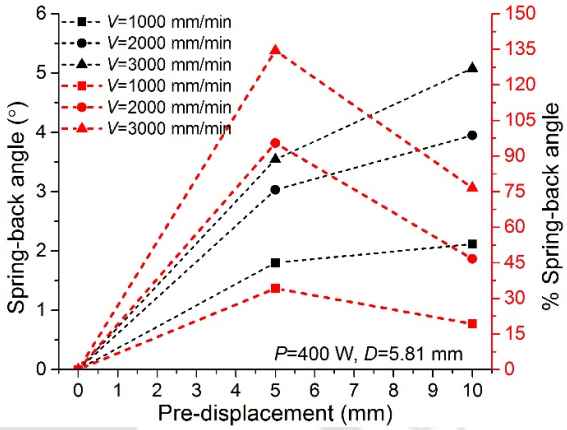

Effect of pre-displacement on spring-back effect at P=400 W and D=5.81 mm.

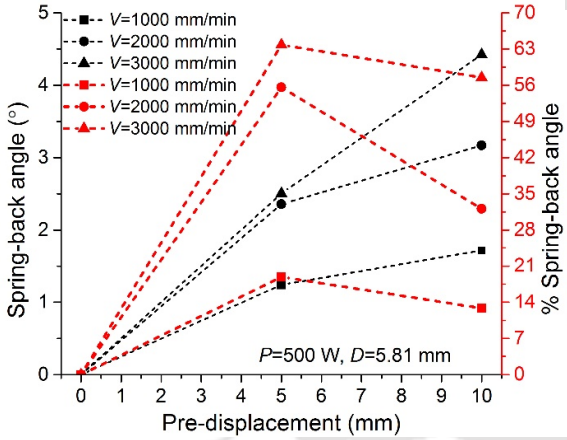

Effect of pre-displacement on spring-back effect at P=500 W and D=5.81 mm.

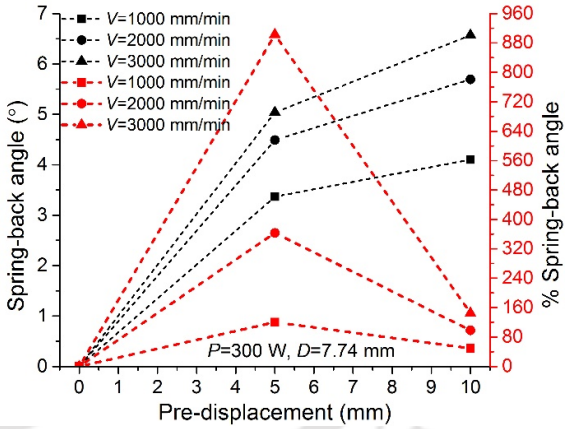

Effect of pre-displacement on spring-back effect at P=300 W and D=7.74 mm.

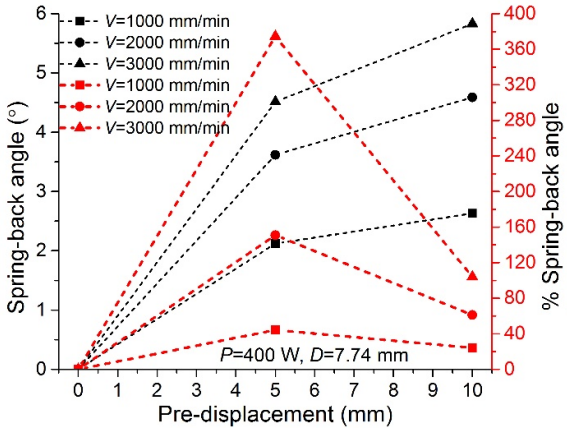

Effect of pre-displacement on spring-back effect at P=400 W and D=7.74 mm.

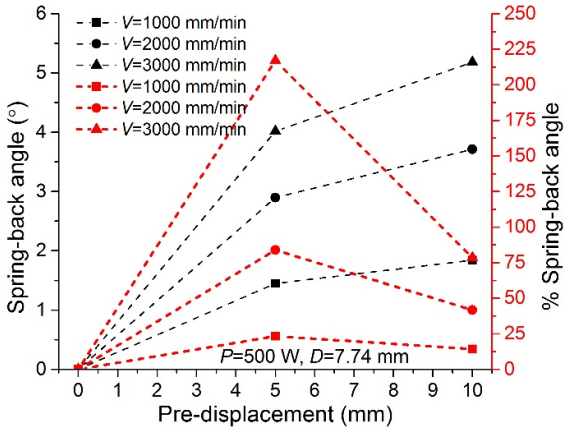

Effect of pre-displacement on spring-back effect at P=500 W and D=7.74 mm.

Appendix 8.5

EFFECT OF PRE-DISPLACEMENT ON EDGE EFFECT

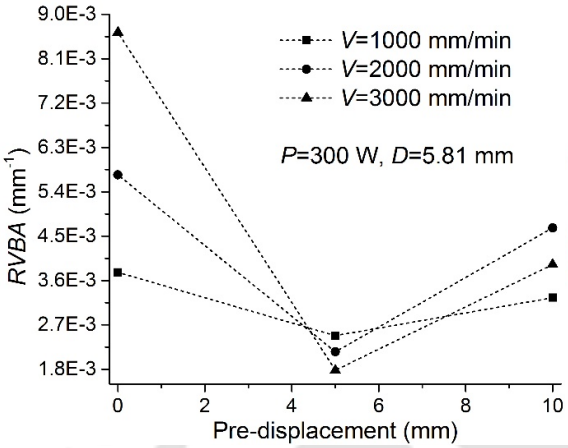

Effect of pre-displacement on edge effect at P=300 W and D=5.81 mm.

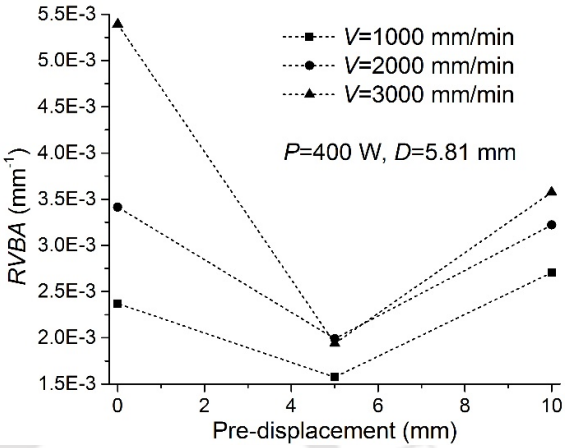

Effect of pre-displacement on edge effect at P=400 W and D=5.81 mm.

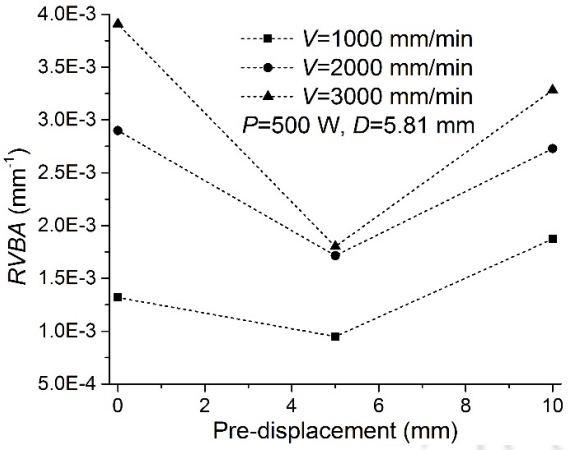

Effect of pre-displacement on edge effect at P=500 W and D=5.81 mm.

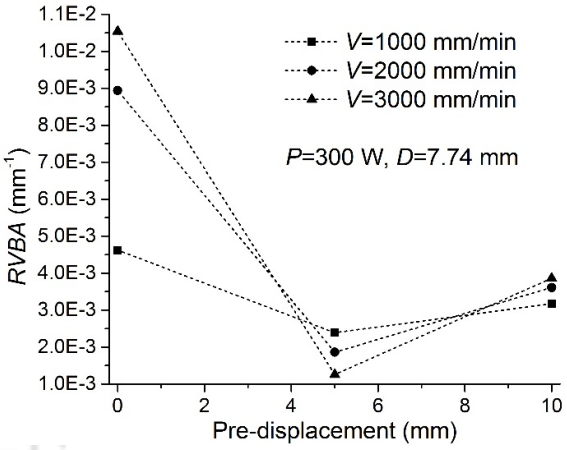

Effect of pre-displacement on edge effect at P=300 W and D=7.74 mm.

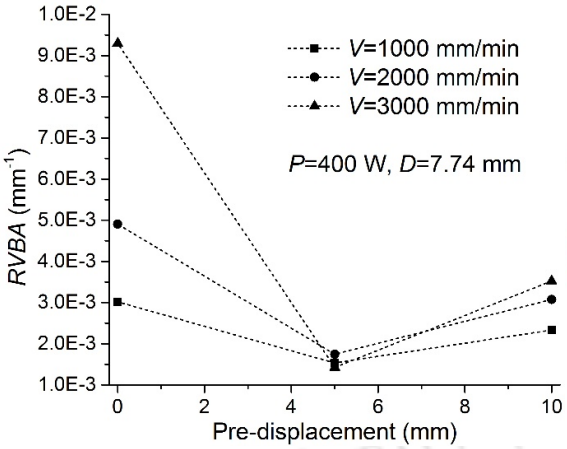

Effect of pre-displacement on edge effect at P=400 W and D=7.74 mm.

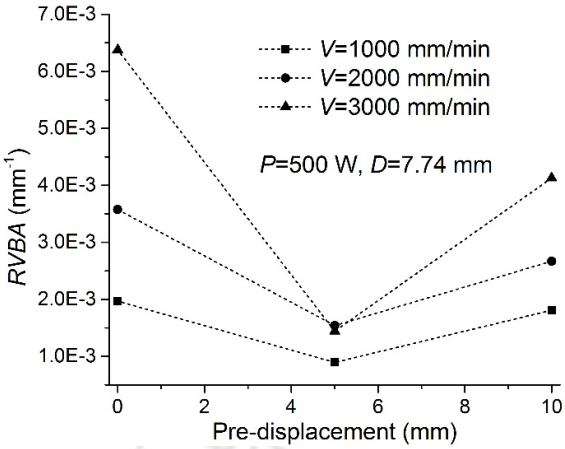

Effect of pre-displacement on edge effect at P=500 W and D=7.74 mm.

LIST OF PUBLICATIONS

Book Chapters

1. Ravi Kant, S. N. Joshi and U. S. Dixit, 2015 "Research issues in the laser sheet bending process" in "Materials Forming And Machining" edited by Paulo J. Devim, Chapter 4, (*Woodhead/Elsevier*, UK)
2. Ravi Kant, P. M. Bhuyan and S. N. Joshi, 2015 "Experimental studies on TGM and BM dominated curvilinear laser bending of aluminum alloy sheets" in "Lasers Based Manufacturing" edited by Shrikrishna N. Joshi and Uday S. Dixit, Chapter 5, pp. 69–91, (*Springer*, India).

Published Research Papers in International Journals

1. Ravi Kant and S. N. Joshi "Numerical and experimental studies on laser bending of magnesium M1A alloy" (In Press, *Lasers in Engineering*)
2. U. S. Dixit, S. N. Joshi and Ravi Kant "Research on laser forming system: A review" *International Journal of Mechatronics and Manufacturing Systems*, Vol. 8, No. (3/4), pp. 160-205, 2015
3. Ravi Kant, S. N. Joshi and U. S. Dixit "An Integrated FEM-ANN model for laser bending process with inverse estimation of absorptivity" *Mechanics of Advanced Materials and Modern Processes*, Vol. 1, p. 6, 2015.
4. Ravi Kant and S. N. Joshi "Numerical Modeling and Experimental Validation of Curvilinear Laser Bending of Magnesium Alloy Sheets" *Proceedings of the Institute of Mechanical Engineering Part B*: *Journal of Engineering Manufacture*, Vol. 228, No. 9, pp. 1036–1047, 2014
5. Ravi Kant and S. N. Joshi "Finite Element Simulation of Laser Assisted Bending with Moving Mechanical Load" *International Journal of Mechatronics and Manufacturing Systems*, Vol. 6, No. 4, pp. 351–366, 2013.

Communicated / To Be Submitted Research Papers in International Journals

1. Ravi Kant and S. N. Joshi "Thermo-mechanical studies on bending mechanism, bend angle and edge effect during multi-scan laser bending of Magnesium M1A Alloy Sheets" (Submitted, *Journal of Manufacturing Processes*, Elsevier)
2. Ravi Kant and S. N. Joshi "Finite element analysis of curvilinear laser bending process: Effect of scanning path curvature" (Submitted, *Journal of Manufacturing Science and Technology*, Springer)

3. Ravi Kant and S. N. Joshi "Enhancement in productivity and product quality during laser based bending using a moving pre-displacement method" (To be submitted, *Journal of Manufacturing Processes*, Elsevier)

Research Papers in National/International Conferences

1. Ravi Kant and S.N. Joshi "Experimental Studies on Laser Bending of Magnesium M1A Alloy Sheets" In: Proceeding of the 3rd International Conference on Laser and Plasma Applications in Materials Science LAPAMS 2015 held at Lake Land Country Club, Kolkata during Jan. 15–17, pp. 135–138, 2015 (Presented in person)
2. Ravi Kant and S. N. Joshi "Finite Element Simulation of Multi-pass Laser Bending Process with Forced Cooling" In: Proceedings of the 8th International Conference COPEN 2013 held at NIT Calicut during Dec. 13–15, pp. 772 – 777, 2013 (Presented by Co-Author)
3. Ravi Kant and S. N. Joshi "Numerical Simulation of Multi-pass Laser Bending Processes using Finite Element Method" In: Proceedings of the 2nd International Conference IRAM 2013 held at IIT Indore during Dec. 16–18, pp. 208 – 213, 2013 (Presented in person)
4. Ravi Kant, S. N. Joshi and U. S. Dixit "State of the Art and Experimental Investigation on Edge Effect in Laser Bending Process" In: Proceedings of the National Conference NCRAME 2013 held at NERIST, Itanagar during Nov. 8–9, pp. 189–197, 2013 (Presented in person)
5. Ravi Kant, S. N. Joshi and U. S. Dixit "Experimental Studies on Laser Bending of Magnesium M1A Alloy Sheet" In: Proceedings of the National Conference MVF 2013 held at IIT Guwahati during Oct. 12–13, pp. 189–197, 2013 (Presented in person)
6. S. N. Joshi and Ravi Kant "Finite Element Simulation of Laser Micro-Bending of Magnesium M1A Alloy" In: Proceedings of the International Conference APM–2013 held at CIPET Lucknow during March 1–3, 2013 (Presented by Co-Author)
7. Ravi Kant and S. N. Joshi "Thermo-mechanical analysis of curvilinear laser bending of magnesium alloy sheet using finite element method" In: Proceedings of the 4th International & 25th AIMTDR Conference held at Jadavpur University, Kolkata during Dec. 14–16, vol. 1, 109–114, 2012 (Presented in person)
8. Ravi Kant, S. N. Joshi and U. S. Dixit "Finite Element Analysis of Laser Bending Process" Asian Academic Seminar held at IIT Bombay during December 3–8, 2012 (Presented in person)
9. Ravi Kant and S. N. Joshi "Numerical simulation of laser bending of magnesium alloy AZ31B using FEM" In: Proceedings of the international Conference IDDRG 2012 held at IIT Bombay during Nov. 25–28, vol. 2, pp. 736–741, 2012 (Presented in person)

10. Ravi Kant and S. N. Joshi “Analysis of Sheet-holding Methods in Laser Bending Process using FEM”, In: Proceedings of the 3rd Asian Symposium on Materials & Processing, ASMP – 2012 held at IIT Madras during Aug. 30–31, MCMT_P6, 2012 (Presented in person)

11. Ravi Kant and S. N. Joshi “Thermo-Mechanical Analysis of Laser Bending of AISI 302 Stainless Steel Thick Sheets”, In: Proceedings of the International Conference ICCMM 2011 held at IIT Guwahati during Dec. 15–16, pp. 486–490, 2011 (Presented in person).